2018-08-01

Dynamic Cone Penetration Tests for Liquefaction Evaluation of Gravelly Soils

Michael H. Talbot
Brigham Young University

BYU ScholarsArchive Citation
Talbot, Michael H., "Dynamic Cone Penetration Tests for Liquefaction Evaluation of Gravelly Soils" (2018). *Theses and Dissertations*. 7542.
https://scholarsarchive.byu.edu/etd/7542

Dynamic Cone Penetration Tests for Liquefaction

Evaluation of Gravelly Soils

Michael H. Talbot

A dissertation submitted to the faculty of
Brigham Young University
in partial fulfillment of the requirements for the degree of

Doctor of Philosophy

Kyle M. Rollins, Chair
T. Leslie Youd
Gus P. Williams
Norman L. Jones
A. Woodruff Miller

Department of Civil and Environmental Engineering

Brigham Young University

ABSTRACT

Dynamic Cone Penetration Tests for Liquefaction Evaluation of Gravelly Soils

Michael H. Talbot
Department of Civil and Environmental Engineering, BYU
Doctor of Philosophy

In North American practice, the Becker Penetration Test (BPT) has become the primary field test used to measure penetration resistance of gravelly soils. However, this test is expensive and uncertainties exist regarding correlations and corrections for rod friction. As an alternative, the dynamic penetration test (DPT) developed in China has recently been correlated with liquefaction resistance in gravelly soils. The DPT equipment consists of a 74 mm diameter cone tip driven by a 120 kg hammer with a free fall height of 100 cm using 60 mm drill rod to reduce friction. The DPT is a very rugged, economical device, capable of penetrating dense gravel layers. During DPT field investigations following the 2008 Wenchuan earthquake in China, liquefaction resistance was correlated with DPT blow count.

Dynamic Cone Penetration tests (DPT) tests were also performed adjacent to Becker Penetration test (BPT) sites at Pence Ranch, Whiskey Springs, and Larter Ranch in Idaho where gravel liquefaction was observed during the 1983 M_w6.9 Borah Peak earthquake. Companion DPT tests were performed using an automatic hammer at two energy levels, namely the energy specified in the original Chinese standard and the energy typical of SPT testing which would be easier to use in practice. Companion testing was undertaken to determine if the cone could be driven in gravelly soil with more standard drilling equipment available to geo-professionals. The second energy level also offers the potential to provide more resolution on the soil layering. PDA measurements were made to determine the energy transferred to the cone rods and the statistical variation in the energy transferred.

Additionally, companion DPT tests were undertaken at the downstream toe of Millsite Dam near Ferron, Utah, where gravelly soils are predicted to liquefy in an earthquake. Two energy levels were used, one using an automatic hammer and the other a manual donut hammer. The blow counts from the BPT and DPT correlated reasonably well for gravels using the automatic hammer, but poor correlation was obtained with the donut hammer. Liquefaction resistance for the BPT and DPT soundings were also in reasonable agreement for gravel layers suggesting that the DPT can provide liquefaction hazard evaluations more economically than the BPT using direct correlations with field performance.

Correlations suggest that the standard energy corrections developed for the SPT can be used for the DPT. In general, the liquefaction resistance from the BPT and DPT correlated reasonably well when using the 30% probability of liquefaction resistance curve developed for the DPT.

Keywords: Michael H. Talbot, liquefaction, Chinese dynamic penetration test, gravelly soils

ACKNOWLEDGEMENTS

This study was funded by the United States Geological Survey (USGS), the US Bureau of Reclamation Dam Safety Office, and the US Bureau of Reclamation Science and Technology Research Program under the Research and Development Office. I am very grateful for their support.

I would like to thank Professor Kyle M. Rollins and T. Leslie Youd (Ret.) from Brigham Young University for their unfailing support throughout the course of this work. I appreciate your patience and guidance. I would also like to thank Brigham Young University and the Department of Civil and Environmental Engineering for having the confidence in me to award a yearly scholarship to me that allowed me to fulfill this life-long dream. I am also grateful for the advice and guidance of Dr. Norm Jones, Dr. Kevin Franke, Dr. Gus Williams, Dr. Woodruff Miller, Dr. Kyle M. Rollins, and Dr. T. Leslie Youd, who served as my committee.

I would like to thank our Chinese research counterparts, Dr. Zhenzhong Cao and Xiaoming Yuan, for their help and guidance.

Thanks is due to the Utah State Division of Water Resources and Eric Dixon for providing valuable information and insight on the Millsite Dam site.

Many thanks are also due to Seth Tykert, Ranch Manager of the Pence Ranch in Idaho, Cody Schmidt and the Idaho Transportation Department, and Todd Kuck from the Challis Idaho Field Office of the Bureau of Land Management, all who provided invaluable help in acquiring and facilitating access to the various Idaho work sites.

Lastly, I would like to thank my wife Lisa for her encouragement, support, and patience in this endeavor. I shall be forever in your debt.

TABLE OF CONTENTS

LIST OF TABLES

LIST OF FIGURES

1 INTRODUCTION

Characterizing gravelly soils in a reliable, cost-effective manner for routine engineering projects is a major challenge in geotechnical engineering. Even for large projects, such as dams, ports, and power projects, characterization is still expensive and problematic. This difficulty is particularly important for cases where liquefaction may occur. The use of DPT methods is well suited for penetration testing in gravelly soils because particle interference is minimized and the test can be carried out efficiently and effectively and with readily available equipment.

1.1 Background

Liquefaction is known to have occurred in gravelly soils at multiple sites during at least 16 earthquakes over the past 130 years as indicated in Table 1. As a result of these case histories, engineers and geologists are frequently called upon to assess the potential for liquefaction in gravels. Therefore, innovative methods for characterizing and assessing liquefaction hazards in gravels are certainly an important objective in geotechnical engineering.

Because of the difficulty of obtaining meaningful results from Standard Penetration tests (SPT) and Cone Penetration tests (CPT) in gravelly soils, the large diameter Becker Penetration test (BPT) was developed. Although the BPT-based approach has provided a reasonable method for liquefaction assessment of gravels, the method is expensive and involves empirical correlations which increase uncertainty. Over the past 60 years, Chinese engineers have developed a dynamic cone penetration test (DPT) which is effective in penetrating coarse or even cobbly gravels and provides penetration data useful for liquefaction assessment, (Chinese Design Code, 2001), (Cao et al. 2013). This test provides an important new procedure for characterization of gravels that fills a void in present geotechnical practice.

Table 1. Case Histories Involving Liquefaction of Gravelly Soil.

Year	Earthquake	Mw	Reference
1981	Mino-Owari, Japan	7.9	(Tokimatsu, 1983)
1948	Fukui, Japan	7.3	(Ishihara, 1985)
1964	Valdez, Alaska	9.2	(Coulter, 1966)
1975	Haicheng, China	7.3	(Wang, 1984)
1976	Tangshan, China	7.8	(Wang, 1984)
1976	Friuli, Italy	6.2	(Sirovich, 1996)
1978	Miyagiken-Oki, Japan	7.4	(Tokimatsu, 1983)
1983	Borah Peak, Idaho	7.3	(Youd, 1985)
1988	Armenia	6.8	(Yegian, 1994)
1992	Roermond, Netherlands	5.8	(Maurenbrecher, 1995)
1993	Hokkaido, Japan	7.8	(Kokusho, 1995)
1995	Kobe, Japan	6.8	(Kokusho, 1995)
1999	Chi-Chi, Taiwan	7.9	(Lin, 2004)
2008	Wenchuan, China	7.9	(Cao, 2013)
2014	Cephalonia Is., Greece	6.1	(Nikolaou, 2014)
2016	Pedernales, Equador	7.8	(Lopez, 2016)

Unfortunately, the probabilistic liquefaction triggering curves based on DPT blow count are only based on case histories from one earthquake in one geologic setting. To make the procedure more robust and reliable, additional case histories are required from other earthquakes and geologic environments. Furthermore, because of the scarcity of field performance case histories, the spread in the DPT probability curves is considerably larger than similar curves for sands based on CPT or SPT blow count. Additional case histories should bring these curves closer together as the effect of potentially misplaced data points becomes less important. In addition, the Chinese implementation of the DPT involves a very heavy hammer with a pulley and free-fall mechanism that contrasts with the typical automatic SPT hammer used in US practice. Additional research is necessary to optimize the DPT procedure for US practice and evaluate appropriate hammer energy corrections. Finally, DPT field case histories are now prevalent enough and DPT tests reliable enough, that the DPT can now be used to verify BPT criteria.

1.2 Objectives

The objectives of this study are:

1. To provide comparative evaluations of the liquefaction resistance estimated by the DPT and the BPT for sites where gravelly soils have liquefied during a major earthquake.
2. To provide comparisons between DPT resistances obtained with the Chinese hammer energy and the energy delivered by an SPT hammer, after appropriate energy corrections in an effort to optimize the method for US practice.
3. To provide additional data points defining the liquefaction resistance as a function of DPT blow count at sites throughout the world where gravels have liquefied in past earthquakes.
4. To use the additional data points from these investigations to improve the probabilistic liquefaction triggering curves for future evaluation of liquefaction hazard in gravelly soils.

To accomplish these objectives, DPT tests were performed at three sites in Idaho where BPT data was previously performed. In addition, DPT test were performed at a site in central Utah where gravelly soils are expected to liquefy in an earthquake.

1.3 Scope of Work

The first Idaho location consisted of a site about 16 km (10 miles) north of Mackay near the Big Lost River in central Idaho where gravelly soil was observed to liquefy near the Pence Ranch house and barns during the 1983 M_s7.3 (M_w6.9) Borah Peak earthquake (Youd et al. 1985). Sand boils, gravelly ejecta, lateral spreading, and fissuring were reported. Testing was carried out at four boring locations to depths of about 10 meters (32.8 ft.) using an automatic hammer but with two different hammer weights to produce varying energy levels.

The second was located about 25.8 km (16 miles) north of Mackay, Idaho near Whiskey Springs in central Idaho, along Highway 93. Coarse grained sediments at the end of an alluvial fan experienced liquefaction effects during the 1983 Borah Peak earthquake such as lateral spreading, fissuring, buckling, and sand boils. Testing was completed at two boring locations to depths of about 10 m (32.8 ft.) using two different hammer weights (energy levels).

The third site was located about 1.6 km (1 mi.) south of the Whiskey Springs site, or about 24.1 km (15 mi.) north of Mackay, Idaho, and also near Thousand Springs Creek in central Idaho, on property known as Larter Ranch. Liquefaction of gravelly soil was observed during the 1983 Borah Peak earthquake with surface fissures, lateral spreading, sand boils, buckled sod, and vertical offsets being the major effects. Testing was carried out at four boring locations to depths of about 10 m (32.8 ft.) using two different hammer weights (energy levels).

The fourth site was in the foundation of Millsite Dam in central Utah, approximately 4.8 km (3 miles) west of the town of Ferron, consisting of sand and gravel layers. Companion testing was carried out at four boring locations to depths of about 6 m (19.7 ft.) using an automatic hammer and a manual donut hammer, which resulted in varied energy levels. Applied energy was measured for all the DPT soundings so that energy corrections could be applied.

1.4 Limitations of Current Methods for Characterizing Gravels

In North American practice, the Becker Penetration Test (BPT) has become the primary field test used to measure penetration resistance of gravelly soils. The BPT was developed in Canada in the late 1950’s and consists of a 168 mm (6.6 in.) diameter, 3 m (36 in.) long double-walled casing whose resistance is defined as the number of blows required to drive the casing through a depth interval of 30 cm (12 inches). For liquefaction resistance evaluations, closed-end casing is specified (Rollins et al. 2016).

2 DEVELOPMENT OF IN-SITU TESTS FOR CHARACTERIZING GRAVELS

Owing to the difficulty of extracting undisturbed samples from gravelly soils, laboratory tests on undisturbed samples have not proven effective or reliable for measurement of shear strength or liquefaction resistance. Freezing of a gravel layer before sampling improves sample quality but the cost is prohibitive for routine projects. Even when undisturbed samples can be extracted, changes in stress conditions between the field and laboratory can limit the usefulness of laboratory results.

For sands and fine-grained soils, standard penetration tests (SPT) and cone penetration tests (CPT) are widely used to measure penetration resistance for applications in engineering design and for assessing liquefaction resistance. However, SPT and CPT are not generally useful in gravelly soils because of interference from large particles. Because of the large particles, the penetration resistance increases and may even reach refusal in cases when the soil is not particularly dense. This limitation often makes it very difficult to obtain a consistent and reliable correlation between SPT or CPT penetration resistance and basic gravelly soil properties.

2.1 The Becker Penetration (BPT) Test for Characterizing Gravels

The Becker Penetration (BPT) Test employs a large diameter penetrometer so that the blow count is less sensitive to the effect of large gravel particles during penetration. The Becker Penetration Test consists of driving a double-walled 168-mm (6.6 in.) outside diameter steel casing shaft and closed drill bit into the ground using an AS-1000 drill rig and an ICE 180 diesel pile hammer. The blow count, N_B, and bounce chamber pressure, BP, are recorded for each 0.3 m (12 in.) of penetration.

The BPT was developed during the late 1950's in Canada by Becker Drills Ltd. as a method for rapid penetration of gravel and cobbles. The main advantages of the Becker test are: (1) it can quickly penetrate through gravelly soils, (2) it has a 168-mm (6.6-in) outside diameter making it less susceptible to influence by large particles than the SPT, and (3) it can provide a sample if an open-end bit is used. The shaft and bit have the same diameter and it is considered one of the oldest methods of penetration testing (Cao et al. 2013).

Andrus reported that "because of the simplicity of the test. The equipment varies considerably. However, it has been shown that probing using properly designed equipment and an adequate procedure based on full understanding of the mechanism of driving a cone into the soil allows measurements to be made that are as reliable as those performed with static equipment." (Andrus 1994).

One disadvantage is that there is a larger bulb of stress associated with the BPT. Research has shown that the bulb of influence can extend five to ten diameters above and below the tip from static cone tests. Because of this the BPT may not adequately measure a layer less than about 2.4 m (7.7 ft.) in thickness.

2.2 Liquefaction Resistance Curve based on BPT Penetration Resistance

Because much of the geotechnical engineering work related to liquefaction evaluation is based on the widely accepted Standard Penetration Test (SPT), there have been many SPT-BPT correlations suggested over the years.

Figure 2-1. Becker Hammer Rig used at Millsite Dam in 2009, view looking north along the downstream toe of the dam.

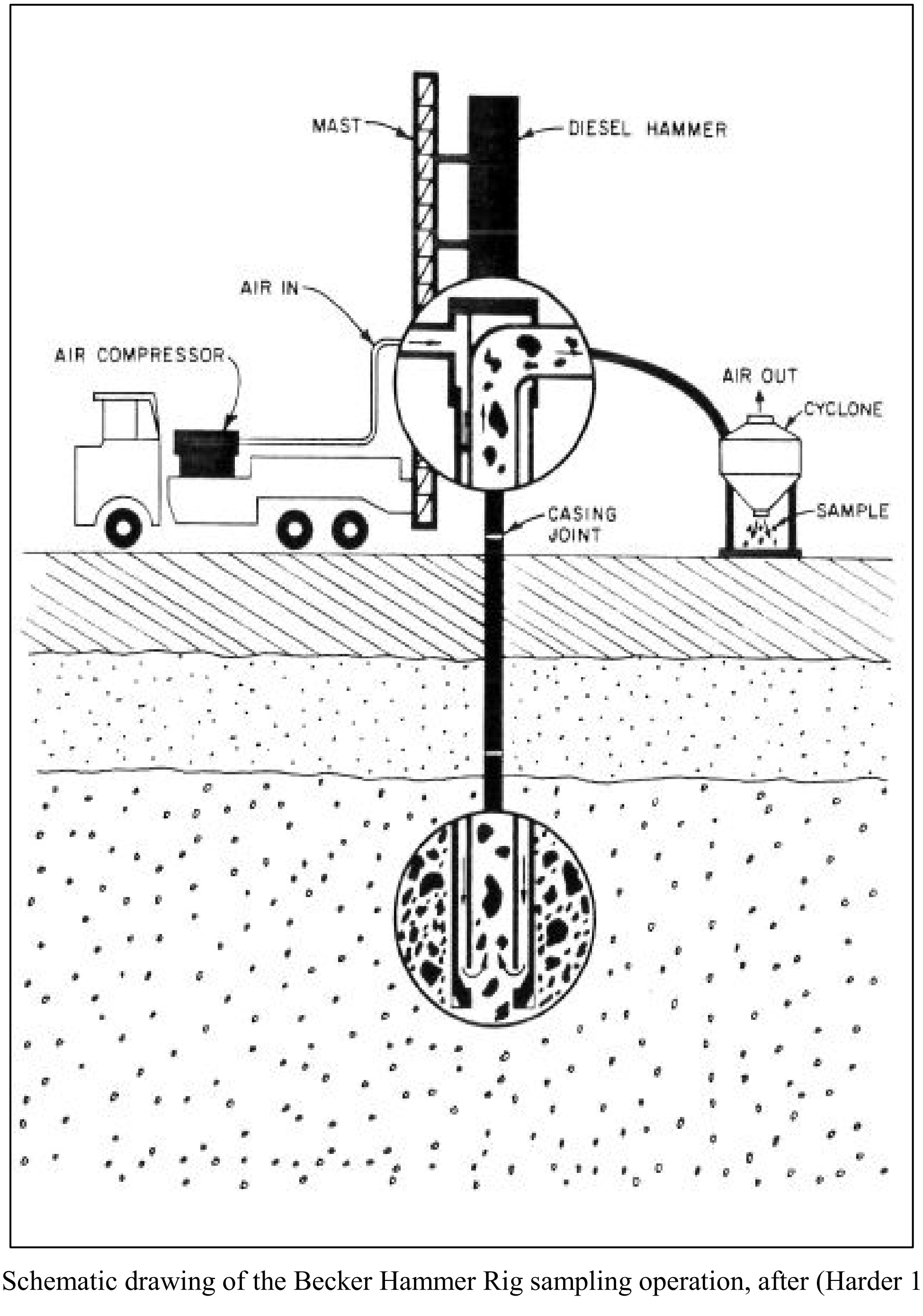

Figure 2-2. Schematic drawing of the Becker Hammer Rig sampling operation, after (Harder 1988).

However, these studies were typically conducted in gravelly soils using non-standard methods. Harder performed side-by-side SPT and BPT tests at several sandy sites in an effort to develop a more accurate correlation and standardization procedures (Harder et al. 1986).

Only the Harder (1988) method will be explained here. In the Harder method the BPT blow count N_B is recorded along with the bounce chamber pressure, BP. After correcting the BP for altitude (say 6000 ft.) to an equivalent pressure at sea level BP_{SL} using Figure 2-3, Figure 2-4 is entered along the x-axis with the BP_{SL}. Next, the BP_{SL} is read vertically until it intercepts the N_B value, which is entered and translated horizontally from the y-axis. The intersection point of these two lines, shown as an open box on Figure 2-4, is then translated down along the combustion efficiency correction curves to Line A-A, keeping the point at approximately the same distance between correction curves. At the point where the translated intersection point (open box) reaches the A-A line, the new N_B is read from the y-axis and is then referred to as the corrected BPT penetration resistance, N_{BC}.

To facilitate use of the BPT for liquefaction resistance calculations, Harder and Seed (1986) developed correlations between the SPT blow count in sand and the BPT N_{BC} after correction for Becker hammer bounce chamber pressure and atmospheric pressure at the elevation of testing as shown in Figure 2-5. Despite the scatter, the correlation appears to be reasonably good considering the typical coefficient of variability for SPT testing (≈ 0.30) (Kulhawy et al. 1990).

Using the correlation between the corrected BPT penetration resistance, N_{BC}, and the SPT penetration resistance corrected for hammer energy, N_{60}, shown in Figure 2-5, the equivalent SPT N_{60} can be obtained.

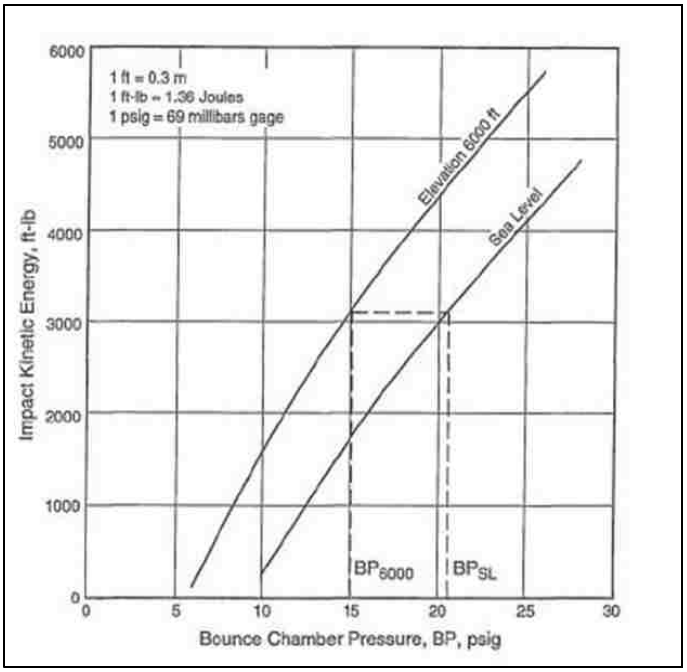

Figure 2-3. Chart for correction of Bounce Chamber Pressure measured at an elevation of 1830 m (6000 ft.), BP_{6000}, to Bounce Chamber Pressure at Mean Sea Level. BPSL after (Harder 1988).

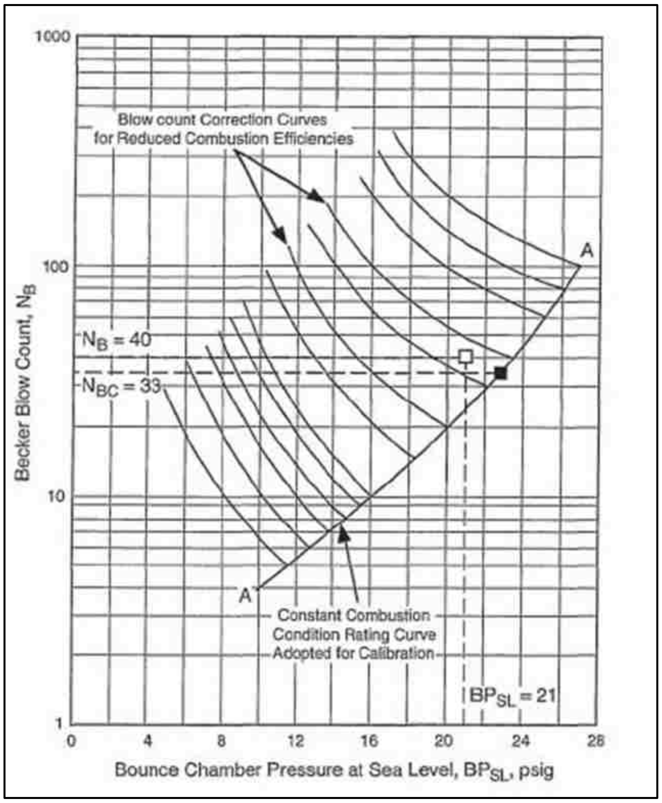

Figure 2-4. Correction curves to correct Becker blow count to constant combustion condition (Harder 1988).

This approach assumes that the Becker hammer is relatively unaffected by the particle size of the gravel. The equivalent SPT blow count must then be corrected for overburden pressure effects to obtain $(N_1)_{60}$, then a liquefaction triggering curve such as that shown in Figure 2-6 (Youd et al. 2001) can be used to evaluate the cyclic resistance ratio for the gravelly soil.

As shown in Figure 2-6, the liquefaction boundary curves (Youd et al. 2001) are essentially vertical at cyclic stress ratios greater than 0.5. For example, with a fines content less than 5%, the CRR is undefined for SPT $(N_1)_{60}$ values greater than 29, although the liquefaction resistance is clearly higher than a value of 0.5.

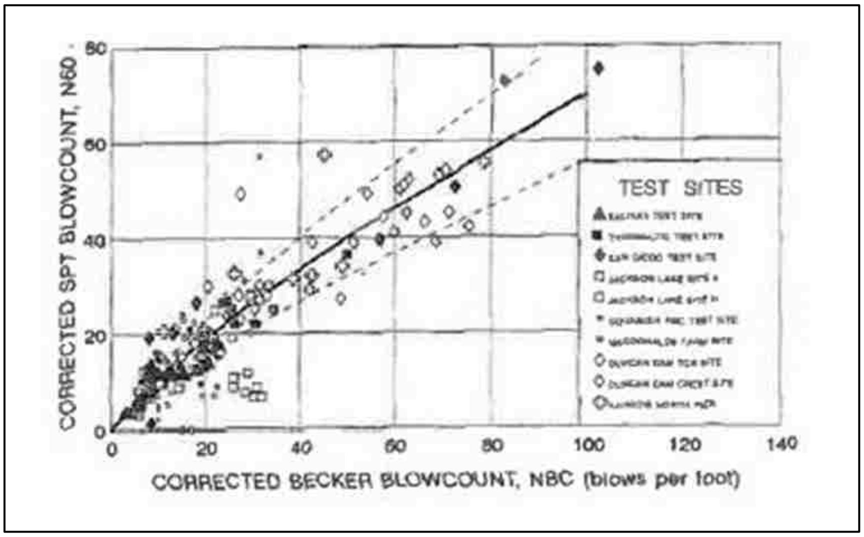

Figure 2-5. Correlation between corrected Becker and SPT blow-counts from (Harder et al 986) supplemented with data from additional test sites (Harder 1997).

Disadvantages in applying the BPT for liquefaction hazard investigations include the high cost of mobilization, uncertainty in measuring BPT resistances, uncertainties in correlations between SPT and BPT blow counts, and friction resistance between the soil and the driven BPT casing. Sy (1994) found that friction on the Becker penetrometer affects the measured penetration resistance. They developed a procedure for correcting BPT measurements for friction resistance by using strain and acceleration measurements to perform a CAPWAP analysis to quantify the effect of casing friction on BPT resistance. Sy (1997) has also used mud slurry injection at the base of the Becker to reduce casing friction, with some success, but both the CAPWAP and the mud injection approaches add to the overall complexity of the test procedure.

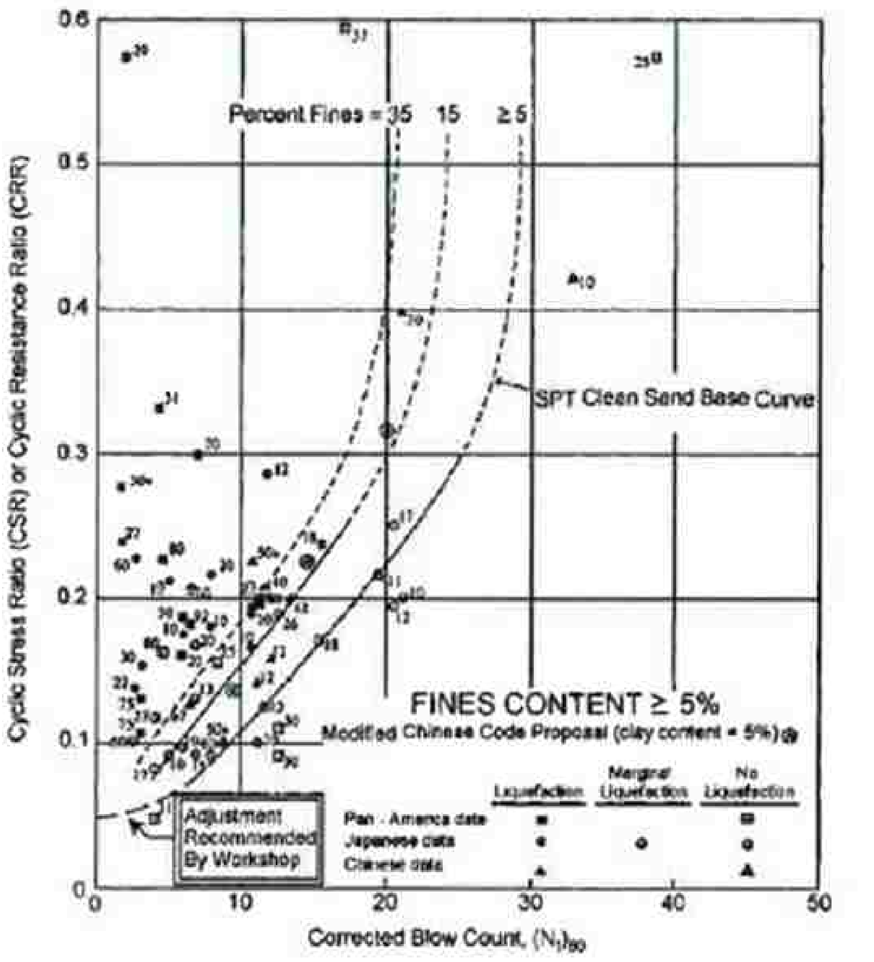

Figure 2-6. Correlation between cyclic resistance ratio and corrected SPT blow count based on liquefaction case histories for Mw7.5 earthquakes (Youd et al. 2001).

More recently, Ghafghazi et al. (2014) have developed more sophisticated instrumentation for determining the energy delivered to the base of the BPT which greatly reduces the uncertainty associated with skin friction. The BPT blow counts adjusted with this procedure have subsequently been correlated with SPT blow counts at several sites (Ghafghazi et al. 2017). This correlation, while representing a major improvement on the Harder (1997) correlation, still leads to increased uncertainty in the liquefaction assessment approach in contrast to a direct correlation with an in-situ test parameter such as the SPT $(N_1)_{60}$ or CPT qc1N, for example.

2.3 The Dynamic Cone Penetration (DPT) Test for Characterizing Gravels

A dynamic penetration test (DPT) apparatus was developed in China during the early 1950s specifically to measure penetration resistance of gravels for bearing-capacity analyses. Based on their experience, standard test procedures and code provisions have been formulated (Chinese Specifications, 1999), (Chinese Design Code, 2001). Because of widespread gravelly deposits beneath the Chengdu Plain, the DPT is commonly used in that region, particularly for the evaluation of liquefaction potential.

DPT equipment is relatively simple, consisting of a 120-kg (264 lb.) hammer, raised to a free fall height of 100 cm (39 in.), then dropped onto an anvil attached to a 60-mm (2.36 in.) diameter drill rod which in turn is attached to a solid steel cone tip with a diameter of 74 mm (2.91 in.) and a cone angle of 60° as shown in Figure 2-7. The smaller diameter rod helps to reduce shaft friction on the rods behind the cone tip.

Prior to testing, the drill rods are marked at 10 cm (4 in.) intervals and the number of blows required to penetrate each 10 cm (4 in.) recorded. The raw DPT blow count is defined as the number of hammer drops required to advance the cone tip 10 cm (4 in.).

A second penetration resistance measure, called N_{120}, is specified in Chinese code applications, where N_{120} is the number of blows required to drive the cone tip 30 cm (12 in.);

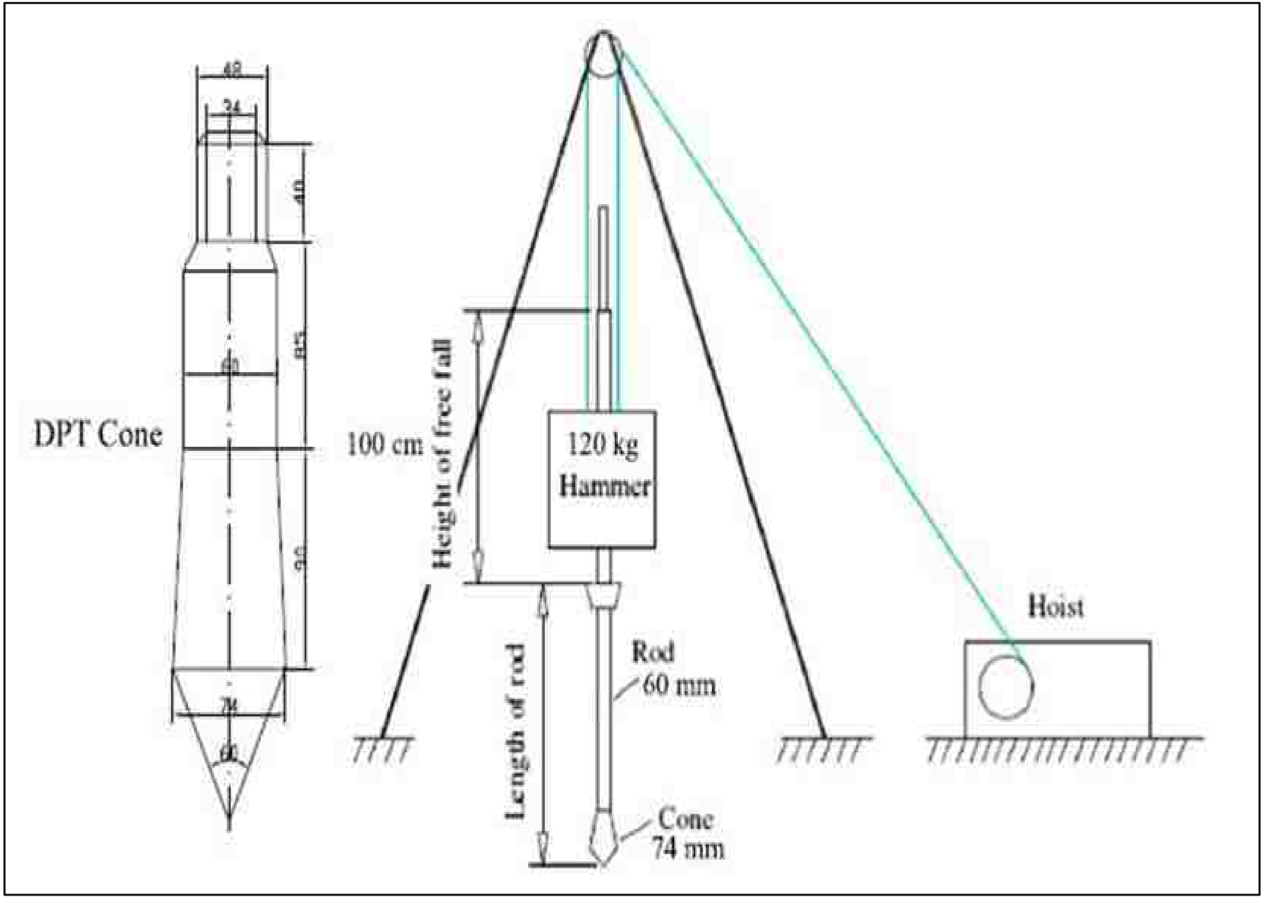

Figure 2-7. Sketch of Tripod and Drop Hammer setup for Dynamic Cone Penetration Tests (DPT) along with the DPT cone tip. (Cao et al. 2011).

however, N_{120} is calculated simply by multiplying the raw blow count by a factor of three which preserves the detail of the raw blow count record.

As with the standard penetration test, a correction for overburden stress on the DPT blow count is applied using equation

$$N'_{120}=N_{120}\,(100/\sigma'_v)^{0.5} \qquad 2\text{-}1$$

Where N'_{120} is the corrected DPT resistance in blows per 30 cm (12 in.), N_{120} is the measured DPT resistance in blows per 30 cm (12 in.), 100 is atmospheric pressure in K=kN/m^2, and σ'_v is the vertical effective stress in kN/m^2 (Cao et al. 2013).

Energy transfer measurements were made for about 1200 hammer drops with the DPT in China using the conventional pulley tripod and free fall drop weight system. These measurements indicate that about 89% of the theoretical hammer energy was transferred to the drill rods with this system on average with a standard deviation between 6.9 and 8.6% (Cao et al. 2013).

2.4 Liquefaction Resistance Curve Based on DPT Penetration Resistance

Following the 2008 M_w=7.9 Wenchuan earthquake in China, 47 DPT soundings were made at 19 sites with observed liquefaction effects and 28 nearby sites without liquefaction effects. Each of these sites was underlain by 2 to 4 meters (6.6 to 13.2 ft.) of clayey soils, which in turn are underlain by gravel beds up to 500 meters (1,640 ft.) thick. Loose upper layers within the gravel beds are the materials that liquefied during the Wenchuan earthquake. Because samples are not obtained with DPT, boreholes were drilled about 2 meters (6.6 ft.) away from most DPT soundings with nearly continuous samples retrieved using 90 mm to 100 mm (3.5 to 3.9 in.) diameter core barrels. DPT soundings reached depths as great as 15 m (49 ft.), readily penetrating gravelly layers that liquefied as well as many layers that were too dense to liquefy.

Layers with the lowest DPT resistance in gravelly profiles were identified as the most liquefiable. At sites with surface effects of liquefaction these penetration resistances were generally lower than those at nearby DPT sites without liquefaction effects. Thus, low DPT resistance became a reliable identifier of liquefiable layers (Cao et al. 2011).

At the center of each layer, the cyclic stress ratio (CSR) induced by the earthquake was computed using the simplified equation

$$CSR = 0.65\ (a_{max}/g)\ (\sigma_{vo}/\sigma'_{v})r_{d} \qquad 2\text{-}2$$

where a_{max} is the peak ground acceleration, σv_o is the initial total vertical stress, $\sigma' v_o$ is the initial vertical effective stress, and r_d is a depth reduction factor as defined by Youd et al. (2001).

Using the DPT data, Cao et al.(2013) plotted the cyclic stress ratio causing liquefaction against DPT blow count as shown in Figure 2-8. Points where liquefaction occurred are shown as solid red dots, while sites without liquefaction are shown with open circles. Cao et al. (2013) also defined boundary curves for 15, 30, 50, 70, and 85% probability of liquefaction based on logistical regression. Most other liquefaction triggering curves are calibrated for $M_w7.5$ earthquakes. To facilitate comparison with data points from other earthquakes, the Cao et al. data points and triggering curves have been shifted upward to represent performance during a $M_w7.5$ earthquake using the equation

$$CSR_{Mw7.5} = CSR/MSF \qquad 2\text{-}3$$

where the Magnitude Scaling Factor (MSF) is given by the equation

$$MSF = 10^{2.24}/M_w^{2.56} \qquad 2\text{-}4$$

proposed by Youd et al. (2001). More recent magnitude scaling factor equations have been developed but they typically require an assessment of relative density or include SPT or CPT based parameters which makes their applicability questionable or problematic for gravel sites. For large magnitude earthquake events the differences in scaling factors are generally small.

The case histories in Idaho with DPT test results provide an excellent opportunity to evaluate the ability of the DPT-based liquefaction triggering curves developed by Cao et al. (2013) to predict accurately liquefaction in gravelly soil. For the Idaho case histories, the geology, earthquake magnitude, and gravel layers are different from those in the Chengdu plain of China and will provide a good test of the method.

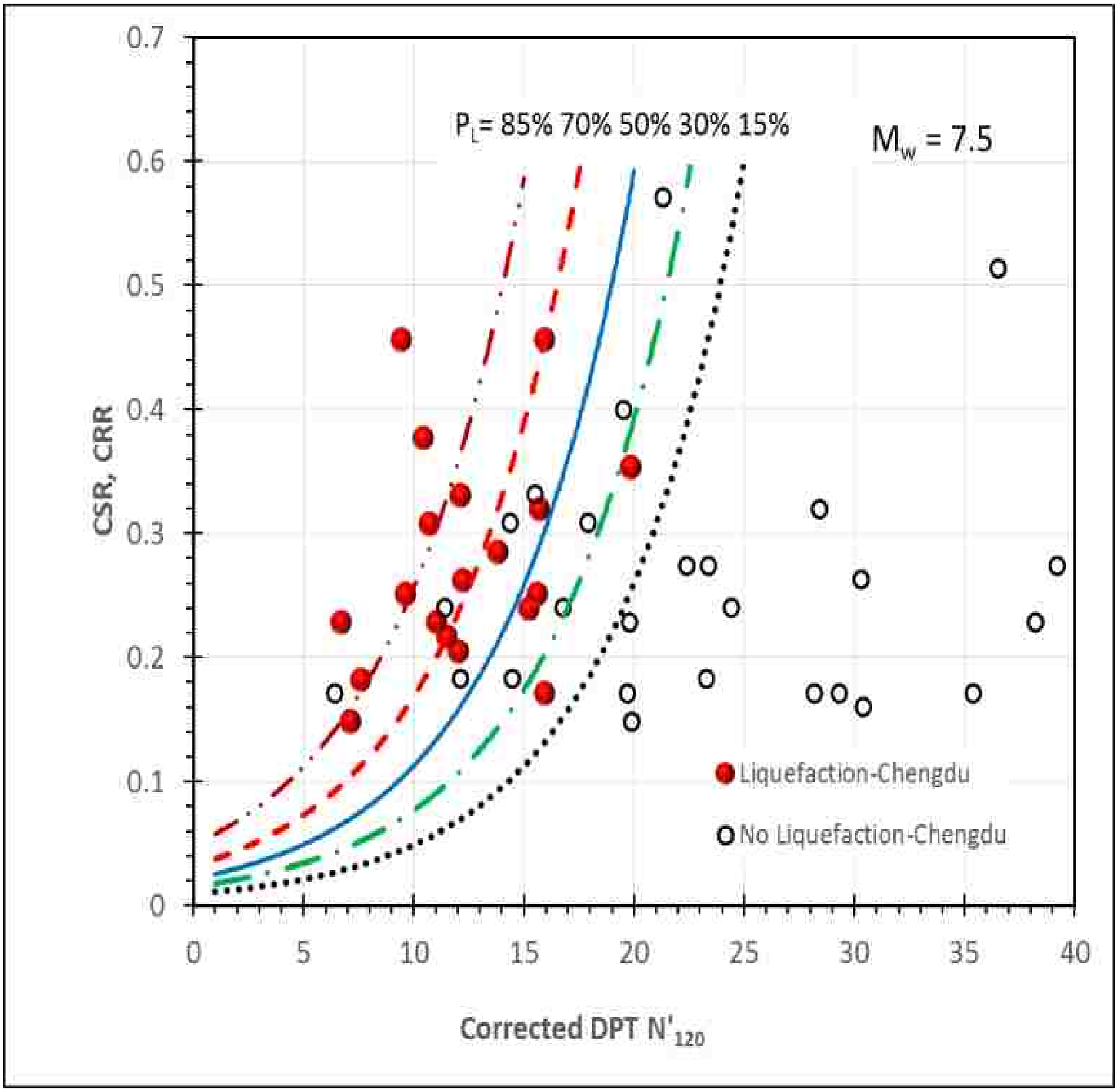

Figure 2-8. CRR vs. DPT N'$_{120}$ triggering curves for various probabilities of liquefaction in gravelly soils developed by (Cao et al. 2013) adjusted for M_w7.5 earthquakes. Liquefaction/no liquefaction data points from sites on the Chengdu plain are also shown after adjustment to M_w7.5.

3 LIQUEFACTION CASE HISTORIES IN GRAVELLY SOILS

3.1 Introduction

The following sections contain four case histories that involve liquefaction of gravelly soils due to earthquake shaking. Although there are many important documented cases world-wide (see Table 1. Page 19), only four will be discussed here because they are of particular interest involving gravely locations.

3.2 Friuli, Italy Gravel Liquefaction Case History

This case history (Sirovich 1996) describes the example of at least two earthquakes with peak ground accelerations lower than former earthquakes which had caused liquefaction. The site at Avasinis is said to have experienced liquefaction effects at least three times.

On May 6, 1976 the area under discussion experienced an earthquake of magnitude M=6.2 that produced numerous liquefaction effects. Near the village of Avasinis, which is located 8 km (5 mi.) northwest of Friuli in northeastern Italy, numerous sand boils consisting of coarse sand and fine gravel were observed, as well as fissures and vents with erupted gravel, and structural damage such as sinking foundations, homes, and sidewalks. On September 15, 1977 an aftershock of M=6.1 struck the area and another the next day on September 16, 1977, M=5.2. Near the village of Mels, located approximately 13 km (8 mi.) SSE of Avasinis and 5 km (3 mi.) south of Friuli, extensive liquefaction occurred during the main shock of May 6, 1976. Mels is about 16 km (10 mi.) from the epicenter and 13 km (8 mi.) from the fault. Numerous vents were documented that spouted fine grey sand, and a two story farm house collapsed.

Evidence of liquefaction in normally consolidated gravels had been observed for the 1948 Fukui earthquake (Ishihara 1985), the 1964 Alaska earthquake (Coulter et al. 1966), the 1975 Hanking (Wang 1984), Tangshan 1974 (Wang 1984), and Borah Peak 1983 quakes (Stokoe et al. 1988a), (Andrus et al. 1991). The majority of liquefaction cases in gravels were either related to alluvial fan deposits or to man-made fills. Only the liquefaction at Pence Ranch (Andrus et al. 1991) is reported to have occurred in gravels belonging to an alluvial terrace, but a less permeable cap favored the development of pore pressure. In all previous cases, liquefaction took place in very loose deposits at shallow to moderate depths. Liquefaction was reported in gravels with clast supported textures and in sediments where the fine matrix prevails.

Sirovich reported that in recent years many new data on the re-liquefaction phenomenon have become available, but a review of case histories has already been given by Youd in a 1984 paper where he also quoted cases of re-liquefaction following prehistoric liquefaction. It was also reported that contemporary data from Japan can be found in Yasuda et al. (1988). Kanamori et al. (1993) presents a case history of archaeological evidence that suggests repetitive liquefactions as early as 500 B.C. Holzer et al. (1994) described two liquefaction cases at the same site in California in 1981 and again in 1987. More information is given by O'Rourke et al. (1994) where it was observed that the locations of the liquefactions caused by the January 17, 1994 Northridge earthquake are approximately the same as those during the 1971 San Fernando event, although the magnitude and extent of ground deformation triggered by liquefaction is considerably less than in 1971. Q_c tip penetration resistances measured in loose sands after the Loma Prieta earthquake were not found to be larger than the values before the earthquake (Chameau et al.

1991). The 1989 Loma Prieta earthquake re-liquefied many 1906 sites (Holzer 1995). In addition, Sims (1995) documented that the distribution of earthquake-induced liquefaction triggered by the 1906 San Francisco and 1989 Loma Prieta quakes are surprisingly similar. They reported finding as many as “three generations of sand blows” at one location with lake sediments where the Loma Prieta main shock (M=7.1) and two aftershocks (M=5.5 and M=4.6) had caused liquefaction at the same sites with sand erupting from fissures created during liquefactions caused by the preceding events. After the measurements reported by Holzer (1989), it was known that not only initial/limited liquefaction, but also extensive liquefaction can occur repeatedly within the same deposit. Less data are available for re-liquefaction caused by an earthquake with magnitude and acceleration lower than that of a previous shock. Yasuda et al. (1988) reported sites where re-liquefaction occurred under these conditions. Following the early shaking table test results by Florin et al. (1961), it was noted that reconsolidation begins at the bottom of liquefied layers. A tentative explanation of re-liquefaction was first proposed by Youd (1984). A similar interpretation was given by Yasuda et al. (1988) following the large shaking table tests by Sasaki et al. (1982), confirming that after liquefaction only the deeper part of the stratum becomes more densely packed. Other shake table and centrifuge tests conducted by Holzer et al. (1995) indicate that similar mechanisms for creating less densely packed zones in the upper part of repeatedly liquefied layers include intrusion of water, loose liquefied sandy material, and dilation in shear zones associated with lateral spreading. Holzer et al. (1995) also showed that soft top layers formed at three liquefaction sites immediately beneath a clay/silt cap.

Redistribution of pressure also plays an important role in liquefaction. It is well known that the strongest liquefaction phenomena in Niigata occurred several minutes after strong motion ceased. Holzer et al. (1989) documented formation of sand blows as much as 19 minutes after the 1987 Superstition Hills, California earthquake. Elgamal et al. (1993) refer to extensive sand boiling from craters 2 meters (6.6 ft.) to 5 meters (16.4 ft.) in diameter which initiated immediately after the October 12, 1992, body-wave magnitude M_b=5.9 Egyptian earthquake. During that event, ejection of sediments as high as 2 meters (6.6 ft.) occurred, and continued for as long as 45 minutes after the main shock. Holzer et al. (1993) observed that there is clear evidence for liquefaction being possible under natural conditions even without strong ground shaking or an increase of applied stress. His observations indicate that "pore pressure buildup during liquefaction is more complex than is suggested by laboratory studies" (Holzer et al. 1989).

Work by Ishihara et al. (1981) and by Holzer et al. (1989) showed that in the case of earthquake-induced liquefaction, there is a threshold acceleration for pore pressure buildup. Seed and others, e.g. Seed et al. (1985); Seed et al. (1986), presented a procedure to estimate liquefaction susceptibility of sands, but also succeeded in predicting liquefaction of the gravelly materials studied by Andrus et al. (1989), a similar observation was made by Sirovich (1996a).

Re-liquefaction has been generally regarded as unlikely because soil grains were believed to always become more densely packed after liquefaction. The author presented additional evidence for the occurrence of re-liquefaction in both sand and gravels.

Sirovich reported that it is possible that before 1976, both the Avasinis and Mels sites had experienced earthquakes with the same magnitude as that of May 6, 1976, or even higher. Therefore the phenomena he described in this case history may be considered the latest one in a series.

3.3 GEER/EERI/ATC Earthquake Reconnaissance, January 26/February 2, 2014, Cephalonia Island Events, Cephalonia, Greece, M=6.1

In a report published June 6, 2014, Sissy Nikolaou, Nikolaou (2014) and colleagues presented an exhaustive review following the 2014 Cephalonia earthquakes. That report is summarized here.

The first of two major earthquakes hit the island of Cephalonia Greece on January 26th with moment magnitude of Mw = 6.0, and the second on February 3rd, with a moment magnitude of Mw = 6.1. Cephalonia has a notable seismic history. In 1953, the island was destroyed by a sequence of destructive shocks that caused more than 450 deaths. But no lives were lost in the 2014 earthquakes. The majority of the structures on the island performed well considering the ground motions were more than twice the elastic code design values. However, other damage was significant enough to affect life, business operations, and economy.

Both events occurred along the Cephalonia Transform Fault, a well-documented active offshore strike-slip fault with a thrust component southwest of the island. Since the seismographic network that recorded the events was installed exclusively east of the fault, epicenters were only approximately located.

Satellite data from the second event revealed a maximum ground deformation of 12 cm (4.7 in.) at the midpoint of the island’s west most peninsula (Paliki), and of 7 cm (2.75 in.) along the east coast of the same peninsula. The highest horizontal Peak Ground Acceleration (pga) recorded during the first event was 0.57 g. The high ground motion amplitude and the characteristic shape of a near-field pulse of the record are consistent with the station’s close proximity to the epicenter. At the same station, the horizontal PGA reached 0.68 g during the second event.

It is likely that site effects played a role in both events. According to the author, the damage concentration in sedimentary soils with poor mechanical properties, like the Lower Pleistocene sequence and younger Holocene alluvial deposits in the Paliki peninsula, is suggestive of significant soil amplification.

Observations included liquefaction of Holocene coarse-grained sediments, rock falls, and landslides. Widespread and repetitive liquefaction and lateral spreading were documented, primarily at the Lixouri and Argostoli ports, within less than 10 km (6.2 mi.) of the epicenters. Very little damage was observed at the ports of Sami and Poros, which are farther from the epicenters. Landslides, rock falls, and retaining wall failures were also concentrated on the western part of the island, closer to the epicenters.

Liquefaction was evident at the ground surface primarily as large horizontal and vertical displacements of pavements on soft sedimentary sites and in areas with widespread liquefaction, mostly in the town of Lixouri. Differential settlement and lateral deformation between pavement and structure were primarily documented for pile-supported structures built on reclaimed land. The relatively mild structural damage in the reclaimed part of Lixouri could be partially attributed to the layer of unsaturated fill on top of the liquefied layers that acted as a protective cap.

Widespread damage was observed in almost all of the 18 cemeteries of the Paliki peninsula and 9 additional cemeteries elsewhere on the island. The main cause of tomb damage was toppling of the grave marble slab. Other failure patterns included slippage, vertical separation, and rotation of blocks and tombstones without toppling.

Extensive structural damage and severe nonstructural damage was also documented for the 49 inspected Greek Orthodox Churches of Cephalonia. The damage was concentrated in the

Paliki peninsula near the epicenters. The extent of damage was found to depend on the structure's age, construction type, and history.

Despite the fact that the island suffered no casualties and the majority of the building stock suffered little to no damage, the economic cost for the Greek government was significant with some estimates as much as $250 million.

The immediate response and thorough reconnaissance by the team, in collaboration with Greek researchers and the local authorities, was invaluable and enabled collection of time-sensitive data on structural and ground failures, such as soil ejecta in areas that experienced liquefaction.

The researchers noted that site amplification and topography effects likely played a role in the damage distribution and strong recorded ground motions. In-situ geophysical testing would be helpful in evaluating the contribution of each. The structural damage at Lixouri and Argostoli ports were composed primarily of rotation and translation of dockside walls at the waterfront, a typical damage mechanism for waterfront structures on soft and/or liquefiable soils.

Seismic response of gravelly fills included liquefaction ejecta in Lixouri and Argostoli ports, which included numerous gravel particles. The fill materials at these locations contained a significant amount of coarse grained particles (greater than #4 sieve).

It was also noted that the minor structural damage at Lixouri could be associated with beneficial effects of structures founded on a stiff non-liquefied soil layer (cap) overlying liquefied soil layers that significantly filter accelerations at the expense of increased lateral displacement.

3.4 Chinese Dynamic Penetration Test for Liquefaction Evaluation in Gravelly Soils, Wenchuan, China, M=7.9

On May 12, 2008 a devastating earthquake (M_s=8.0, M_w=7.9), with an epicenter in Wenchuan County, struck Sichuan Province in southwestern China killing more than 100,000 people. The earthquake was the largest and most destructive to strike China since the 1976 Tangshan earthquake (M_s=7.8, M_w=7.6), which killed more than 240,000 people (Liu 1989). Shortly after the Wenchuan earthquake, a team of geotechnical specialists, organized by the Institute of Engineering Mechanics (IEM), China Earthquake Administration (CEA) traveled to the affected area to investigate occurrences of liquefaction and consequent damage. Through several months of detailed field investigations, 118 liquefaction sites were identified, effects documented, and 47 sites drilled and tested. Most of these sites are located on the Chengdu plain or in the Mianyang area to the northeast. Nearly all of the investigated liquefaction sites are underlain by loose gravels at shallow depth.

Two months were spent identifying, mapping, and documenting surface liquefaction effects including sand boils and ground fissures. Another 2 1/2 months were spent conducting dynamic penetration tests (DPT), drilling sites to extract core samples, and measuring shear wave velocities. Results from these investigations and tests were published in Cao et al. (2011), documenting the distribution and character of gravelly soils that liquefied. The author also developed a probabilistic shear-wave correlation for evaluation of liquefaction resistance of gravels, provided a case history database for future research, and provided comparisons of results from the Wenchuan earthquake with those from previous earthquakes.

Following the 2008 Wenchuan earthquake, 118 liquefaction sites were documented in the Chengdu, Deyang, Mianyang, Meishan, Leshan, and Suining areas of Sichuan Province; the affected region is ~500 km (311 mi.) long and 200 km (124 mi.) wide (Cao et al. 2011). A rectangular region 160 km (99.4 mi.) long and 60 km (37 mi.) wide contained most of the liquefied sites (Yuan et al. 2009).

The Chengdu plain is underlain by a 1–4 m (3.3-13.1 ft.) thick layer of Holocene clayey soil, which is underlain by thick deposits of gravelly sediment (as thick as 540 m, or 1771 ft.) overlying bedrock. The gravel layers beneath the Chengdu plain were formed as alluvial fans along ancient courses of the Minjiang and Tuojiang Rivers. The rivers now flow northwesterly across the plain from the Long-men Mountains and join the Yangzi River that flows along the northwestern edge of the plain. The topography of Chengdu plain is composed primarily of two terraces that lie 2–3 m (6.6-9.8 ft.) and 4–6 m (13.1-19.7 ft.) above present river levels.

The surface effects of liquefaction included sand-boil deposits, ground fissures, lateral ground displacements, ground settlement, and fractured, settled, or tilted structures. The liquefaction sites were located primarily in agricultural areas, but numerous sites were located in urban areas. Fields, roads, bridges, buildings, and industrial facilities were damaged to various extents by the effects of liquefaction. Many houses and small buildings were damaged beyond repair, or entirely collapsed.

The village of Minzhu is located on an alluvial fan terrace 2–3 m (6.6-9.8 ft.) above the water level of a small nearby river. Sand-boil deposits were randomly scattered across approximately 10 hectare (25 ac.) of farmland. Single sand-boil deposits were as large as 5 m^2 (53.8 ft^2), with volumes of ejected reaching 0.5 m^3 (17.6 ft^3). Most of the ejected sediment was reported to be fine to coarse sand with gravel particles up to 5 cm (2 in.) in diameter.

In the village of Baihutou, residents observed sand boils with water spouts as high as 1 m (3.28 ft.) in an area of 66.7 hectare (16 ac.) The sand boils were accompanied by ground fissures, the largest of which was 300 m (984 ft.) long and 3 to 5 cm (1.2-1.9 in.) wide. The sand-boil deposits along those fissures were bordered by what was described as brown to purple fine sand ejecta. In one instance a 3 m (9.8 ft.) deep and 1 m (3.28 ft.) diameter water well was clogged with sand and gravel where gravelly soils were not noted during excavation of the well, indicating that the boiled-up sand and gravel originated beneath the well.

Near the village of Songbai, it was reported that half of a house collapsed because of the fracture of foundations and superstructures caused by ground fissures and ground displacements. Sand boil deposits were observed in an area 7 km (4.4 mi.) long X 3.3 km (2.0 mi.) wide. The deposits ranged from yellow medium sand to gray gravelly sand.

The volumes of ejected sand and gravel and the durations of sand-boil activity during the Wenchuan earthquake were much smaller and shorter than that observed following the earthquakes in Haicheng in 1975 and the Tangshan in 1976, even though shaking duration, intensity, and the inflicted damage were greater during the Wenchuan event. It was postulated that for the smaller sand boil deposits from the Wenchuan earthquake, the liquefaction occurred in gravelly layers, where in the earlier quakes it occurred in thick layers of fine sand. Further, it was suspected that the short durations and lesser volumes of ejected sediment during the Wenchuan even were a consequence of the high permeability of the gravel deposits that liquefied, which allowed rapid dissipation of pore water pressure.

DPT were used to measure penetration resistance and construct DPT resistance profiles. Chinese DPT has been in use for over 50 years although the tests conducted in this study were the first tests conducted in gravelly soils that had liquefied. Forty-seven sites were tested during 2008 and 2010, including 19 with observed surface effects of liquefaction effects and 28 sites without. Most of these sites were located in the Deyang and Dujiangyan districts, which suffered extensive liquefaction effects and damage.

The test sites ranged from 20 km (12.4 mi.) to 40 km (24.8 mi.) away from the fault rupture (Longmen fault). Since no instrumental acceleration data were recorded near the test sites, peak accelerations were interpolated from PGA contour maps prepared by the CEA based on data collected from the China National Strong Motion Network.

DPT were conducted at numerous sites and because samples are not obtained with DPT, boreholes were drilled ~2m (6.5 ft.) away from most DPT soundings for soil logging purposes; nearly continuous samples were retrieved using 90–100-mm (3.5-3.9 in.) diameter core barrels. The retrieved samples were logged to note sediment types and general grain-size properties. Intact gravel samples were cut from the various cores, bagged, and taken to the laboratory for grain-size and soil-classification tests. Geotechnical logs developed from extracted core samples and laboratory tests indicate that a 4 m (13.1 ft.) thick layer of clayey sediment overlies thick beds of gravel in the area surrounding the test sites. Fine-grained clayey soils and soils above the water table were classed as non-liquefiable and the penetrated sediments were divided into layers based on soil type, saturation, and uniformity of N_{120} values. For sites with surface-liquefaction effects, the layer below the water table with the lowest general N_{120} values was identified as the layer that liquefied. For sites without surface-liquefaction effects, the layer below the water table with the lowest average N_{120} was identified as the most liquefiable layer, but was assumed not to have liquefied. Some layers may have liquefied without generating surface-liquefaction effects. Average N_{120} were consistently less than 15 blows/30 cm (12 in.) and at depths less than 10 m (32.8 ft.) in layers identified as liquefiable. Each of the liquefaction sites was strongly shaken by the Wenchuan earthquake with seismic intensities between VII and IX (Chinese Intensity Scale) and PGA between 0.15 g and 0.45 g. The Chinese Intensity Scale is roughly comparable to the Modified Mercalli Intensity Scale.

Soil samples were extracted from layers that did and did not liquefy. Grain-size distribution curves from these samples were plotted and the curves provide general information on the gravels sampled. Mean grain size, D_{50}, of samples retrieved from layers that liquefied ranged from 0.4 to 40 mm (.02 – 1.6 in.) with gravel contents (particles larger than 5 mm, or 0.2 in.) ranging up to 75% (These were considered are minimum values because due exclusion of particles larger than 100 mm, or 3.9 in.). There were no distinguishable differences in grain size between soils classed as having liquefied and those classed as having not liquefied.

Important aspects of the DPT were revealed by the penetration resistance profile. Spikes in the record were caused by the DPT tip striking a large particle or cobble where the particle impeded penetration of the cone tip requiring extra blows to either fracture the particle or push it aside. Once the tip passed the large particle, the blow count returned to the gravel matrix value, where the DPT matrix value is the penetration resistance of the gravel without interference from gravel particles or cobbles. When the tip penetrated an extra loose or finer-grained layer, the blow count dipped on the plot and then returned to the gravel matrix value once the soft zone was passed. As the tip penetrated into denser or coarser layers, the matrix penetration resistance increased, but the peaks and dips continued as large particles or soft lenses were penetrated. During the field investigation, the DPT readily penetrated gravelly sediments to depths of 7 to 15 m (22.9 - 49.2 ft.), including all layers that liquefied.

It was observed that liquefaction mostly occurred in upper layers of the gravelly deposits; these layers are the youngest (Holocene) and loosest layers in the gravel section. Most of the liquefaction sites were near rivers and are underlain by fluvial or alluvial layers with relatively low DPT blow counts. Many liquefaction sites occurred in what are believed to be elongated zones that may be the courses of ancient and buried stream channels and floodplain deposits. Youd et al. (1978) noted that the sediments that liquefied followed previously noted trends of younger, looser, and shallower sediments, being more susceptible to liquefaction than older, denser, and deeper sediments.

As stated earlier, dynamic penetration tests were conducted at 19 sites with liquefaction effects and 28 nearby sites without liquefaction effects. Because soil samples are not obtained with DPT, boreholes with continuous core sampling were drilled near many DPT sounding to define the soil profile with nearly all of the tested sites are underlain by gravel.

Several important results came from this work. First, the Chinese DPT was used for the first time to measure penetration resistance of gravelly soils that liquefied. Results from these tests were used to develop probabilistic criteria for estimation of liquefaction resistance of the gravelly soils. Second, data from 79% of sites with surface liquefaction effects plot above the 50% probability curve and 82% of data from sites without surface-liquefaction effects plot below the 50% probability curve. Third, for sites with surface-liquefaction effects, the layers that liquefied were identified as the layer below the water table with the lowest average DPT penetration resistance. For sites without surface-liquefaction effects, the layer below the water table with the lowest average DPT resistance was identified as the most liquefiable layer, but those layers were assumed not to have liquefied during the Wenchuan earthquake. Fourth, the investigated sites were underlain by cobbley gravels with mean grain sizes ranging from 1 mm (0.04 in.) to more than 30 mm (1.2 in.). Fifth, the DPT readily penetrated gravelly sediments to depths of 7 m–15 m (22.9 – 49.2 ft.), including all tested gravel layers that liquefied. And sixth, the DPT is a robust, efficient, and effective test for measurement of penetration resistance in gravelly soils for liquefaction hazard investigations. With further development, the DPT could become a useful test for measurement of penetration resistance of gravelly soils in other parts of the world, including the United States and other countries where liquefaction resistance of gravels is an important issue.

3.5 In-Situ Investigation of Liquefied Gravels at Seward, Alaska

In this study (Koester et al. 2000), dynamic in-situ penetration tests and cross hole shear wave velocity measurements were performed in deep alluvial gravel deposits at Seward, Alaska that were shaken and reportedly liquefied by the March 27, 1964 Alaska Earthquake. The researchers used two sizes each of split spoon and dynamic cone penetrometers were they driven into gravels near the mouth of the Resurrection River that had exhibited settlement and lateral spreading as a result of earthquake shaking. The researchers used two safety hammers of different sizes and the energy delivered using various hammer and penetrometer combinations was measured. Limited measurements were also made of hammer velocity using a radar system developed for that purpose, to allow for kinetic energy determination. Soil samples were collected and evaluated for classification and to determine stratigraphy. Procedures used at the Seward site were summarized as well as correlation of penetration resistance measured by alternate means and normalized for overburden stress and driving energy.

The author noted that in situ material properties of soils containing gravels and cobbles, including inference of liquefaction resistance and residual strength, are currently estimated by converting results of several different dynamic penetration tests (Becker Hammer Penetration Test - BPT, and Large Penetration Test- LPT) to equivalent Standard Penetration Test (SPT) blow counts. BPT/SPT correlations employed for U. S. Army Corps of Engineers projects have considered diesel combustion efficiency like those described by Harder et al. (1986) and Harder (1988). Field measurements using Pile Driving Analyzer (PDA) equipment have also shown that BPT efficiency is strongly influenced by mechanical energy losses, including friction acting along the driven casing (Sy 1993), (Sy et al. 1993), and (Sy et al. 1994).

Koester stated that liquefaction and resulting post-earthquake instability has been observed during moderate to strong earthquakes in loose to medium dense gravels, both naturally deposited and artificially placed. In his paper, the author lists field occurrence data on liquefaction in gravels during earthquakes worldwide during the last 20 years (similar to Table 1). In most of the cases liquefaction occurrence is only confirmable through surface expression such as sand boils or lateral spreads, or by subsurface instrumentation.

He affirms that in situ tests are not yet developed to confirm or deny the occurrence of liquefaction in any soils, but gravels are especially difficult. The BPT has been widely used to sample and characterize stiffness of coarse grained deposits, and shows promise as a tool to investigate properties associated with liquefaction potential evaluation. In place density tests are extremely valuable but are usually impractical to conduct in saturated gravel deposits at depths greater than about 3.05 m. (10 ft.). And finally, although sampling and testing of gravels is difficult, in situ freezing techniques such as those utilized in Japan e.g. Tanaka et al. (1989), have been successfully used for recovery of high quality specimens of coarse-grained soils.

Test results from several soundings in a sand and gravel river bed using a safety hammer with rope and cathead to advance a 6.35 cm (2.5 in.) solid dynamic cone penetration tip demonstrated that penetration resistance is strongly dependent on probe size in gravelly sand and sandy gravel.

In summary, a new set of field data was produced from penetration tests conducted in gravels at a site that exhibited liquefaction as a result of the 1964 Alaska Earthquake. These data represented one of the first collections of a variety of types of penetration tests and shear wave velocity measurements in gravels associated with liquefaction behavior where energy was measured to support adjustment of the results for varying equipment and procedures.

The author expected that more rigorous evaluation of their data would follow and anticipated that more and better field procedures and interpretation methods for in situ determination of cyclic strength and behavior of coarse grained soils would be developed. They hypothesized that if the gravels at the Seward sit did in fact liquefy during the 1964 Alaska Earthquake, that pore pressure build up and strength loss in the gravelly soils was probably attributable to the siltier gravels found between 7.6 m (25 ft.) and 15.2 m (50 ft.) in depth.

4 THE BOROAH PEAK EARTHQUAKE OF OCTOBER 28, 1983-LIQUEFACTION, M_W=6.9

The most prevalent and damaging effects of liquefaction generated by the 1983 Borah Peak, Idaho earthquake occurred in the Big Lost River and Thousand Springs Valleys north of Mackay Reservoir. Less severe effects occurred in the Big Lost River Valley south of Mackay Reservoir, and in the nearby Pahsimeroi Valley to the north. Nearly all of the liquefaction effects developed in floodplain alluvium of late Holocene age. However, the sediment that liquefied beneath the alluvial fans on the east side of the Thousand Springs Valley was deposited in late Pleistocene time. The distance from the fault to the farthest effect of liquefaction was unusually short for an M_s7.3 event. The distribution of liquefaction effects were consistent, however, with the distribution of MMI intensity and estimated peak ground motion parameters, both of which attenuated more rapidly than is generally expected for an earthquake of this type and magnitude. Figure 4-1 shows the location of the sites relative to the epicenter of the earthquake.

A magnitude 6.9 (M_w) earthquake (7.3 M_s) struck the Borah Peak area of south central Idaho on October 28, 1983, creating a 38 km (23 mi.)-long rupture along the Lost River fault.

The shock caused building damage in several communities, landslides and rock falls, and numerous other liquefaction effects including sand boils, fissures, lateral spreads, and buoyant rise of a buried pump house.

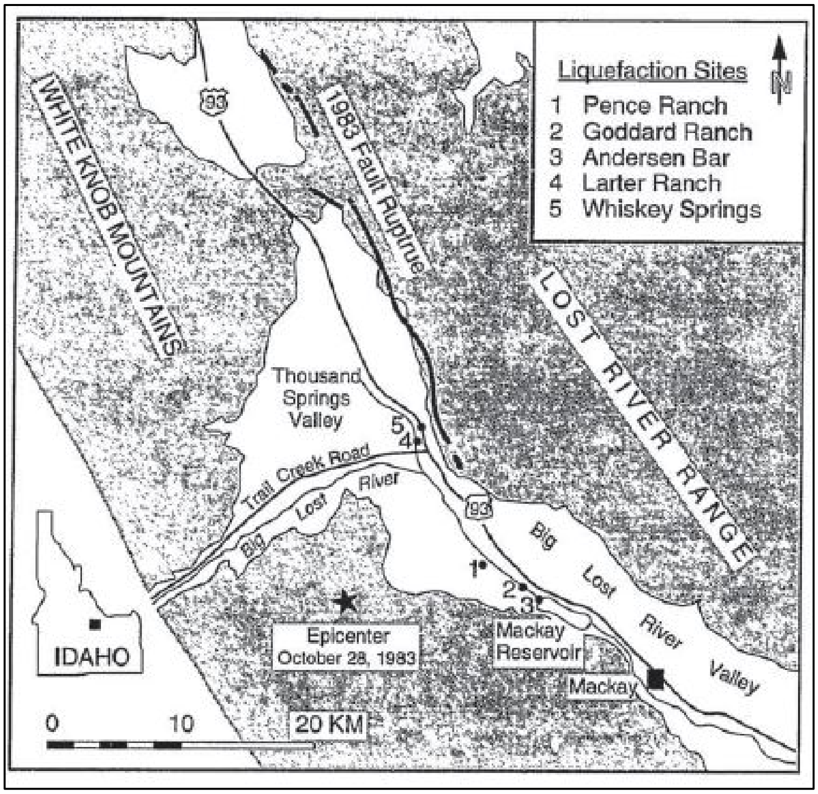

Figure 4-1 Area map showing location of investigation sites with respect to Big Lost River Valley (Andrus 1994).

The disturbances disrupted roadways and pastures, and damaged two buildings. All locations of reported damage in the epi-central area were examined and nearly all the major roads within 64 km (40 miles) of the fault rupture were driven. Low altitude reconnaissance flights over the area were also made. The authors described the liquefaction effects observed, plotted their locations on a map, and compared their distribution with those of past earthquakes.

Youd et al. (1985) reported that liquefaction effects generated by the 1983 earthquake developed only in the intermountain valleys surrounding the Lost River Range. The valleys are filled with Quaternary alluvial, fluvial, and glacial sediment. The youngest sediment in the valleys are channel and floodplain deposits of late Holocene age. These young fluvial deposits lie along rivers and creeks that drain the intermountain valleys. Alluvial fan, glacial, and fluvial deposits of earlier Holocene and late Pleistocene age flank the young fluvial deposits and cover the lower slopes of the valleys. It was reported that most liquefaction effects developed in the late Holocene deposits, but several effects also developed in the older sediment.

Permanent artesian conditions beneath the valleys generated numerous springs and seeps that lead to high ground water conditions beneath many lowland areas. Nearly all of the liquefaction effects occurred in these areas of high water table. Although some lateral spreads extended into areas where free ground water is tens of feet deep.

Youd reported that fissures similar to those southeast of Leslie developed in most roadways passing over marshy areas in the Big Lost River valley to the north of Leslie. In the vicinity of Mackay, three zones of fissures on Highway 93 and several other zones on county roads were noted. In general, the fissures were wider and more disruptive the nearer they were to the surface rupture on the Lost River fault. The fissures in Highway 93 about 5 km (3 mi.) northwest of Mackay and 20 km (12 mi.) from the fault rupture were as wide as 10 cm (4 in.) and disrupted the roadway sufficiently to impede traffic. Near this same area, sand boils with deposits as large as 0.6 m (2 ft.) in diameter erupted in the flood plain of the Big Lost River. These were the only sand boils observed south of Mackay Reservoir.

Approximately 5 km (3 mi.) northwest of Mackay Reservoir and 10 km (6 mi.) southeast of the southern terminus of the fault rupture a lateral spread developed on a low terrace near the Big Lost River, known as Pence Ranch. A curved zone of fissures and sand boils marked the head of the spread and passed beneath a house, barn, and adjacent ranch yards. The fissures were as wide as 0.3 m (1 ft.) with scarps as high as 0.3 m (1 ft.). Sand boil deposits as wide as 2.5 m (8 ft.) were composed of gravelly sand with pebbles as large as 25 mm (1 in.) across.

The cause of lateral spreading was liquefaction of a subsurface sediment layer. The eruption of sand boils at several places along the toe and on the spread were evidence of this phenomenon. The sediment deposited by sand boils was fine sand and silt, indicating that the layer that liquefied contains similarly fine grained material.

No sand boil deposits on marsh grass in the Thousand Springs Valley were seen other than those near fan fronts, and many of those sand boils erupted through cracks in the sod at the toes of lateral spreads. Considering the high water table and generally thick section of late Holocene sediment in the grassy areas, liquefiable material should have been abundant. Two possible reasons for the absence of sand boils are: (1) The sediment may be too fine grained to liquefy, or (2) the thick mat of roots and dead vegetation beneath the grass may have acted as a filter preventing sediment carried by sand boils from reaching ground surface. The authors expressed that the latter explanation seemed more likely. Very few cracks were seen in areas covered by marsh grass. One reason for this absence is the ductility of the upper soil and grass layer which readily stretches rather than cracks.

Some of the most spectacular effects of the earthquake were the violent eruptions of large sand boils and springs in a l.6 km (1 mi.)-long northwest trending zone that cuts across the eastern tip of Chilly Buttes. The sand boils on the valley floor reportedly spewed water and sediment 4.5 to 6m (15 to 20 ft.) into the air for several minutes after the earthquake and lesser flows occurred for several hours. This action flooded part of the Thousand Springs Valley, spread hundreds of cubic yards of sediment across the ground surface in the vicinity of the boils, and pocked the surface with craters. Where the zone cuts across the tip of Chilly Buttes, water gushed from transient springs as high as 30 m (100 ft.) on the hillside above the valley floor. These springs washed sediment from the hillside, cut gullies, and blocked a ranch road and irrigation ditch. The cratered area east of Chilly Buttes was mapped by the researchers and they noted widths and depths of craters and delineated the areas covered by sediment. They recorded that 47 craters were larger than 0.6 m (2 ft.) in diameter and 19 had diameters greater than 6 m (20 ft.) and depths greater than 1.5 m (5 ft.). The largest crater had a diameter of 23 m (75 ft.) and the deepest was 5 m (16 ft.). At least one and possibly five craters existed before the earthquake and were reactivated by the outburst of water during the event. They indicated that a local rancher reported that several of the craters were created by a similar eruption of water during the 1959 Hebgen Lake, Montana, earthquake.

Most liquefaction effects developed in floodplain alluvium of late Holocene age. This sediment fills the bottom of the valleys that surround the Los River Range. The valley bottoms are also generally characterized by high ground water levels. The development of liquefaction in saturated late Holocene sediment of fluvial origin is consistent with behavior of similar materials in other parts of the world. Youd et al. (1978) classify this type and age of sediment as one of the materials most susceptible to liquefaction.

During the earthquake, liquefaction also developed in one area of late Pleistocene sediment beneath the far ends of fans along the east edge of the Thousand Springs Valley. These fans are composed primarily of late Pleistocene materials, although some Holocene deposition has occurred near the larger streams that flow across the fan surfaces (McIntyre et al. 1978); (Nelson et al. 1969); (Pierce et al. 1982); (Rember et al. 1979a); (Rember et al. 1979b). The parts of the alluvial fans affected by liquefaction are quite far from the larger channels and thus presumed late Pleistocene age. The layer that liquefied beneath the fans must be equally as old as or slightly older than the overlying fan deposit and also of late Pleistocene age. No other liquefaction effects were observed or reported by the researchers in the extensive area of Pleistocene fan deposition in the epi-central region. This restriction of liquefaction to a very limited part of the Pleistocene materials is also consistent with behavior in other parts of the world. Sediment of that age has a low susceptibility to liquefaction, as described by Youd et al. (1978).

Youd reported that the distance from the fault rupture to the farthest location where liquefaction occurred was much smaller for this earthquake than was predicted from worldwide correlations. The fissures in Highway 93 near Leslie, ID, 37.6 km (23.5 mi.) from the fault rupture, were the most distant effects attributable to liquefaction. For a magnitude 7.3 event, that distance was less than half of the 85 km (53 mi.) limit estimated by Youd et al. (1978).and only about a quarter of the 149 km (93 mi.) limit given by Keefer (1984). This shorter than expected distance to the limit of liquefaction effects is consistent with modified Mercalli Intensity and with peak ground motions measured during aftershocks, both of which were smaller at Leslie than would normally be expected. Maps of modified Mercalli intensity place the outer bound of the intensity VII zone just east of Mackay near Leslie (Stover 1985). The distance from the source to that bound was much shorter than generally would be expected for an earthquake with the magnitude and length of fault rupture produced by the 1983 event. The absence of liquefaction effects beyond the zone of intensity VII is consistent with past behavior as reported by Keefer. Peak ground motions measured at a station near Leslie, ID were much smaller for magnitude 4 and 5 aftershocks than were expected, based on measurements from other earthquakes. For example, peak motions measured following the 1975 Oroville, CA earthquake, also generated by normal faulting, were approximately twice as large as those at Leslie for similar sized aftershocks at similar distances from the recording instruments. Peak motions at Leslie during the main shock of the 1983 event were also smaller than expected for an event of that size (Jackson et al. 1985). Youd concluded that the reason liquefaction effects did not occur farther from the seismic energy source for the 1983 Borah Peak event is that intensity of ground motion was less than normal at these distances for an event of this magnitude (Youd et al. 1985).

The nearest strong-motion sensors to record the main shock were located at the Idaho National Engineering Laboratory, INEL, located approximately 88 to 110 km (55 to 68 mi.) southeast of the epicenter (Andrus 1994). The maximum horizontal ground surface accelerations, a_{max}, recorded at the two free-field INEL accelerographs were 0.05 and 0.078 g. Based on studies of the far-field records and near-field aftershock data, Jackson et al. (1987) concluded that the town of Mackay experienced peak ground surface accelerations during the main shock of about 0.15 to 0.24 g. They also suggested 0.54 and 0.58 for a_{max} at an epicentral distance of 11 and 12 km (6.8 and 7.5 mi.). These were presumably in the vicinity of the surface rupture.

Andrus (1994) estimated peak ground accelerations for Pence Ranch of 0.33 g at a distance of 12.8 km (8 mi.) from the rupture surface. He also estimated peak ground accelerations for Larter Ranch of 0.5 g at a distance of 3.2 km (2 mi.) and 0.5 g for Whiskey Springs at a distance of 2.6 km (1.6 mi.). These ground motions are generally consistent with estimations of peak ground accelerations estimated using NGA prediction equations except in the case of Pence Ranch where a peak ground acceleration of 0.39 was calculated in this study.

5 DPT TESTING AT PENCE RANCH, IDAHO AND LIQUEFACTION ASSESSMENT

5.1 Introduction

Liquefaction of gravelly soil was observed at the Pence Ranch during the M_s7.3 (M_w6.9) Borah Peak earthquake in 1983 (Andrus 1994), (Youd et al. 1985). Pence Ranch is located on a low-lying river terrace about 16 km (10 mi.) north of Mackay near the Big Lost River in central Idaho (latitude 43.99º, longitude -113.77º). Strong ground shaking during the earthquake caused the loose, saturated sediments beneath the terrace to liquefy. Peak ground acceleration was estimated to be about 0.39g at the ranch. This site was chosen because of the availability of information and easy accessibility to the site. Figure 5-1 shows the general location with the number 1 identifying Pence Ranch.

5.2 Liquefaction Effects

In his 1994 PhD. Dissertation, Andrus (1994) reported that liquefaction effects at Pence Ranch included ground failure in the form of lateral spreading, sand boils, and flotation of a partially buried concrete utility box.

A number of boils were observed at the surface consisting of sand and gravel as shown in Figure 5-2. In addition, gravelly sand ejecta erupted from a fissure formed as a result of lateral spreading near what is described as the hay yard as depicted in Figure 5-3.

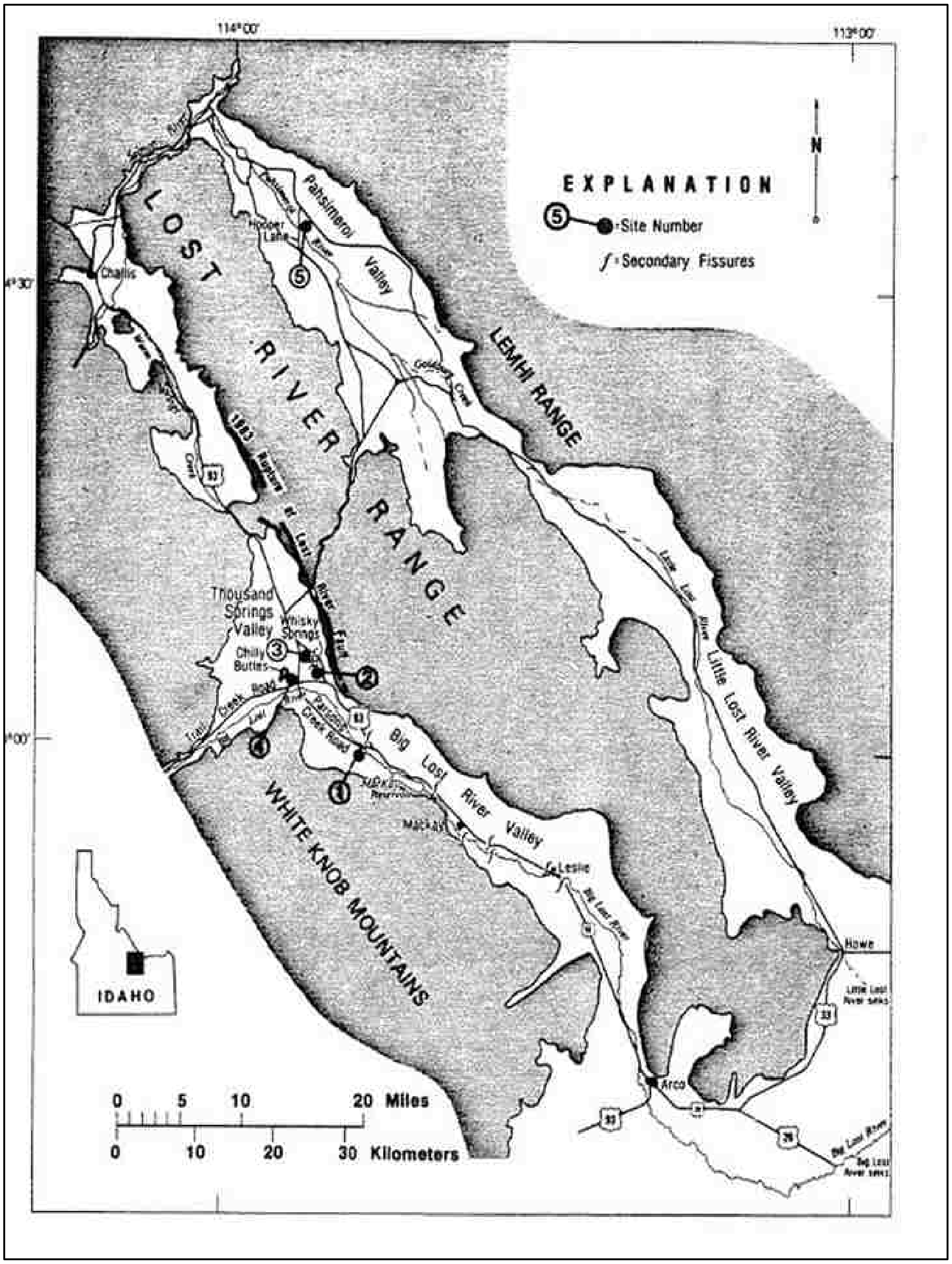

Figure 5-1. Regional map of central Idaho showing geographic features and approximate trace of fault rupture. Site 1 is Pence Ranch (Andrus et al. 1987).

The zone of fissures at Pence Ranch was reported to be 246 m (800 ft.) long and 30 m (100 ft.) wide with the fissure openings as wide as 0.3 m (1 ft.) and scarps as high as 0.3 m (1 ft.). The maximum horizontal displacement was approximately 0.75 m (2.5 ft.) downslope towards the nearby marshy flood plain. Water carrying sand and gravel was ejected at several locations up through the fissures and onto the ground surface.

After the earthquake, site investigations were conducted by the University of California Berkeley in 1984 using SPT and BPT testing. In 1985 researchers from the University of Texas at Austin conducted SPT and SASW testing at the site while the U.S. Bureau of Reclamation conducted CPT tests. The University of Texas at Austin conducted additional BPT and SASW tests in 1990 and cross-hole shear wave velocity tests in 1991 (Andrus 1994). Site conditions in 1983 are shown in Figure 5-2 and 5-3.

The locations of closed-end BPT holes are shown in Figure 5-4 and the interpreted soil profile is shown in Figure 5-5. Site conditions in 2015 are shown in Figure 5-6 and it will be noted that the shed has been constructed since the BPT tests. A picture of the two auto-hammer weights used for the testing is shown in Figure 5-7.

Figure 5-2. Photograph showing sand and gravel ejecta that erupted through a fissure in the ground at Pence Ranch after the M_w7.3 Borah Peak Earthquake in 1983 (Youd et al. 1985).

Figure 5-3. Hay yard fence at Pence Ranch, looking south, pulled apart 0.25 m (30 in.) by lateral spread movement (to the left) in 1983. Sand boils erupted along the large fissure leaving deposits on the ground surface (Youd et al. 1985).

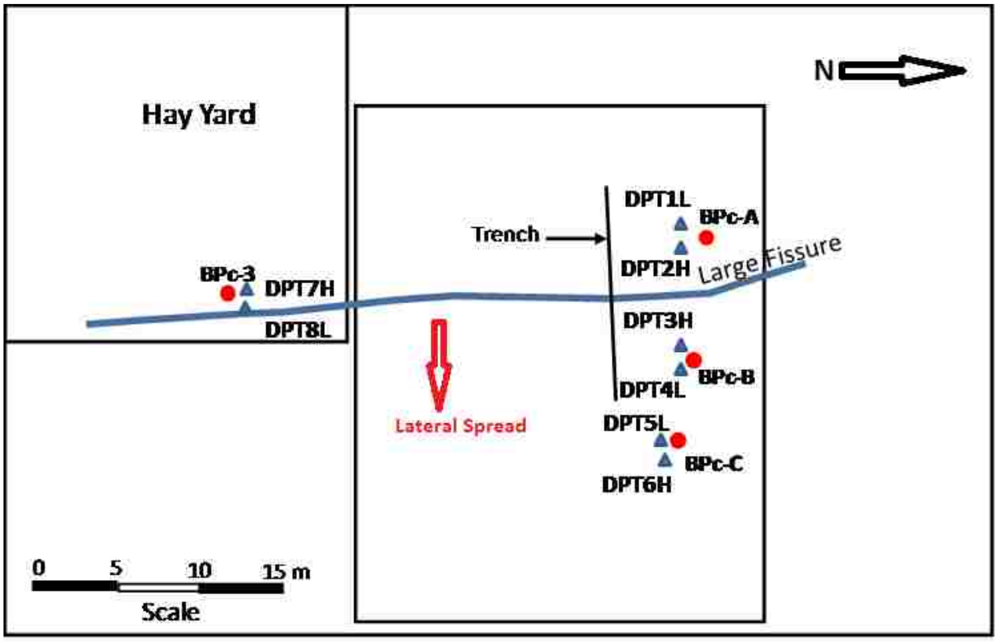

Figure 5-4. Plan view drawing showing location of closed-end Becker Penetration tests (BPc-A, BPc-B, BPc-C and BPc-3) at Pence Ranch relative to hay yard and large fissure that formed due to lateral spreading. Simplified from Andrus et al. (1986). Location of companion DPT soundings are also shown.

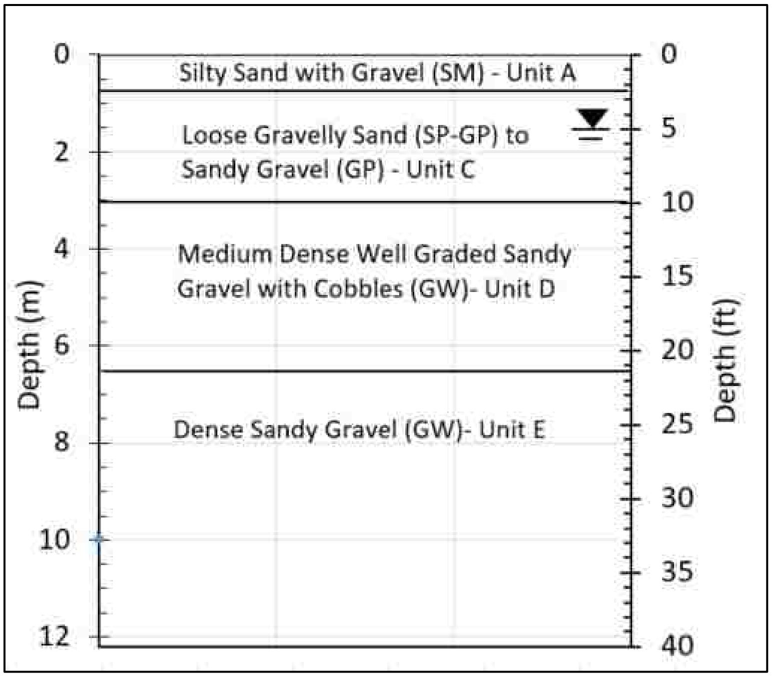

Figure 5-5. Interpreted soil profile near DPT tests based on soil property descriptions provided by Andrus (1994).

Figure 5-6. View looking northeast showing CME rig set up at Pence Ranch site near BPc-B, November, 2016. Shed is of recent construction.

Figure 5-7. View of the two different hammers, the heavy hammer is on the left, 154.4 kg (340 lb.), and the light hammer on the right, 63.6 kg (140 lb.).

5.3 Soil Description

In his 1994 report, Andrus reported several trench investigations at the site where samples were collected, and classified the soils as follows:

A dark brown silty sand, sediment Unit A in Figure 5-8, lies immediately beneath the ground surface. Unit A is less than a meter thick and overlies fluvial sediments, Units B and C. Unit B is divided into subunits B1, B2, and B3. Subunit B1 is reported as a clean, dense sandy gravel (GP) with N-values as large as 62, cone tip resistances as high as 48 MPa (500 ton/ft^2), and in-place dry densities on the order of 21.2 kN/m$_3$ (135 lb/ft^3). Subunit B2 is a channel-fill that grades upward from clean sand to silty sand (SW to SM). Characteristic of sub-unit B2 are cone profiles with tip resistance decreasing with depth, from

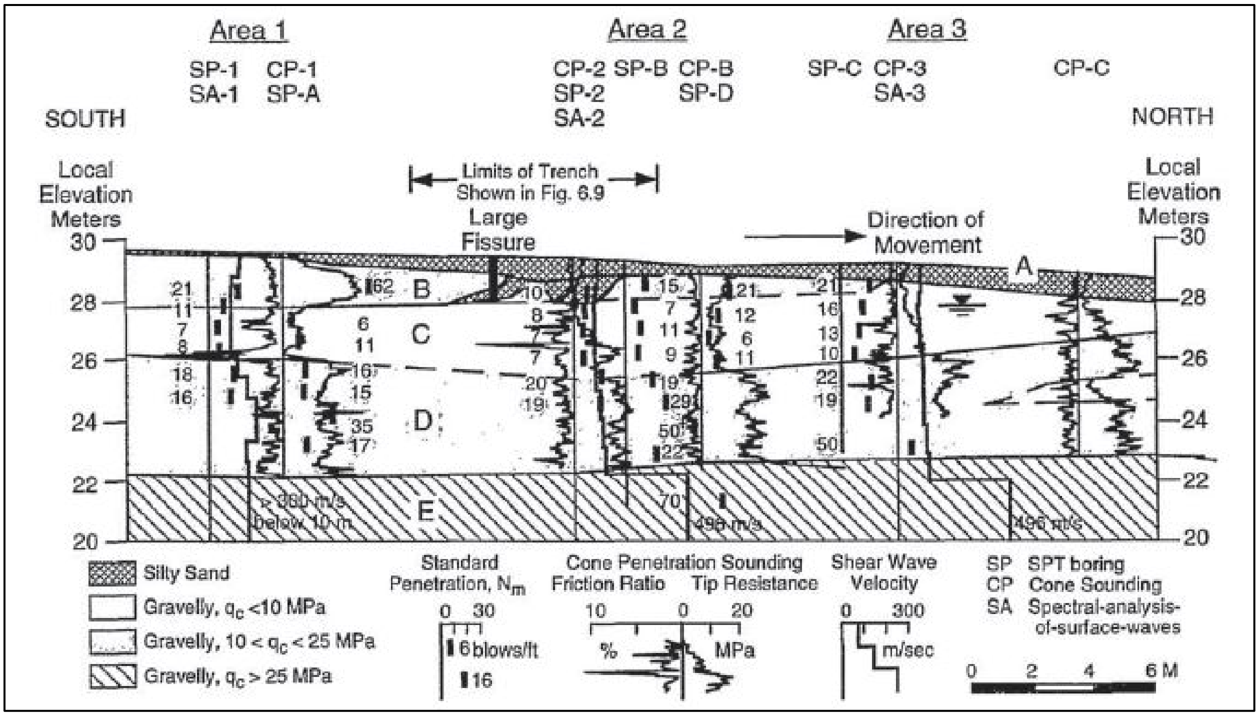

Figure 5-8. North-South cross section at Pence Ranch showing soil units (Andrus 1994).

about 4 to 0.5 MPa (40 to 5 tons/ft^2), and in-place dry densities of about 14.1 kN/m3 (90 lb/ft^3). Subunit B2 locally separates subunit B1 from a clean, medium dense sandy gravel (GP), subunit B3. N-values measured in subunit B3 range from 15 to 21 and tip resistances are greater than about 10 MPa (100 ton/ft^2). It is not possible to delineate these subunits without more penetration testing or trenching.

Beneath units A and B, a loose gravelly stratum labeled Unit C was identified. SPT N_{60} values range from 1 to 18, with an average value of approximately 7. Cone tip resistances, with lowest values near the top of Unit C, vary from 0.4 to 19 Mpa (4 to 201 tons/ft^2), with an average value of 6 MPa (65 tons/ft^2). Cone friction ratios range from 0 to 11 percent, with an average value of 1.2 percent. Uncorrected Becker blow counts (closed bit) range from 7 to 13 blows per 0.3 m (1 ft.). Equivalent N_{60}-values determined from the Becker blow counts range 2 to 8, with an average of 5. Shear wave velocities for Unit C range between 91 and 162 m/sec (300 and 520 ft/sec), with an average on the order of 120 m/sec (390 ft/sec). The minimum in-place dry density of Unit C is less than 17.4 kN/m^3 (111 lb/ft^3), the lowest measurement above the water table. Sediments within Unit C classify as gravelly sand (SP-GP) to sandy gravel (GP) with less than a few percent fines. The amount of sand contained in the samples indicate the gravel to be packed in a sand matrix-supported to a clast-supported structure. Saturated layers of gravelly sand are likely interbedded with sandy gravel, as suggested by the ring density samples taken from Unit C above the water table. The occasional high friction ratios in the cone soundings suggest thin, discontinuous layers of sandy silt within Unit C. The thickness of Unit C varies from 1.5 to 2.8 m (5 to 9 ft.).

The sediments beneath Unit C have much higher penetration and velocity properties (Units D and E). Unit D is characterized by an average SPT N_{60}-value of about 22; and average CPT tip resistance of about 17 MPa (180 tons/ft^2); uncorrected Becker blow count between 15 and 46 blows per 0.3 m (1 ft.); and an average shear wave velocity on the order of 170 m/sec (550 ft. /sec). The average equivalent Becker N_{60}-value is 16. Borehole samples from Unit D classify as clean, well-graded sandy gravel (GW) with cobbles. The thickness of Unit D ranges from 2.7 to 4.2 m (9 to 14 ft.).

Below local elevation of 22.3 (73 ft.), the material (Unit E) is characterized by CPT tip resistance greater than about 40 MPa (400 tons/ft^2); uncorrected Becker blow count ranging from about 46 to over 140 blows per 0.3 m (1 ft.); and shear wave velocities generally exceeding 250 m/sec (820 ft./sec).

Borehole gravel from Units C, D, and E are hard, predominantly sub-rounded with low plasticity, and consist of rock strata similar to the trench gravel.

The water table at Pence Ranch slopes very gently to the east. Near the house, the water table in July 1985 was about 1.8 m (6 feet) beneath the surface of the ground. At the hay yard, nearly 183 m (600 ft.) east of the house, the water table was at a depth of 2.6 m (8.6 ft.). No measurable elevation difference was observed in the north-south direction at the test area near the hay yard. In August, 1990 the water table beneath the hay yard site was about 2.7 m (9 feet) below the ground surface.

The water table was estimated to be at a depth of 1.5 m (6 ft.) during the earthquake but was at a depth of about 1.5 m (5 ft.) at the time of the DPT testing in November 2016. In all cases, with the exception of Whiskey Springs, the water table depth was measured with an electronic m-scope and recorded. At Whiskey Springs the hole caved and did not allow a measurement. The water table was then assumed to be as recorded in the reports.

A plot showing the corrected Becker penetration resistance N_{BC}, as a function of depth is provided in Figure 5-11 for BPT hole BPc-A. The BPT sounding suggests that the critical zone for liquefaction was a layer of sandy gravel located between about 1.5 and 4.0 m (4.9 and 13.1 feet) below the ground surface (Unit C). Previous trenching showed that the ejecta originated from this layer. The BPT blow count increases to between 15 and 20 between 4 and 6.5 m (13.1 and 21.3 feet) (Unit D), then jumps above 25 at about 7.5 m (24.6 feet) (Unit E), and increases linearly to about 60 at a depth of 11 m (36 feet). Andrus identified the soils at the site as generally Holocene alluvial deposits.

5.4 Identification of Liquefiable Material

Based on the low penetration resistance and low shear wave velocities, liquefaction most likely occurred within Unit C (Andrus et al. 1991). This conclusion is supported by the trench studies and his three dimensional model. Further, he reported that from an examination of the large fissure exposed in the trench, ejecting sediment flowed from Unit C. Although samples taken from Unit C are much coarser than the gravelly sand boil deposits, the coarser particles likely became wedged in the narrow openings of the fissure near the bottom of the trench while the finer gravel and sand continued to flow upward.

In Andrus' report, the three-dimensional model showed that the loosest material of Unit C and the large fissure appear geometrically connected. Pore water pressures may have risen in the medium dense Unit D layer. However, since Unit D is present at all test locations and only part of the Pence Ranch site experienced lateral spreading, the development of pore pressures within Unit D does not appear to have controlled sliding. The lower penetration resistance and relationship to the large fissure provided strong evidence that Unit C liquefied.

5.5 Identification of Most Likely Failure Zone for Lateral Spreading

Andrus stated that most of the measurable lateral displacement occurred along the large fissure. The silty cap north of the fissure is as much as 1.4 m (4.6 ft.) thick. Located close to the water table and the loosest material, the low-permeability cap makes the area most vulnerable to liquefaction and shear deformation. The most likely failure zone extended northward from the large fissure, passing just below the water table and through the sediment most susceptible to liquefaction, Unit C.

5.6 Age of Deposit

The report also indicated that radiocarbon dating of the organic compounds bound to the clay fraction of subunit B2 material and a charcoal fragment provided evidence that trench sediments are of Holocene age. An age of 3150 +/- 60 years B.P. (Tx-7103; corrected for $\delta^{13}C$, increased 10 years). For the charcoal fragment that were collected near the first soil sample, an age of 3430 +/- 70 years B.P. (AA-8429) was determined. These dates indicate a maximum age of subunit B2 of 3500 years.

Andrus (1994) reported that alluvial accumulation of calcium carbonate below Unit A is small. Fines from Unit A react strongly with a weak solution of hydrochloric acid. While fines from Unit B and C exhibit a very weak to no reaction with a weak solution of HCl, indicating no significant accumulation of calcium carbonate. The lack of variation in soil development on top of Unit B and C suggested deposition around the same time period, on the order of 3000 years ago.

Andrus (1994) also reported that borehole samples exhibit characteristics (grain-size, grain-shape, sorting, and rock lithologies) similar to the coarse-grained fluvial sediments comprising Units B and C. Cone soundings were suggestive of a geometrical connection between the loose gravelly sediment below the water table and the loose gravelly sediment comprising Unit C in the trench. For these reasons, the loose sediment below the water table is also designated as Unit C. Unit C includes the cross-bedded, gravel and pebbly sand layers (GP and SP), and is on the order of 3000 years old. Andrus concludes that liquefaction occurred in Holocene river sand and gravel. These findings agreed with the criteria relating geologic origin and age of sediment to liquefaction by Youd et al. (1978), where Holocene river deposits have a high liquefaction susceptibility.

Finally, Andrus (1994) reported that sediments comprising Units D and E are more densely packed and possibly coarser than Unit C, indicative of higher flow regimes. Unit D may be similar to the dense Subunit B1, a massive gravel facies (GM) characteristic of longitudinal bars. Unit E could be of late Pleistocene to early Holocene age when the last major episode of gravel deposition by large streams occurred (Pierce et al. 1982).

5.7 DPT Soundings

For this study, two companion DPT soundings were performed within about a meter of each of four previous BPT soundings using a CME 85 drill rig with the capability of using two different hammer energies. In one sounding the DPT cone was advanced using a conventional automatic SPT (light) hammer with a weight of 63.6 kg (140 lb.) dropped from a height of 0.76 m (30 in.). The second sounding was performed using a 154.4 kg (340 lb.) automatic hammer (heavy) with a drop height of 0.76 m (30 in.). Hammer energy measurements were made using an instrumented rod section and a PDA device for each hammer weight to determine the energy transferred to the drill rod. The ratio of the measured energy to the theoretical drop energy is referred to as the Energy Transfer Ration (ETR). Histograms showing the frequency distribution of the Energy Transfer Ratio are provided in Figures 5-9 and 5-10, for the light and heavy hammers, respectively.

The mean ETR for the light hammer was 92.8% with a standard deviation of 4.4, while the mean for the heavy hammer was 85.4% with a standard deviation of 3.7. These standard deviation values are somewhat lower than the 6.9 to 8.6 values measured with the DPT hammers in China. This improvement in precision is likely associated with the automatic hammer drop mechanism used in the US in comparison to the free-fall mechanism used in China as described by Cao et al. (2013).

Because the delivered energies are less than the energy typically supplied by a Chinese DPT hammer, it was necessary to correct the measured blow count downward using the equation

$$N_{120} = N_{measured}(E_{Delivered}/E_{Chinese\ DPT}) \quad 5\text{-}1$$

where $E_{Delivered}$ is the mean energy delivered by a given hammer to the drill rod and $E_{Chinese\ DPT}$ is the mean energy delivered in a typical Chinese DPT test. Cao et al. (2013) found that the measured energy from a typical Chinese DPT was about 90% of the theoretical drop energy.

Equation 5-1 follows the pattern for energy correction recommended for SPT testing by (Seed et al. 1985). The ratio of energy actually delivered divided by the energy delivered by the Chinese DPT hammer was 0.42 and 0.93 for the 63.6 kg (140 lb.) (light) and 154.4 kg (340 lb.) (heavy) hammers, respectively.

Plots of energy corrected DPT N_{120} values versus depth for the 63.6 kg (140 lb.) and 154.4 kg (340 lb.) hammers, near BPT holes BPc-A, BPc-B, BPc-C, and BPc-3 are provided in Figures 5-11 through 5-14, respectively, compared with the BPT N_{BC}. Generally, layers below the water table with the lowest average DPT resistances were identified as the critical liquefiable layers. When two layers below the water table had similar blowcounts, the upper layer was generally selected as being more critical because sand boils could more easily rise to the surface.

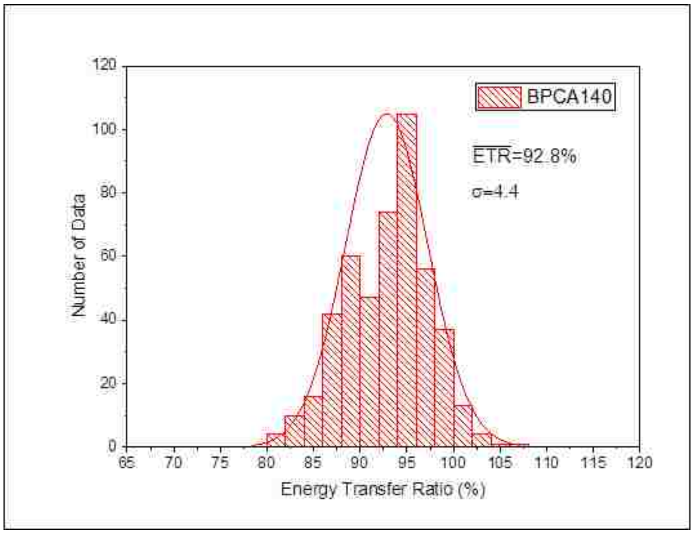

Figure 5-9. Frequency diagram showing number of hammer drops and ETR values for Pence Ranch Hole BPc-A using light hammer (SPT hammer energy of 63.6 kg, 140 lbs., weight dropped 0.76 m, 30 in.).

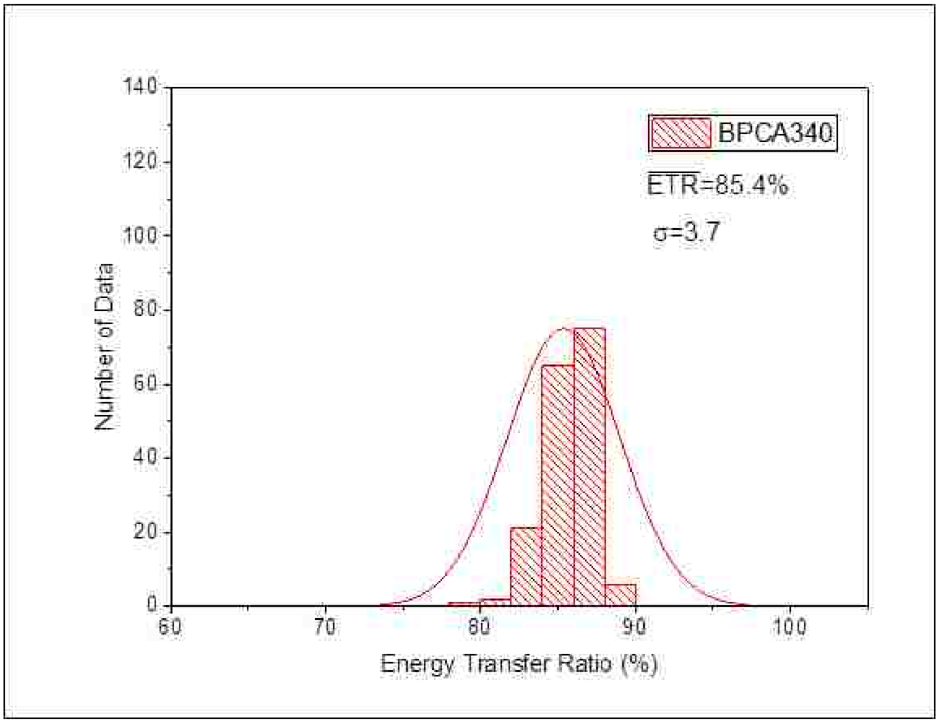

Figure 5-10. Frequency diagram showing number of hammer drops and ETR values for Pence Ranch Hole BPc-A using heavy hammer (Hammer of 154.4 kg, 340 lb., dropped from 0.76 m, 30 in.).

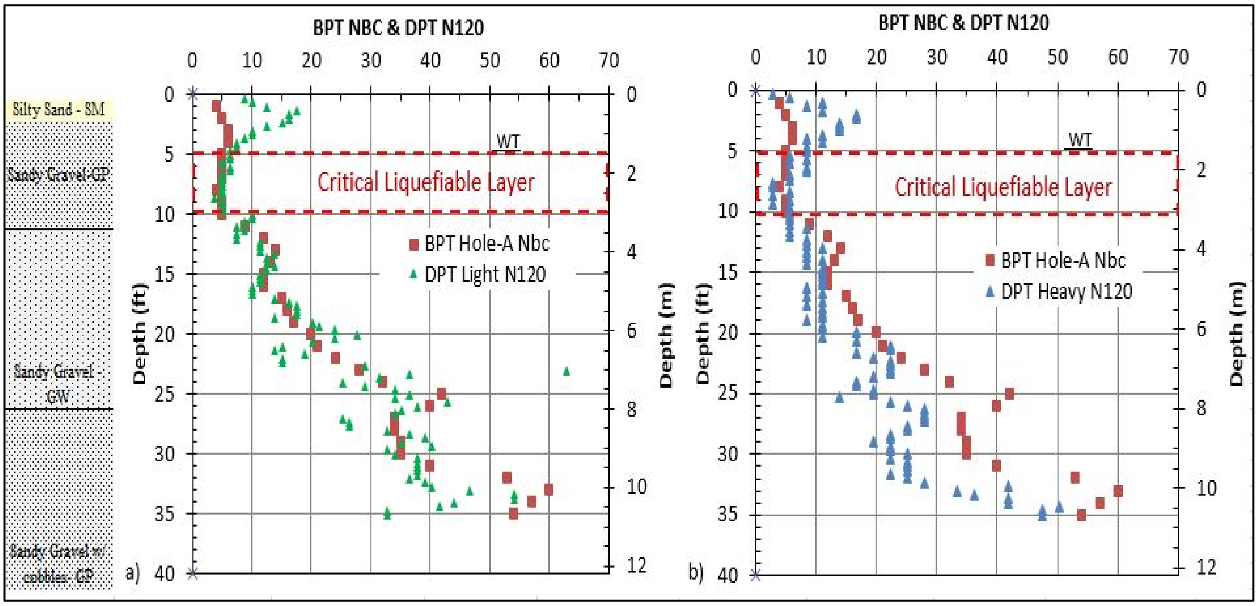

Figure 5-11. Plots of DPT N_{120} versus Depth using (a) light 63.6 kg (140 lb.) hammer and (b) heavy 154.4 kg (340 lb.) hammer, after energy correction to account for lower hammer energies, compared to BPT N_{BC} for Pence Ranch Hole BPc-A. BPT data from Andrus et al. (1994).

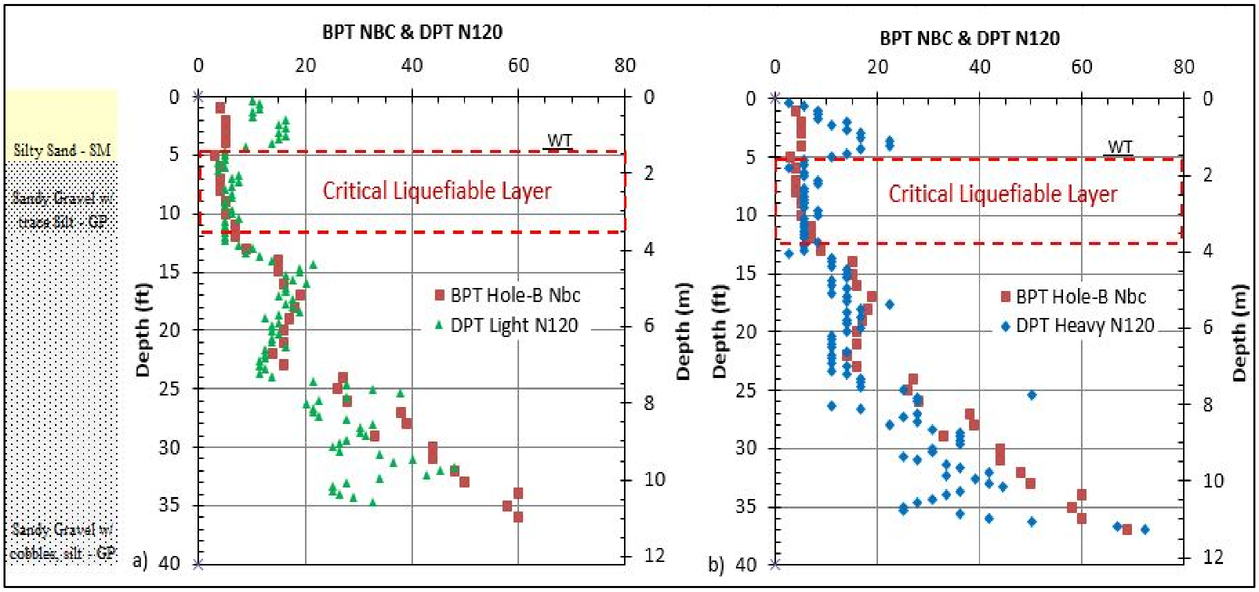

Figure 5-12. Plots of DPT N_{120} versus depth using (a) light 63.6 kg (140 lb.) hammer and (b) heavy 154.4 kg (340 lb.) hammer, after energy correction to account for lower hammer energies, compared to BPT N_{BC} for Pence Ranch Hole BPc-B. BPT data from Andrus et al. (1994).

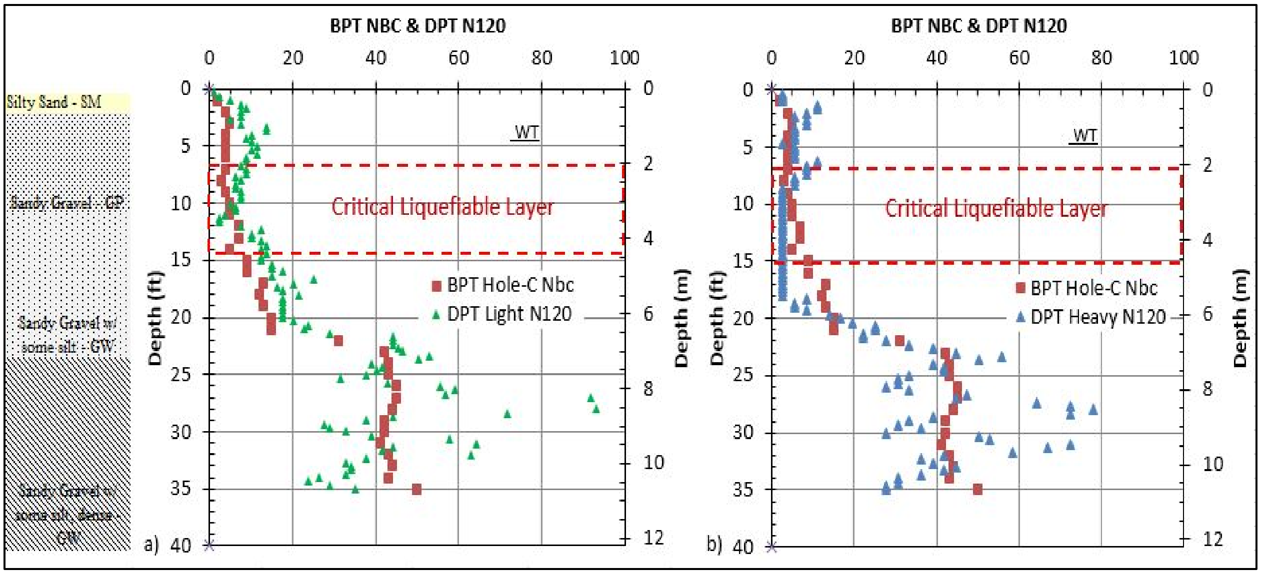

Figure 5-13. Plots of DPT N_{120} versus depth using (a) light 63.6 kg (140 lb.) hammer and (b) heavy 154.4 kg (340 lb.) hammer, after energy correction to account for lower hammer energies, compared to BPT N_{BC} for Pence Ranch Hole BPc-C. BPT data from Andrus et al. (1994).

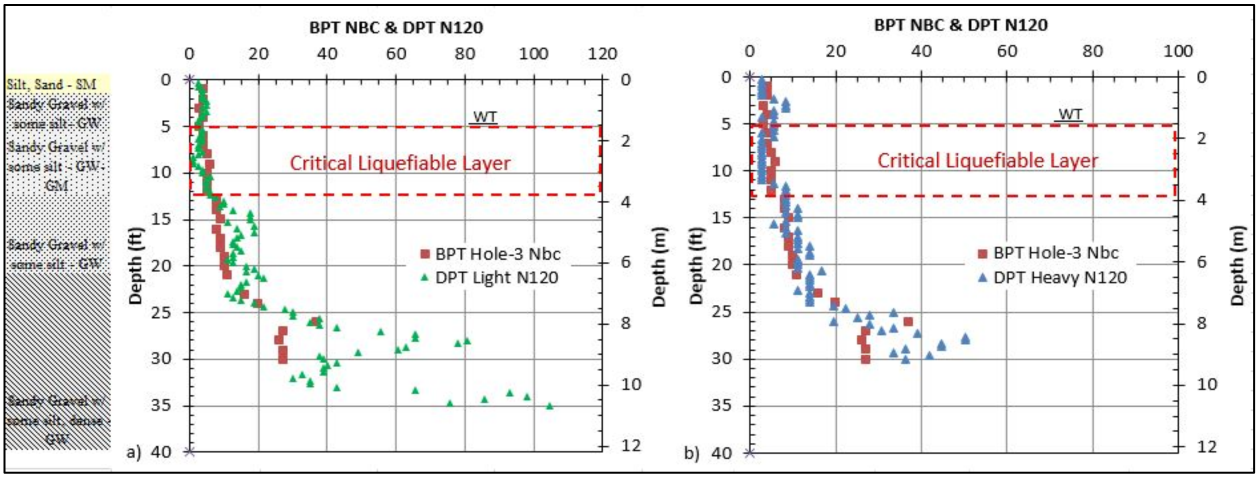

Figure 5-14. Plots of DPT N_{120} versus depth using (a) light 63.5 kg (140 lb.) hammer and (b) heavy 154.4 kg (340 lb.) hammer, after energy correction to account for lower hammer energies, compared to BPT N_{BC} for Pence Ranch Hole BPc-3. BPT data from Andrus et al. (1994).

For both hammer energies, the energy corrected DPT N_{120} value is quite consistent with the trend defined by the BPT N_{BC} value with depth. The agreement is best within the depth range from 1.5 to 7.5 m (4.9 to 24.6 ft.) and when BPT N_{60} is less than about 20. However, at shallower depths, the DPT soundings near BPc-A and BPc-B appear to identify a denser layer within the top 1.5 m (4.9 ft.) of the profile than observed in the BPT testing. This could be a result of compaction associated with construction of the foundations for the new shed at the site. In addition, at depths greater than 7.5 m (24.6 ft.), where the BPT blow count began to increase significantly, the DPT N_{120} was typically less than the BPT N_{BC} for both hammer energies. This may suggest that the cone tip is somewhat more efficient in penetrating the denser gravels than the Becker hammer, although the exact reason is unknown at present. In terms of liquefaction assessment the difference may not be overly significant as the blow counts in these cases are relatively high and liquefaction would not be predicted with either in-situ test. It should be noted that the triggering curve for the DPT curves upward at a lower blow count than for the SPT based method so differences at higher blow counts should be expected.

A comparison of the N_{120} blow counts obtained from the two different hammer energies after energy correction is provided in Figure 5-15 for each DPT sounding. The data points generally fall within a reasonable range of the 1:1 line. Results from additional testing will be necessary to define the error bands and to determine if adjustments in the energy correction factor may be necessary for depth or gravel particle size. For sites BPc-A and BPc-3 the light hammer test became inclined beyond 5° from vertical when impacting gravel particles which led to artificially high blowcounts relative to the DPT sounding with the heavy hammer (similar for all tests). For inclined rod, increased friction on the rod reduces the energy delivered to the cone tip and artificially increases the blowcount. In contrast, for site BPc-B and BPc-C the DPT's remained vertical for both soundings and the Blowcounts are relatively consistent after correction for hammer energy. These results highlight the importance of maintaining a vertical rod. When the DPT rods get more than about 5° from vertical, the DPT cone should be withdrawn and the test repeated.

5.8 CSR vs. DPT N'_{120}

Liquefaction potential was evaluated using both the DPT and BPT methods of analysis. In the case of the BPT, the N_{BC} value was converted to the equivalent sand SPT N_{60} using the Harder et al. (1986) correlation approach. The SPT N_{60} value was then corrected for overburden pressure effects using the equation proposed by Youd et al. (2001). The cyclic stress ratio, or CSR, was computed using equation 2-2 which was originally developed by Seed et al. (1971), where a_{max} is the peak ground acceleration of 0.39g. The CSR was adjusted for the Borah Peak earthquake using the magnitude scaling factor in equation 2-3.

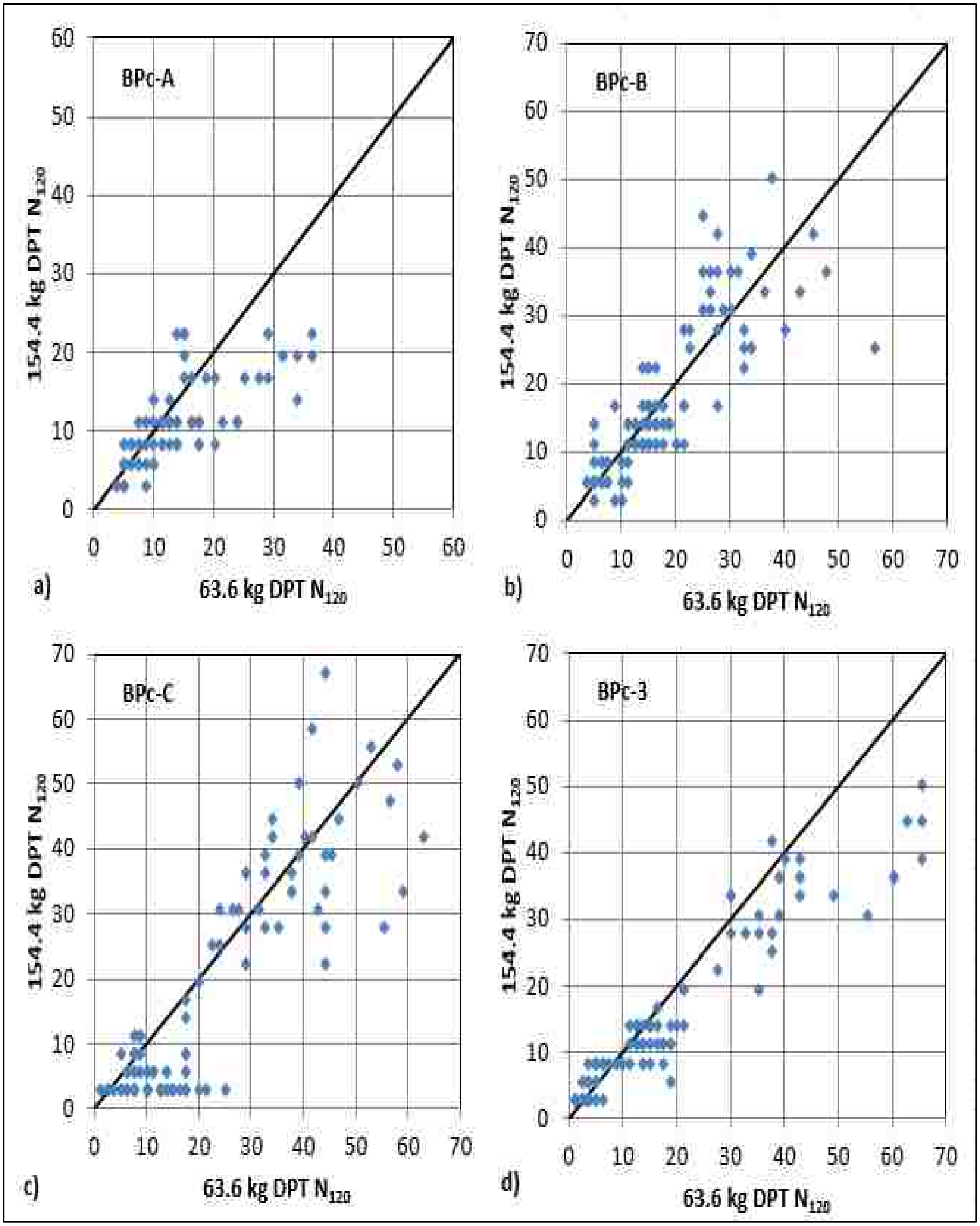

Figure 5-15. Comparison of DPT N_{120} obtained using the 63.6 kg (140 lb.) and the 154.4 kg (340 lb.) hammers after energy correction, for Pence Ranch a) Hole BPc-A, b) Hole BPc-B, c) Hole BPc-C, and d) Hole BPc-3.

The cyclic stress ratio, CSR, is plotted as a function of DPT-based N'_{120} for the zone between 1.5 and 4 m (4.9 and 13.1 ft.) below the ground surface for all four Becker holes at Pence Ranch in Figures 5-16 through 5-19. The adjusted triggering curve for the M_w6.9 Borah Peak earthquake is also plotted for comparison. Solid dots indicate liquefaction and open dots indicate a layer that had no liquefaction.

The cyclic stress ratio, CSR, is summarized as a function of BPT-based $(N_1)_{60}$ for the zone between 1.5 and 4 m (4.9 and 13.1 ft.) below the ground surface in Figure 5-20 a). The adjusted triggering curve for the M_w6.9 Borah Peak earthquake is also plotted in Figure 5-20 for comparison.

In the case of the DPT, the N_{120} value was first converted to N'_{120} using equation 2-1. Then the average CSR was plotted as function of N'_{120} within the zone of liquefaction from 1.5 to 4 m (4.9 to 13.1 ft.) in Figure 5-20 b). The liquefaction triggering curve was based on the 30% probability curve develop by Cao et al. (2013) shown in Figure 2-2. The data pairs in Figure 5-20 b) were adjusted downward using the magnitude scaling factor to account for the lower magnitude of the Borah Peak earthquake (M_w6.9) earthquake relative to the M_w7.5 DPT liquefaction curve developed from the Wenchuan China earthquake.

All the CSR values are high enough to produce liquefaction for the range of N'_{120} values within the susceptible layer. N'_{120} values in the layer range from 4 to 12, but are more typically between 6 and 10. Liquefaction factors-of-safety range from 0.18 to 0.45.

The CSR-DPT pairs for each hole at Pence Ranch were averaged to obtain a single point that represents the entire data *set*, and plotted in Figure 5-21, in comparison with the triggering curve for 30% probability of liquefaction.

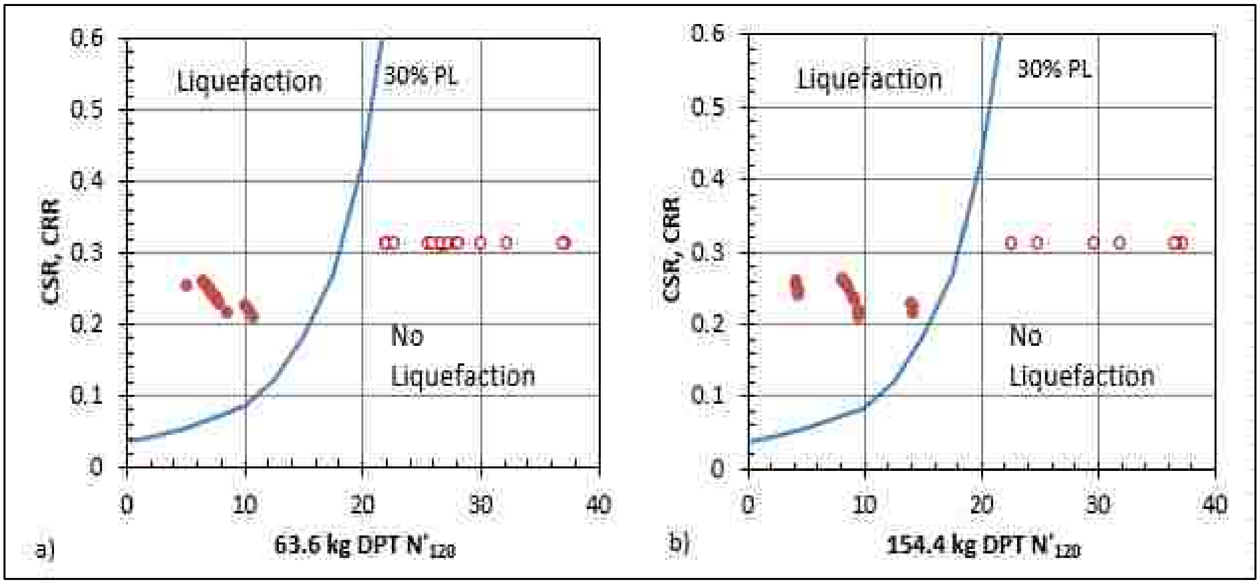

Figure 5-16. Comparison of CSR vs DPT N'$_{120}$, using a) the 63.6 kg (140 lb.) hammer and b) the 154.4 kg (340 lb.) hammer, for Pence Ranch Hole BPc-A. Solid dots are from the liquefiable unit (Unit C) and open dots are from the non-liquefiable unit (Unit E).

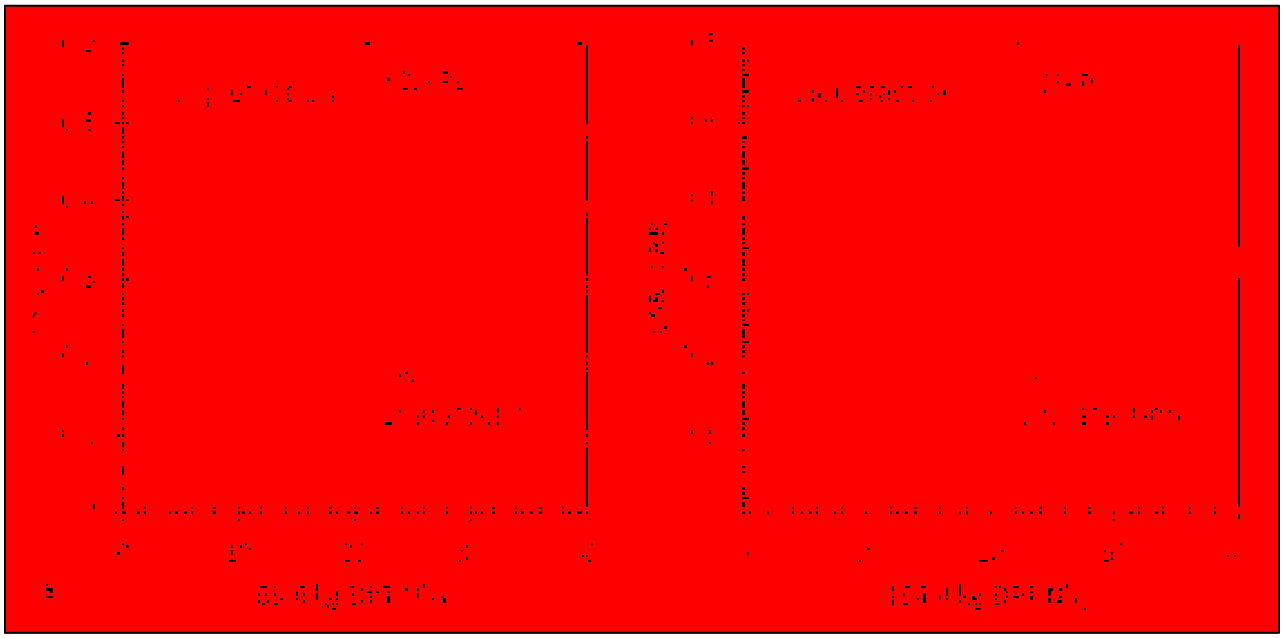

Figure 5-17. Comparison of CSR vs DPT N'$_{120}$, using a) the 63.6 kg (140 lb.) hammer, and b) the 154.4 kg (340 lb.) hammer, for Pence Ranch Hole BPc-B. Solid dots are from the liquefiable unit (Unit C) and open dots are from the non-liquefiable unit (Unit E).

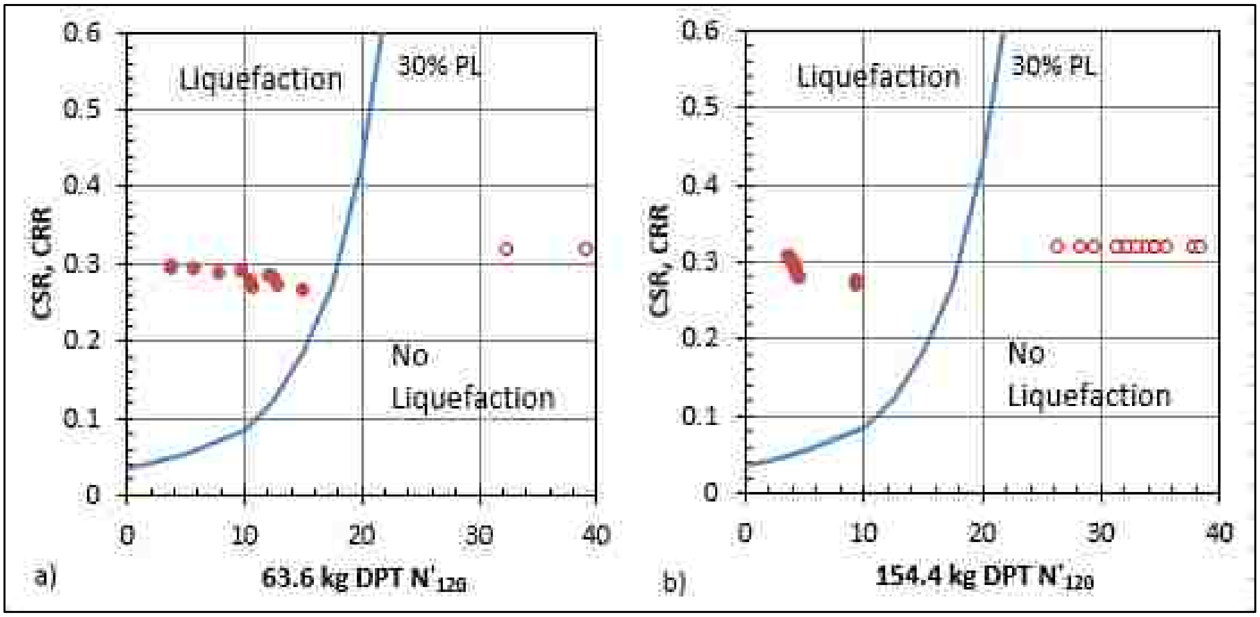

Figure 5-18. Comparison of CSR vs DPT N'120, using a) the 63.6 kg (140 lb.) hammer, and b) the 154.4 kg (340 lb.) hammer, for Pence Ranch Hole BPc-C. Solid dots are from the liquefiable unit (Unit C) and open dots are from the non-liquefiable unit (Unit E).

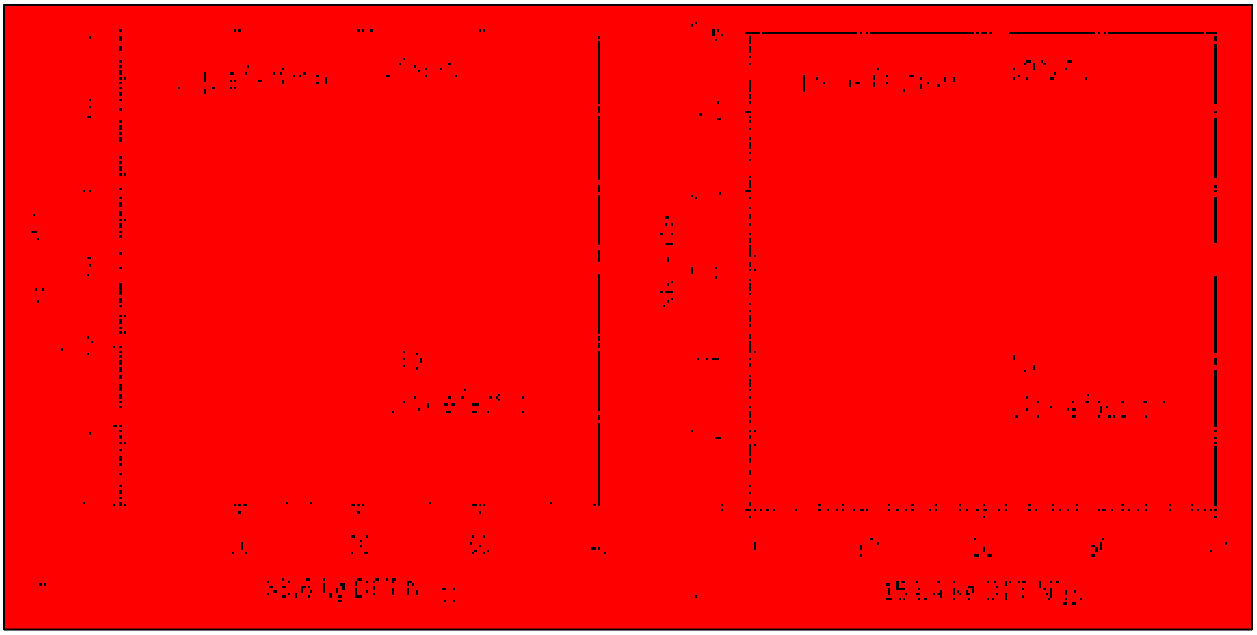

Figure 5-19. Comparison of CSR vs DPT N'120, using a) the 63.6 kg (140 lb.) hammer, and b) the 154.4 kg (340 lb.) hammer, for Pence Ranch Hole BPc-3. Solid dots are from the liquefiable unit (Unit C) and open dots are from the non-liquefiable unit (Unit E).

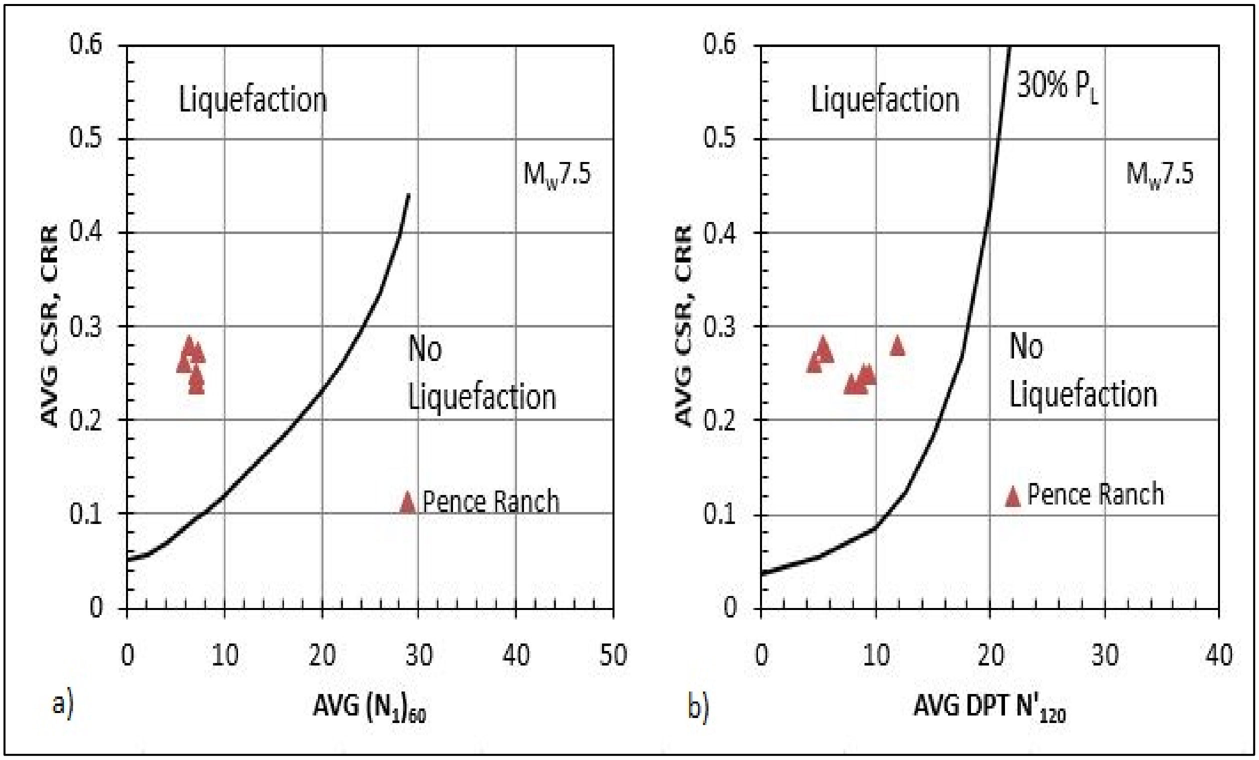

Figure 5-20. Comparison of a) CSR vs BPT-based $(N_1)_{60}$ data points for Pence Ranch in comparison with triggering curve, and b) CSR vs. DPT N'_{120}, data points for Pence Ranch in comparison with triggering curve for 30% probability of liquefaction (Cao et al. 2013) for M_w7.5 earthquakes.

The CSR-DPT N'_{120} points from Figure 5-20 b) are plotted in Figure 5-22 in comparison with the probabilistic liquefaction triggering curves (Cao et al. 2013), after magnitude scaling adjustments which shifted the measured CSR values slightly downward. In all cases the data pairs plot above the 50% probability of liquefaction curve which is consistent with the observed liquefaction at both sites. In Figure 5-23, a single data point is shown that represents the DPT N'_{120} data set, as compared to the liquefaction triggering curve.

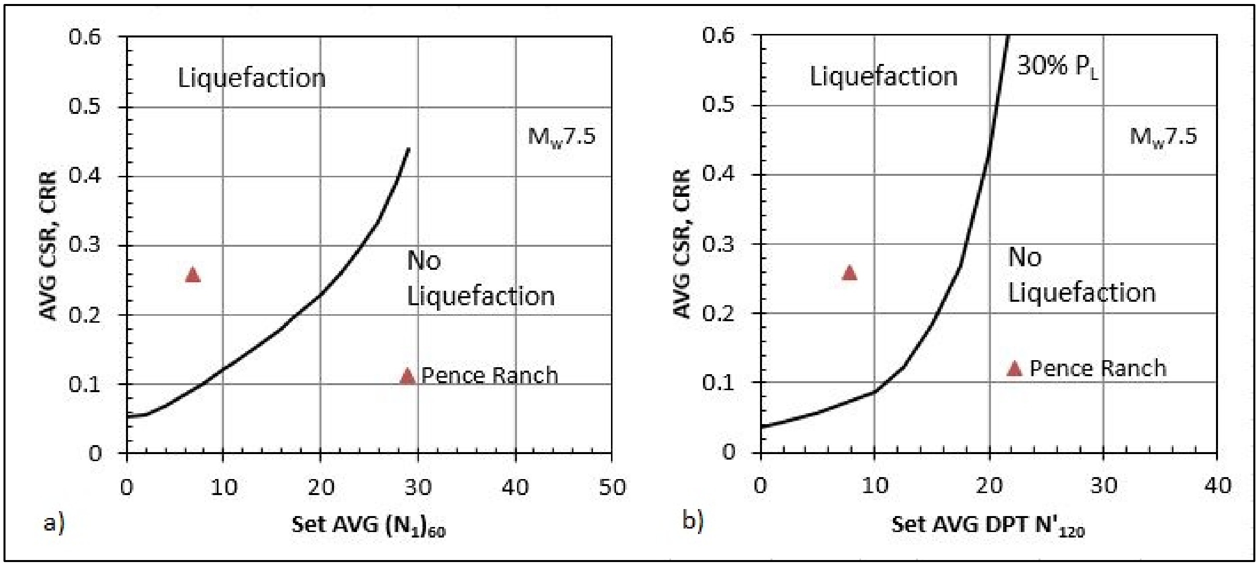

Figure 5-21. Comparison of the set average (Figure 5-21) for a) CSR vs BPT-based $(N_1)_{60}$ data points for Pence Ranch in comparison with triggering curve, and b) CSR vs. DPT N'$_{120}$, data points for Pence Ranch in comparison with triggering curve for 30% probability of liquefaction (Cao et al. 2013) for M_w7.5 earthquakes.

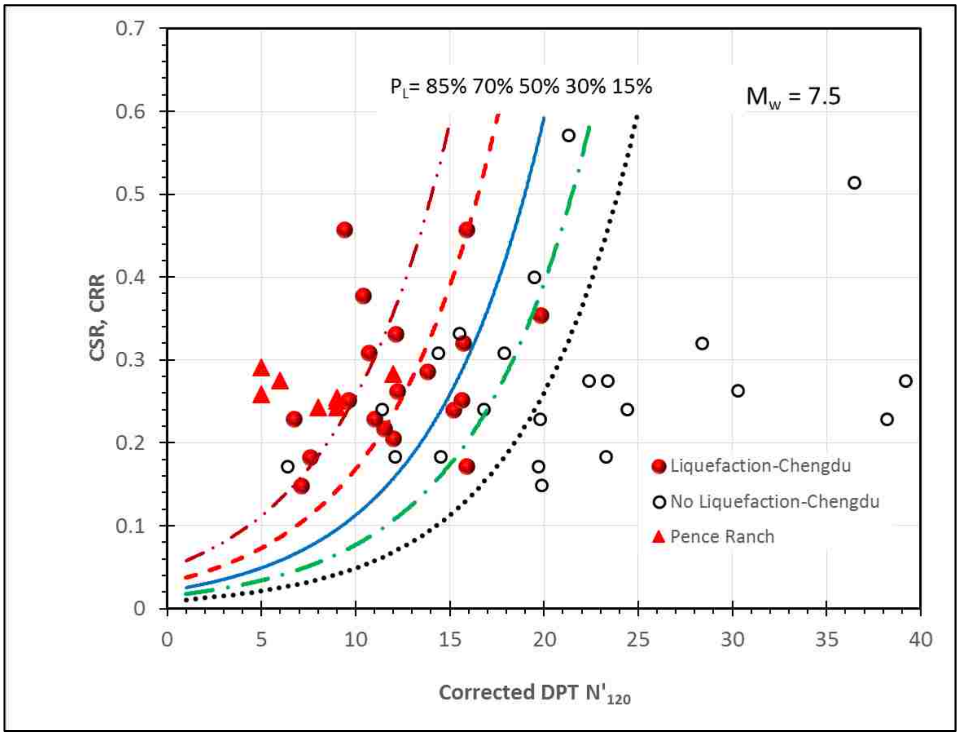

Figure 5-22. CSR vs. DPT N'$_{120}$ curves for various probabilities of liquefaction in gravelly soils developed by Cao et al. (2013) along with liquefaction/no liquefaction data points from Chengdu Plain. Points from Pence Ranch, Figure 5-22 b) are shown.

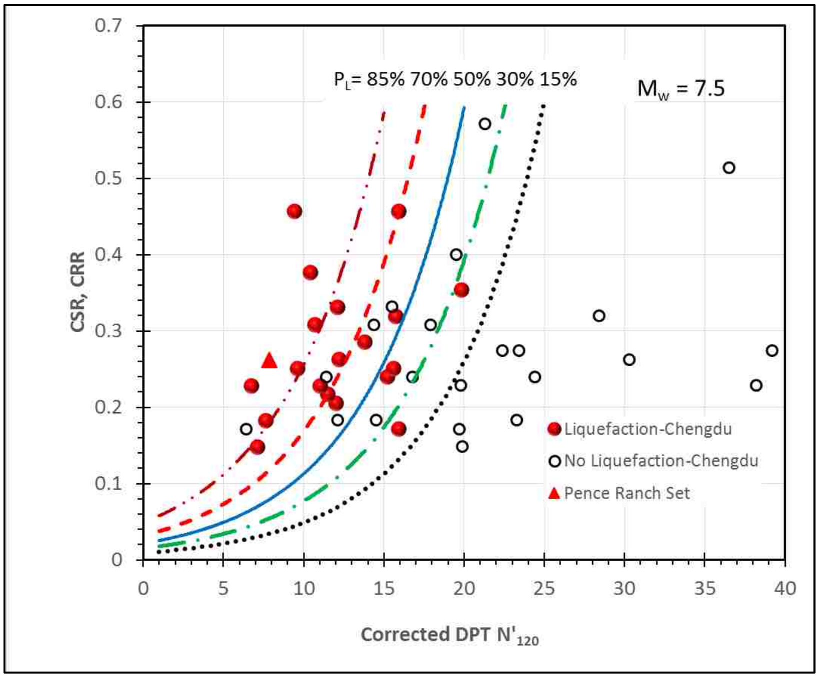

Figure 5-23. CSR vs. DPT N'$_{120}$ curves for various probabilities of liquefaction in gravelly soils developed by Cao et al. (2013) along with liquefaction/no liquefaction data points from Chengdu Plain. Set point from Pence Ranch, Figure 5-23 is shown.

5.9 DPT vs. SPT

Another indicator of the results of the study is the comparison of the DPT results with previous SPT results. Figures 5-24 through 5-26 show the correlation between the SPT N_{60} and the DPT N_{120} at Pence Ranch.

The 2016 DPT combined for heavy and light hammers was plotted against the 1990 SPT N_{60} data to gain a better understanding of the correlation between the DPT soundings accomplished at the site and the previous SPT soundings. As can be seen from Figure 5-27 there is reasonable correlation between the two. Even though the R^2 value is 0.58, indicating a fairly weak correlation (R^2=1.0 is a perfect fit), the value associated with x in the correlation equation is the slope of the regression line and should be close to 1.0 for good correlation. 0.80 is reasonably good.

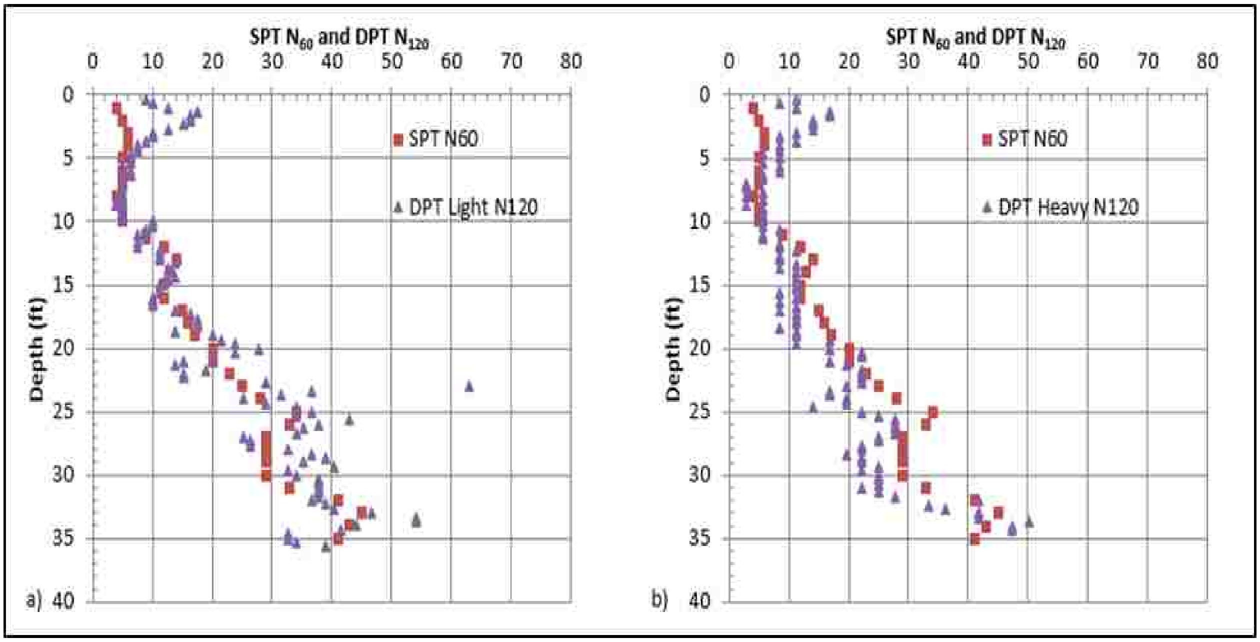

Figure 5-24. Correlation of DPT N_{120} and 1990 SPT N_{60} for Hole number BPc-A given a) the light 63.6 kg (140 lb.) hammer and b) the heavy 154.4 kg (340 lb.) hammer at Pence Ranch.

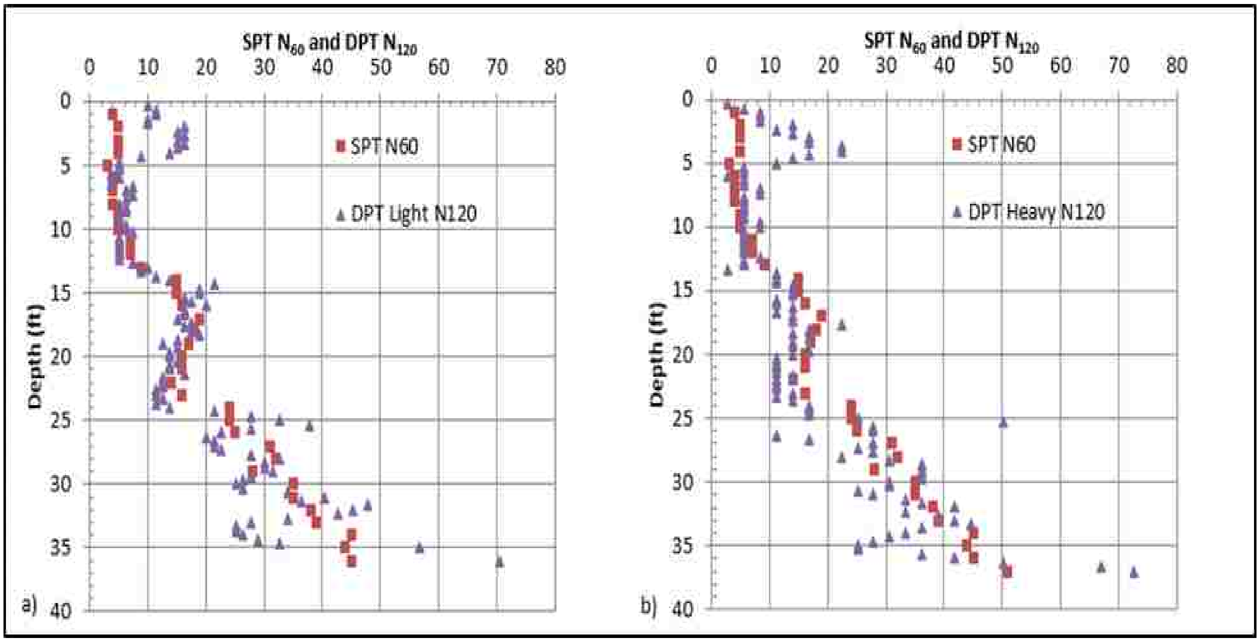

Figure 5-25. Correlation of DPT N_{120} and 1990 SPT N_{60} for Hole number BPc-B given a) the light 63.6 kg (140 lb.) hammer and b) the heavy 154.4 kg (340 lb.) hammer at Pence Ranch.

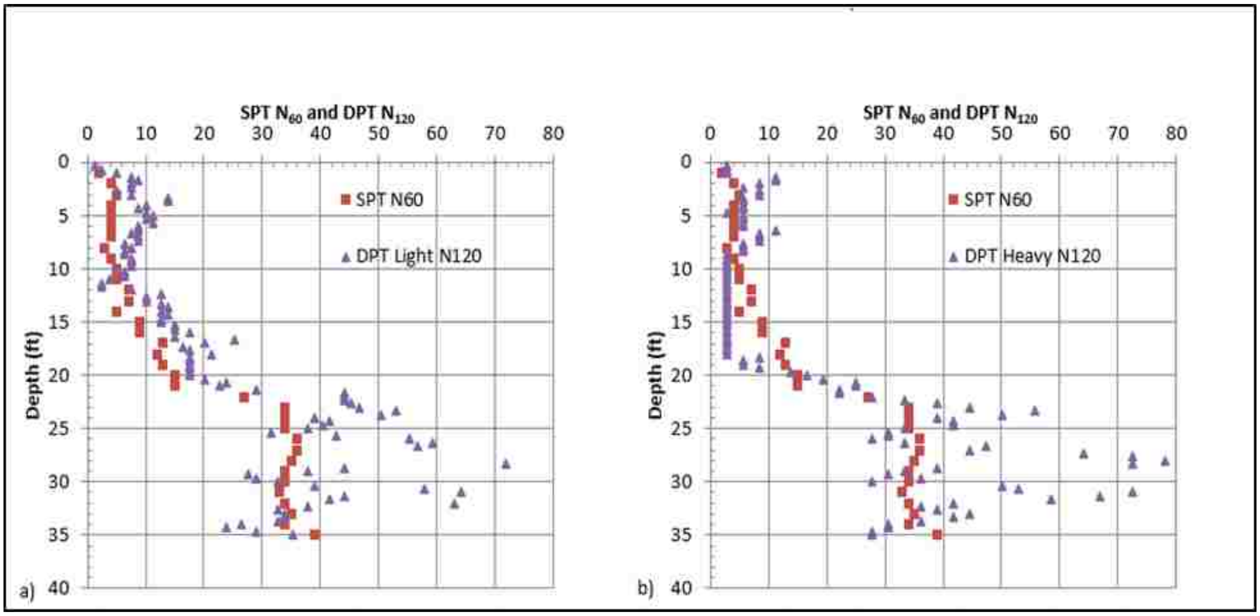

Figure 5-26. Correlation of DPT N_{120} and 1990 SPT N_{60} for Hole number BPc-C given a) the light 63.6 kg (140 lb.) hammer and b) the heavy 154.4 kg (340 lb.) hammer at Pence Ranch.

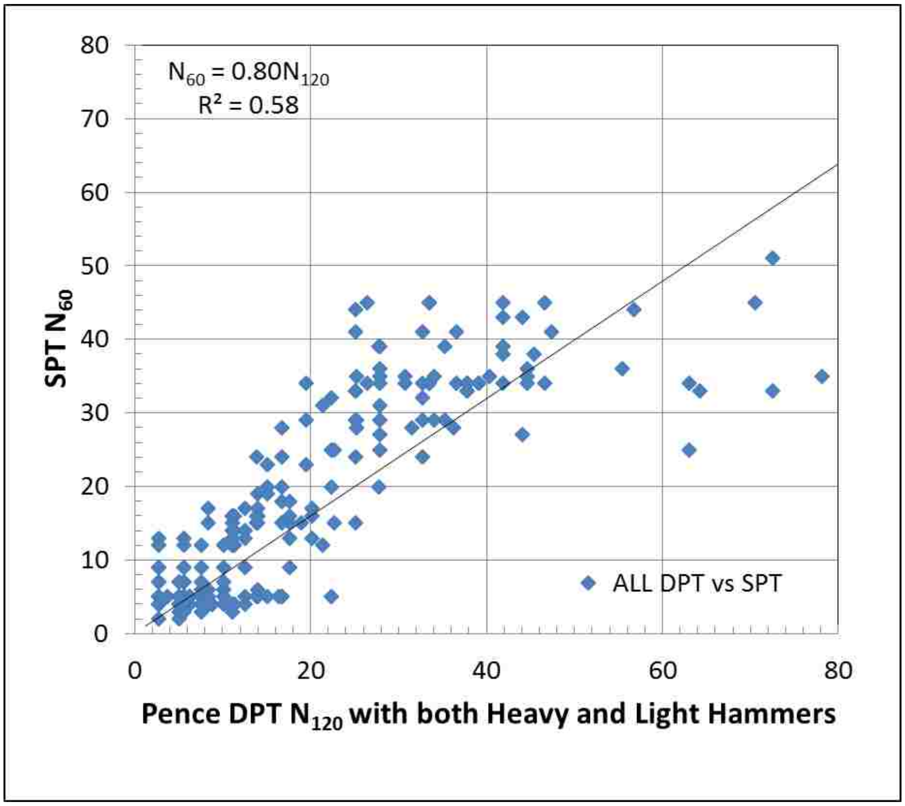

Figure 5-27. Plot comparing the 2016 DPT N_{120} vs. 1990 SPT N_{60} for all holes at Pence Ranch using both the 63.6 kg (140 lb.) hammer, and the 154.4 kg (340 lb.) hammer.

5.10 Probability of Liquefaction vs. Depth from DPT

The probability of liquefaction P_L was calculated and plotted for all DPT holes at Pence Ranch and is shown in Figure 5-28 below. Equation 5-2 (Cao et al. 2013), is referred to as the probability function for liquefaction.

$$P_L = 1/\left(1+ \exp\left(- [8.4 - 0.35N'_{120} + 2.12\mathrm{Ln}\,(CSR)]\right)\right) \qquad 5\text{-}2$$

Cao et al. (2013) validated this equation using data from the Wenchuan event where 15 of 19 sites with surface liquefaction effects (79%) plotted on or above the P_L=50% curve of Figure 2-8, and 17 of 19 (89%) liquefaction sites plot on or above the P_L=30% curve. Similarly, 23 of 28 (82%) of sites exhibiting no surface liquefaction effects plot on or below the P_L=50% curve and 26 of 28 (93%) non-liquefaction sites plot on or below the P_L=70% curve. He states that this correlation is therefore generally verifiable for gravelly soils in the Chengdu plain shaken by the 2008 Wenchuan earthquake, and that this relationship may be used for other sites underlain by gravelly soils with soil types similar to those that liquefied during the Wenchaun quake.

It can be clearly seen that the probability of liquefaction corresponds closely with the calculated critical zone of liquefaction, 1.5 to 4 m (4.9 to 13.1 ft.) in Hole-A, where a number close to 1.0 would indicate liquefaction and a number such as 0.50 or 0.30, diminishing downward from 1.0, would indicate less susceptibility to liquefaction. Hole-B corresponds well with the calculated critical liquefaction zone between 1.5 and 3.7 m (5 and 12 ft.). Hole-C corresponds reasonably well with the calculated critical zone of 1.8 to 4.6 m (6 to 15 ft.). At Hole-3 also corresponds reasonably well with the calculated critical liquefaction zone between 1.5 and 4.0 m (5 and 13 ft.).

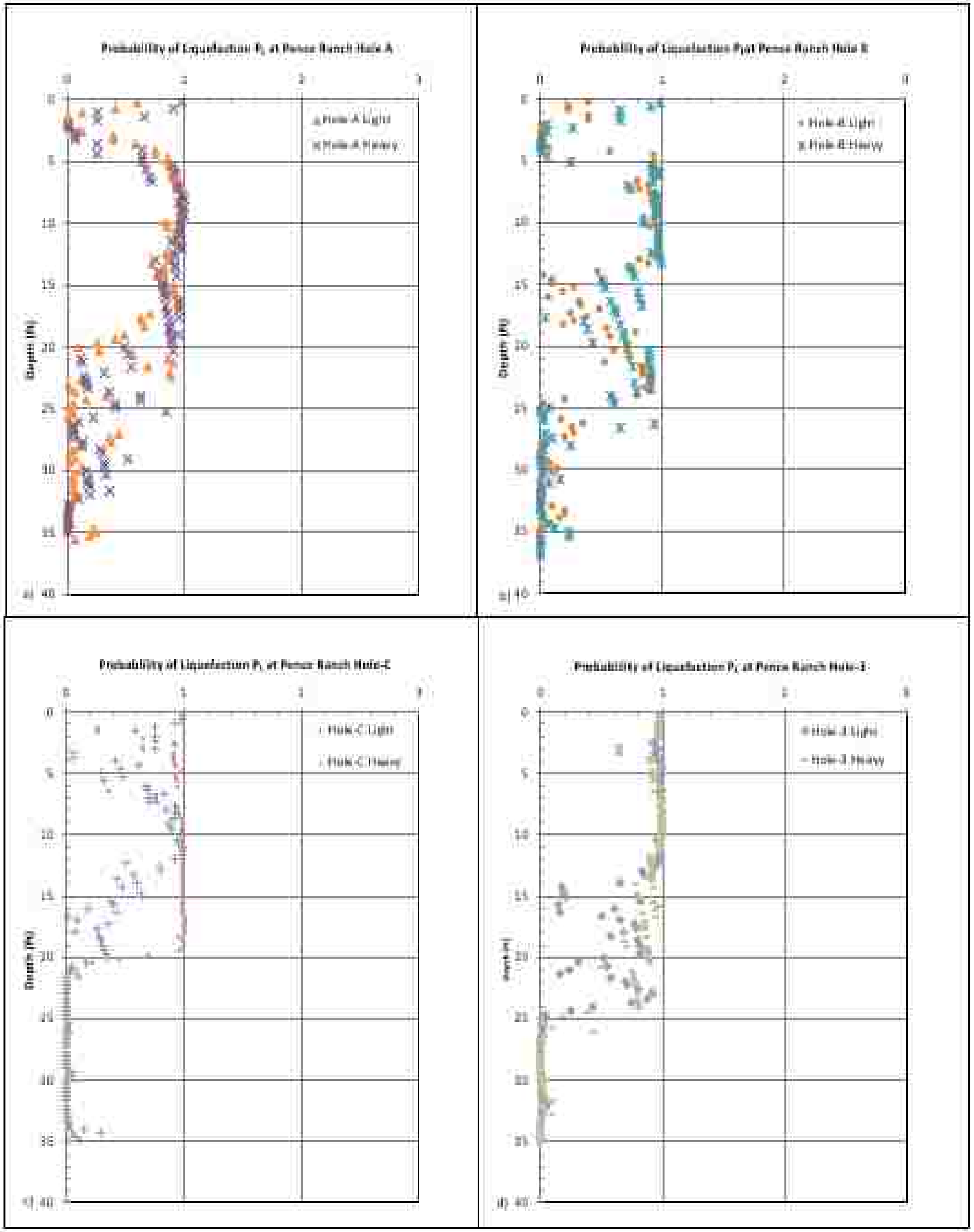

Figure 5-28. Probability of Liquefaction, P_L, for all holes at Pence Ranch, vs. Depth, from DPT soundings. A) Hole-A, b) Hole-B, c) Hole-C, and d) Hole-3.

6 DPT TESTING AT WHISKEY SPRINGS, IDAHO AND LIQUEFACTION ASSESSMENT

6.1 Introduction

Whiskey Springs is located about 25.7 km (16 mi.) north of Mackay near the Thousand Springs Creek in central Idaho (latitude 44.0851º, longitude -113.8412º) along Highway 93. Peak ground acceleration was estimated to be about 0.5g.

The Lost River, Lemhi, and Beaverhead mountains are three parallel, northwest trending ranges separated by alluvium-filled valleys that form the basin-and-range structure in central Idaho. Range-front normal faults occur along the southwest fronts of all three mountain ranges. These faults all show signs of latest Quaternary movement. Until October 28, 1983 this area had experienced little historic seismicity. The Borah Peak Earthquake reactivated the Thousand Springs segment of the Lost River Fault.

The subject mountain valleys are mostly flanked by Pleistocene alluvial-fan and glacial-outwash deposits. Holocene floodplain and older Holocene deposits are found along major drainages. Although mudflow deposits are uncommon in these gravelly fans, Holocene boulder mudflow deposits reportedly occur at the head and along the main drainage of the Elkhorn fan (Andrus et al. 1987). Figure 6-1 shows the general location with the number 3 identifying Whiskey Springs.

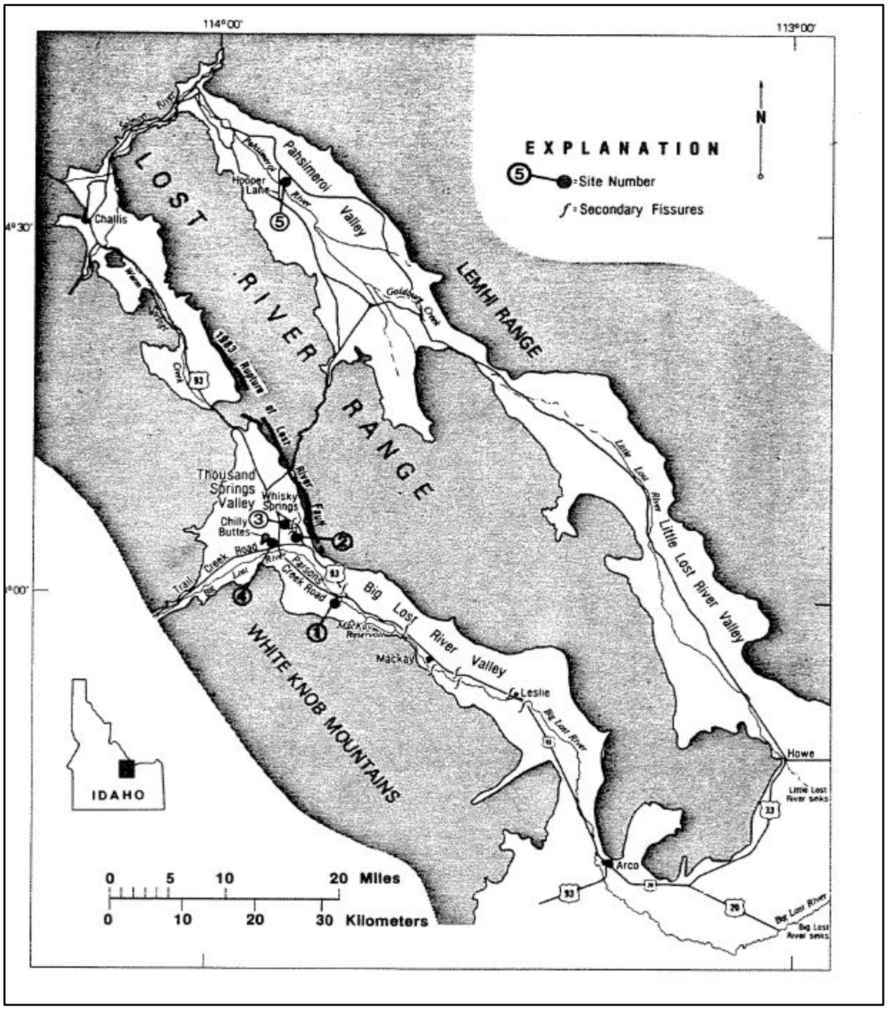

Figure 6-1. Regional map of central Idaho showing geographic features and approximate trace of fault rupture. Site number 3 is Whiskey Springs (Andrus et al. 1987).

Drainage from the mountains quickly sinks into the coarse-grained fan deposits and resurfaces through several springs into Thousand Springs Creek to the west. Flow of the creek through most of the valley is not channelized and forms a marsh. Midway between Whiskey Springs and Trail Creek Road most of the flow passes through a narrow channel. The northeast boundary of the creek along this section is formed by two alluvial fans, the Elkhorn fan, and a smaller unnamed fan. Liquefaction of subsurface sediment along and upslope from this fan-marsh interface induced lateral spreading of the distal end of the fans.

6.2 Liquefaction Effects

Shortly after the 1983 Borah Peak earthquake, Andrus et al. (1987) made a reconnaissance trip to the area, concentrating on the area between Whiskey Springs and Trail Creek Road on the east side of Thousand Spring Valley. In this area numerous occurrences of lateral spreads, ground fissures, buckled sod, and sand boils were reported.

Andrus indicated that the zone of lateral spreading in the Thousand Springs Valley was 2.1 km (1.3 mi.) long and 75m (250 ft.) wide. Large parallel fissures and cracks were concentrated at the head of the spread, but smaller fissures were seen throughout the zone. Lateral Soil at the toe of the spread caused the ground to buckle into ridges as high as 1.2 m (4 ft.). Sand boils erupted at several locations along cracks on the lower half of the failure zone. Maximum lateral movement was estimated to be 0.8 m to 1.0 m (2.6 ft. to 3.3 ft.).

Movement along the lateral spread was reported as primarily horizontal, as indicated by extensional displacement with little vertical separation across fissures at the head of the failure, compressional buckling of sod with little or no uplift of the toe, and horizontal displacement with about 3 ft. of offset along Highway 93. Figures 6-2 to 6-4 below show some of the effects of the lateral spread.

Liquefaction effects shown on the map in Figure 6-5, include major fissures, areas of buckled sod, and sand boils. Site conditions in 2015 are shown in Figure 6-6.

6.3 Soil Description

In their 1987 report on the subsurface investigations at this site Andrus and Youd reported the following:

"The Whiskey Springs site lies on the distal end of an alluvial fan that is covered by a thin mantle of reworked loess (loess that has been carried by flowing water and redeposited in another locality). Beneath this mantle lies a thick complex sequence of interbedded sandy silts and cobbley gravels." A generalized soil profile is shown on Figure 6-9 with DPT test sites indicated.

Figure 6-2. Photograph showing buckled and overturned sod at the toe of the lateral spread along Highway 93 at the 1985 Whiskey Springs investigation site (Youd et al. 1985).

Figure 6-3. Photograph showing lateral displacement of Highway 93 near the 1985 Whiskey Springs investigation site (Youd et al. 1985).

Figure 6-4. Aerial photograph showing the 1985 Whiskey Springs investigation site and lateral spread effects, left to right in this view is east to west (Andrus et al. 1987).

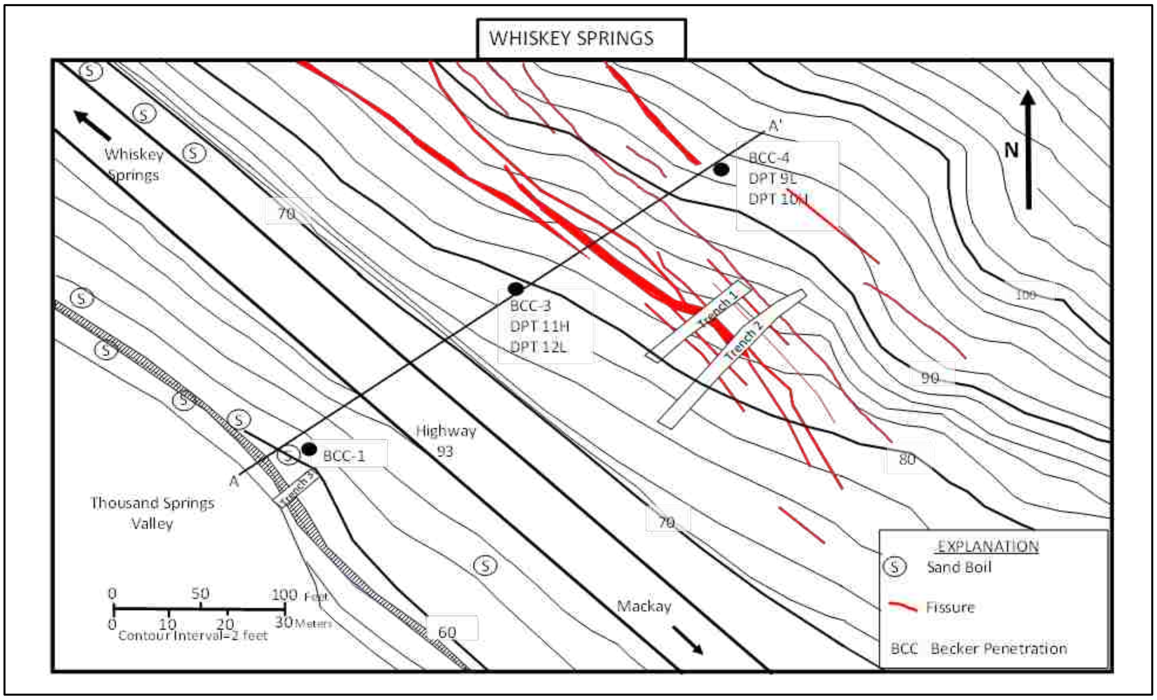

Figure 6-5. Plan view drawing of the 1985 site showing location of closed-end Becker Penetration tests (BCC-4, BCC-3, and BCC-1). Simplified from Andrus et al. (1987).

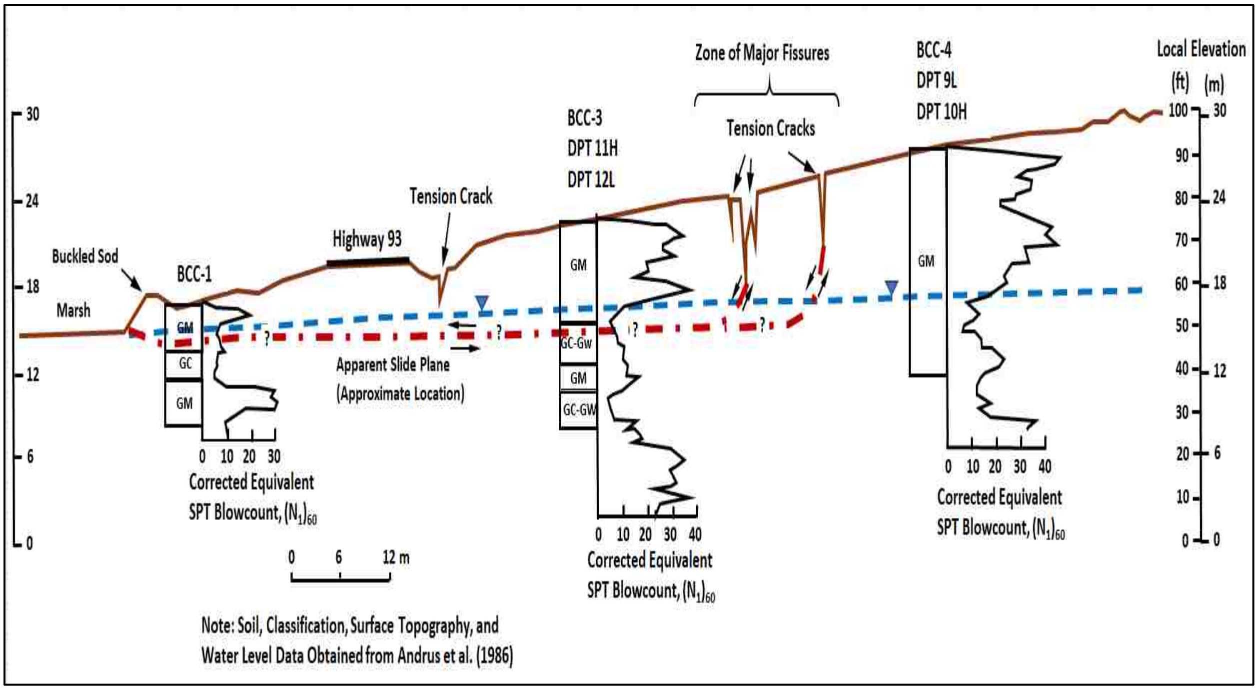

Figure 6-6. Plot showing a generalized cross section showing sediment layers beneath the Whiskey Springs site. Simplified from Andrus et al. (1987).

Figure 6-7. Photograph showing site conditions at Whiskey Springs in 2015 near BC3, looking southwest. Highway 93 can be seen in the background.

In 1985, trenches were excavated across major zones of fissures that developed at the head of the lateral spread and across the buckled sod that developed at the toe of the failure. These trenches are documented in the 1987 report (Andrus et al. 1987).

The excavated trench sediments were divided into an upper matrix-rich sequence, units A2 through A3c, and a lower relatively matrix-poor gravel, unit A4. The term matrix was used to describe the sand, silt, and clay fraction of gravelly sediment. In general these sediment units were poorly sorted and have gap-graded grain-size distributions. Gravel and cobbles were either suspended in the matrix (matrix-supported) or were in contact with each other (clast-supported). Clast-supported fabrics are mostly filled with matrix. Stratification was poorly defined and generally dipped down fan. Distinct beds within units were usually better sorted than overlying and underlying material. However, these beds were generally lenticular, discontinuous, and displayed progressive changes in particle size within a sediment layer. Individual beds were presumably formed by a single episode of deposition (Bull 1972).

Only the north end of trench 2 was mapped in detail. As in trench 1, the surficial material is a mantle of dark brown loess, unit A1. Directly below unit A1 lies a fairly thick, 0 to 0.4 m (0 to 1.3 ft.) very loose brown silty gravel, unit A2a. This unit is not apparent in trench 1. Unit A2a overlies a clast-supported gravelly sediment that appears to correlate with unit A2b in trench 1. This correlation is based on the fact that unit A2b is a nearly horizontal lying, apparently un-bedded clast-supported gravel with stage I to II carbonate development, and overlies a nearly horizontal matrix-supported gravel.

Gravel and cobble clasts in these sediments are mostly quartzite with lesser amounts of limestone and dolomite. Minor amounts of sandstone and volcanic clasts are also present. Based on the angularity of the clasts and the presence of nearby outcrops of quartzite (Ross 1947), these gravels apparently were transported no more than a few kilometers.

Since deposition of the trenched sediments, a soil profile has formed near the present ground surface. This profile consists of 1) an organic horizon 0.1 to 0.4 m (0.3 to 1.3 ft.) thick, that is generally confined to unit A1, 2) a thin (generally less than 10 cm (0.3 ft.) thick, weak reddish brown, and 3) a stage I to II calcic horizon. This calcic horizon was formed by surface water infiltrating into the upper soil surface, then evaporating before it reached the ground water table. This process caused calcium carbonate (caliche) and other soluble minerals to accumulate in the zone of evaporation. The thickness of the calcic horizon is highly variable, depending on the permeability of the upper sediment layers and the erosional processes reworking these sediments. In very permeable material, the calcic horizon is as thick as 1.5 m (5 ft.), but strongest development is generally confined to a thickness of 0.5 m (1.6 ft.).

A soil profile similar to the profiles in trenches 1 and 2 was found in trench 3 located near the marsh. Near the marsh, unit A1 is much thicker, 0.4 to 0.7 m (1.3 to 2.4 ft.) and much more humic than unit A1 exposed in the upland trenches. Unit A1 overlies a thin, 5 cm (0.16 ft.) thick reddish brown horizon and a 1.5 m (4.9 ft.) thick stage I to II calcic horizon that has formed in a gravelly sediment. This soil profile suggests that the fan surface near the marsh and at the head of the lateral spread have existed for a similar period of time.

The trenching investigations revealed interbedded fine- and coarse-grained sediments of probable latest Pleistocene age (10,000 to 15,000 years) 4.6 m (15 ft.) beneath the Whiskey Springs site. The very gravelly sediments are characteristic of braided channels and bars deposited by high-energy flows, whereas the finer-grained matrix supported gravels indicate fluctuations in flow conditions to lower energy flows.

Figure 6-7 is a generalized cross section showing sediment layers beneath the Whiskey Springs site. The sediment units A through E are delineated on the basis of penetration resistance and sample classification. Nearly all of the sediment is poorly sorted, gap-graded, sub-angular gravel. Units A and C generally have greater percentages of fines than units B, D, and E.

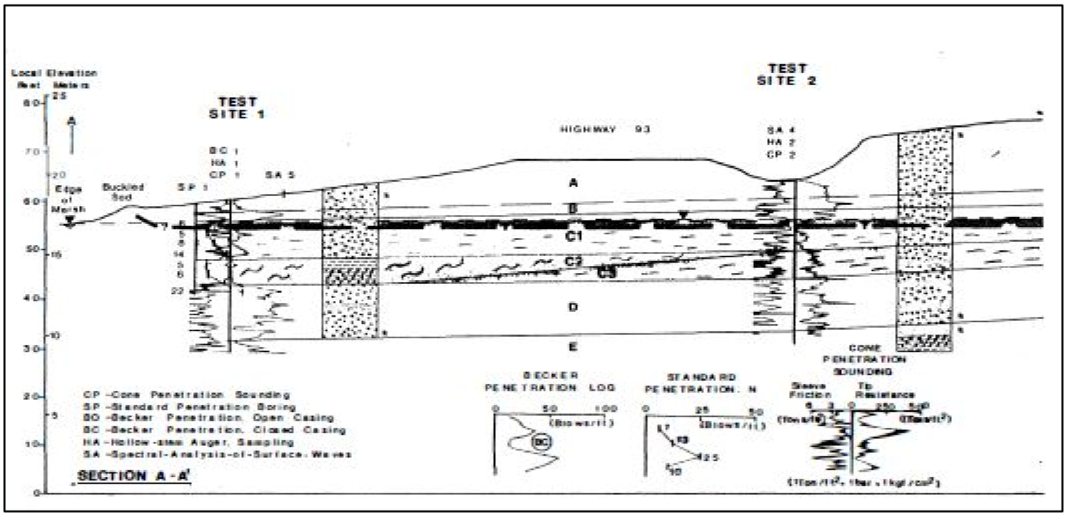

Figure 6-8. Cross section of the lateral spread near Whiskey Springs showing SPT, CPT, BPT penetration data, and stratigraphic logs. A heavy line delineated the most likely position of the failure zone (Andrus et al. 1987).

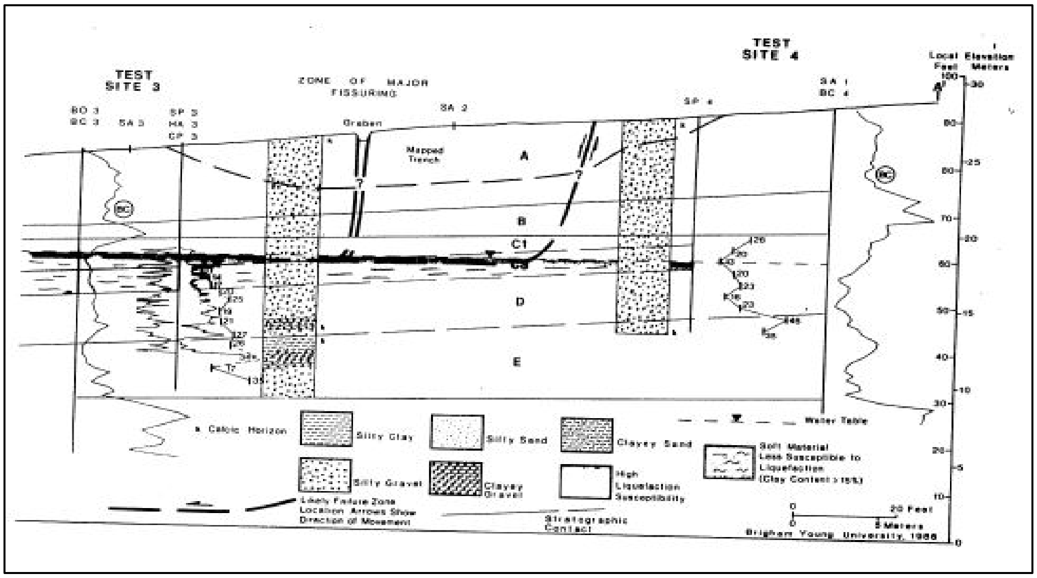

Figure 6-8. Continued.

The area is capped by a dense to very dense silty gravel (sediment units A and B). At the top of unit A, a calcic soil horizon has formed. Unit A thins downslope from 5.5 m (18 ft.) at test site 4 to 0.8 m (2.5 ft.) at test site 1. Unit B is characterized by a BPT penetration resistance about twice as high as in unit A. Unit B thins from 3 m (10 ft.) at test site 4 to 0.6 m (2 ft.) at test site 1. A looser and finer-grained gravelly sediment, unit C, lies below unit B.

Unit C has been subdivided into three subunits, Cl, C2, and C3, based on clay content and cone penetration resistance. All the samples recovered from unit Cl classified as silty gravel (GM) with an appreciable sand content. Unit Cl thickens downslope from 1.2 m (4 ft.), at test site 4, to over 2 m (7 ft.), at test site 1. The lower half of unit Cl appears to be coarser. N-values for unit Cl range between 5 and 14; CPT tip resistances range from 1 to 120 kgf/cm^2 (15 cm^2 cone; kilogram force per square centimeter); and BDT blow counts are 4 to 9 blows/foot (0.3 m). Below Cl, at test site 1, is a silty clay to clayey gravel, unit C2. Unit C2 is 1.8 m (6 ft.) thick at test site 1 but thins rapidly with distance upslope and is not detectable across the road at test site 2. Unit C2 is distinguished by a high clay content (14 to 22 percent finer than 0.005 mm), a liquid limit from 25 to 26 percent, low CPT tip resistances of 2 to 52 kgf/cm^2, and sleeve resistances, 0.1 to 1 kgf/cm^2. It was reported that in a piston sample taken at site 1 from units Cl and C2 the material had a moisture content of 15 to 16 percent (the piston sampler was pushed 61 cm (24 in.) and a 7-cm-long (2.75 in.) sample was recovered). Unit C2 has N-values of 5 and 6, and BDT blow counts from 4 to 6 blows/foot (0.3 m).

From the reported work, Unit C3 was not detected in CPTlb, but was detected 15 m (50 ft.) to the southeast in CPTla. This unit is more than 1.5 m (5 ft.) thick at the other test sites. For unit C3, N-values range from 11 to 14; CPT tip resistance varies from 100 to 175 kgf/cm^2; and BDT blow counts range from 9 to 13 blows/foot (0.3 m). Split-spoon samples from units Cl, C3, and D at test sites 3 and 4 have similar grain-size distributions and the boundaries are drawn based on N-values.

Unit D, lying below unit C, is approximately 3.4 m (11 ft.) thick and consists of interbedded silty gravels with sand. The upper half of the layer is generally denser than the lower half. N-values range from 17 to 27; CPT tip resistance varies from 100 to 300 kgf/cm^2; and BDT blow counts vary from 12 to 46 blows/foot (0.3 m). Unit E, clayey silts and gravels, is characterized by a calcic horizon, lower penetration resistance, and finer material in the top half of the unit. Below unit E the material is very dense having BDT blow count over 100 blows/foot (0.3 m).

The water table in July 1985 sloped very gently toward the marsh, lying below unit B at test site 4, at elevation of 18 m (59 ft.), or about 35 feet below the ground surface, and surfacing in the marsh near test site 1, at elevation 17 m (56 ft.), or about 5 feet below the ground surface (Andrus et al. 1987).

The water table was not found at the time of the DPT testing in November 2015. A plot showing the corrected Becker penetration resistance, N_{BC}, as a function of depth is provided in Figure 6-12 for BPT hole BC3. Conclusions reached by Andrus and Youd suggest that the critical zone for liquefaction was a silty gravel layer located at or just above what was the water table (Andrus et al 1987).

6.4 Identification of Liquefiable Material

Andrus et al. (1987) also reported the following:

“Based on the sediment cross section developed for the site and relative penetration resistances, we conclude that liquefaction and shear deformation occurred in the loose silty gravel in unit C1. A comparison of grain-size distributions between sand boil material and samples from unit C1 also support this conclusion. Figure 6-8 gives distributions for two samples from sand boil deposits (Youd et al. 1985) and representative samples from units C1 and C2. Samples 1 and 2 were collected from sand boils along the fence near test site 1.”

Curves 3 and 5 are from samples taken from drill hole SP1. Curve 3 indicates that unknit C1 is much coarser than both sand boil samples. On the other hand, curve 5, from unit C2, closely parallels one of the sand boil curves. Because sand boil deposits are formed from sediment transported by water flowing upward through fissures above the liquefied layer, coarse particles tend to segregate out. Therefore, a better comparison would be between the sand boil samples and the portion of the drill hole samples less than 2 mm (0.08 in.). Grain-size curves 4 and 6 show the distribution of material finer than 2 mm (0.08 in.) for the samples used for curves 3 and 4, respectively. Curve 4 closely parallels curve 1 for sand boil sample 1; this is another indication that liquefaction occurred in unit C1. If the fraction less than 2 mm (0.08 in.) from the sample from unit C2, curve 6, and the curve for sand boil sample 2 are compared, a correlation still exists. If liquefaction occurred in unit C2, sand boil movement through the coarser material above, unit C1, could have been contaminated with the coarser material and explain the differences between curve 6 and the sand boil sample. Another explanation would be that liquefaction occurred in parts of C3, but erosion and mixing with clay occurred during upward movement of sand boil material through finer grained material.

Although these comparisons look relatively good they are not conclusive in determining the origin of the sand boil material. Material from units C3, D, and E have similarly close correlations. Had the matrix material been more variable between units, this comparison between sand boil and drill hole samples may have been more diagnostic. The low penetration resistance of unit C1 plus the match of sand boil and matrix sediment provide strong evidence that unit C1 liquefied (Andrus et al. 1987).

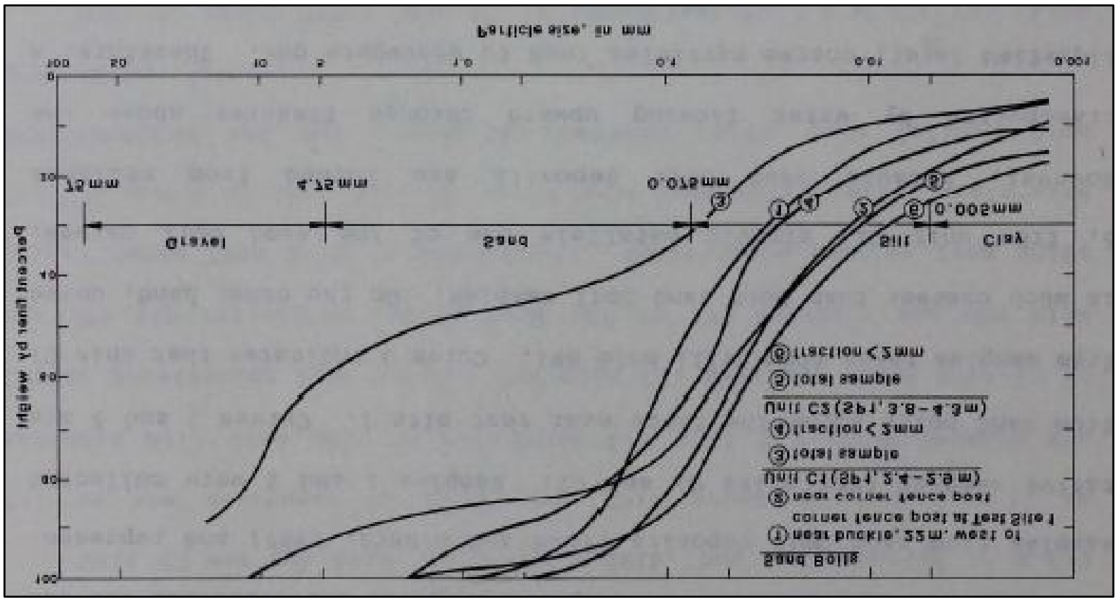

Figure 6-9. Grain-size distribution curves for samples taken from two sand boil deposits near the buckled sod at the Whiskey Springs site and representative distribution curves for two samples from drill hole samples from sediment units Ca and C2 at test site 1. To account for sediment segregation during sand boil formation, distribution curves for drill hole material finer than 2 mm are also shown. The curves for the finer fraction of the drill-hole samples (curves 4 and 5) match rather closely the curves from the sand boil samples (curves 1 and 2) (Andrus et al 1987).

6.5 Identification of Most Likely Failure Zone

The most likely failure zone passed through what is identified as Unit C1 in Figure 6-7. Near test site 1 at the toe of the hill, the previous testing, CPT, SPT, and BPT results indicated a loose liquefiable layer at a depth of 1.5-2.0 m (5-7 ft.) below the ground surface.

This corresponds to the estimated top of Unit C and is at the water table. This liquefiable zone extends down to a depth of 3.7 m (12 ft.). At test site 2 immediately to the east of highway

93. The failure zone was assumed to pass through Unit C1 at a depth between 2.4 m (8 ft.) and 4.3 m (14 ft.) below the ground surface. Here the water table was located at a depth of 2.4 m (8 ft.). Neat test site 3 farther up the hill to the east, the most likely location of the failure zone was estimated to still be within Unit C1, between the water table and the top of the denser underlying unit C3 at a depth of 16.8 m (55 ft.). Progressing up the hill and to the east to test site 4, Unit C1 is believed to thin, rise above the water table, and increase in penetration resistance (Andrus 1994).

6.6 Age of Deposit

Trenching investigations carried out in 1985 revealed interbedded fine and coarse grained sediments of probably late Pleistocene age (10,000 to 15,000 years), 4.6 m (15 ft.) beneath the site. The gravelly sediments are characteristic of braided channels and bars deposited by high energy flows, whereas the finer-grained matrix-supported gravels indicate fluctuations in flow conditions to lower-energy flows (Andrus et al. 1987). Figure 6-9 shows the principle liquefaction features, along with drill hole and sounding locations on the lateral spread.

For the 1985 campaign, four test sites were laid out that line up parallel to the direction of movement and perpendicular to the fan fronts. These tests sites provided subsurface information for delineating sediment layers beneath the lateral spread and defined soil properties and liquefaction susceptibility of the sediments.

6.7 DPT Soundings

Two DPT soundings each were performed within about a meter or two of the old BPT soundings using a CME 85 drill rig with the capability of using two different hammer energies.

In one sounding the DPT cone was advanced using a conventional automatic SPT hammer with a weight of 63.6 kg (140 lbs.) dropped from a height of 0.76 m (30 in). The second sounding was performed using a 154.4 kg (340 lb.) automatic hammer with a drop height of 0.76 m (30 in). Hammer energy measurements made at Pence Ranch in the days previous to Whiskey Springs were made using an instrumented rod section and a PDA device as described in Chapter 5 and are assumed to be the same for Whiskey Springs. There the measurements indicated that the SPT hammer delivered 93% and 85% of the theoretical free-fall energy, respectively, and with the same standard deviations.

Similar to Pence Ranch the measured blow count was corrected downward using the same equations. Because of this, the ratio of energy actually delivered divided by the energy delivered by the Chinese DPT hammer was the same, i.e. 0.42 and 0.93 for the 63.6 kg (140 lb.) and 154.4 kg (340 lb.) hammers, respectively.

For the Whiskey Springs drilling, the very same drill rig and crew were used in the days immediately following the work at Pence Ranch. Therefore, the PDA Frequency diagrams showing the number of hammer drops and Energy Transfer Ratio (ETR) are assumed to be the same and are presented for convenience in Figures 6-10 and 6-11, for the light and heavy hammers, respectively.

Plots of the energy corrected DPT N_{120} versus depth for the 63.6 kg (140 lb.) and 154.4 kg (340 lb.) hammers are provided in Figures 6-12 and 6-13, respectively, in comparison with the BPT N_{BC}.

For both hammer energies, the energy corrected DPT N_{120} value is moderately consistent with the trend defined by the BPT N_{BC} value with depth. The agreement is best within the depth range from 6.7 to 8.5 m (22-28 ft.) in Hole BC3, and 10.7 to 13.4 m (35 to 44 ft.) in Hole BC4, and when the BPT N_{60} is less than about 30.

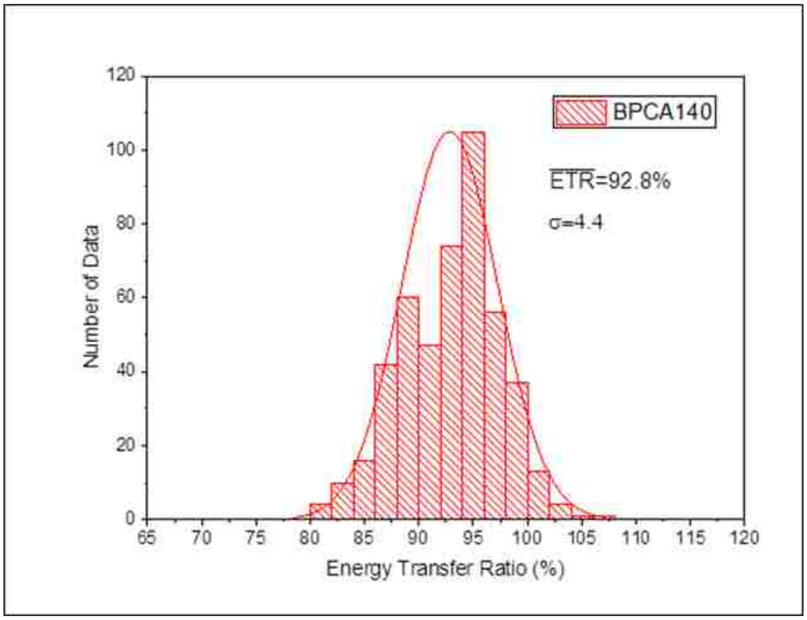

Figure 6-10. Frequency diagram showing number of hammer drops and ETR values for the light hammer, 63.5 kg (140 lb.) at Pence Ranch and assumed to be the same for the Whiskey Springs site.

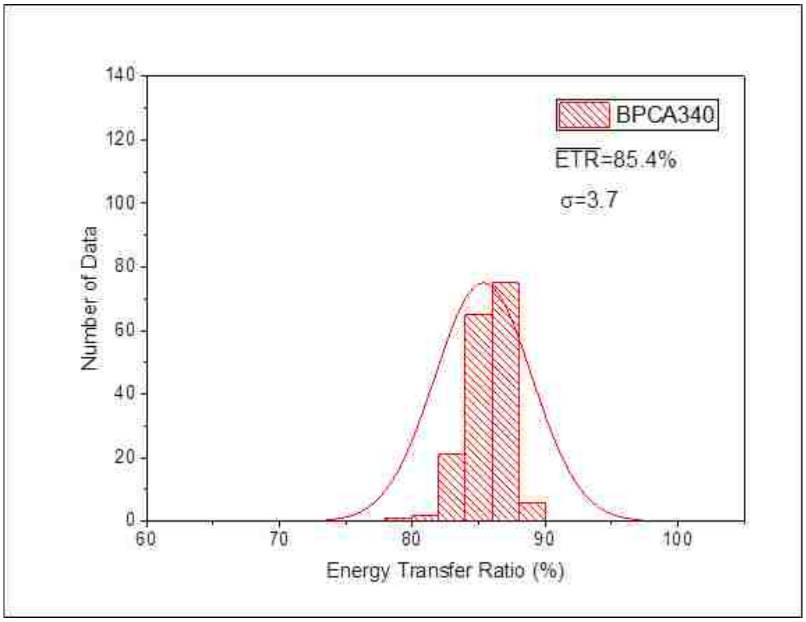

Figure 6-11. Frequency diagram showing number of hammer drops and ETR values for the heavy hammer at Pence Ranch and assumed to be the same for the Whiskey Springs site.

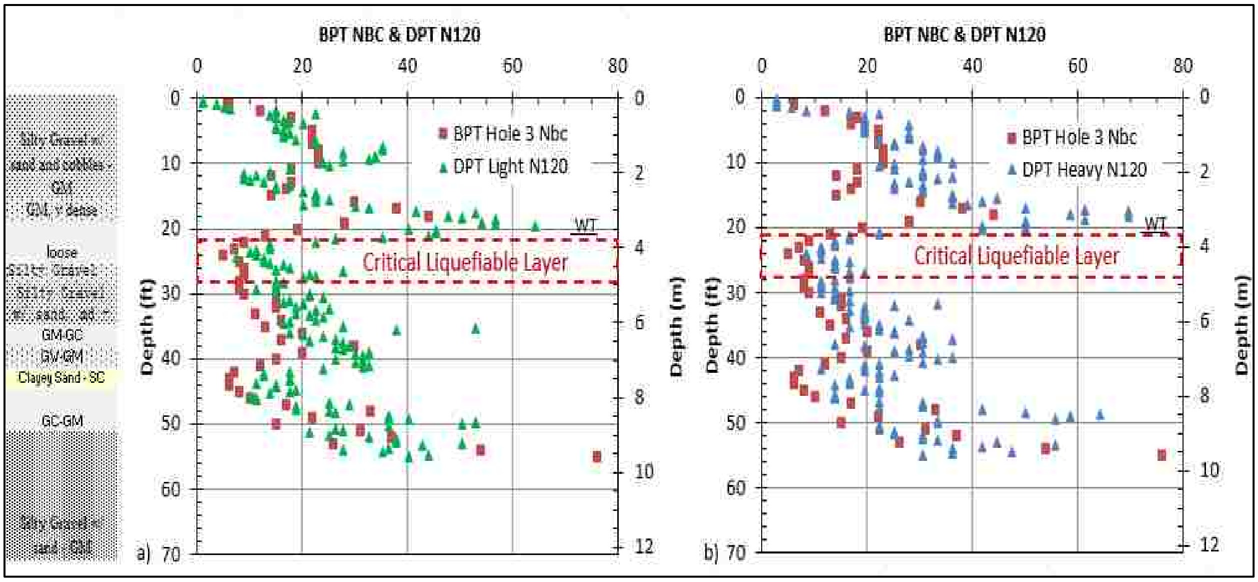

Figure 6-12. Plots of DPT N_{120} versus Depth using (a) light 63.6 kg (140 lb.) hammer and (b) heavy 154.4 kg (340 lb.) hammer, after energy correction to account for lower hammer energies, compared to BPT for Whiskey Springs Hole BC3. BPT from Andrus et al. (1987).

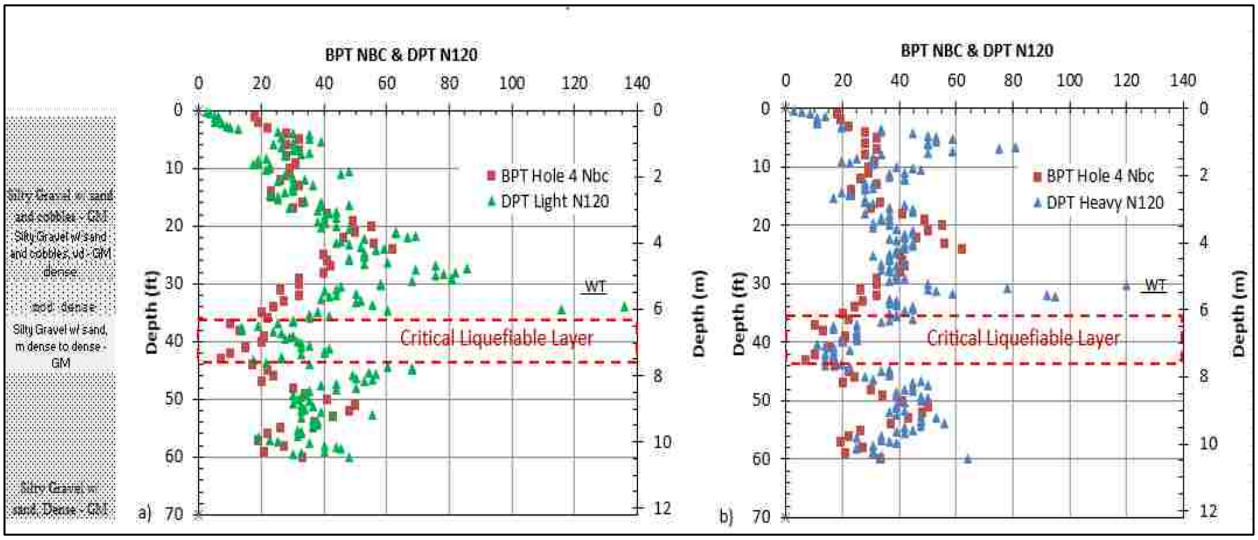

Figure 6-13. Plots of DPT N_{120} versus depth using (a) light 63.6 kg (140 lb.) hammer and (b) heavy 154.4 kg (340 lb.) hammer, after energy correction to account for lower hammer energies, compared to BPT for Whiskey Springs Hole BC4. BPT from Andrus et al. (1987).

It can also be readily seen that, in this instance, the correlation is somewhat better for the heavy hammer than for the light hammer, probably because of the dense nature of the material.

Because of the dense nature of the material at this site, these soundings were a significant test of the SPT hammer.

A comparison of the N_{120} blow counts obtained from the two different hammer energies after energy correction is provided in Figure 6-16. The data points generally fall within a reasonable range of the 1:1 line. Results from additional testing will be necessary to define the error bands and to determine if adjustments in the energy correction factor may be necessary for depth or gravel particle size.

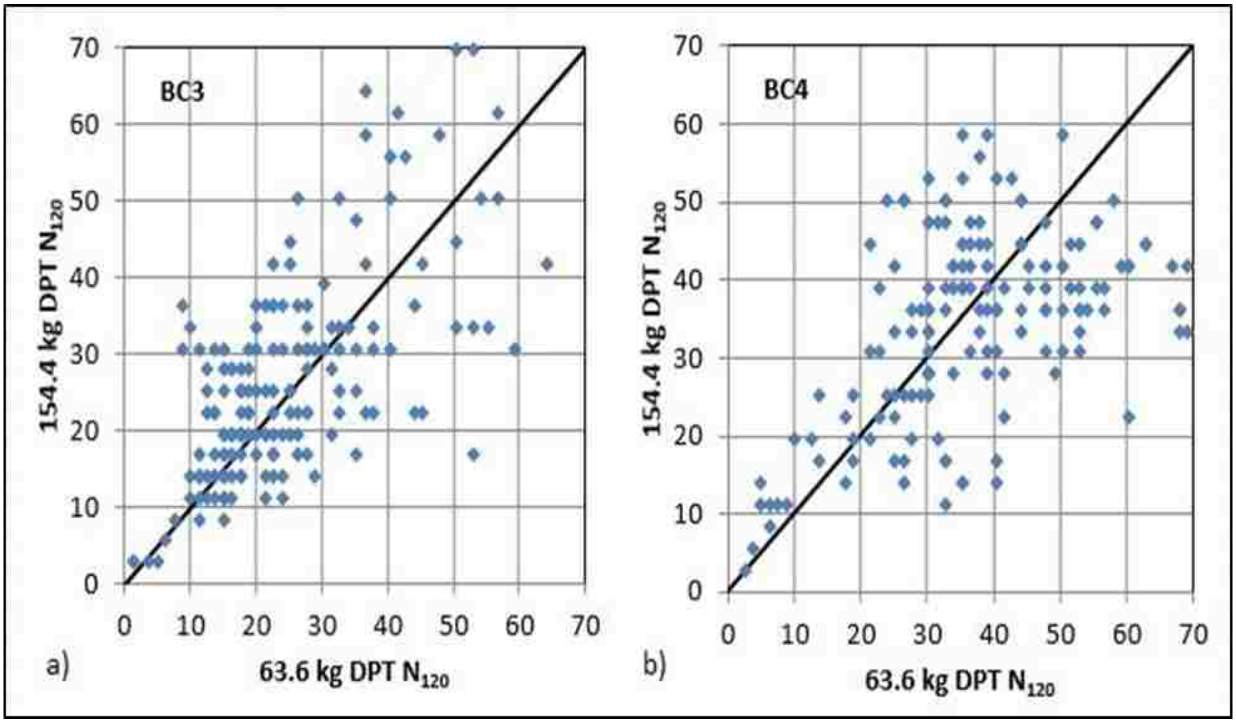

Figure 6-14. Comparison of DPT N_{120} obtained using the 63.6 kg (140 lb.) and the 154.4 kg (340 lb.) hammers after energy correction, for Whiskey Springs a) Hole BC3, and b) Hole BC4.

6.8 CSR vs. DPT N'_{120}

As in Chapter 5, liquefaction potential was evaluated using both the DPT and BPT methods of analysis for the Whiskey Springs sites. In the case of the BPT, the N_{BC} value was converted to the equivalent sand SPT N_{60} using the Harder et al. (1986) correlation approach.

The SPT N_{60} value was then corrected for overburden pressure effects using the equation proposed by Youd et al. (2001). The cyclic stress ratio, or CSR, was computed using equation 2-2 which was originally developed by Seed et al. (1971) where a_{max} is the peak ground acceleration of 0.5g. The CSR was adjusted for the Borah Peak earthquake using the magnitude scaling factor equation 2-3.

The cyclic stress ratio, CSR, is plotted as a function of DPT-based N'_{120} for the zone between 10.0 to 13.7 m (33 to 45 ft.) below the ground surface for both holes at Whiskey Springs in Figures 6-15 and 6-16. The adjusted triggering curve for the $M_s7.3$ Borah Peak earthquake is also plotted for comparison. Solid dots indicate liquefaction and open dots indicate a layer that had no liquefaction.

The cyclic stress ratio, CSR, is summarized as a function of BPT-based $(N_1)_{60}$ for the zone between 10.0 to 13.7 m (33 to 45 ft.) below the ground surface in Figure 6-17 a). The adjusted triggering curve for the $M_s7.3$ Borah Peak earthquake is also plotted in Figure 6-17 for comparison.

In the case of the DPT, the N_{120} value was first converted to N'_{120} using equation 2-1. Then the CSR was plotted as function of N'_{120} within the zone of liquefaction from 10.0 to 13.7 m (33 to 45 ft.) in Figure 6-17 b). The liquefaction triggering curve was based on the 30% probability curve develop by Cao et al. (2013) shown in Figure 2-2. The triggering curve in Figure 6-17 b) was adjusted upward using the magnitude scaling factor to account for the lower magnitude of the Borah Peak earthquake ($M_w7.3$) earthquake relative to the $M_w7.9$ Wenchuan China earthquake used to develop the DPT triggering curves.

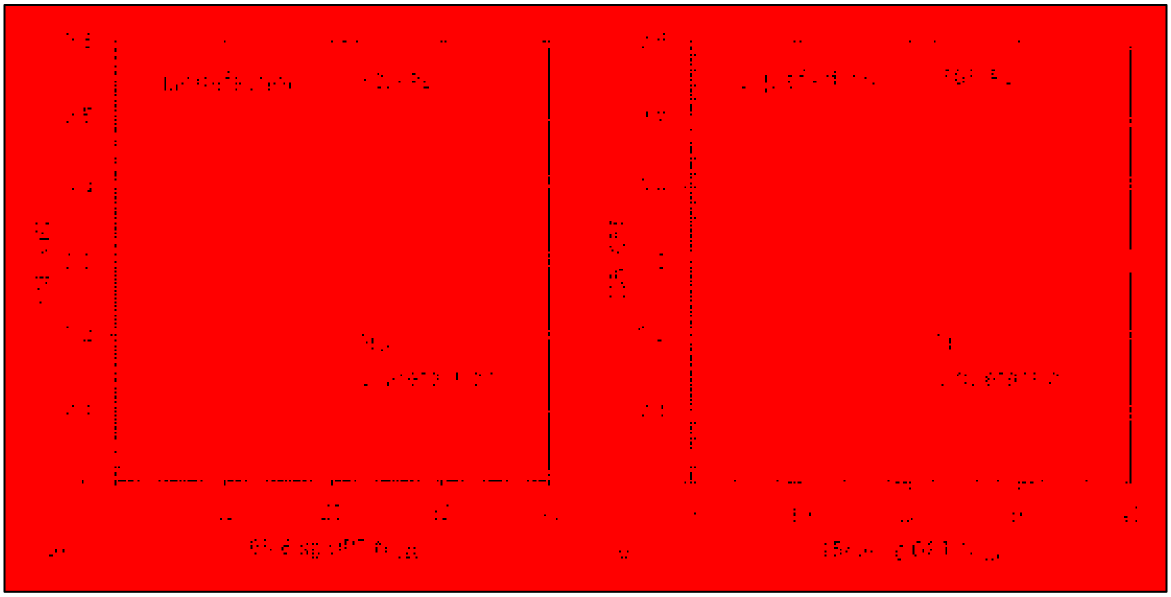

Figure 6-15. Comparison of CSR vs DPT N'$_{120}$, using a) the 63.6 kg (140 lb.) hammer, and b) the 154.4 kg (340 lb.) hammer, for Whiskey Springs BC3. Solid dots are from the liquefiable unit and open dots are from the non-liquefiable unit.

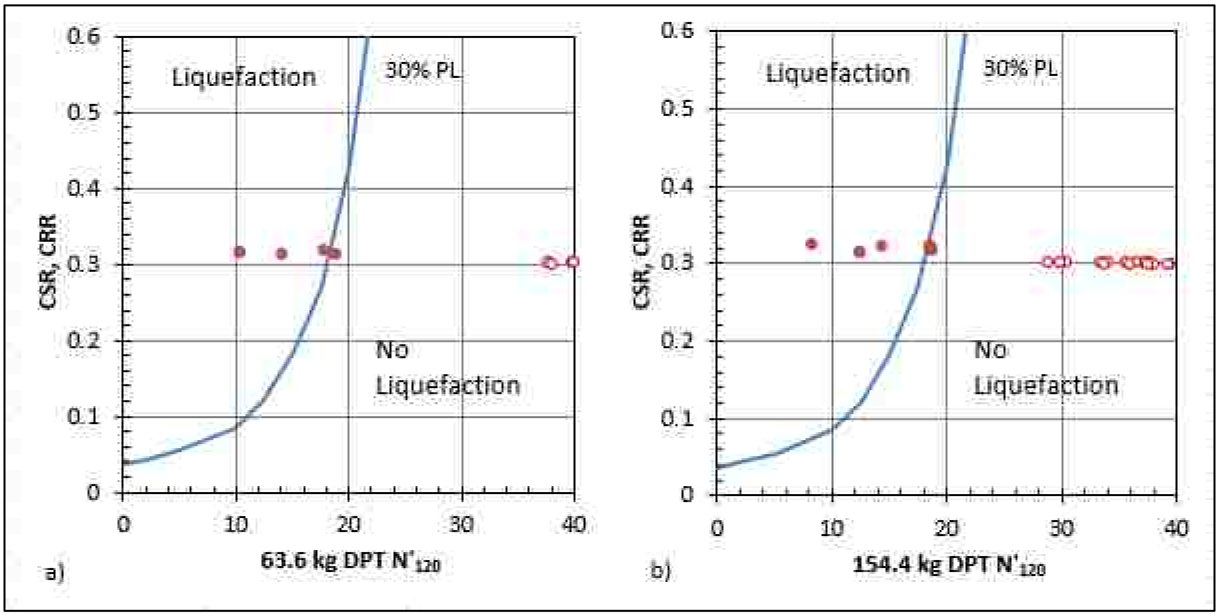

Figure 6-16. Comparison of CSR vs DPT N'$_{120}$, using a) the 63.6 kg (140 lb.) hammer, and b) the 154.4 kg (340 lb.) hammer, for Whiskey Springs BC4. Solid dots are from the liquefiable unit and open dots are from the non-liquefiable unit.

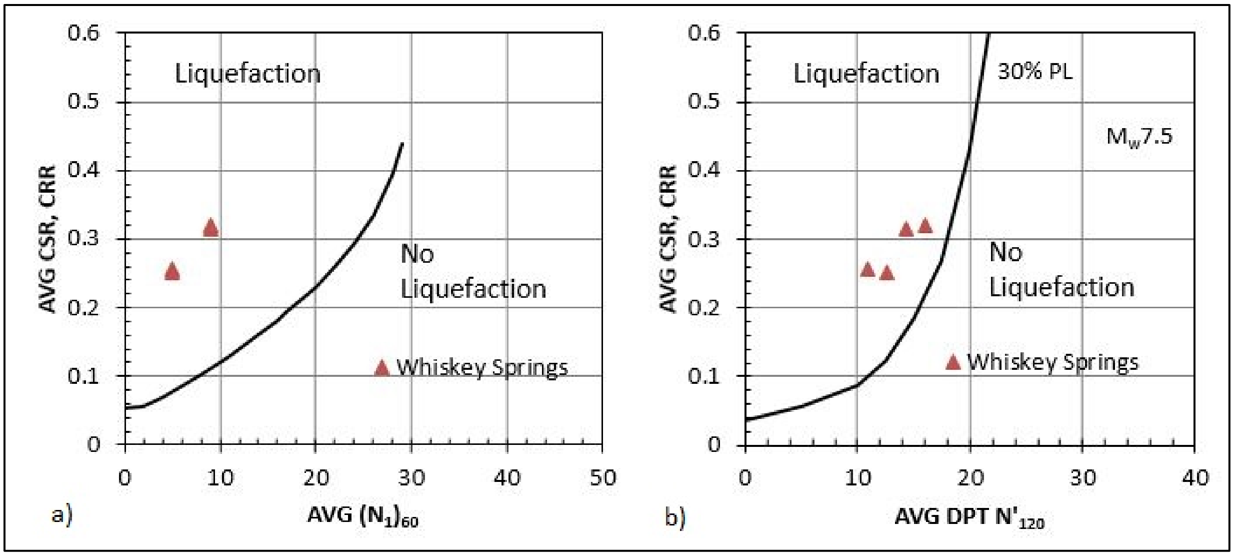

Figure 6-17. Comparison of a) CSR vs BPT-based $(N_1)_{60}$ data points for Whiskey Springs in comparison with triggering curve, and b) CSR vs. DPT N'_{120}, data points for Whiskey Springs in comparison with triggering curve for 30% probability of liquefaction (Cao et al. 2013) for M_w7.5 earthquakes.

The CSR-DPT pairs for each hole at Whiskey Springs were averaged to obtain a single point that represents the entire data *set*, and plotted in Figure 6-18, in comparison with the triggering curve for 30% probability of liquefaction.

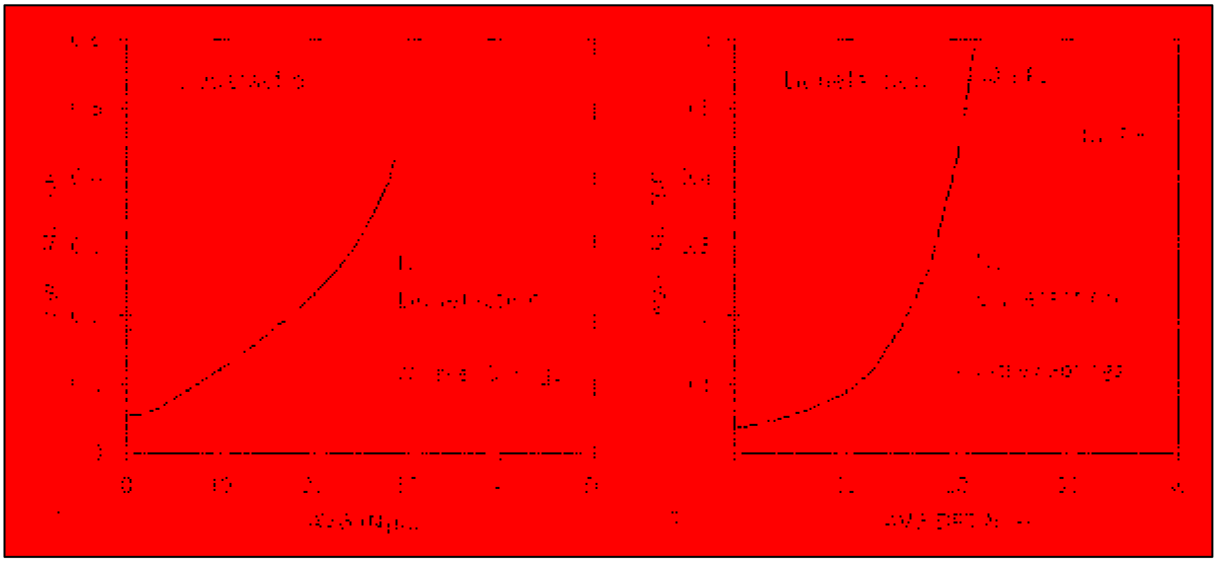

Figure 6-18. Comparison of the set average (Figure 5-21) for a) CSR vs BPT-based $(N_1)_{60}$ data points for Whiskey Springs in comparison with triggering curve, and b) CSR vs. DPT N'_{120}, data points for Whiskey Springs in comparison with triggering curve for 30% probability of liquefaction (Cao et al. 2013) for M_w7.5 earthquakes.

The CSR-DPT N'_{120} points from Figure 6-17 b) are plotted in Figure 6-19 below in comparison with the probabilistic liquefaction triggering curve (Cao et al. 2013), after magnitude scaling adjustments which shifted the measured CSR values slightly downward. In all cases the data pairs plot above the 50% probability of liquefaction curve which is consistent with the observed liquefaction at both sites. In Figure 6-20, a single data point is shown that represents the DPT N'_{120} data set, as compared to the liquefaction triggering curve.

6.9 DPT vs. SPT

Similar to Chapter 5, a good indicator of the results of the study is the comparison of the DPT results with previous SPT results. Figures 6-21 and 6-22 illustrate the correlation between the SPT N_{60} and the DPT N_{120} at Whiskey Springs.

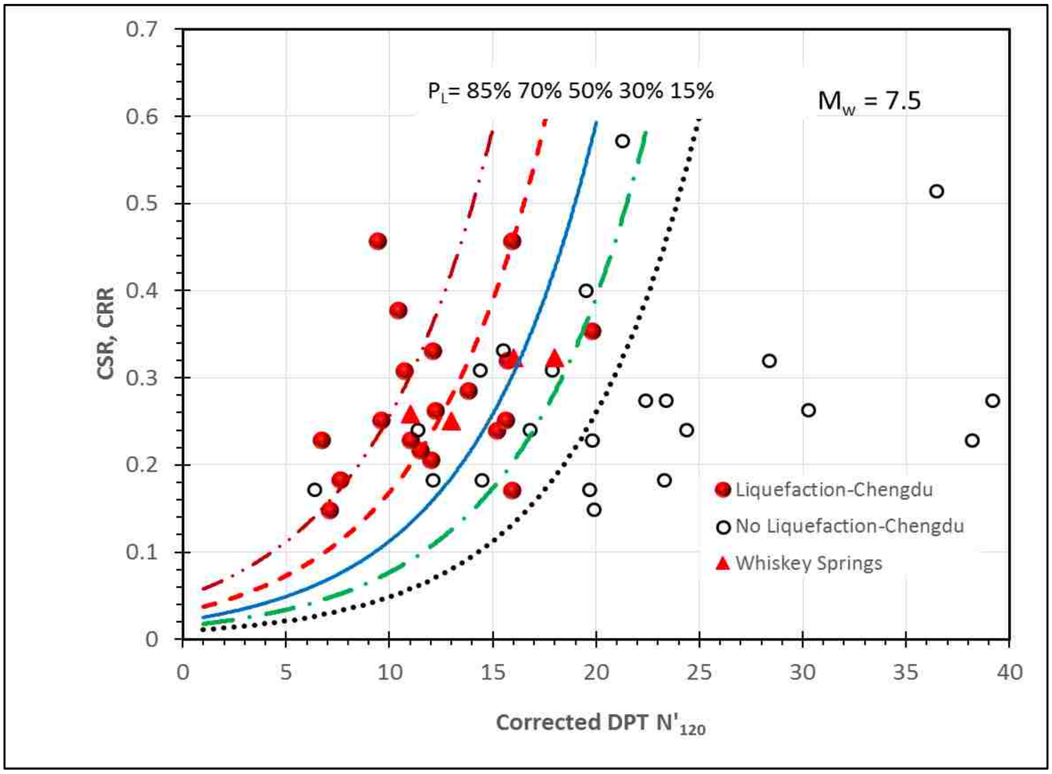

Figure 6-19. CSR vs. DPT N'_{120} curves for various probabilities of liquefaction in gravelly soils developed by Cao et al. (2013) along with liquefaction/no liquefaction data points from Chengdu Plain. Points from Whiskey Springs, Figure 6-19 b) are shown.

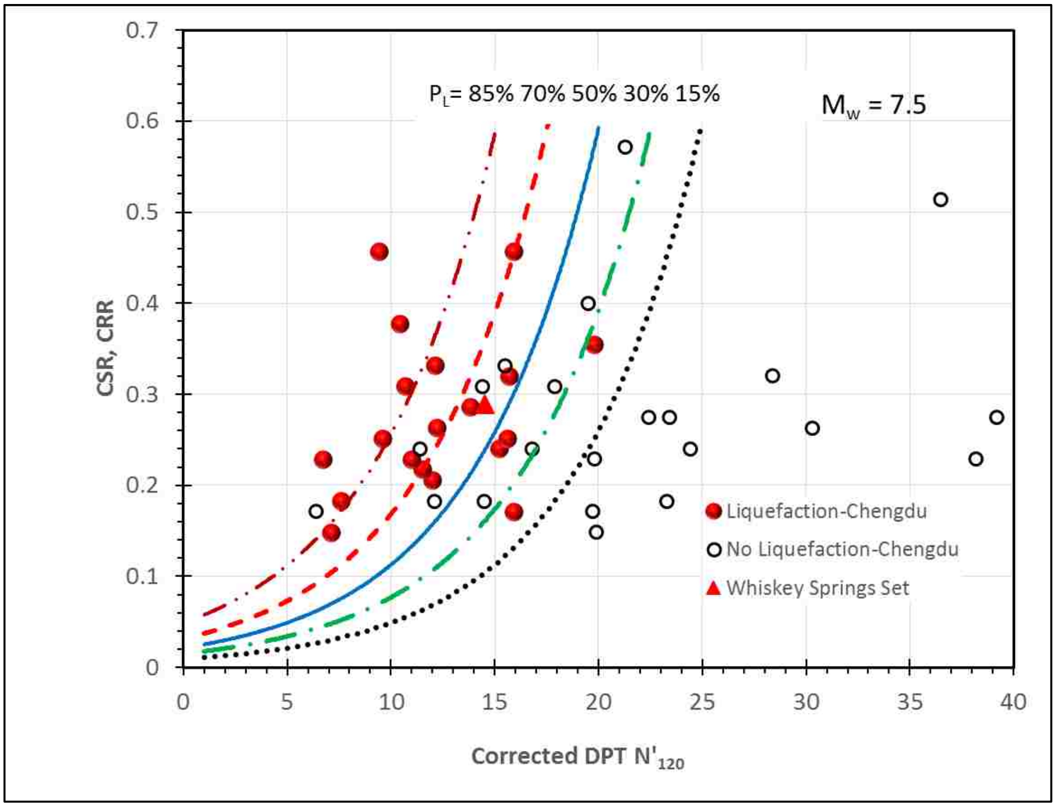

Figure 6-20. CSR vs. DPT N'$_{120}$ curves for various probabilities of liquefaction in gravelly soils developed by (Cao et al. 2013) along with liquefaction/no liquefaction data points from Chengdu Plain. Set point from Whiskey Springs, Figure 6-20 is shown.

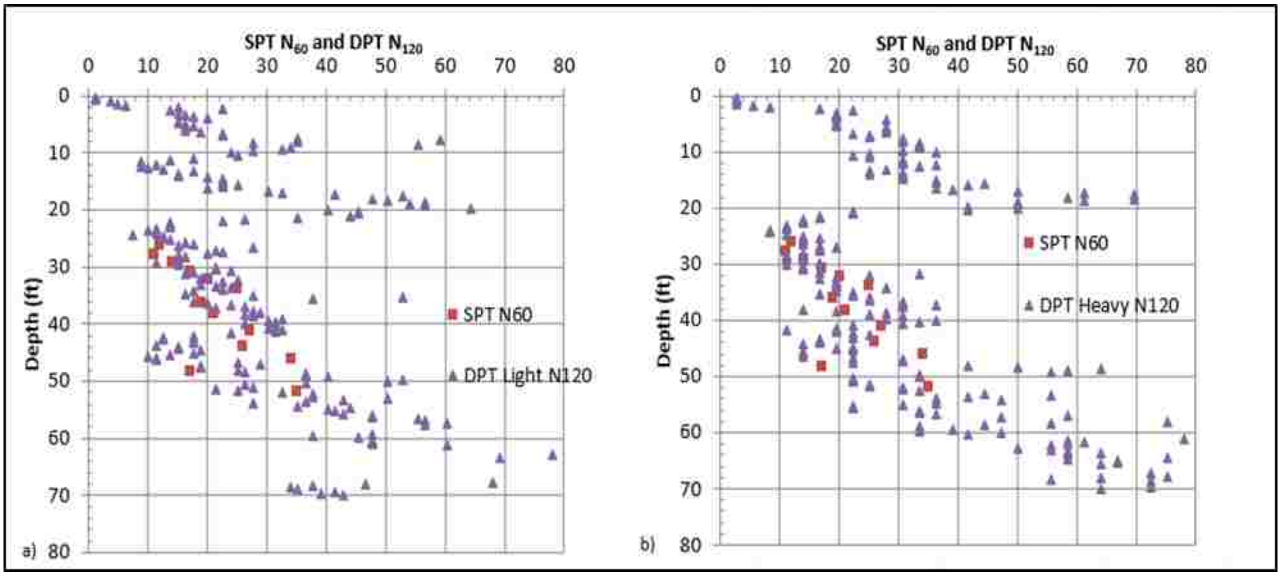

Figure 6-21. Correlation of DPT N$_{120}$ and 1990 SPT N$_{60}$ for Hole number BP3 given a) the light 63.6 kg (140 lb.) hammer and b) the heavy 154.4 kg (340 lb.) hammer at Whiskey Springs.

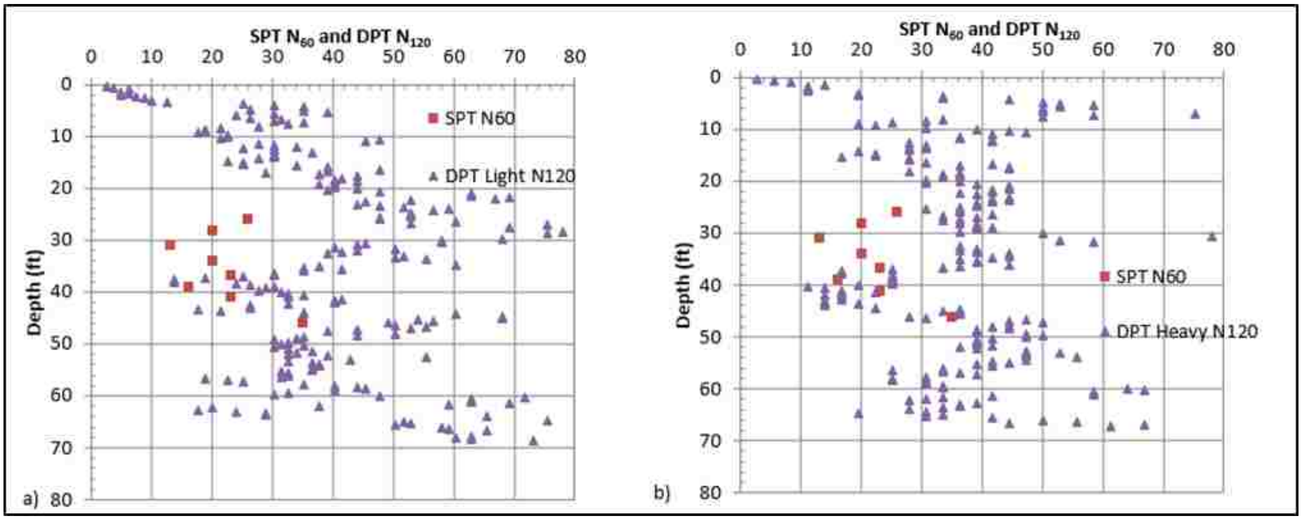

Figure 6-22. Correlation of DPT N_{120} and 1990 SPT N_{60} for Hole number BP4 given a) the light 63.6 kg (140 lb.) hammer and b) the heavy 154.4 kg (340 lb.) hammer at Whiskey Springs.

The 2016 DPT vs. 1987 SPT data was plotted to gain an understanding of the correlation between the DPT soundings accomplished at the site and the SPT soundings. As can be seen from Figure 6-23 there is only weak to no correlation between the two.

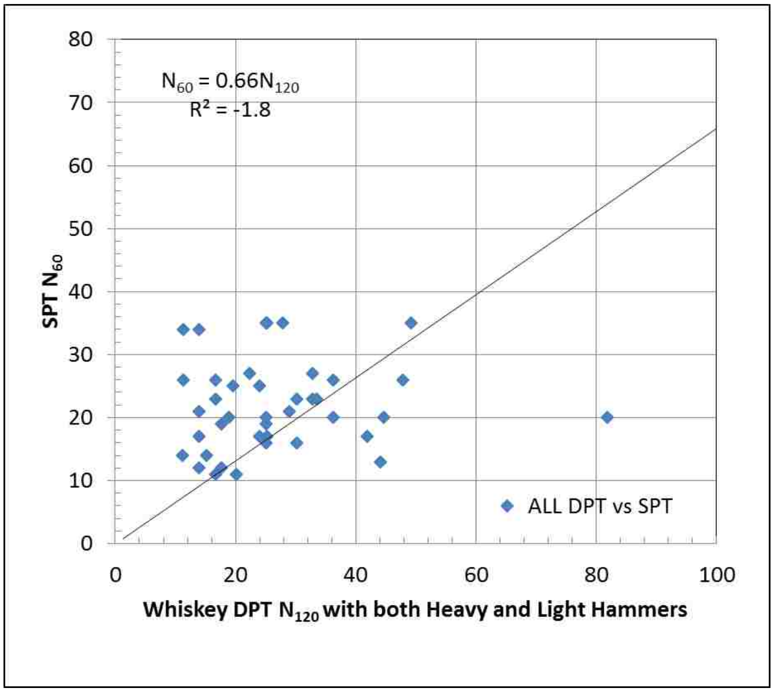

Figure 6-23. Plot comparing the 2016 DPT N_{120} vs. 1987 SPT N_{60} for all holes at Whiskey Springs using both the 63.6 kg (140 lb.) hammer, and the 154.4 kg (340 lb.) hammer.

The R^2 values for this correlation of all holes at Whiskey Springs is marginal given that a perfect fit would have an R^2 of 1.0. The regression equation factor on x is the slope of the regression line and should be close to 1.0 but is only 0.66, this signifies a weak correlation.

6.10 Probability of Liquefaction vs. Depth from DPT

The probability of liquefaction P_L was calculated and plotted for all DPT holes at Whiskey Springs and is shown in Figure 6-24 below. Equation 5-2 was used and is the same as that used for Pence Ranch and is referred to as the probability function for liquefaction. Cao et al. (2013) validated this equation using data from the Wenchuan event where 15 of 19 sites with surface liquefaction effects (79%) plotted on or above the P_L=50% curve of Figure 2-8, and 17 of 19 (89%) liquefaction sites plot on or above the P_L=30% curve. Similarly, 23 of 28 (82%) of sites exhibiting no surface liquefaction effects plot on or below the P_L=50% curve and 26 of 28 (93%) non-liquefaction sites plot on or below the P_L=70% curve. He states that this correlation is therefore generally verifiable for gravelly soils in the Chengdu plain shaken by the 2008 Wenchuan earthquake, and that this relationship may be used for other sites underlain by gravelly soils with soil types similar to those that liquefied during the Wenchaun quake.

The probability of liquefaction corresponds well with the calculated critical zone of liquefaction in the interval of 6.7 to 8.5 m (22 to 28 ft.) in Hole-3, and also well from 10.9 to 13.7 m (36 to 44 ft.) in Hole-4.

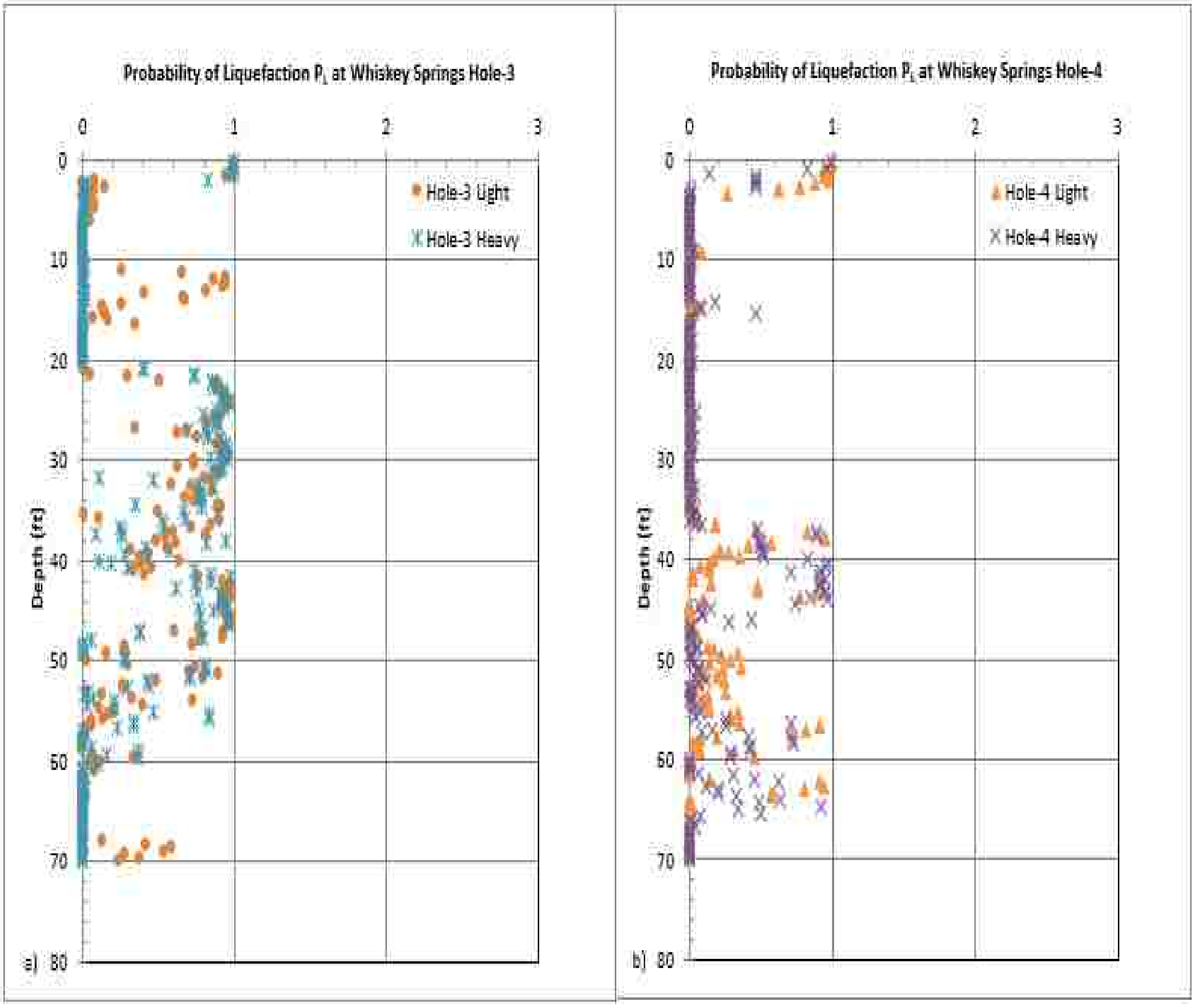

Figure 6-24. Probability of Liquefaction, P_L, for all holes at Whiskey Springs, vs. Depth, from DPT. a) Hole-3, and b) Hole-4.

7 DPT TESTING AT LARTER RANCH, IDAHO AND LIQUEFACTION ASSESSMENT

7.1 Introduction

Liquefaction of gravelly soil was also observed at the Larter Ranch during the M_s7.3 Borah Peak earthquake in 1983 (Andrus 1994) (Youd et al. 1985). Larter Ranch is located about 24.1 km (15 miles) north of Mackay near Thousand Springs Creek in central Idaho (latitude 44.0743º, longitude -113.8429º) and about 0.75 miles SSW of the Whiskey Springs site and approximately 2 km (1.2 mi.) SW of the fault rupture. Similar to the Whiskey Springs site, the earthquake generated zones of lateral spreading, fissuring, buckling, and sand boils in a coarse-grained sediment. Peak ground acceleration was estimated to be about 0.5g at the site.

Figure 7-1 shows a general map with an approximate location of the site with the number 2 identifying Larter Ranch.

7.2 Liquefaction Effects

Locations of liquefaction effects as shown by surface manifestations are noted on the map shown on Figure 7-2. The parallel fissures mark the head of the lateral spread. In many areas these fissures intersect at an angle roughly 10 degrees to the trend of the set, suggesting movement in the downslope and slightly downstream direction.

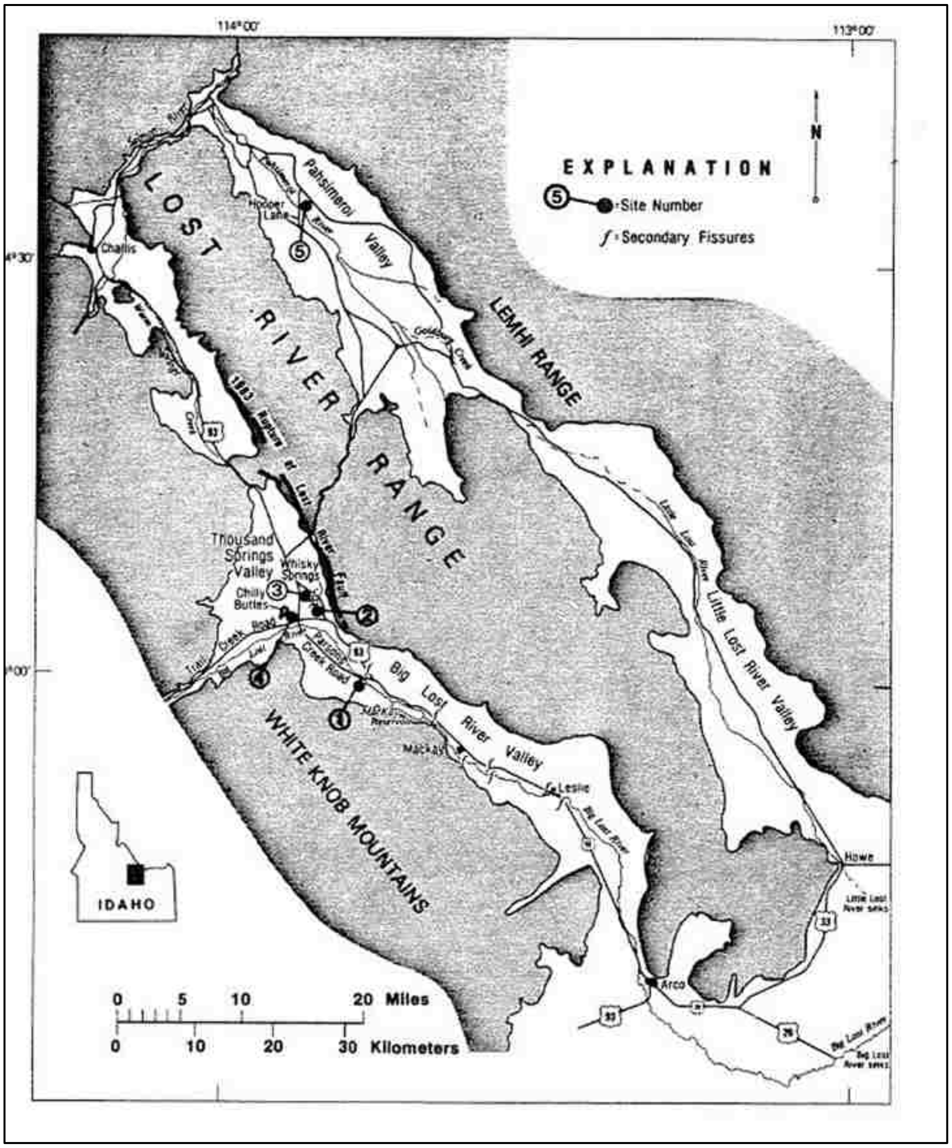

Figure 7-1. Regional Map of central Idaho geographic features and approximate fault rupture. Site number 2 is Larter Ranch (Andrus et al. 1987).

The larger fissures are filled by blocks of soil that dropped vertically downward. These graben-type structures are as wide as 2.4 m (8 feet). At the edge of the marsh, the soil buckled forming ridges as high as 1.2 m (4 feet). The buckled sod marked the toe of the lateral spread.

The movement was primarily horizontal, as indicated by the large tension cracks and the buckled sod. The maximum horizontal displacement was about 1 m (3 ft.). Some vertical movement did occur, with vertical offsets as much as 0.3 m (1 ft.).

Water carrying silt and sand reportedly erupted up through cracks along the lower areas of the lateral spread. First-hand accounts from the area describe a large dust cloud that rose up along Thousand Spring Creek just after the earthquake. The reporting party recounted seeing water spouts flowing up to 0.9 m (3 ft.) into the air along the toe of the slide that lasted for nearly 30 minutes.

The locations of 1990 BPT and 2017 DPT holes are shown in Figure 7-2. 2016 site conditions are shown in Figure 7-3 and a view of the dynamic cone and thread adapter used in the DPT drilling in Figure 7-4.

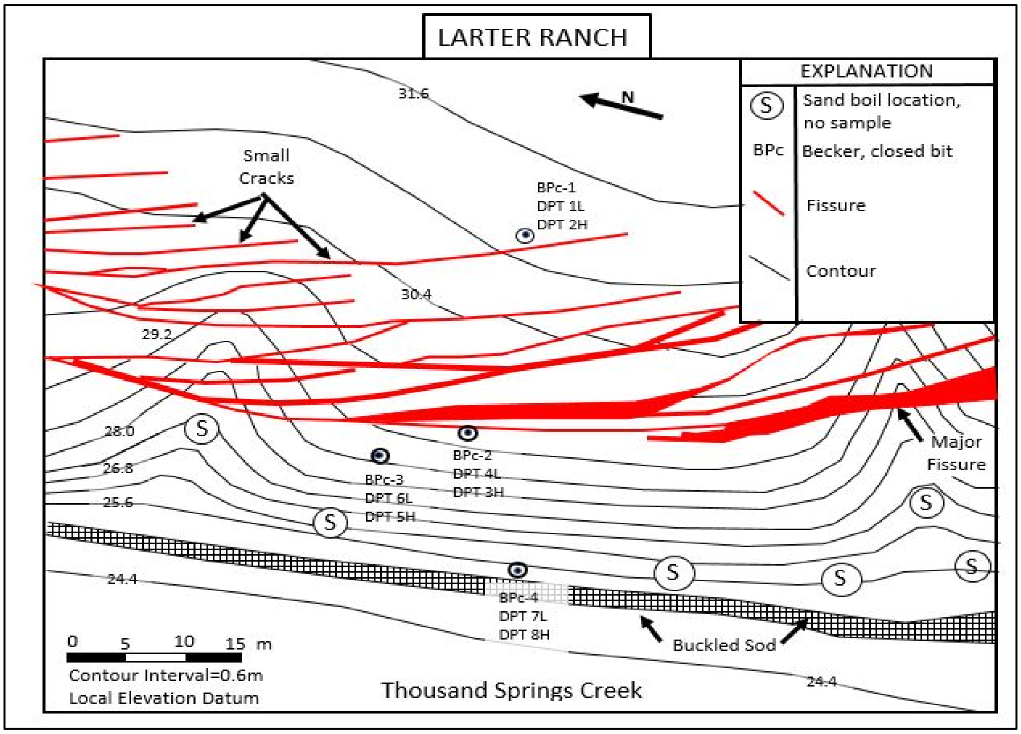

Figure 7-2. Map of the Larter Ranch Site north of Mackay, Idaho showing topographic liquefaction effects and sites of testing. Simplified from Andrus (1994).

Andrus (Andrus 1994) reported that site investigations at Larter Ranch were conducted at three principal areas: near the buckled sod at the toe of the lateral spread, below the major fissures at the head of the lateral spread, and above the zone of fissures. In 1985, SASW methods were used in each area. In 1990, the same sites were retesting with SASW, SPT, and BPT. In 1991, cross-hole seismic tests were conducted near the toe of the slope.

Figure 7-3. View looking north of drillers setting up on BPc-2, also showing 2017 site conditions near a large fissure caused by liquefaction induced lateral spreading towards Thousand Springs Creek to the left.

7.3 Soil Description

Field investigation were carried out in 1985, 1990, and 1991 and were conducted in three principle areas: near the buckled sod at the toe of the lateral spread below the major fissures at the head of the lateral spread, and above the zone of fissures as shown in Figure 7-5.

A generalized cross section delineating the sediment layers beneath the Larter Ranch site is shown in Figure 7-5. A 1.0 m (3 foot) thick, non-plastic, dark grayish brown silty sand and gravel lies below the ground surface at test Area 1.

Figure 7-4. View of cone tip, thread adapter, and PDA rod section.

This is referred as Unit A and is an organic-rich silty sand. It grades laterally eastward into weak humic silty sand that is less than 0.3 m (12 inches) thick at test area 2. Unit A has formed on top of a coarse-grained alluvial fan deposit, Unit B.

Unit B is a medium dense to dense sandy gravel with silts and cobbles (GM-GW). It is characterized by shear wave velocities, V_s, generally exceeding 200 m/sec (650 ft/sec), N-values as high as 94, and corrected Becker blow counts as much as 49 blows/0.3m (blows/ft.). The gravel particles are packed in a clast-supported structure with a filled framework of silty sand to somewhat matrix-supported (clast separated by a small amount of silt and sand). The maximum particle size is 250 x 180 x 130 mm (10 x 7 x 4 in.). The silty sand fraction is pale to yellowish brown, non-to slightly-plastic, and reacts moderately to a weak hydrochloric acid solution (HCl; about 0.1 N solution). Unit B is nearly 6.1 m (20 feet) thick beneath Area 3 and less than 1.4 m (4.6 feet) thick beneath Area 1.

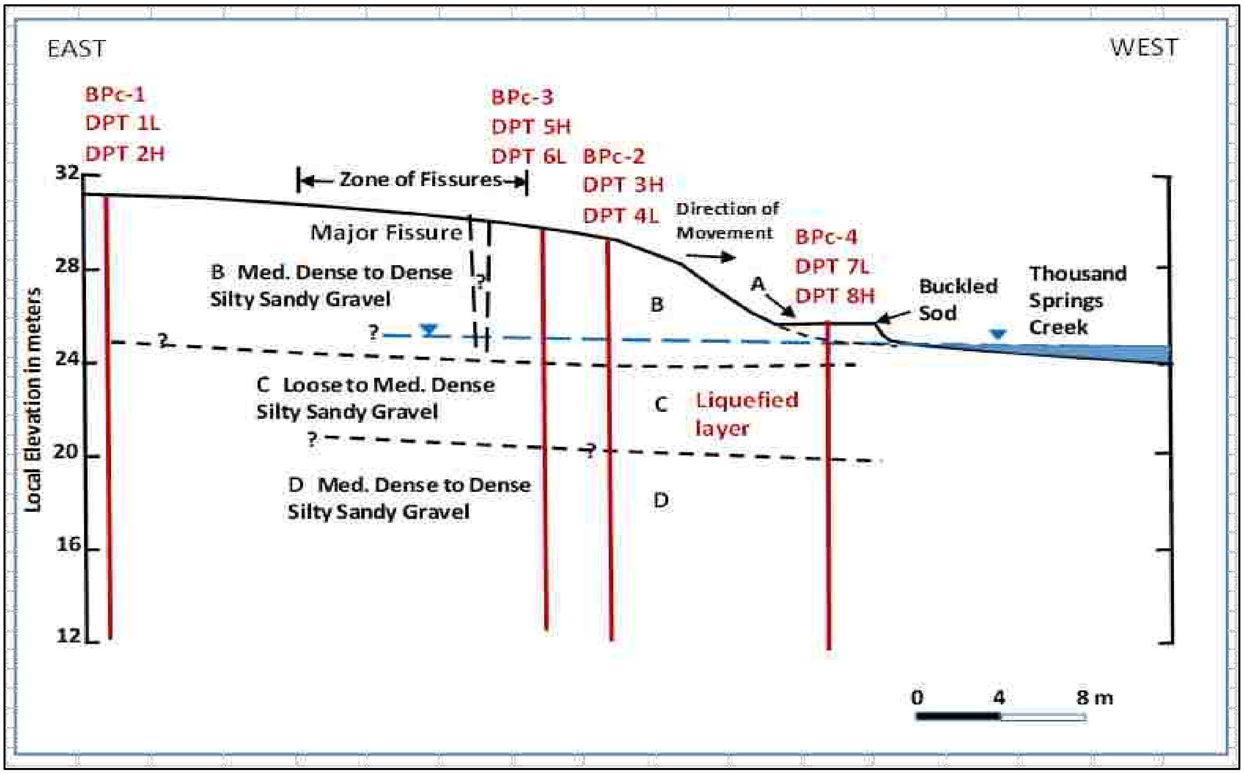

Figure 7-5. Cross Section of the Thousand Springs lateral spread at the Larter Ranch site. After Andrus (1994).

Beneath Unit B lies a loose to medium dense silty sandy gravel with few cobbles (GM-GW) sediment, Unit C. Unit C can be further subdivided into subunits (C1 and C2). Subunit C1 is characterized by N_{60}-values ranging from 4 to 11, with an average value of 9; cone tip resistances between 1 and 10 MPa (8 and 106 tons/ft^2), with an average value of 4.4 MPa (46 tons/ft$_2$); cone friction ratios between 0 and 5 percent, with an average value of 1.2 percent; uncorrected Becker blow counts (closed bit) varying from 5 to 13 blows per 0.3 m (1 ft.), with an average value of 8. The equivalent N_{60}-values range between 148 and 211 m/sec (484 and 692 ft/sec), with an average value of about 170 m/sec (540 ft/sec). Subunit C1 sediments are gap-graded, and contain about 7 percent silt and clay. The finer fraction is yellowish brown, non to slightly plastic, and exhibits a weak reaction to a weak hydrochloric acid solution. The top of subunit C1 in Area 1 lies at a local elevation of about 23.4 m (76.6 ft). Subunit C1 is about 1.4 m (4.4 ft) thick.

Subunit C2, a silty sandy gravel (GM), exhibits higher penetration resistance and greater fines content (silt and clay) than C1. Subunit C2 is characterized by N60-values ranging from 8 to 17, with an average value of 10; cone tip resistances between 1 and 21 MPa (1 and 215 tons/ft^2), with an average value of 6.3 MPa (66 tons/ft^2); cone friction ratios between 0 and 28 percent, with an average value of 2.7 percent; uncorrected Becker blow counts (closed bit) varying from 6 to 17 blows per 0.3 m (1 ft), with an average value of 12. Equivalent N_{60}-values determined from Becker blow count range from 4 to 8, with an average value of 6. Average Vs-values range from 153 and 274 m/sec (500 and 900 ft/sec), with an average of about 200 m/sec (660 ft/sec). Split-barrel samples taken from subunit C2 contain about 17 percent fines. The finer fraction of subunit C2 is gray to light brownish gray, slightly plastic, and exhibits a weak reaction to a weak HCl solution. Subunit C2 is about 2.7 m (8.7 ft) thick in Area 1.

Beneath Area 2 and 3, sediment between local elevations of 20 and 25 m (66 and 82 ft.) seems related to Unit C beneath Area 1. At Area 2, N_{60}-values range from 22 to 43, with an average value of 32. At Areas 2 and 3, uncorrected Becker blow counts (closed bit) ranged from 6 to 44 blows per 0.3 m (1 ft), with an average value of 24. The equivalent N_{60}-values determined from Becker blow count range from 4 to 23, with an average value of 12. V_s-values range between 180 and 404 m/sec (590 and 1330 ft/sec), with an average value of 290 m/sec (960 ft/sec). These average values of penetration and shear wave velocity for Unit C at areas 2 and 3 are higher than average values for Unit C in Area 1, because of increase confinement as well as increase stiffness.

Below Unit C, sediment is medium dense to very dense. This dense material, Unit D, is characterized by Becker blow counts (closed bit) exceeding 18 blows per 0.3 m (1 ft) and V_s-values greater than 248 m/sec (812 ft/sec). The water table was located at approximately the elevation of Thousand Springs Creek (or slightly higher as reported by the local ranch owner), where it remains today.

7.4 Identification of Liquefiable Material

Andrus related that based on the low penetration resistances and low shear wave velocities, liquefaction and shear deformation most likely occurred within Unit C. Subunit C1 is considered the most likely to have liquefied because it exhibits the lowest penetration resistances and shear wave velocities. Liquefaction may also be possible within parts of subunit B1 having low penetration resistances (Andrus 1994).

Sand boil material can sometimes be used to identify the liquefiable layer, if each sediment layer exhibits unique characteristics (such as grain-size distribution, color, or chemical composition). Grain-size distribution curves of samples collected from five sand boil deposits along the toe of the lateral spread are shown in Figure 7-6, with the curves for two test pits taken from the top of subunit C1 included for comparison. Although the test pit samples are much coarser than the sand boil samples, one would expect the coarser particles to segregate out during upward transport through narrow fissures and cracks. Perhaps the gap-graded character of Unit C also contributed to the transport of only the finer grain sizes. The grain size curves of the test pit samples exhibit a gap between particle sizes of 0.4 mm and 3 mm. Sand boil samples consist of material finer than 3 mm. The sand boil material and the finer fractions of subunits B1, C1, and C2 are pale brown, pale yellow, yellowish brown and gray, respectively. If subunits C1 and C2 liquefied, materials from each could have mixed together to produce a pale brown color. Subunit C1 material could have mixed with subunit B1 materials during upward transport. Variations of color may also be explained by exposure to the sun.

Sand boil deposits were exposed to the sun for two years prior to sampling. Materials from sand boils and subunits C1 and C2 react mildly to a weak hydrochloric acid solution.

Pore-water pressures may have risen in Unit D. The finer material within layer D also matches the sand boil material. However, similar medium dense to dense material lies beneath test Area 3 but this area is above the zone of significant lateral movement. The low penetration resistances and geometrical relationship to the lateral spread are strong evidence that Unit C liquefied. Unfortunately, sand boil material could not be used to conclusively identify the liquefiable material.

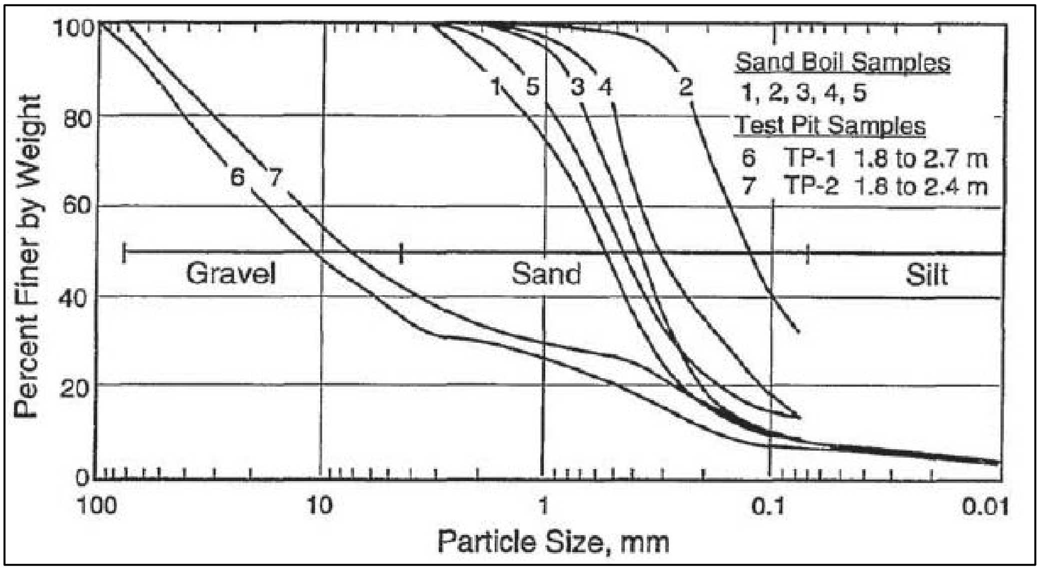

Figure 7-6. Comparison of Grain-Size Distribution Curves for Samples Taken from Five Sand Boil Deposits and Two Test Pit Samples taken from the top of Subunit C1 at the Larter Ranch Site (Andrus 1994).

7.5 Identification of Most Likely Failure Zone

The most likely failure zone at Larter Ranch passed through the top of Unit C and below the water table, see Figure 7-7 below. Unit C was identified as the zone of lowest penetration resistance and shear wave velocity. The failure zone is also presumed to connect the zone of fissures at the head of the slide and the buckled sod at the toe. Penetration resistances and shear wave velocities in Unit C were reported to have increased between Areas 2 and 3, moving uphill (refer to Figure 7-5). This would provide a plausible explanation for the location of the fissures.

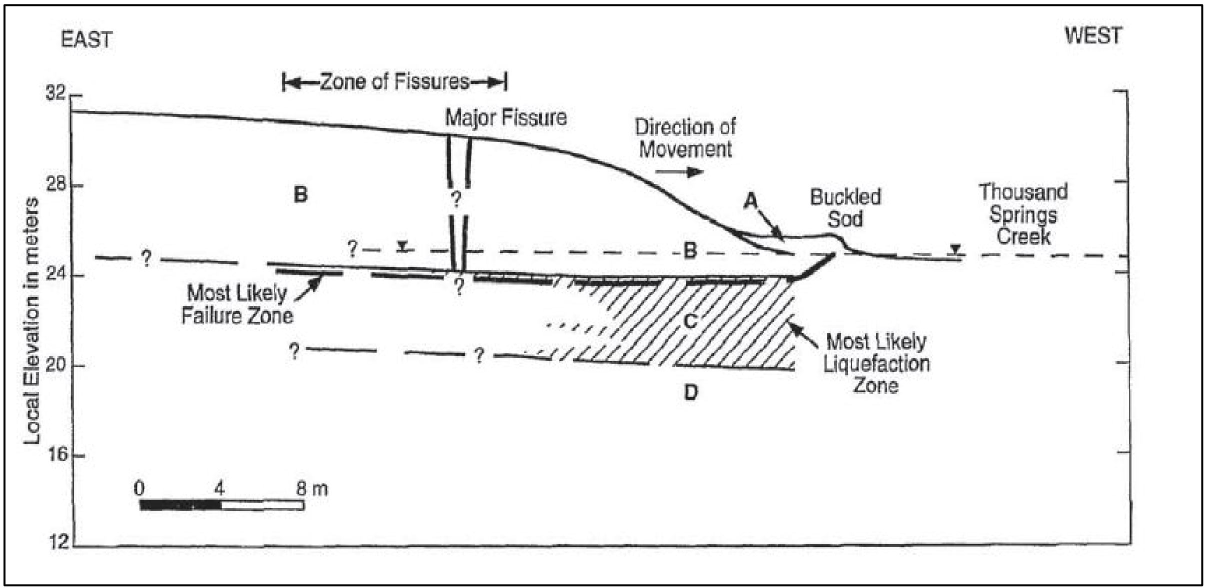

Figure 7-7. Cross Section of the Thousand Springs Valley lateral spread at the Larter Ranch site showing zones of likely liquefaction, after Andrus (1994).

7.6 Age of Deposit

Sediments at the Larter Ranch site are similar to sediments at the Whiskey Springs site investigated by Andrus et al. (1987). A dense gravelly alluvial fan deposit overlies a loose gravelly layer (Unit C) at both sites. Unit C can be subdivided into an upper sandy gravel with silt (subunit C1) and a lower layer containing more silt and clay (Subunit C2). Subunit C1 at the

Larter Ranch and Whiskey Springs sites contains about 7 and 18 percent fines, respectively. Subunit C2 at Whiskey Springs consists of more clay. Sediments at both sites are gap-graded (sand mode clearly separate from the gravel mode), with sub-angular quartzite gravel and cobble particles. The mountain adjacent to these fans consists of an isolated quartzite outcrop. Subunit C1 at Whiskey Springs is a braided channel-fill characteristic of proximal regions of alluvial fans in south-central Idaho (Funk 1976); (Pierce et al. 1982). Subunit C1 likely formed when heavy rainfall or rapid snow melt mobilized loess and coarse fan materials for a short distance (say less than a few kilometers).

Andrus et al. (1987) studied stratigraphic relationships, thicknesses of carbonate coats on stones, and radiometric dates of pedogenic carbonate and charcoal at the Whiskey Springs site. They concluded the fan sediments at the Whiskey Springs site are of probable latest Pleistocene age (10,000 to 15,000 years). Fan sediments at the Larter Ranch site might be of similar latest Pleistocene age, since the site is located on an adjacent fan at about the same elevation. However, significantly less calcium carbonate has accumulated in the fan gravels at the Larter Ranch site, suggesting a younger age or less favorable conditions for pedogenic carbonate accumulation.

Pleistocene alluvial fan deposits should have a low liquefaction susceptibility (Youd et al. 1978). Andrus et al. (1987) suggested three reasons for liquefaction at the Whiskey Springs site. First, alluvial fans can be dominated by wither debris flows or stream flows. Liquefaction has been reported in area associated with distal fan environments dominated by stream flows. Therefore, fans dominated by stream flows should be considered as having a higher liquefaction susceptibility than do fans deposited by debris flows. Second, conditions during the Holocene may not have allowed significant compaction nor cementation of sediments, Unit C contains very little cementing agents, as indicated by only a slight reaction to weak hydrochloric acid solution. Third, evidence in the trenches near Whiskey Springs (exposed roots follow the 1983 fissures) suggest Unit C sediments were disturbed during a pre-1983 earthquake, probably by liquefaction with small horizontal displacement. Such disturbance could destroy cementation and loosen sediments.

7.7 DPT Soundings

As this site also, two DPT soundings were performed within about a meter of the previous BPT soundings using a CME 85 drill rig with the capability of using two different hammer energies. In one sounding the DPT cone was advanced using a conventional automatic SPT hammer with a weight of 63.6 kg (140 lbs.) dropped from a height of 0.76 m (30 in). The second sounding was performed using a 154.4 kg (340 lb.) automatic hammer with a drop height of 0.76 m (30 in). Hammer energy measurements were made using an instrumented rod section and a PDA device for each hammer weight to determine the energy transferred to the drill rod.

The ratio of the measured energy to the theoretical drop energy is referred to as the Energy Transfer Ration (ETR). Histograms showing the frequency distribution of the Energy Transfer Ratio are provided in Figure 7-8 and 7-9 for the light and heavy hammers, respectively. The mean ETR for the light hammer was 90.9% with a standard deviation of 2.8, while the mean for the heavy hammer was 90.8% with a standard deviation of 1.9. These standard deviation values are substantially lower than the 6.9 to 8.6 values measured with the DPT hammers in China. This improvement in precision is likely associated with the automatic hammer drop mechanism used in the US in comparison to the free-fall mechanism used in China as described by Cao et al. (2013).

Because the delivered energies are less than the energy typically supplied by a Chinese DPT hammer, it was necessary to correct the measured blow count downward using the equation 5-1. Cao et al. (2013) found that the measured energy from a typical Chinese DPT was about 90% of the theoretical drop energy. Equation 5-1 follows the pattern for energy correction recommended for SPT testing by Seed et al. (1985). The ratio of energy actually delivered divided by the energy delivered by the Chinese DPT hammer was 0.42 and 0.93 for the 63.6 kg (140 lb.) (light) and 154.4 kg (340 lb.) (heavy) hammers, respectively.

Frequency diagrams showing the numbers of hammer drops and the ETR values using the light and heavy hammers are shown in Figures 7-8 and 7-9, respectively. Once again, the standard deviation of the energy transfer ratio with the automatic hammer is about half of that for the Chinese hammer system.

Plots of the energy corrected DPT N_{120} versus depth for the 63.6 kg (140 lb.) and 154.4 kg (340 lb.) hammers near BPc-1, BPc-2, BPc-3, and BPc-4 are provided in Figures 7-10 through 7-13, respectively, in comparison with the BPT N_{BC}.

For both hammer energies, the energy corrected DPT N_{120} value is quite consistent with the trend defined by the BPT N_{BC} value with depth. The agreement is best within the depth range from 4.6 to 9.1 m (15 to 30 ft.). It can also be seen that in Hole BPc-4, the DPT identified a much denser layer in the upper reaches in the interval 0.9-3.0 m (5-10 ft.) that was apparently not picked up by the BPT. This loss of detail is inherent in the BPT process.

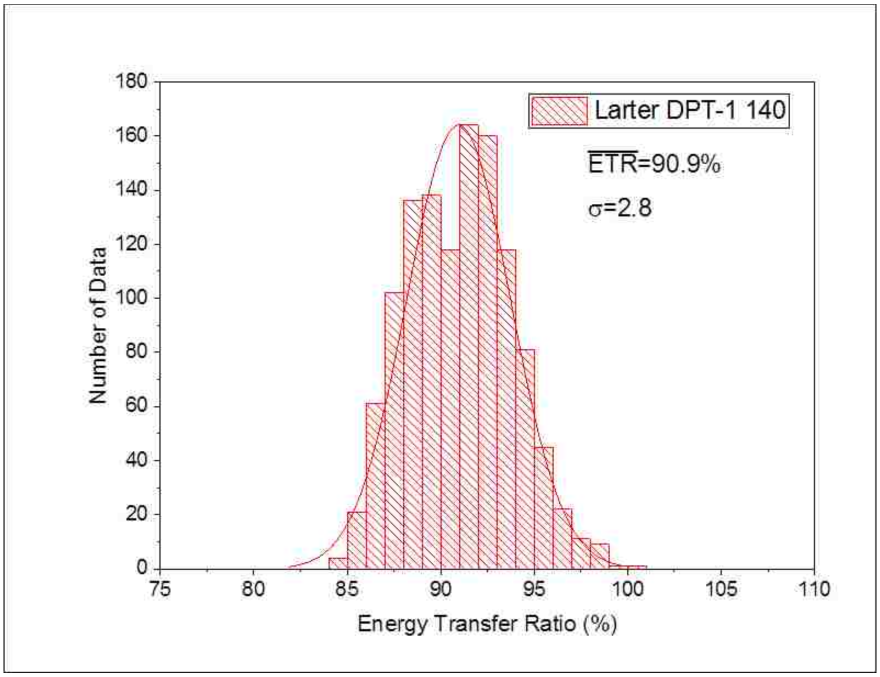

Figure 7-8. Frequency diagram showing number of hammer drops and % ETR values for Larter Ranch DPT-1, using light hammer (63.6 kg (140 lb.), dropped from 0.76 m, 30 in.).

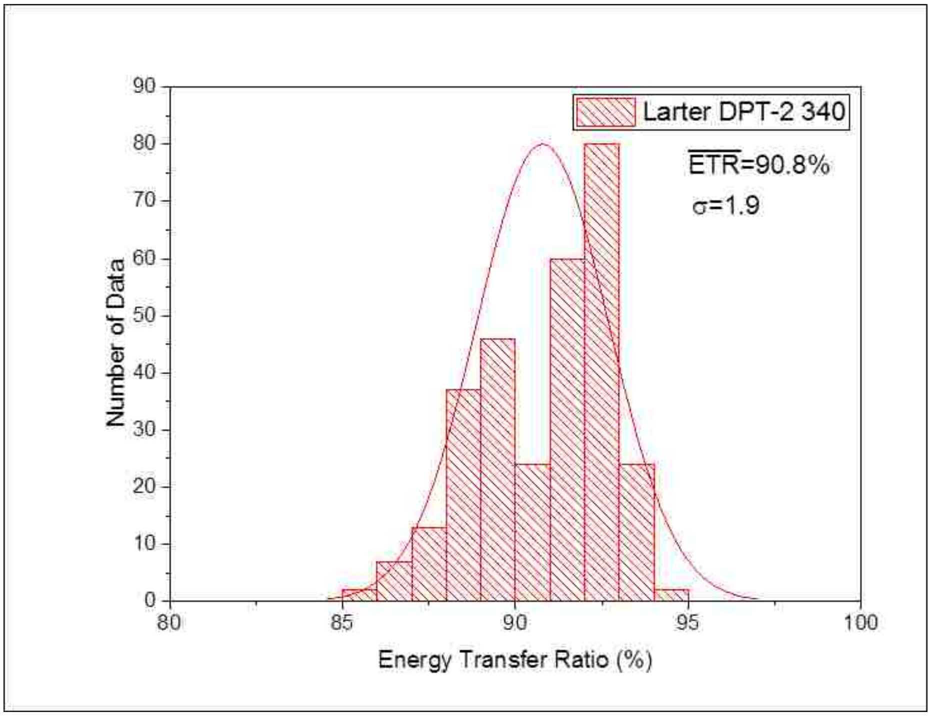

Figure 7-9. Frequency diagrams showing number of hammer drops and % ETR values for Larter Ranch DPT-2, heavy hammer (154.4 kg (340 lb.), dropped from 0.76 m, 30 in.).

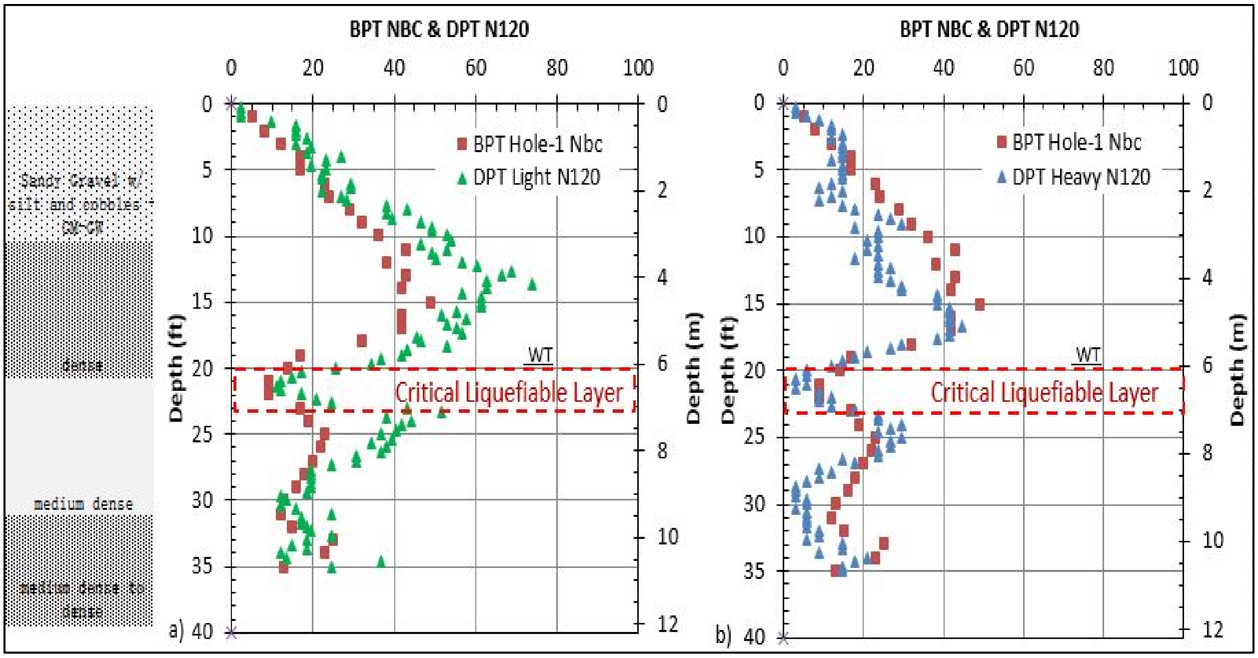

Figure 7-10. Plots of DPT N_{120} versus depth using (a) light 63.6 kg (140 lb.) hammer and (b) heavy 154.4 kg (340 lb.) hammer, after energy correction to account for lower hammer energies, compared to BPT for Larter Ranch Hole BPc-1. BPT data from Andrus (1994).

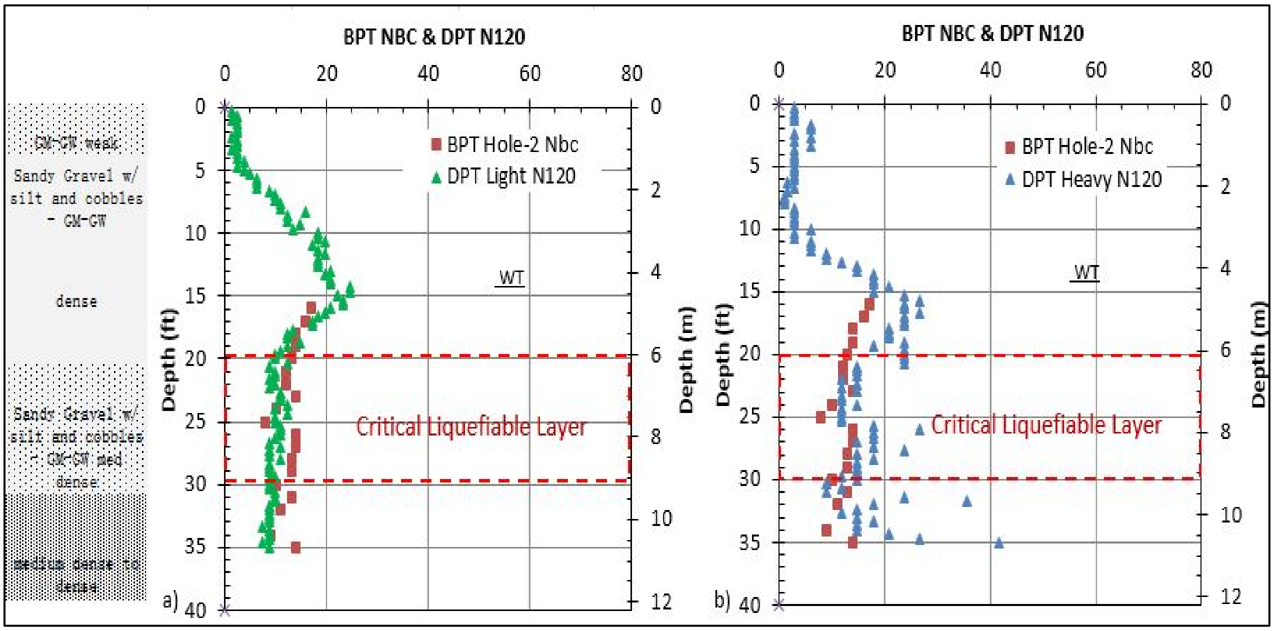

Figure 7-11. Plots of DPT N_{120} versus depth using (a) light 63.6 kg (140 lb.) hammer and (b) heavy 154.4 kg (340 lb.) hammer, after energy correction to account for lower hammer energies, compared to BPT for Larter Ranch Hole BPc-2. BPT data from Andrus (1994).

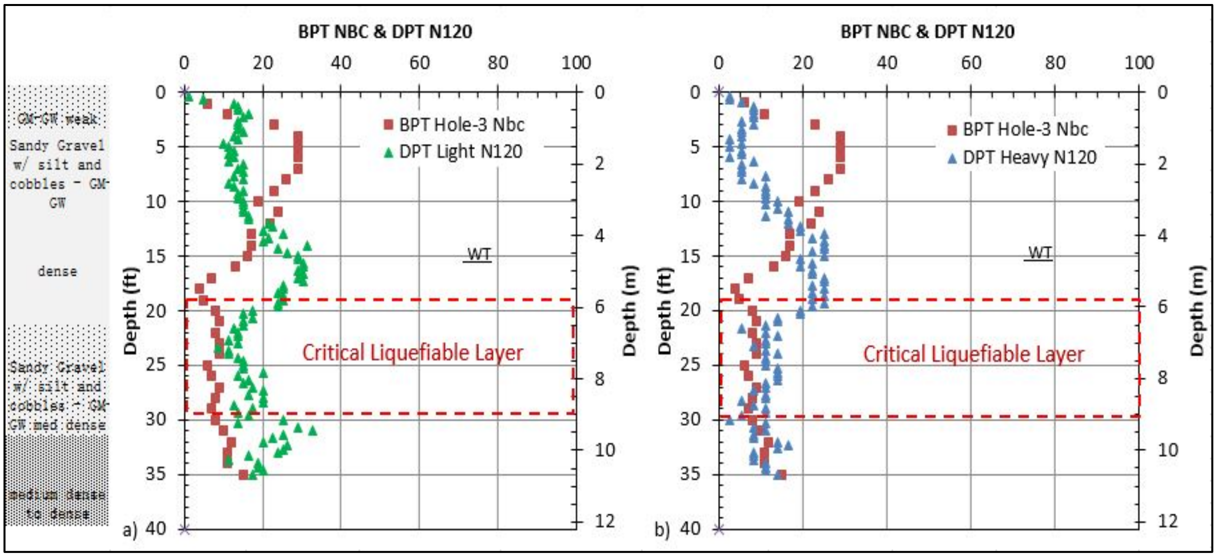

Figure 7-12. Plots of DPT N_{120} versus depth using (a) light 63.6 kg (140 lb.) hammer and (b) heavy 154.4 kg (340 lb.) hammer, after energy correction to account for lower hammer energies, compared to BPT for Larter Ranch Hole BPc-3. BPT data from Andrus (1994).

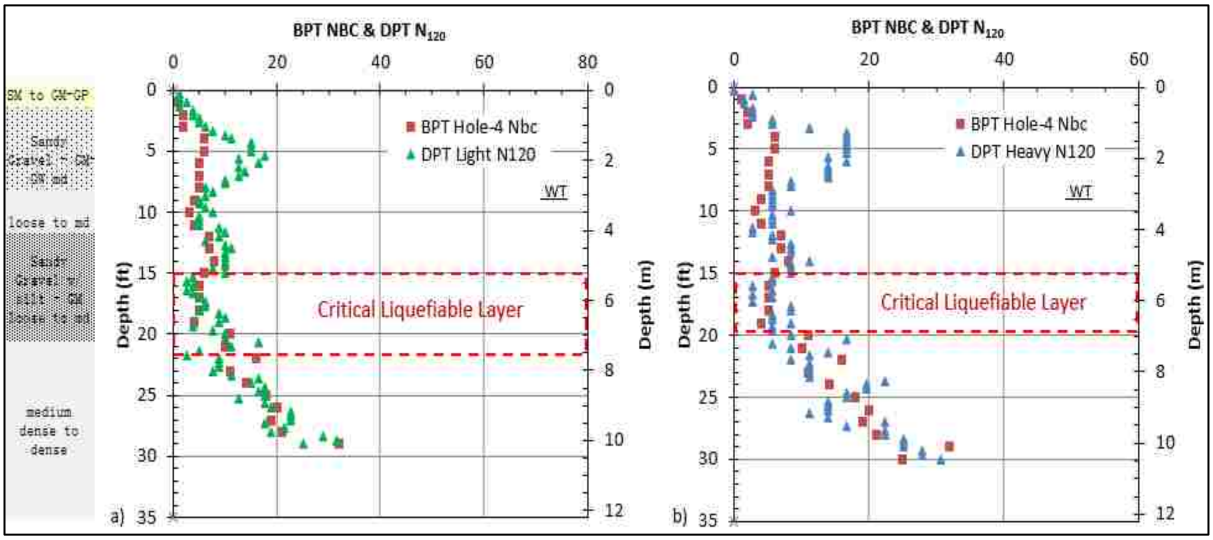

Figure 7-13. Plots of DPT N_{120} versus depth using (a) light 63.6 kg (140 lb.) hammer and (b) heavy 154.4 kg (340 lb.) hammer, after energy correction to account for lower hammer energies, compared to BPT for Larter Ranch Hole BPc-4. BPT data from Andrus (1994).

A comparison of the N_{120} blow counts obtained from the two different hammer energies after energy correction is provided in Figure 7-14 for each DPT sounding. The data points generally fall within a reasonable range of the 1:1 line. Results from additional testing will be necessary to define the error bands and to determine if adjustments in the energy correction factor may be necessary for depth or gravel particle size. The deviation in BPc-1 may indicate a problem with drill rod verticality being more than 5°.

7.8 CSR vs. DPT N'_{120}

Liquefaction potential was evaluated using both the DPT and BPT methods of analysis. In the case of the BPT, the N_{BC} value was converted to the equivalent sand SPT N_{60} using the Harder L. et al. (1986) correlation approach. The SPT N_{60} value was then corrected for overburden pressure effects using the equation proposed by Youd et al. (2001). The cyclic stress ratio, or CSR, was computed using equation 2-2 which was originally developed by Seed and Idriss (1971) where a_{max} is the peak ground acceleration of 0.33g. The CSR was adjusted for the Borah Peak earthquake using the magnitude scaling factor in equation 2-3.

The cyclic stress ratio, CSR, is plotted as a function of DPT-based N'_{120} for the zone between 4.6 to 9.1 m (15 to 30 ft.) below the ground surface for all four Becker holes at Larter Ranch in Figures 7-15 through 7-18.

The cyclic stress ratio, CSR, is summarized as a function of BPT-based $(N_1)_{60}$ for the zone between 4.6 to 9.1 m (15 to 30 ft.) below the ground surface in Figure 7-19 a). The adjusted triggering curve for the M_s7.3 Borah Peak earthquake is also plotted in Figure 7-19 for comparison. All the CSR values are sufficiently high to produce liquefaction for the range of blow counts within this layer. The adjusted triggering curve for the M_w7.3 Borah Peak earthquake is also plotted for comparison. Solid dots indicate liquefaction and open dots indicate a layer that had no liquefaction.

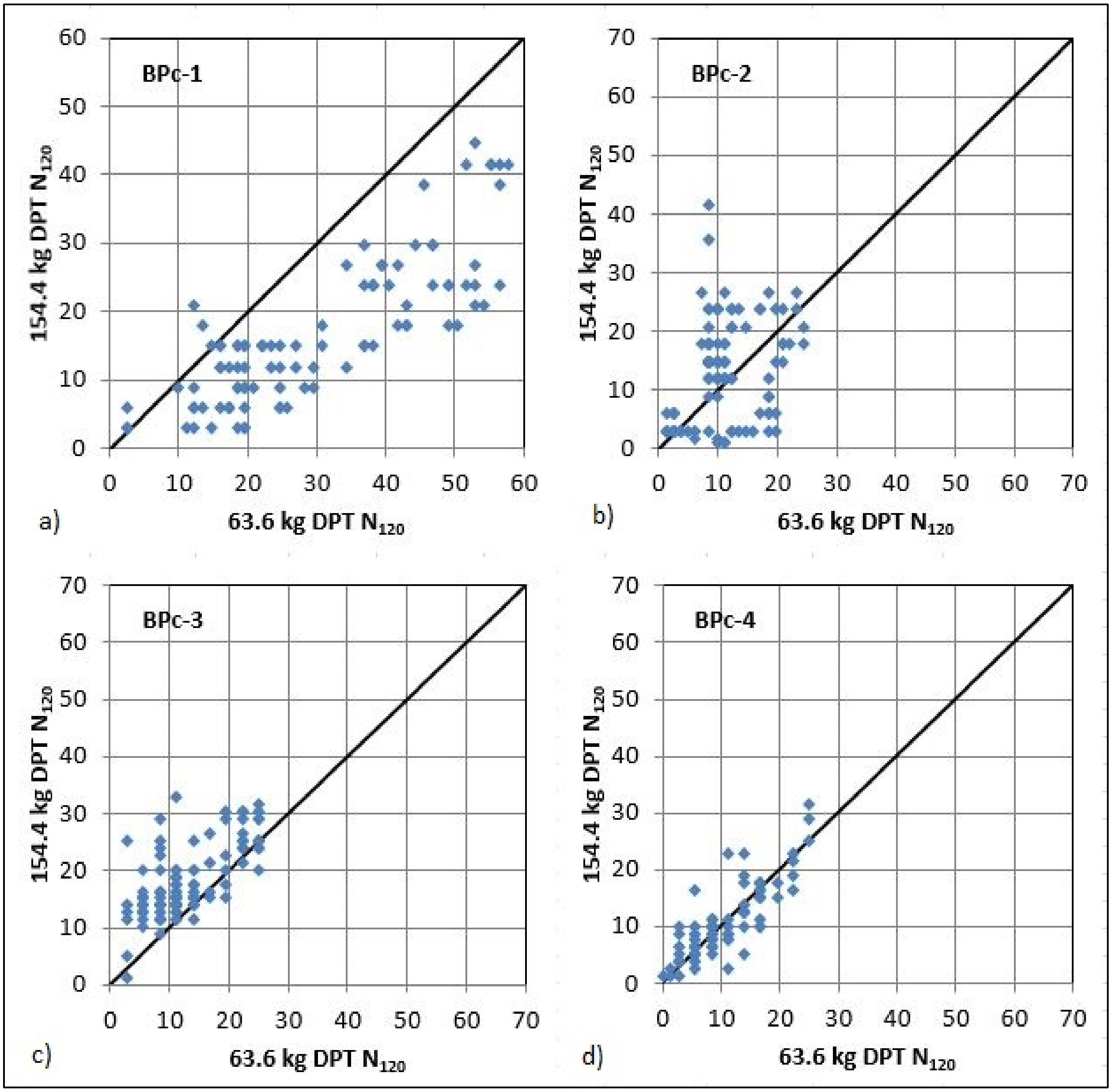

Figure 7-14. Comparison of DPT N_{120} obtained using the 63.6 kg (140 lb.) and the 154.4 kg (340 lb.) hammers after energy correction, for Larter Ranch a) Hole BPc-1, b) Hole BPc-2, c) Hole BPc-3, and d) BPc-4.

In the case of the DPT, the N_{120} value was first converted to N'_{120} using equation 2-1. Then the CSR was plotted as function of N'_{120} within the zone of liquefaction from 4.6 to 9.1 m (15 to 30 ft.) in Figure 7-19 b). The liquefaction triggering curve was based on the 30% probability curve develop by Cao et al. (2013) and shown in Figure 2-2.

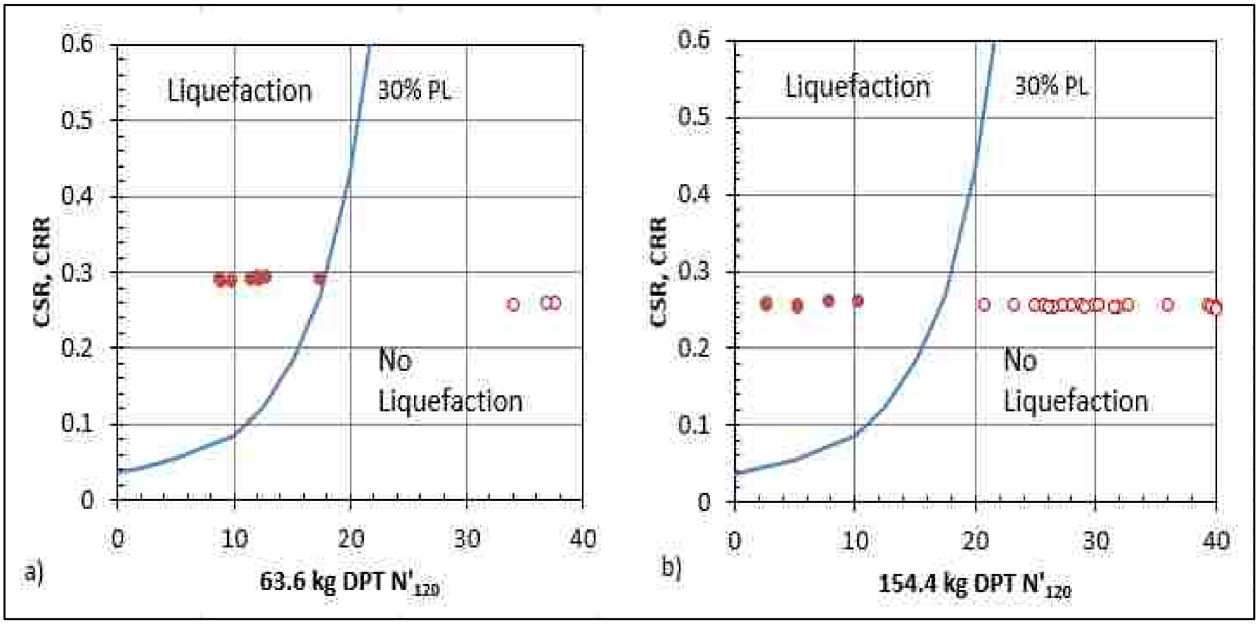

Figure 7-15. Comparison of CSR vs DPT N'120, using a) the 63.6 kg (140 lb.) hammer, and b) the 154.4 kg (340 lb.) hammer, for Larter Ranch Hole BPc-1. Solid dots are from the liquefiable unit and open dots are from the non-liquefiable unit.

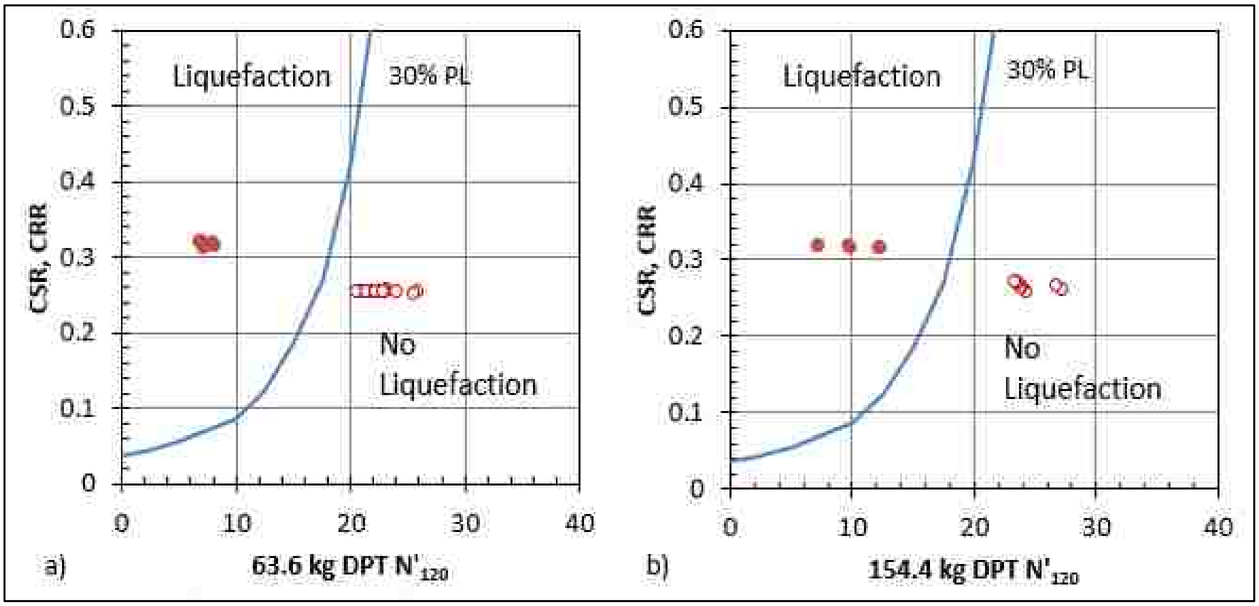

Figure 7-16. Comparison of CSR vs DPT N'120, using a) the 63.6 kg (140 lb.) hammer, and b) the 154.4 kg (340 lb.) hammer, for Larter Ranch Hole BPc-2. Solid dots are from the liquefiable unit and open dots are from the non-liquefiable unit.

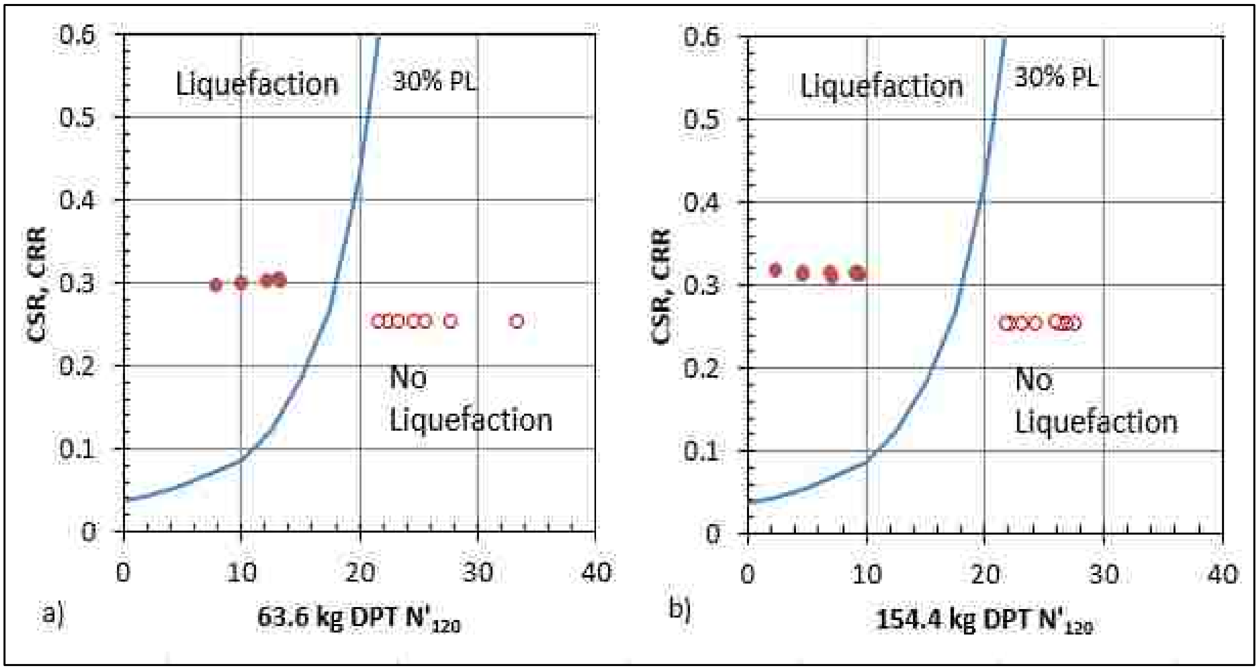

Figure 7-17. Comparison of CSR vs DPT N'120, using a) the 63.6 kg (140 lb.) hammer, and b) the 154.4 kg (340 lb.) hammer, for Larter Ranch Hole BPc-3. Solid dots are from the liquefiable unit and open dots are from the non-liquefiable unit.

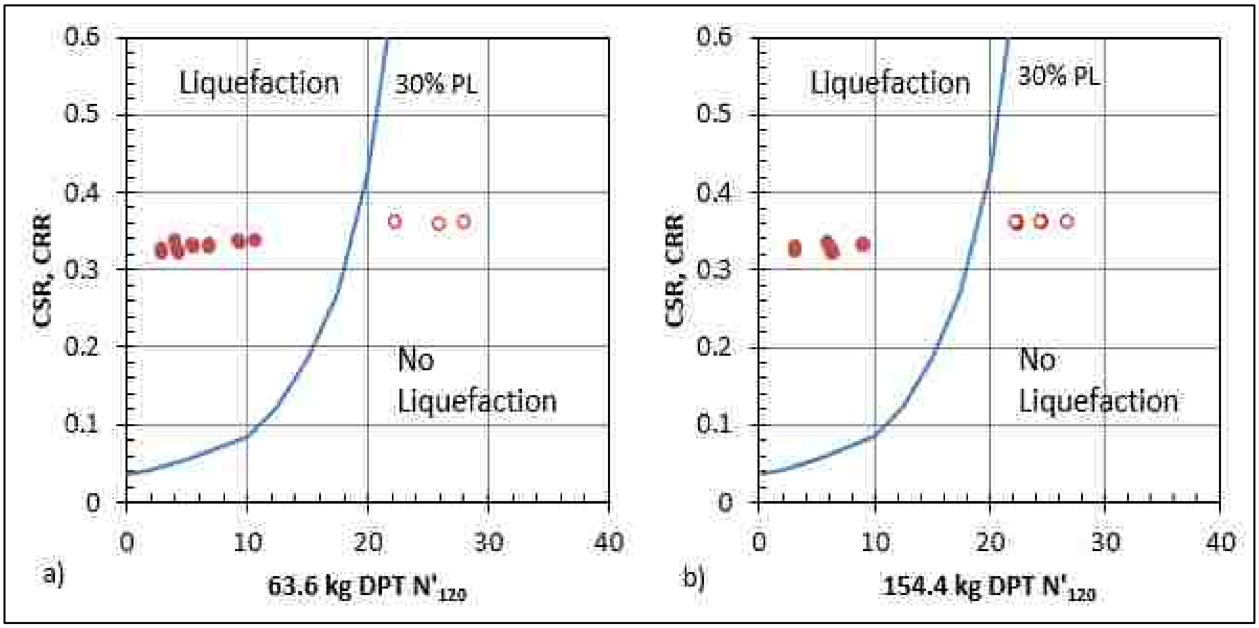

Figure 7-18. Comparison of CSR vs DPT N'120, using a) the 63.6 kg (140 lb.) hammer, and b) the 154.4 kg (340 lb.) hammer, for Larter Ranch Hole BPc-4. Solid dots are from the liquefiable unit and open dots are from the non-liquefiable unit.

The triggering curve in Figure 5-19 b) was adjusted upward using the magnitude scaling factor to account for the lower magnitude of the Borah Peak earthquake (M_w7.3) earthquake relative to the M_w7.9 Wenchuan China earthquake used to develop the DPT triggering curves.

The CSR-DPT pairs for each hole at Pence Ranch were averaged to obtain a single point that represents the entire data *set*, and plotted in Figure 7-20, in comparison with the triggering curve for 30% probability of liquefaction.

The CSR-DPT N'$_{120}$ points from Figure 7-19 b) are plotted in Figure 7-21 in comparison with the probabilistic liquefaction triggering curves (Cao et al. 2013), after magnitude scaling adjustments which shifted the measured CSR values slightly downward.

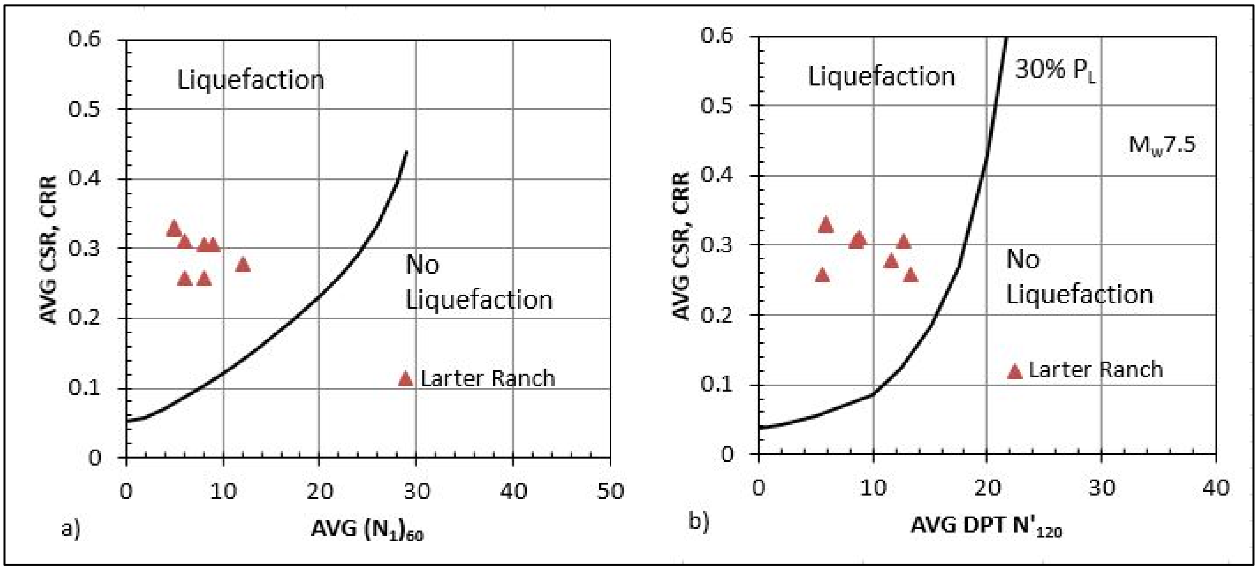

Figure 7-19. Comparison of a) CSR vs BPT-based $(N_1)_{60}$ data points for Larter Ranch in comparison with triggering curve, and b) CSR vs. DPT N'$_{120}$, data points for Larter Ranch in comparison with triggering curve for 30% probability of liquefaction (Cao et al. 2013) for M_w7.5 earthquakes.

In all cases the data pairs plot above the 50% probability of liquefaction curve which is consistent with the observed liquefaction at both sites. In Figure 7-22, a single data point is shown that represents the DPT N'$_{120}$ data set, as compared to the liquefaction triggering curve.

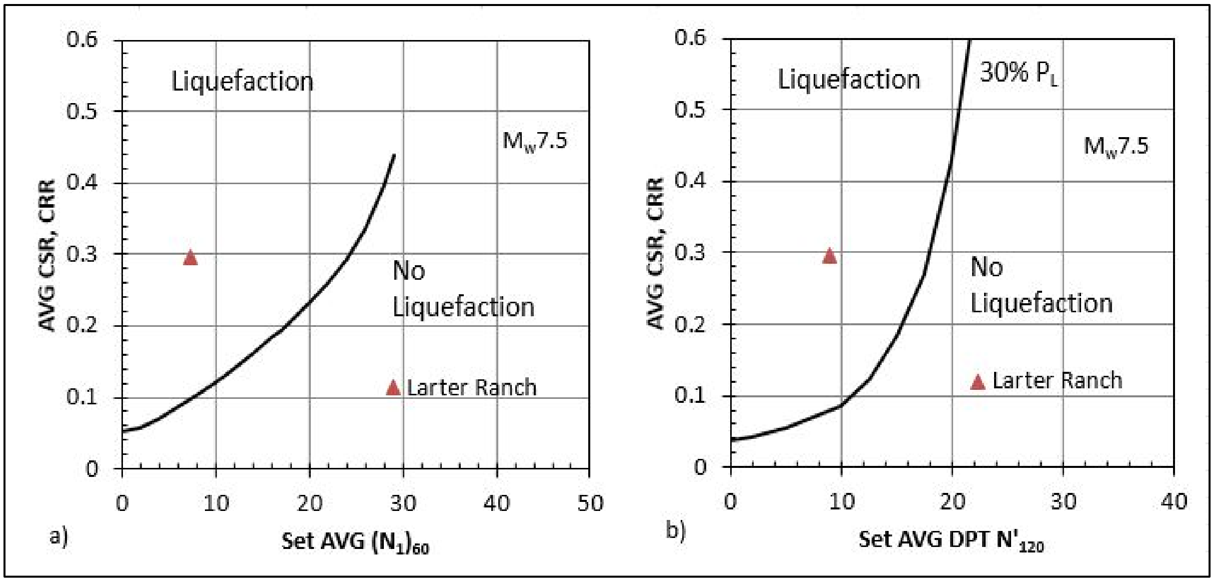

Figure 7-20. Comparison of the set average (Figure 7-21) for a) CSR vs BPT-based $(N_1)_{60}$ data points for Larter Ranch in comparison with triggering curve, and b) CSR vs. DPT N'_{120}, data points for Larter Ranch in comparison with triggering curve for 30% probability of liquefaction (Cao et al. 2013) for M_w7.5 earthquakes.

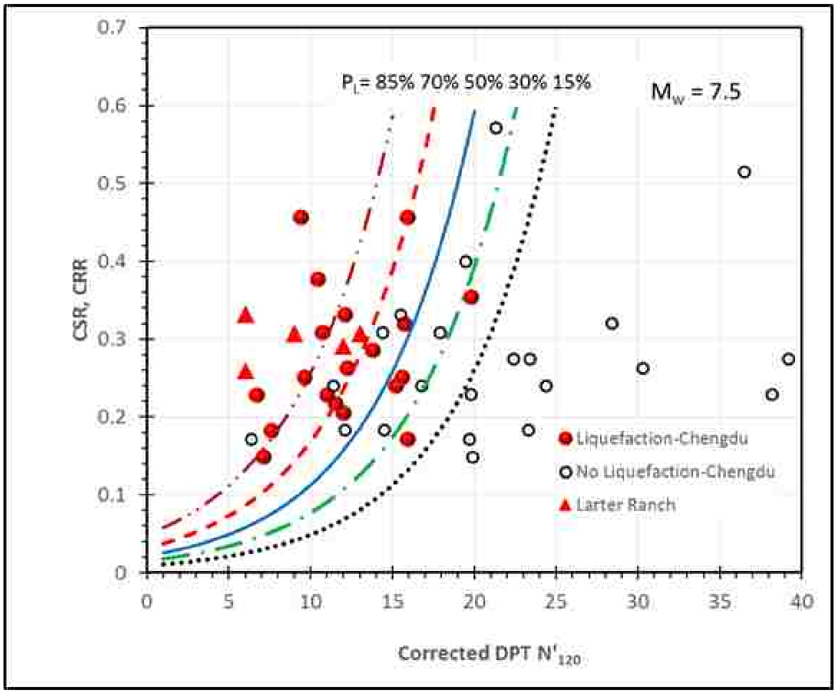

Figure 7-21. CSR vs. DPT N'_{120} curves for various probabilities of liquefaction in gravelly soils developed by (Cao et al. 2013) along with liquefaction/no liquefaction data points from Chengdu Plain. Points from Larter Ranch, Figure 7-21 b) are shown.

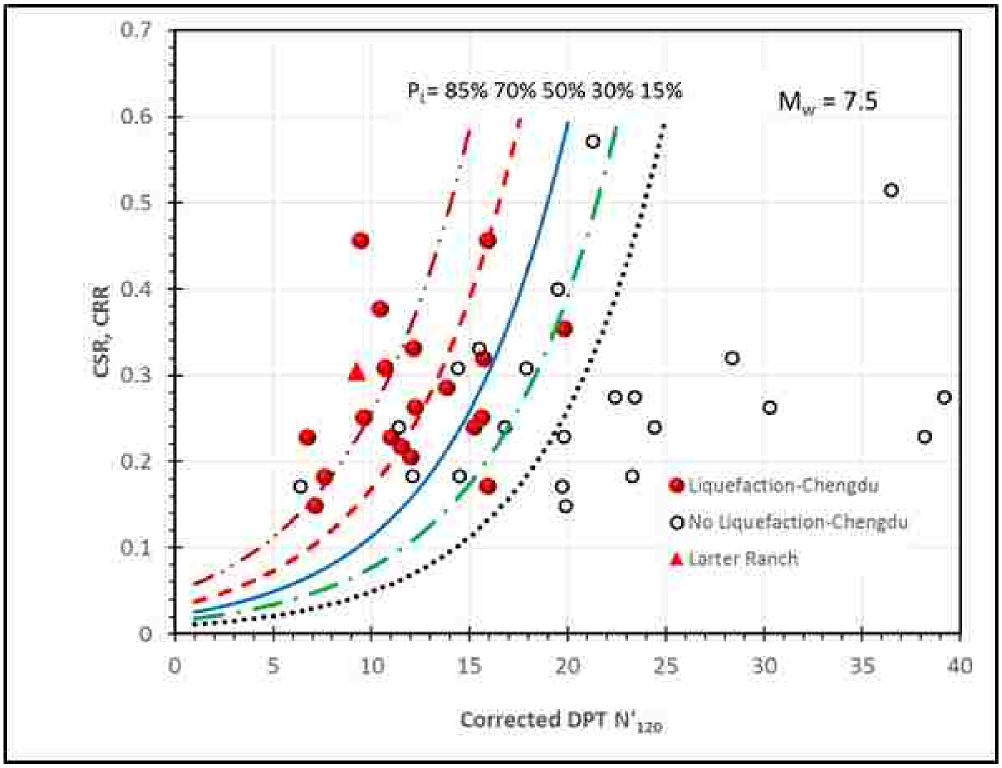

Figure 7-22. CSR vs. DPT N'$_{120}$ curves for various probabilities of liquefaction in gravelly soils developed by (Cao et al. 2013) along with liquefaction/no liquefaction data points from Chengdu Plain. Set point from Larter Ranch, Figure 7-20 is shown.

7.9 DPT vs. SPT

Similar to Chapter 6, a good indicator of the results of the study is the comparison of the DPT results with previous SPT results. Figures 7-23 through 7-26 illustrate the correlation between the SPT N_{60} and the DPT N_{120} at Larter Ranch.

The 2017 DPT vs. 1990 SPT data was plotted to gain an understanding of the correlation between the DPT soundings accomplished at the site and the SPT soundings. As can be seen from Figures 7-27 there is only weak correlation between the two. The R^2 value of 0.36 indicates a weak correlation, (R^2=1.0 is a perfect fit but growing weaker below 0.80 and very weak below 0.50). The slope of the regression equation would ideally be close to 1.0 for a perfect fit. 0.68 indicates a fairly weak correlation.

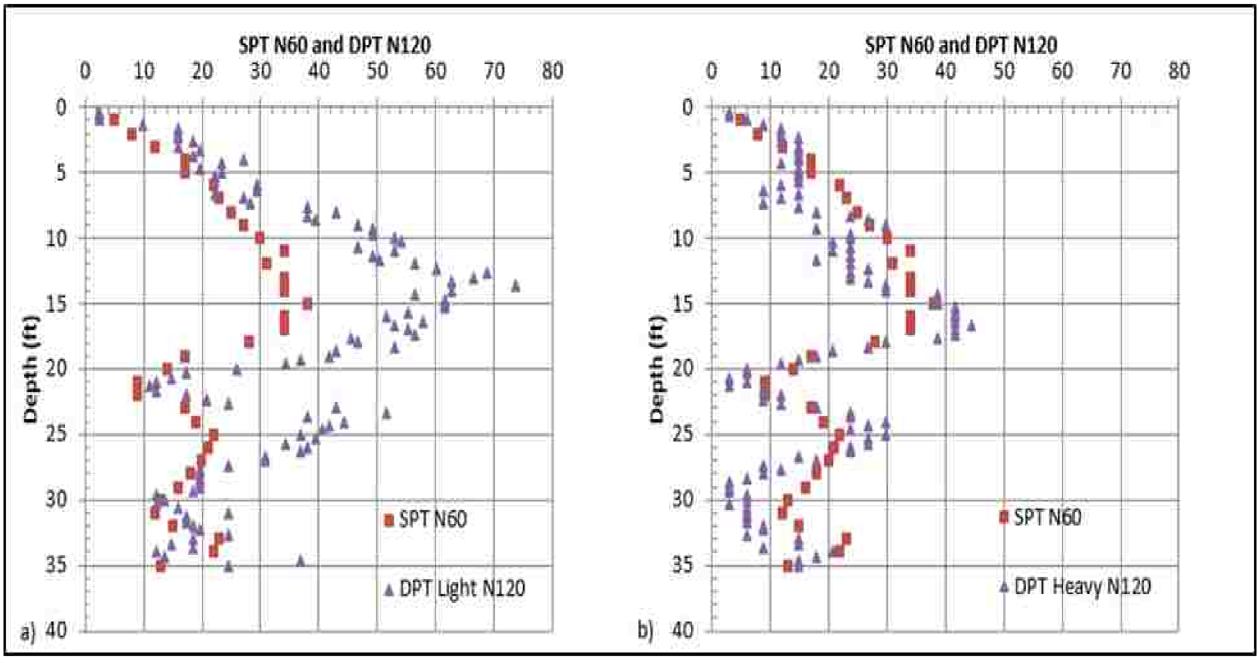

Figure 7-23. Correlation of DPT N_{120} and 1990 SPT N_{60} for Hole number BPc-1 given a) the light 63.6 kg (140 lb.) hammer and b) the heavy 154.4 kg (340 lb.) hammer at Larter Ranch.

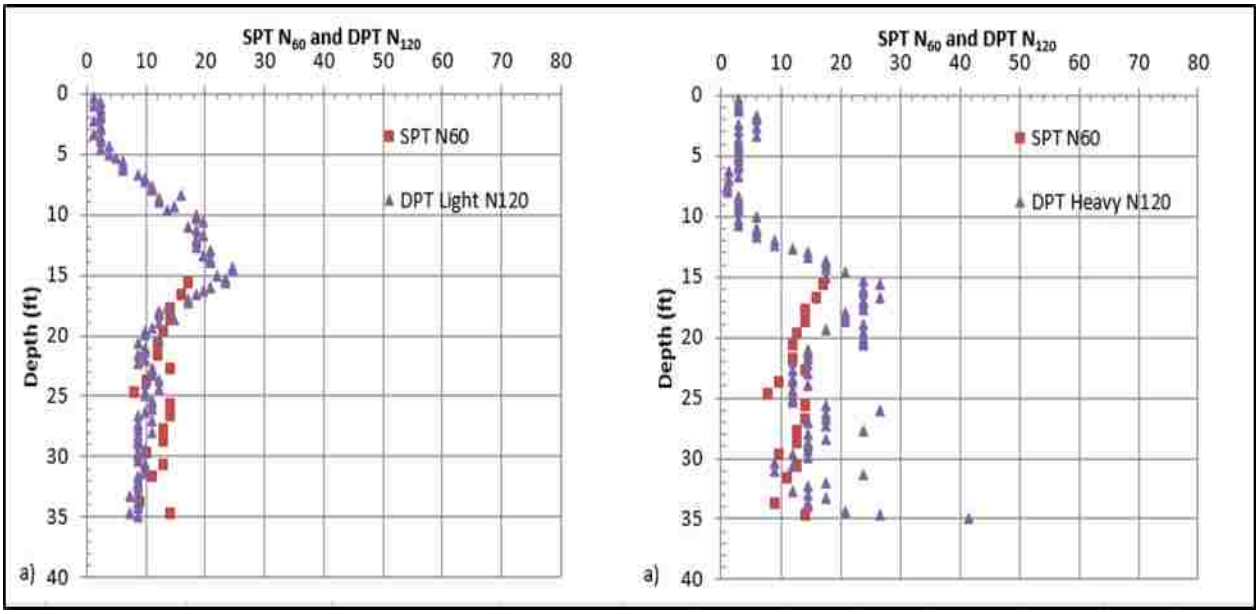

Figure 7-24. Correlation of DPT N_{120} and 1990 SPT N_{60} for Hole number BPc-2 given a) the light 63.6 kg (140 lb.) hammer and b) the heavy 154.4 kg (340 lb.) hammer at Larter Ranch.

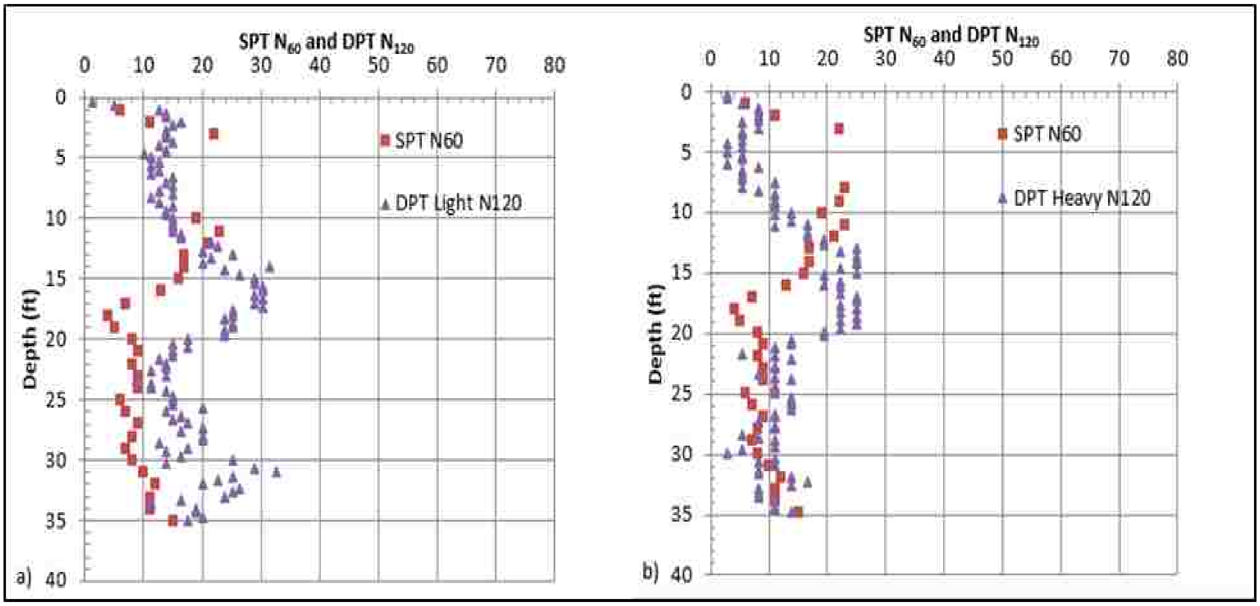

Figure 7-25. Correlation of DPT N_{120} and 1990 SPT N_{60} for Hole number BPc-3 given a) the light 63.6 kg (140 lb.) hammer and b) the heavy 154.4 kg (340 lb.) hammer at Larter Ranch.

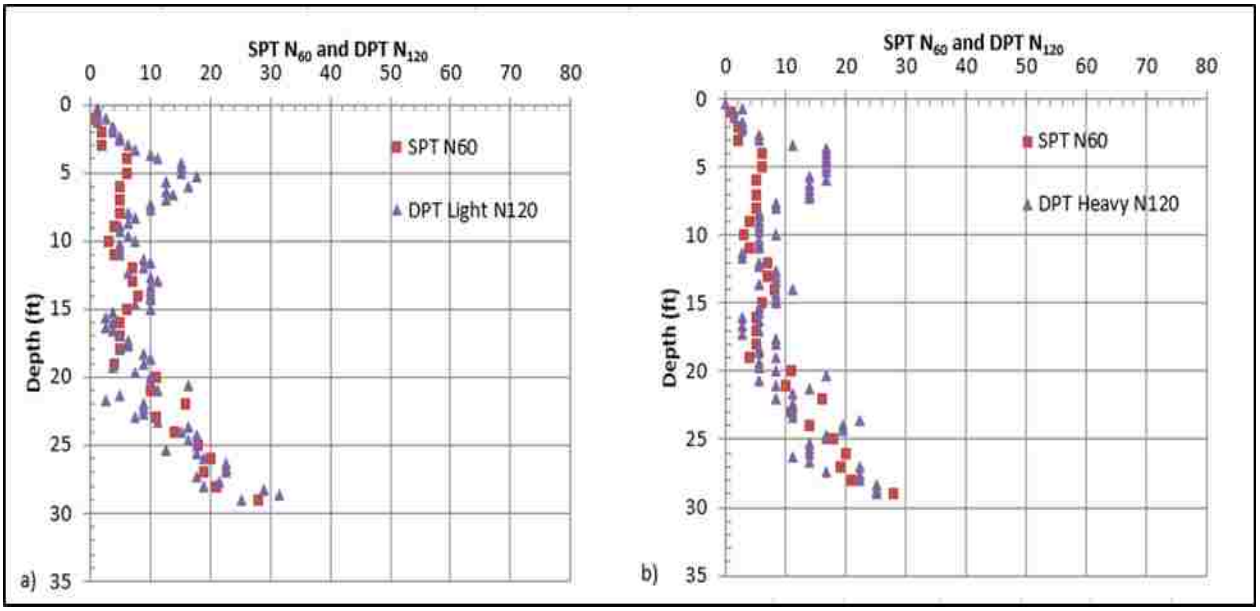

Figure 7-26. Correlation of DPT N_{120} and 1990 SPT N_{60} for Hole number BPc-4 given a) the light 63.6 kg (140 lb.) hammer and b) the heavy 154.4 kg (340 lb.) hammer at Larter Ranch.

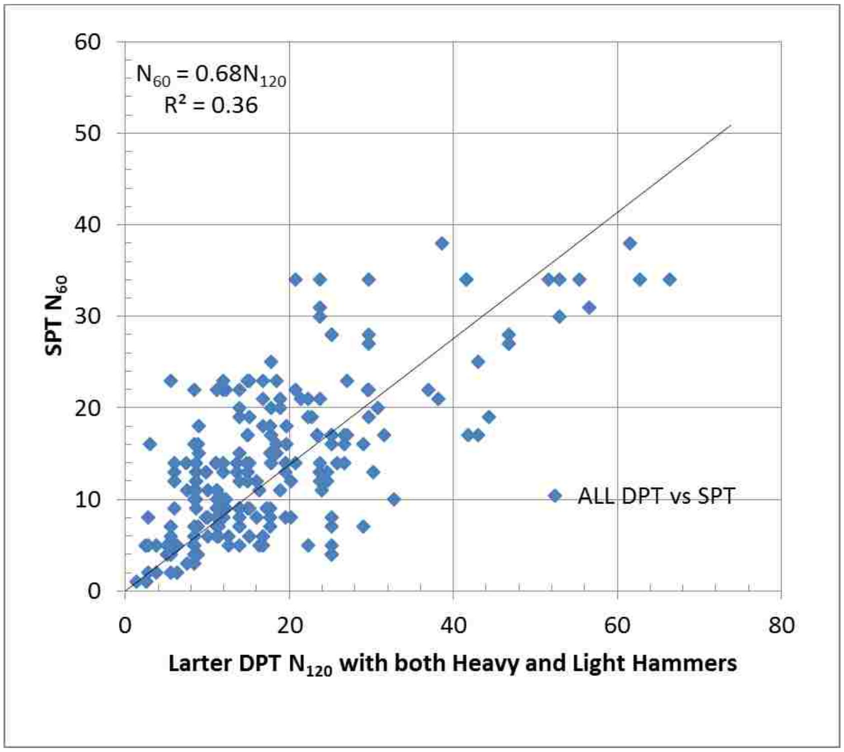

Figure 7-27. Plot comparing 2017 DPT N_{120}vs. 1990 SPT N_{60} for all holes at Larter Ranch using both the 63.6 kg (140 lb.) hammer, and the 154.4 kg (340 lb.) hammer.

7.10 Probability of Liquefaction vs. Depth from DPT

The probability of liquefaction P_L was calculated and plotted for all DPT holes at Larter Ranch and is shown in Figure 7-28 below. Equation 5-2, used for this calculation, is referred to as the probability function for liquefaction.

Cao et al. (2013) validated this equation using data from the Wenchuan event where 15 of 19 sites with surface liquefaction effects (79%) plotted on or above the P_L=50% curve of Figure 2-8, and 17 of 19 (89%) liquefaction sites plot on or above the P_L=30% curve. Similarly, 23 of 28 (82%) of sites exhibiting no surface liquefaction effects plot on or below the P_L=50% curve and 26 of 28 (93%) non-liquefaction sites plot on or below the P_L=70% curve. He states that this correlation is therefore generally verifiable for gravelly soils in the Chengdu plain shaken by the

2008 Wenchuan earthquake, and that this relationship may be used for other sites underlain by gravelly soils with soil types similar to those that liquefied during the Wenchaun quake.

The probability of liquefaction corresponds reasonably well with the calculated critical zone of liquefaction in Hole-1 of approximately 6.1 to 7.3 m (20 to 24 ft.), and also reasonably well in Hole-2 for the calculated critical interval between 6.1 and 9.1 m (20 and 30 ft.). For Hole-3 the calculated critical zone exists between 19 and 30 ft. and shows a good correlation. The probability of liquefaction for Hole-4 corresponds well with the critical zone of liquefaction from 4.6 to 6.7 m (15 to 22 ft.).

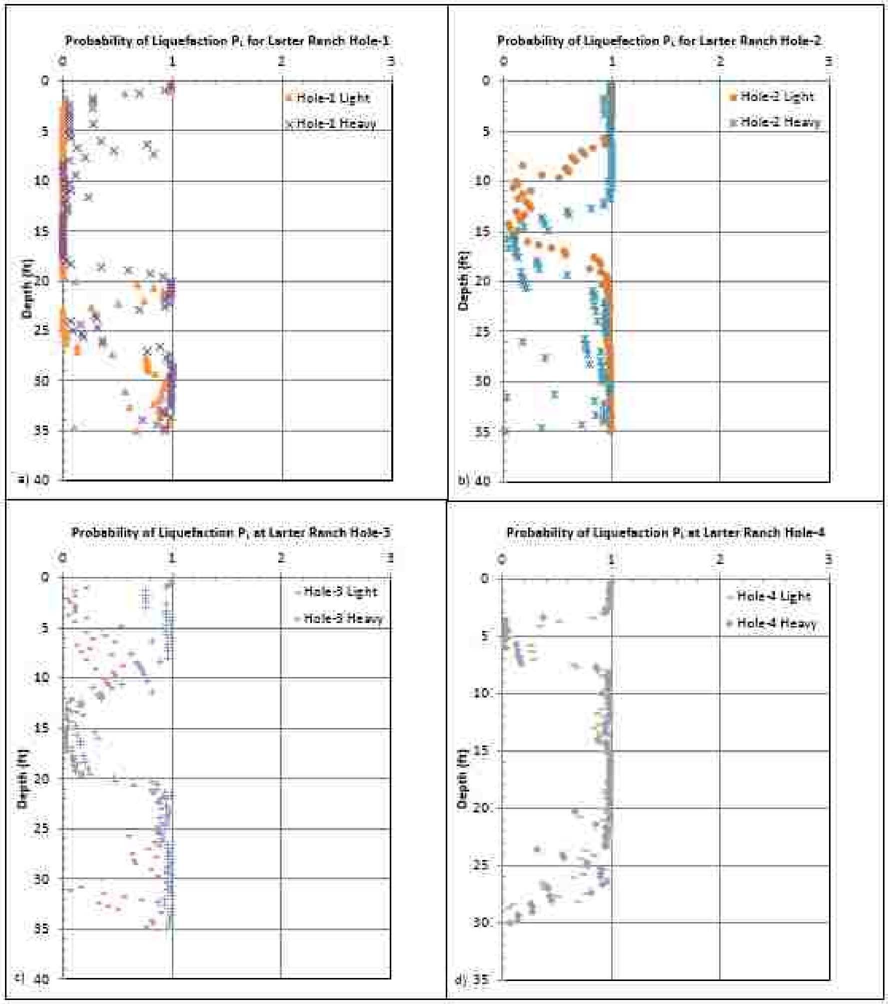

Figure 7-28. Probability of Liquefaction, P_L, for all holes at Larter Ranch, vs. Depth, from DPT. a) Hole-1, b) Hole-2, c) Hole-3, d) Hole-4.

8 DPT TESTING AT MILLSITE DAM, UTAH AND LIQUEFACTION ASSESSMENT

8.1 Introduction

Millsite Dam (39.09733°, -111.1877°) is located near Ferron, Utah about 45 miles south of Price, Utah. Because the foundation soils beneath the dam contain saturated sand and gravel layers that are potentially liquefiable, the Utah State Division of Water Resources carried out a drilling program at the dam in 2007 and 2010 to better define the potentially liquefiable layers. Figure 8-1 shows the general location of the dam.

Figure 8-1. Regional map of central Utah showing location of Millsite Dam.

In particular, the Becker hammer was used to evaluate the liquefaction resistance of the gravel layers. Becker penetration tests were performed at 8 locations along the downstream toe of the dam. Companion SPT soundings were accomplished alongside the Becker soundings. At 5 of these locations, DPT soundings were also performed about 1 m (3.28 ft.) away from the BPT and SPT soundings using the Chinese DPT cone tip.

BPT tests at Millsite Dam were carried out in 2009 by the Rollins, Brown, and Gunnel Engineering for the Utah State Division of Water Resources. Five total soundings were accomplished that generally agreed with the locations of the 2007/10 SPT holes. Becker Penetration Test number BPT09-1 was located near Standard Penetration Test SPT07-1 (and what would be Dynamic Cone Penetration Test number DCPT-1) as can been seen in Figure 8-2 below. BPT09-2 was located near SPT07-2 (and DCPT-2), BPT09-4 was located near SPT07-4 (and DCPT-3), BPT09-6 was located near SPT10-6 (and DCPT-4), and BPT09-5 near SPT10-9 (and DCPT-5). SPT tests at Millsite were carried out in 2007 and 2010 by the US Bureau of Reclamation. Figure 8-2 shows a general overhead view of the site and layout of the test sites.

In contrast to the Chinese DPT where applied energy was produced by a 120 kg (264 lb.) weight dropped from a 1 m (3.28 ft.) height, DPT soundings at Millsite in this study used two different hammers: (1) a 102.1 kg (225 lb.) donut hammer weight dropped from 0.91 m (36 in.) and (2) a 63.6 kg (140 lb.) automatic hammer dropped from a height of 0.76 m (30 inches). Energy transfer measurements were made with a Pile Driver Analyzer (PDA) for each hammer at the site. The donut hammer and the automatic hammer delivered 52% and 98% of the theoretical freefall energy, respectively. Remarkably, despite the different applied hammer energies, both hammers transferred approximately 53% of the energy transferred by the Chinese hammer. Figures 8-3 and 8-4 show conditions at the site.

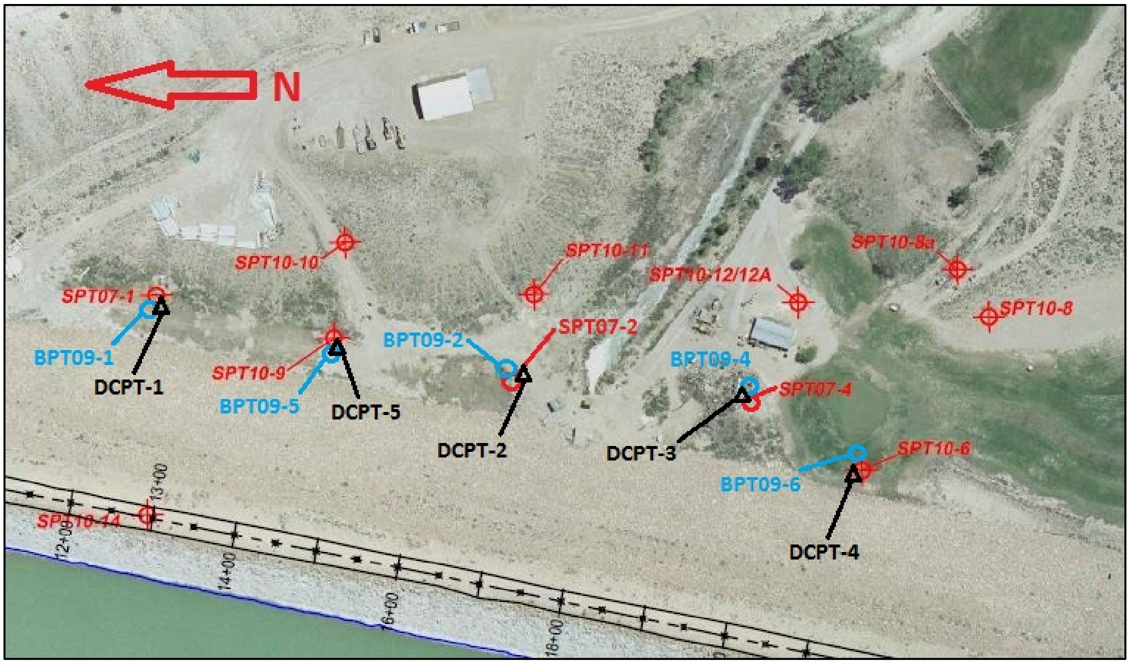

Figure 8-2. Plan view of layout at Millsite Dam site showing test sites from previous drilling and location of DPT soundings.

Figure 8-3. View of drill rig used at Millsite Dam looking north along the downstream toe of the dam, January 2015.

Figure 8-4. View of conditions and topography at Millsite Dam, looking south along the downstream toe of the dam, January 2015.

To account for these energy differences, the measured blow counts were corrected to obtain N'_{120} values using the equation:

$$N'_{120} = (N'_{120})_F(E_F/E_{CDPT}) \qquad 8\text{-}1$$

where $(N'_{120})_F$ is the uncorrected blow count obtained with the hammer in the field, E_{CDPT} is the energy delivered by the Chinese DPT and E_F is the energy delivered by the hammer in the field. This linear adjustment factor is based on the energy correction approach used for the SPT hammer. In this case, the energy adjustment factor increased the measured blow counts by a factor of 1.89.

8.2 Soil Description

Drill logs collected by the Natural Resource Conservation Service (NRCS) in 2007 describe the soil strata at Millsite Dam as follows:

Near DPT-1: A review of the drill logs for SPT sounding SPT07-01, accomplished in November of 2007, describe the top three feet of ground as FILL, consisting of Clay (CL), soft, low to medium plasticity with 75% fines and 25% fine to medium grained sand. This layer is underlain by several alternating thin layers of Sand (SP to SP-SM) and Clay (CL), each about 0.3-0.5 m (12-18 in.) thick, extending to a depth of about 2.3 m (7.5 ft.). These thin sand layers are described as loose and moist, approximately 85%-90% medium to fine grained, with 10%-15% non-plastic fines. The thin Clay layers are described as soft and moist, with 75% low to moderately plastic fines and 25% fine Sand. At a depth of 2.3 m (7.5 ft.), an approximately 12 inch thick layer of Gravel (GM) was encountered, and identified as Alluvium (Qal). This gravel layer is described as sandy, silty, medium dense and wet, with 15% non-plastic fines, 60% coarse to fine gravel, and 25% coarse to fine sand with 0.09 m (3.5 in.) cobbles. The soil down to this depth was determined to be the critical liquefiable layer.

Below this gravel layer is an approximately 0.6 m (2 foot) thick layer of Sand (SP), extending to a depth of 11 feet. This layer is described as gravelly, medium dense, and wet, with 10% non-plastic fines 50% coarse to fine sand, and 40% coarse to fine gravel with a maximum diameter of 7.6 cm (3 in.).

From 3.35 m (11 ft.) to 5.7 m (18.6 ft.) there is a Gravel (GP-GM) layer that is described as sandy, medium dense, and wet, with an estimated 10% non-plastic fines, 60% coarse to fine poorly-graded gravel to maximum 6.3 cm (2.5 in.) diameter, and 30% coarse to fine sand. At a depth of 4.14 m (13.6 ft.) the fines increase to 10-15%, the gravel content stays at about 60%, and the coarse to fine sand decreases to 25%, with 5% cobbles appearing, up to 8.0 cm (3.5 in.) in diameter. At a depth of 4.9 m (16.1 ft.) in this gravel layer, the sand increases to 30%, the gravel stays at 60%, and cobbles increase to 25% with an 11.4 cm (4.5 in.) maximum diameter. At 5.15 m (16.9 ft.) the sand decreases to 15% and the gravel content increases to 70% with a 6.3 cm (2.5 in.) maximum diameter, and the fine content remaining at 10%.

From 5.7 m (18.6 ft.) to 6.4 m (21.1 ft.) there is a Sand (SM) layer that is described as very dense, moist to wet, with 15% non-plastic fines, 45% coarse to fine sand, and 40% coarse to fine gravel.

Near DPT-2: A review of the drill logs for SPT sounding SPT07-02, also accomplished in November of 2007, describe the top 1.2 m (4.2 ft.) as EMBANKMENT MATERIALS consisting of Sand (SM), silty with some gravel, medium dense, and slightly moist. Non-plastic fines were estimated at 15%, very fine to coarse grained sand at 75%, and 10% fine to coarse grained gravel with minor (5%) cobbles having a maximum diameter of 7.6 cm (3 in.).

From 1.2 m (4.2 ft.) to 2.8 m (9.2 ft.) the layer is described as Sand (SP-SM), medium dense, slightly moist, with 10% non-plastic fines, 70% fine to coarse grained sand, and 20% fine to coarse grained gravel. At a depth of 1.7 m (5.7 ft.), 5% cobbles are noted with a maximum diameter of 10.1 cm (4 in.). At 2.0 m (6.7 ft.) the sand continues with 10% non-plastic fines but the sand content increases to 75%, and the gravel decreases to 15%.

At a depth of 2.8 m (9.2 ft.), the log calls out ALLUVIUM consisting of Gravel (GP-GM) that extends to a depth of more than 12.5 m (41 ft.). The gravel is described as medium to very dense and wet, with 10% non-plastic fines, 60% fine to coarse grained gravel, and 30% fine to coarse grained sand. At 3.3 m (10.7 ft.), and again at 4.0 m (13.2 ft.), the drill log notes that 5% cobbles are present with a maximum diameter of 10.2 cm (4 in.) and 15.2 cm (6 in.), respectively. At 4.4 m (14.4 ft.) a 7.6 cm (3-in.) thick layer of fine sand is noted, and again at 4.8 m (15.6 ft.), with the thickness decreasing to 5.1 cm (2 in.). At 4.8 m (15.7 ft.) the gravel layer continues with 10% cobbles noted, and having a maximum diameter of 17.8 cm (7 in.). At 5.2 m (16.9 ft.) a 10.2 cm (4 in.) thick layer of fine sand is noted containing 20% small rounded gravel. At 5.4 m (17.8 ft.) the gravel layer continues with 15% cobbles having a maximum diameter of 20.3 cm (8 in.).

From 5.9 m (19.2 ft.) to 6.1 m (20.0 ft.), a Sand (SP-SM) layer is described as moderately dense and wet with 10% non-plastic fines, 60% fine to coarse grained sand, and 30% fine to coarse grained gravel.

At a depth of 6.1 m (20 ft.) the Gravel (GP-GM) layer continued and is described as very dense, wet with 15% non-plastic fines, 55% fine to coarse grained gravel, and 30% fine to coarse grained sand, with 5% cobbles having a maximum diameter of 12.7 cm (5 in.). The sample recovered from this depth contained soft sandstone fragments. At 7.1 m (23.2 ft.) the cobble fractioned changed to 10.2 cm (4 in.) maximum diameter. At 7.4 m (24.2 ft.) the gravel content increased to 75%, and the sand content decreased to 15%. At 7.8 m (25.7 ft.) the cobble fraction increased back to 12.7 cm (5 in.) maximum diameter. At 8.9 m (29.2 ft.) the gravel content increased to 80% and the sand content decreased to 10%. At 9.2 m (30.1 ft.) the soil is described as wet with 10% non-plastic fines, 85% fine to coarse grained gravel, and 5% fine to coarse grained sand with 15% cobbles having a maximum diameter of 12.7 cm (5 in.). At 9.7 m (31.7 ft.) the gravel content decreased to 70% and the sand content increased to 20%.

At 10.4 m (34.2 ft.) the gravel content increased to 75% and the sand content deceased to 15%. From there to a depth of 12.7 m (41.8 ft.), the gravel and sand contents varied up and down by 5% but the fines content stayed 10%. The cobble volume and maximum diameter vary slightly.

Near DPT-3: A review of the drill logs for SPT sounding SPT07-04, also accomplished in November of 2007, describe the top 1.1 m (3.5 ft.) as FILL, consisting of Sand (SC), slightly moist with 15% low to non-plastic fines, 60% fine to coarse grained sand, and 25% fine to coarse grained gravel, with organic material in upper 0.3 m (1 ft.). At a depth of 1.1 m (3.5 ft.) moderately hard sandstone cobbles and boulders were noted.

At a depth of 1.8 m (5.8 ft.) the soil changed to ALLUVIUM, and is described as Sand (SM), dry with 15% low to non-plastic fines, 65% fine to coarse grained sand, and 20% fine to coarse grained gravel. This sand changed to Sand (SC) at a depth of 2.5 m (8.2 ft.), also with 15% low to non-plastic fines, 65% very fine to coarse grained sand, and 20% fine to coarse grained gravel, with traces of cobbles to 10.2 cm (4 in.) maximum diameter. From 2.5 m (8.2 ft.) to 3.4 m (11.2 ft.) the Sand changed back to (SM) and is described as dry, with 10% non-plastic fines, 65% very fine to coarse grains sand, and 25% fine to coarse grained gravel with 15% cobbles having a maximum diameter of 15.2 cm (6 in.). At 5.1 m (16.7 ft.) the fines content remained at 10%, the sand content decreased to 60%, and the gravel content increased to 30%, with the 15% cobble fraction being described as soft to hard and a maximum diameter of 17.8 cm (7 in.). A large sandstone cobble was noted at the bottom of the sample.

Near DPT-4: SPT sounding SPT10-06, accomplished in June of 2010, described the top 2.1 m (7.0 ft.) as FILL, consisting of Sand (SM), silty and gravelly with cobbles, damp and dense. At 2.1 m (7.0 ft.) the sand changed to (SP) and is described as very dense, fine to medium grained, with minor gravel. Drill logs noted that the sample at 2.1 m (7.0 ft.) was driven into a large limestone cobble with possible sandstone cobble beneath. At a depth of 3.1 m (10 ft.)

gravel was increasing from above, was dense and fine to coarse grained, and the sample was driven through an 20.2 cm (8 in.) piece of sandstone.

At a depth of 4.3 m (14 ft.) the soil profile changed to ALLUVIUM, and is described as Sand (SP), gravelly, very dense to hard, and fine to medium grained with grey limestone and brown cherty limestone gravel pieces ranging to cobble size. At 5.2 m (17 ft.) the soil was described as gravelly and dense. This layer continued down to 6.7 m (22 ft.) where it was described as gravelly, layered, fine to medium grained, clean-of alluvial origin with fine round gravel and scattered larger gravel pieces to 20.3 cm (8 in.) in diameter.

Near DPT-5: SPT sounding SPT10-09, accomplished in May of 2010, described the top 0.7 m (2.5 ft.) as FILL/SLOPE WASH, consisting of Sand (SM), silty, medium dense very fine to fine grained, moist to wet and streaked with brownish yellow organics. At a depth of 1.5 m (5 ft.) the logs noted the soil becoming wet and loose with medium firm to stiff clay in tip of sampler, 1.5 m to 1.9 m (5 to 6.3 ft.). From 1.9 m (6.3 ft.) to 2.6 m (8.5 ft.) a band of Clay (CL) is described as sandy, soft to firm, organic, wet, dark grey, with charcoal fragments, and rock in tip of sampler from 2.3 m (7.5 ft.) to 2.6 m (8.5 ft.).

At 2.6 m (8.5 ft.) the strata changed to ALLUVIUM, and is described as Sand (SP), with minor gravel, medium dense, fine to coarse grained and wet. At 3.1 m (10 ft.) the sand is described as loose to medium dense, with the sample driven into sandstone from 3.1 m (10 ft.) to 3.5 m (11.5 ft.).

At 4 m (13 ft.) the layer changed to Sand (SP/GP), gravelly, medium dense, fine to coarse grained with rounded gravel pieces to 5.1 cm (2 in.) in diameter, and wet. At 4.6 m (15 ft.) the log states that the sand is becoming dense, with some clay in matrix- SP/SC with gravel, gravel sized pieces of sandstone in tip of sample from 4.6 m (15 ft.) to 5.0 m (16.5 ft.).

At a depth of 5.8 m (19 ft.) the log indicated that the strata turns to Sand (SM), silty, loose to medium dense and wet, and continues to a depth of 7.3 m (24 ft.) with a note at 6.7 m (22 ft.) indicating interlayering with yellowish brown sand and gravel pieces of sub-round cherty limestone to 5.1 cm (2 in.) diameter.

From 7.3 m (24 ft.) to 8.1 m (26.5 ft.) the logs call out Sand (SP/GP), gravelly, dense, with gravel pieces of sub-round cherty limestone to 5 cm (2 in.) in diameter.

The blow counts from the BPT and DPT correlated reasonably well for gravels using the automatic hammer, but poor correlation was obtained with the donut hammer. Liquefaction resistance for the BPT and DPT soundings were also in reasonable agreement for gravel layers suggesting that the DPT can provide liquefaction hazard evaluations more economically than the BPT using direct correlations with field performance.

In addition, analyses indicated that separate correlations were necessary for DPT tests in sand and in gravel layers, even with the automatic hammer. For example, for a given DPT N'_{120} the BPT $(N_1)_{60}$ in sand was typically about 65% of the value in gravel. This result suggests that the correlation may be dependent on the maximum grain size at least for the lower energy levels used in this study. Therefore, the correlation between liquefaction resistance and DPT N'_{120} proposed by (Cao et al. 2013) should probably be restricted to gravel layers at present.

A comparison of liquefaction resistance obtained from the BPT and DPT evaluations within (a) gravel layers and (b) sand layers was investigated. In most of the holes the BPT soundings indicated that the $(N_1)_{60}$ was higher than 29 meaning the soil is non-liquefiable. This indicates that the CRR would be greater than 0.5. Therefore, the CSR is plotted as 0.5 in this figure as a reference point. It should be noted that the 30% probability DPT CSR's are generally considerably higher than the 0.5 boundary throughout the majority of the profile consistent with the BPT results in the gravel layers. However, some relatively thin 0.3- 0.6 m (12 -24 in.)-thick (potentially liquefiable layers are identified by the DPT). The consistency of the layer across the site suggests that the identification is accurate. These results also indicate that the DPT with values at 0.10 m (4 in.) intervals may provide better resolution for thin layers than the BPT at 0.3 m (12 in.). Similar problems have been previously reported by Harder (1997) for thin silt layers.

8.3 Identification of Liquefiable Material

At the location of DCPT sounding number 1 (DCPT 1 on Figure 8-2), situated at the northern-most end of the site, approximately 161 m (539 ft.) north of the dam outlet, potentially liquefiable layers exist from the ground surface down to a depth of 2.4 m (8 ft.), and again at a depth of 3.7 m (12 ft.) with a thickness of 30 cm (1 ft.)

At the location of DCPT sounding number 2 (DCPT 2 on Figure 8-2), located approximately 140 m (460 ft.) to the south of DCPT 1, or 25 m (84 ft.) north of the outlet, no potentially liquefiable layers exist.

At the location of DCPT sounding number 3, located approximately 59 m (193 ft.) south of the outlet, potentially liquefiable layers exist between a depth of 2.4-3.4 m (8-11 ft.), and again at a depth of 7.9-8.2 m (26-27 ft.).

At the location of DCPT sounding number 4, located approximately 107 m (350 ft.) south of the outlet, a potentially liquefiable layer was identified by BPT tests at a depth of 18.3-19.5 m (60-64 ft.). For DCPT sounding number 4, the sounding met refusal at very shallow depths even after moving the drill rig 3 times. Therefore, DCPT 4 will not be used for the purposes of this study.

At the location of DCPT sounding number 5, located between DCPT 1 and DCPT 2, and approximately 94 m (307 ft.) north of the outlet, potentially liquefiable layers exist at a depth of 0.6-2.4 m (2- 8 ft.), and at 4.3 m (14 ft.).

8.4 Identification of Most Likely Failure Zone

Although there has not been an occurrence of liquefaction at the site, it would be generally accepted that if liquefaction occurred due to an earthquake, the potentially liquefiable layer identified by the testing would occur near at a depth of about 0.91-3.3 m (3-11 ft.).

8.5 DPT Soundings

For this study, two companion DPT soundings were performed within about a meter of each of four previous BPT soundings using a CME 85 drill rig with the capability of using two different hammer energies. In one sounding the DPT cone was advanced using a conventional automatic SPT (light) hammer with a weight of 63.6 kg (140 lb.) dropped from a height of 0.76 m (30 in.). The second sounding was performed using a 102.1 kg (225 lb.) automatic hammer (heavy) with a drop height of 0.91 m (36 in). Hammer energy measurements were made using an instrumented rod section and a PDA device for each hammer weight to determine the energy transferred to the drill rod. The ratio of the measured energy to the theoretical drop energy is referred to as the Energy Transfer Ration (ETR). Histograms showing the frequency distribution of the Energy Transfer Ratio are provided in Figure 8-5 and 8-6 for the light and heavy hammers, respectively. The mean ETR for the light hammer was 79.9% with a standard deviation of 1.5, while the mean for the heavy hammer was 52.5% with a standard deviation of 5.8. These standard deviation values are somewhat lower than the 6.9 to 8.6 values measured with the DPT hammers in China. This improvement in precision is likely associated with the automatic hammer drop mechanism used in the US in comparison to the free-fall mechanism used in China as described by Cao et al. (2013).

Because the delivered energies are less than the energy typically supplied by a Chinese DPT hammer, it was necessary to correct the measured blow count downward using the equation 5-1. Cao et al. (2013) found that the measured energy from a typical Chinese DPT was about 90% of the theoretical drop energy. Equation 5-1 follows the pattern for energy correction recommended for SPT testing by (Seed et al. 1985). The ratio of energy actually delivered divided by the energy delivered by the Chinese DPT hammer was 0.42 and 0.93 for the 63.6 kg (140 lb.) (light) and 154.4 kg (340 lb.) (heavy) hammers, respectively.

Frequency diagrams showing the numbers of hammer drops and the ETR values using the light and heavy hammers are shown in Figures 8-5 and 8-6, respectively.

As noted above, for DPT site number 1, the 2011 liquefaction study carried out by the Utah State Division of Water Resources found potentially liquefiable layers (using a design earthquake of M7 and pga=0.38) at depths of 0-2.4 m (0-8 feet) and again at 3.7 m (12 ft.).

Figure 8-7 below shows very good correlation between these findings and the results of the DPT soundings accomplished for this study.

For DPT site number 2, the liquefaction study carried out by the Utah State Division of Water Resources did not identify any potentially liquefiable layers, although their results did show somewhat lower blow counts between 2.4 and 3.3 m (8 and 11 ft.). Figure 8-8 below shows reasonably good correlation between these findings and the results of the DPT soundings accomplished for this study.

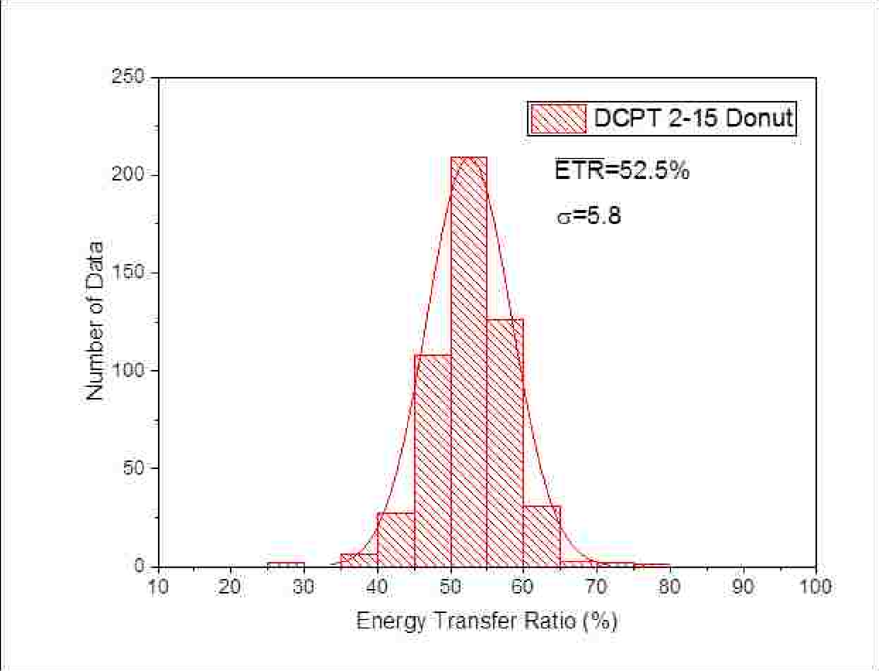

Figure 8-5. Frequency diagrams showing number of hammer drops and ETR values for Millsite Dam Hole DCPT 2-15 using the manually operated donut hammer (102.1 kg, 225 lb., weight dropped 0.91 m, 36 in.).

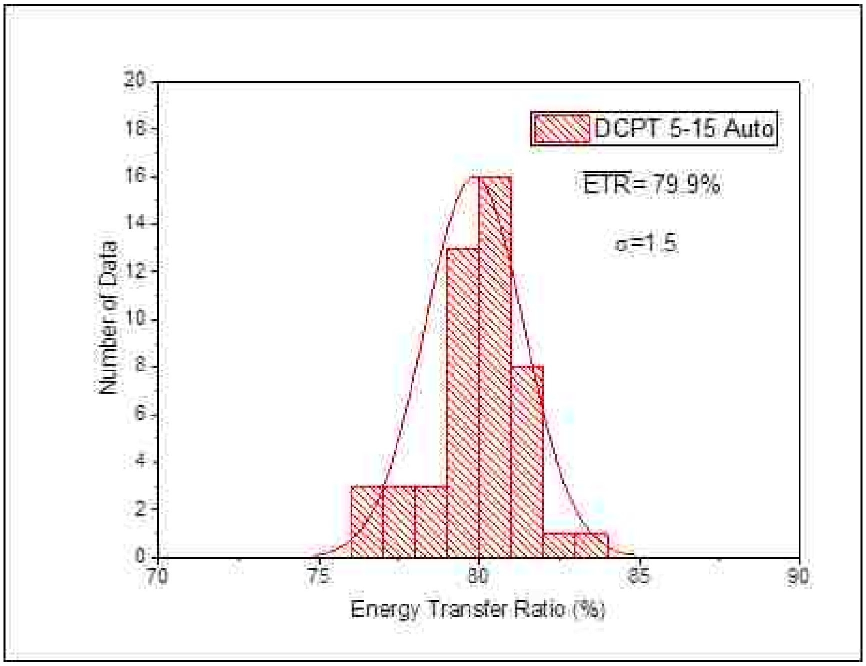

Figure 8-6. Frequency diagrams showing number of hammer drops and ETR values for Millsite Dam Hole 5-15, using light auto hammer (63.6 kg, 140 lb., weight dropped 0.76 m, 30 in.).

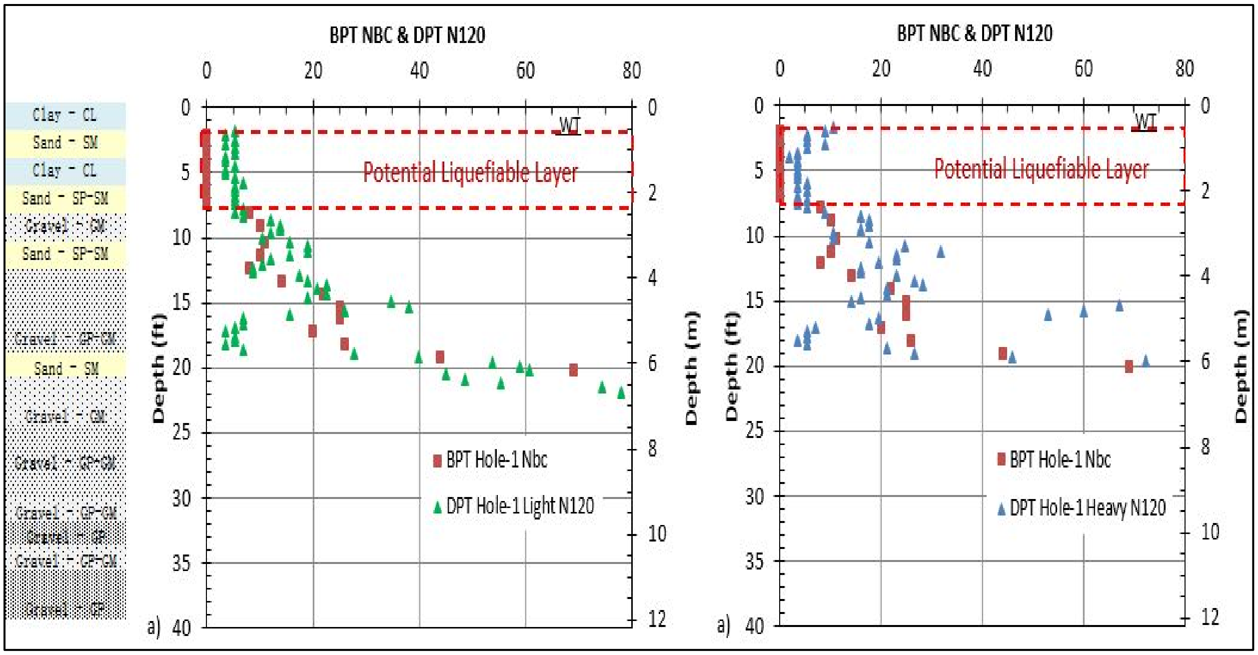

Figure 8-7. Plots of DPT N_{120} versus depth using (a) light 63.6 kg (140 lb.) auto-hammer and (b) heavy 102.1 (225 lb.) donut-hammer, after energy correction to account for lower hammer energies, compared to BPT for Millsite Dam Hole DPT-1-15.

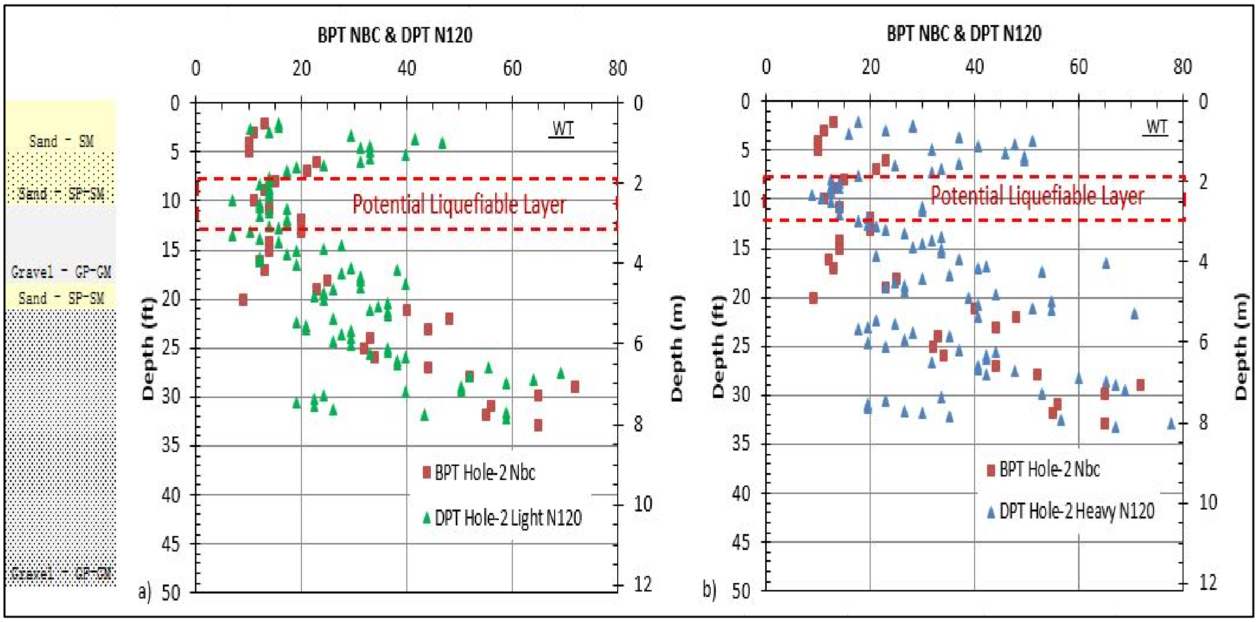

Figure 8-8. Plots of DPT N_{120} versus depth using (a) light 63.6 kg (140 lb.) auto-hammer and (b) heavy 102.1 kg (225 lb.) donut-hammer, after energy correction to account for lower hammer energies, compared to BPT for Millsite Dam Hole 2-15.

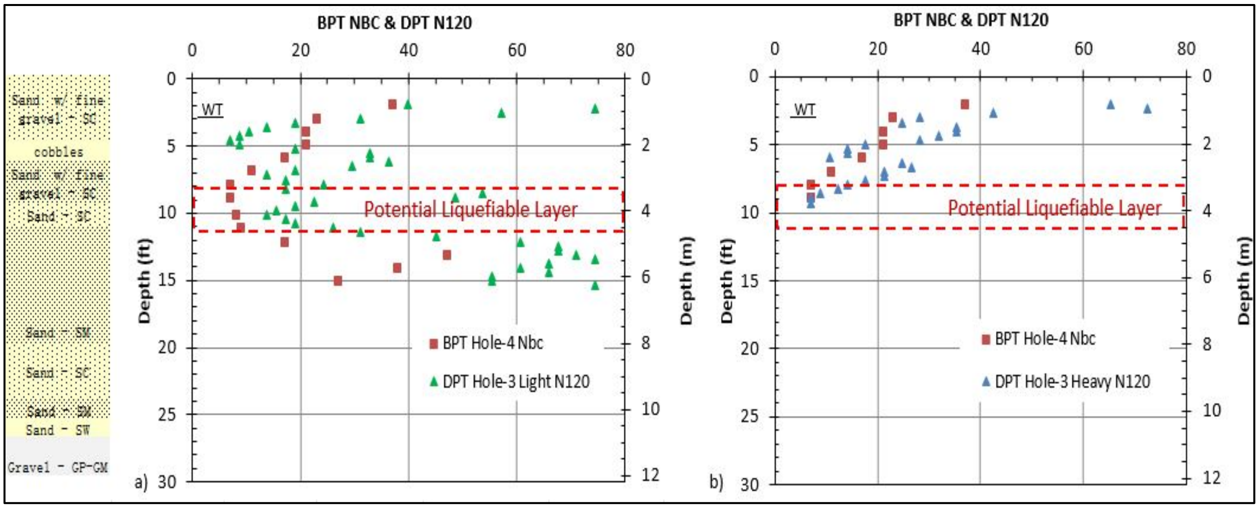

Figure 8-9. Plots of DPT N_{120} versus depth using (a) light 63.6 kg (140 lb.) auto-hammer and (b) heavy 102.1 kg (225 lb.) donut-hammer, after energy correction to account for lower hammer energies, compared to BPT for Millsite Dam Hole 3-15.

As noted above, for DPT site number 3, the liquefaction study carried out by the Utah State Division of Water Resources found potentially liquefiable layers at depths of 2.4-3.3 m (8-11 ft.) and again at 7.9-8.3 m (26-27 ft.). Figure 8-9 below shows reasonably good correlation between these findings and the results of the DPT soundings accomplished for this study.

DPT 4 met shallow refusal and therefore is not included here. It is worth noting however, that the 2011 State liquefaction BPT study experienced very high blow counts, on the order of hundreds per foot, to a depth of 18 m (60 ft.), where they encountered a 1.5 m (5 ft.) thick potentially liquefiable layer.

For DPT site number 5, the 2011 liquefaction study carried out by the Utah State Division of Water Resources found potentially liquefiable layers at depths of 0.6-2.1 m (2-7 ft.) and again at 4.3 m (14 ft.). Figure 8-10 below shows varying correlation between these findings and the results of the DPT soundings accomplished for this study. These results seem to show an over-estimation of blow counts in sandy material which would lead to an under-estimation of liquefaction potential.

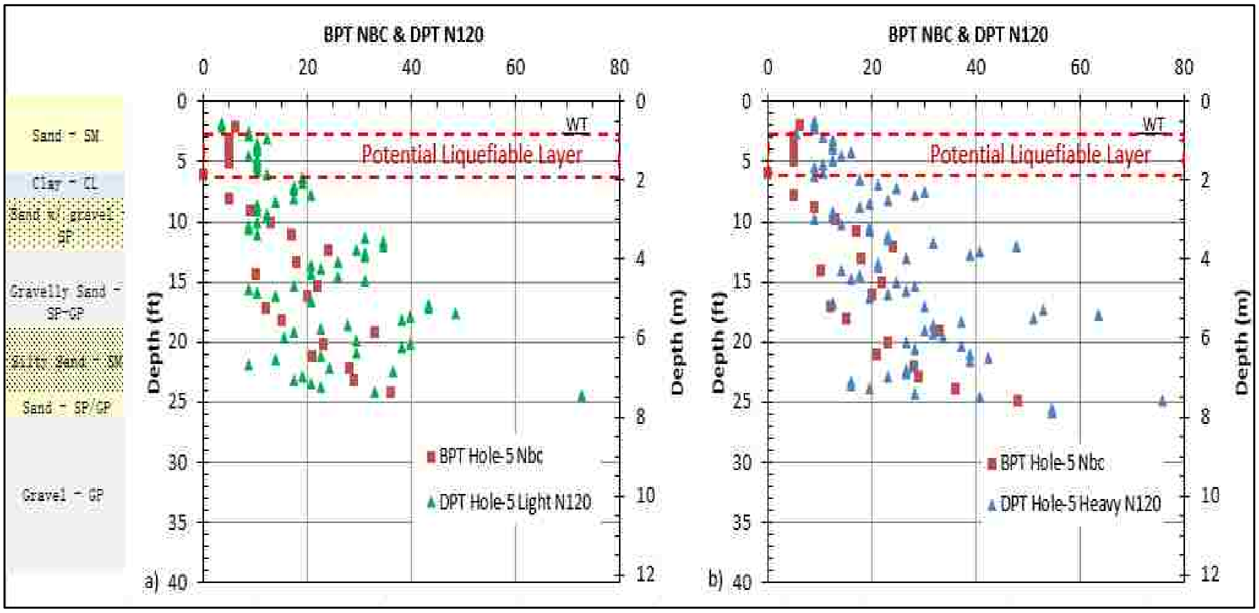

Figure 8-10. Plots of DPT N_{120} versus depth using (a) light 63.6 kg (140 lb.) auto-hammer and (b) heavy 102.1 kg (225 lb.) donut-hammer, after energy correction to account for lower hammer energies, compared to BPT for Millsite Dam Hole 5-15.

Furthermore, to facilitate comparisons between the liquefaction resistance obtained with the DPT which is based on data from a $M_w8.0$ earthquake and the BPT which is based on $M_w7.5$ earthquake data, a magnitude scaling factor approach was used. For example, the cyclic stress ratio, CRR, obtained from a DPT-based liquefaction triggering curve in Figure 3 was adjusted using the equations below to obtain the CRR for a $M_w7.5$ earthquake.

$$CRR_{M7.5} = CRR_{M8.0}/MSF \qquad 8\text{-}2$$

Where $MSF=10^{2.24}/M_w^{2.56}$ and $M_w=8.0$.

This had the effect of increasing the CRR values obtained from the DPT correlation by a factor of about 15%.

Correlations between BPT $(N_1)_{60}$ and DPT N'_{120} were attempted for both the donut hammer and the automatic hammer data. Correlations were much improved with the automatic hammer relative to the donut hammer which was operated manually. The difficulty for the driller in consistently raising the heavier donut hammer (102.1 kg (225 lb.) vs. 63.6 kg (140 lb.)) led to much greater scatter in the test data relative to the automatic hammer. This finding is consistent with results obtained by Cao et al. (2013). For both hammer energies, the energy corrected DPT N_{120} value is fairly consistent with the trend defined by the BPT N_{BC} value with depth. The agreement is best within the depth range from 0.91-3.3 m (3-11 ft).

A comparison of the N_{120} blow counts obtained from the two different hammer energies after energy correction is provided in Figure 8-11. The data points generally fall within a reasonable range of the 1:1 line. Results from additional testing will be necessary to define the error bands and to determine if adjustments in the energy correction factor may be necessary for depth or gravel particle size.

8.6 CSR vs. DPT N'_{120}

Liquefaction potential was evaluated using both the DPT and BPT methods of analysis. In the case of the BPT, the N_{BC} value was converted to the equivalent sand SPT N_{60} using the Harder et al. (1986) correlation approach. The SPT N_{60} value was then corrected for overburden pressure effects using the equation proposed by Youd et al. (2001). The cyclic stress ratio, or CSR, was computed using equation 2-2 which was originally developed by Seed et al. (1971) where a_{max} is the peak ground acceleration estimate of 0.37g.

The cyclic stress ratio, CSR, is plotted as a function of DPT-based N'$_{120}$ for the zone between 0.91-3.3 m (3-11 ft.) below the ground surface for four holes at Millsite Dam in Figures 8-12 through 8-15.

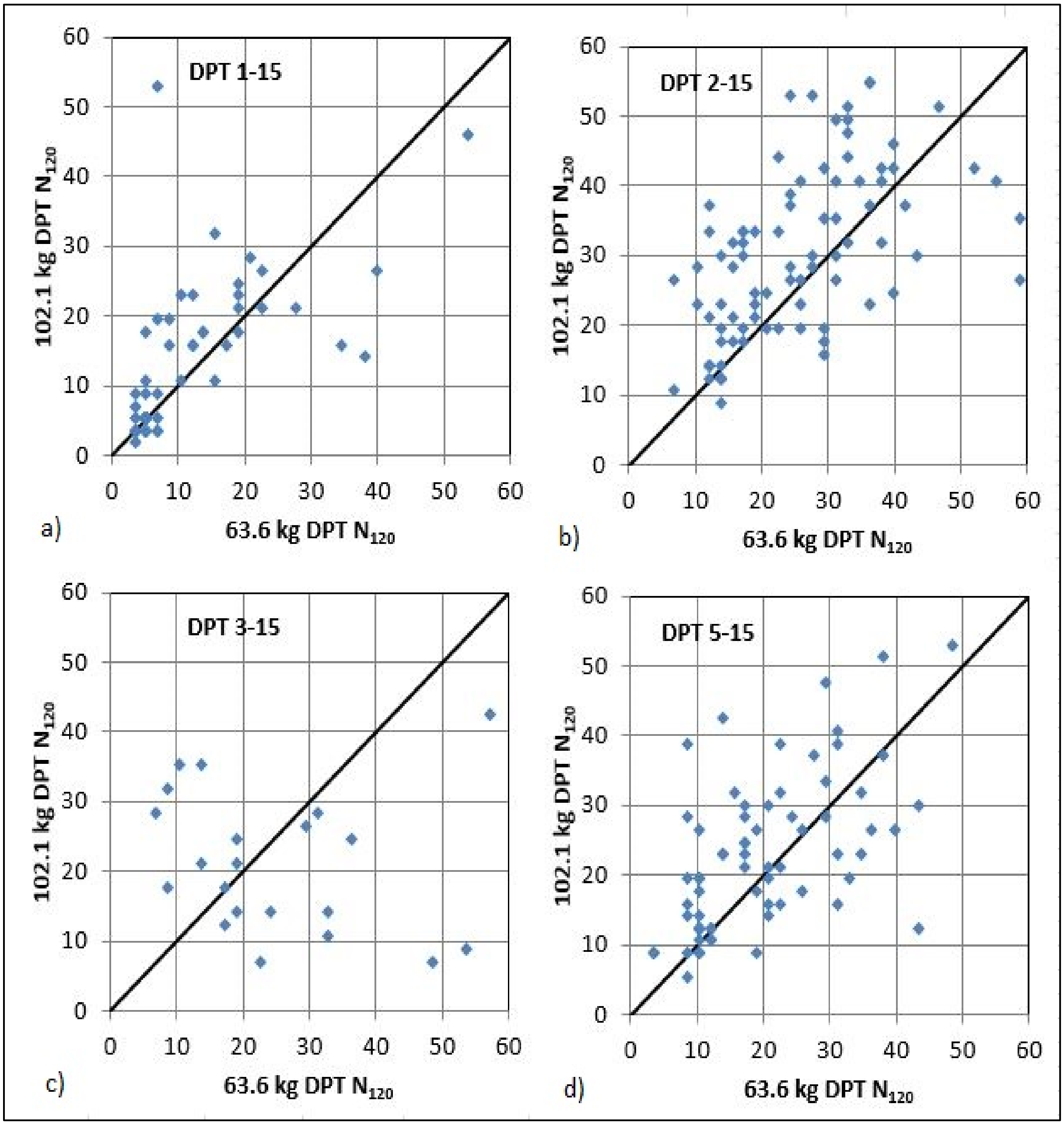

Figure 8-11. Comparison of DPT N_{120} obtained using the 63.6 kg and the 102.1 kg hammers after energy correction, for Millsite Dam a) Hole DPT 1-15, b) DPT 2-15, c) DPT 3-15, and d) DPT 5-15.

The adjusted triggering curve for the M_w7.3 Borah Peak earthquake is also plotted for comparison. Solid dots indicate liquefaction and open dots indicate a layer that had no liquefaction.

Following are results from each DPT site. All blow counts are for critical zones identified as liquefiable (solid dots) and non-liquefiable (open dots).

The cyclic stress ratio, CSR, is summarized as a function of BPT-based $(N_1)_{60}$ for the zone between 0.91-3.3 m (3-11 ft.) below the ground surface in Figure 8-16 a). The adjusted triggering curve for the M_w7.3 Borah Peak earthquake is also plotted in Figure 8-16 for comparison.

In the case of the DPT, the N_{120} value was first converted to N'_{120} using equation 2-1. Then the CSR was plotted as function of N'_{120} within the zone of liquefaction from 0.91-3.3 m (3-11 ft.) in Figure 8-16 b). The liquefaction triggering curve was based on the 30% probability curve develop by Cao et al. (2013) shown in Figure 2-2. The triggering curve in Figure 8-16 b) was adjusted upward using the magnitude scaling factor to account for the lower magnitude of the Borah Peak earthquake (M_w7.3) earthquake relative to the M_w7.9 Wenchuan China earthquake used to develop the DPT triggering curves.

Not all the CSR values were sufficiently high to produce liquefaction for the range of blow counts within this layer, see Hole DPT-2 specifically where liquefaction was not estimated by BPT.

The CSR-DPT pairs for each hole at Millsite were averaged to obtain a single point that represents the entire data *set*, and plotted in Figure 8-17, in comparison with the triggering curve for 30% probability of liquefaction.

The CSR-DPT N'$_{120}$ points from Figure 8-16 b) are plotted in Figure 8-18 in comparison with the probabilistic liquefaction triggering curves (Cao et al. 2013), after magnitude scaling adjustments which shifted the measured CSR values slightly downward. Not all data pairs plot above the 50% probability of liquefaction curve, but are consistent with the observed liquefaction potential. In Figure 8-19, a single data point is shown that represents the DPT N'$_{120}$ data set, as compared to the liquefaction triggering curve.

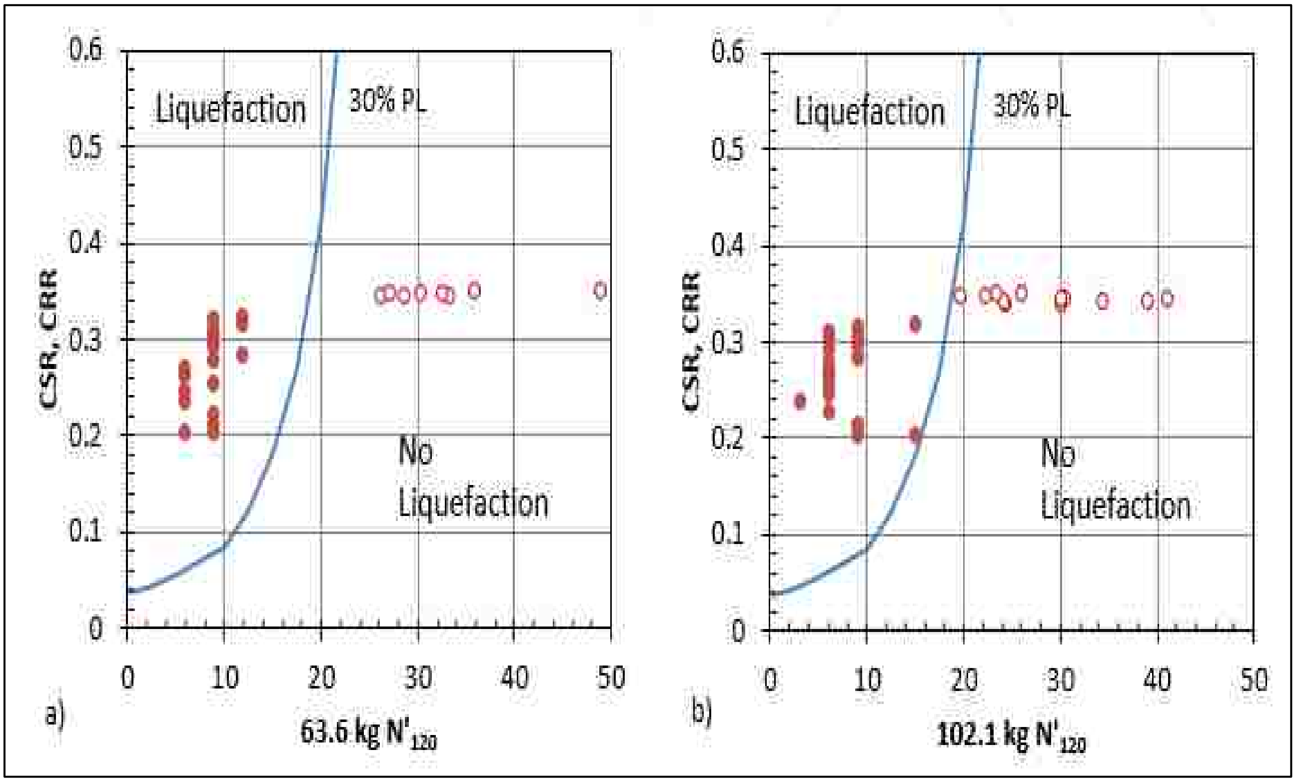

Figure 8-12. Comparison of CSR vs DPT N'$_{120}$, using a) the 63.6 kg (140 lb.) hammer, and b) the 102.1 kg (225 lb.) hammer, for Millsite Dam Hole 1-15. Solid dots are from a potentially liquefiable unit and open dots are from a non-liquefiable unit.

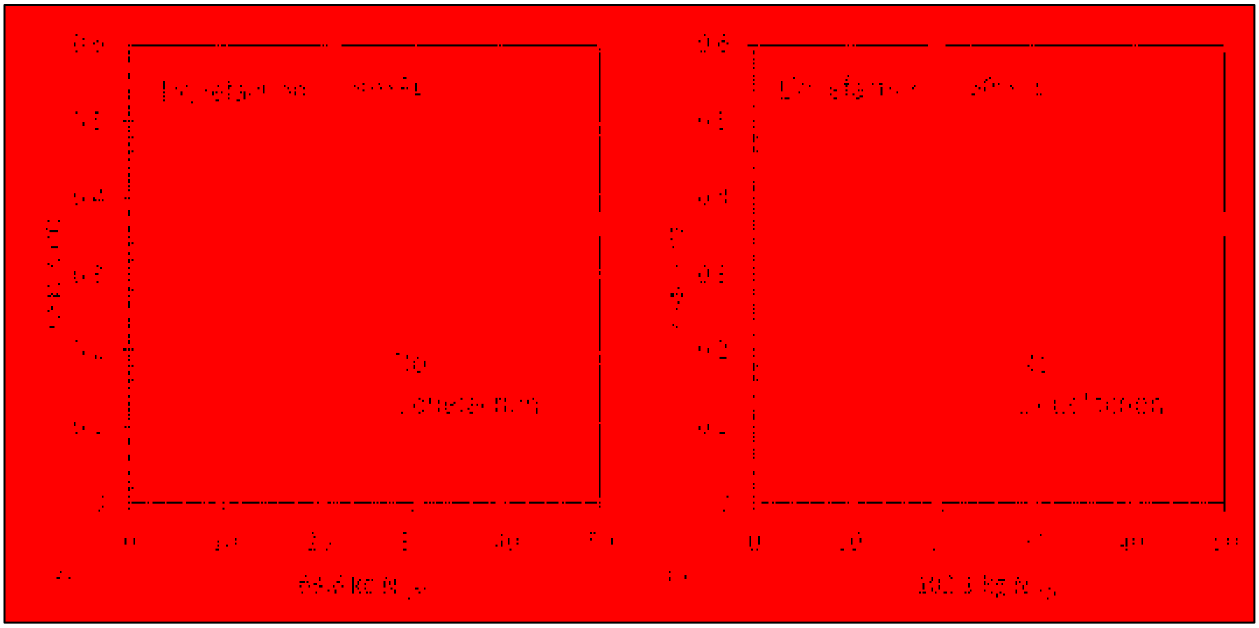

Figure 8-13. Comparison of CSR vs DPT N'$_{120}$, using a) the 63.6 kg (140 lb.) hammer, and b) the 102.1 kg (225 lb.) hammer, for Millsite Dam Hole 2-15. Solid dots are from a potentially liquefiable unit and open dots are from a non-liquefiable unit.

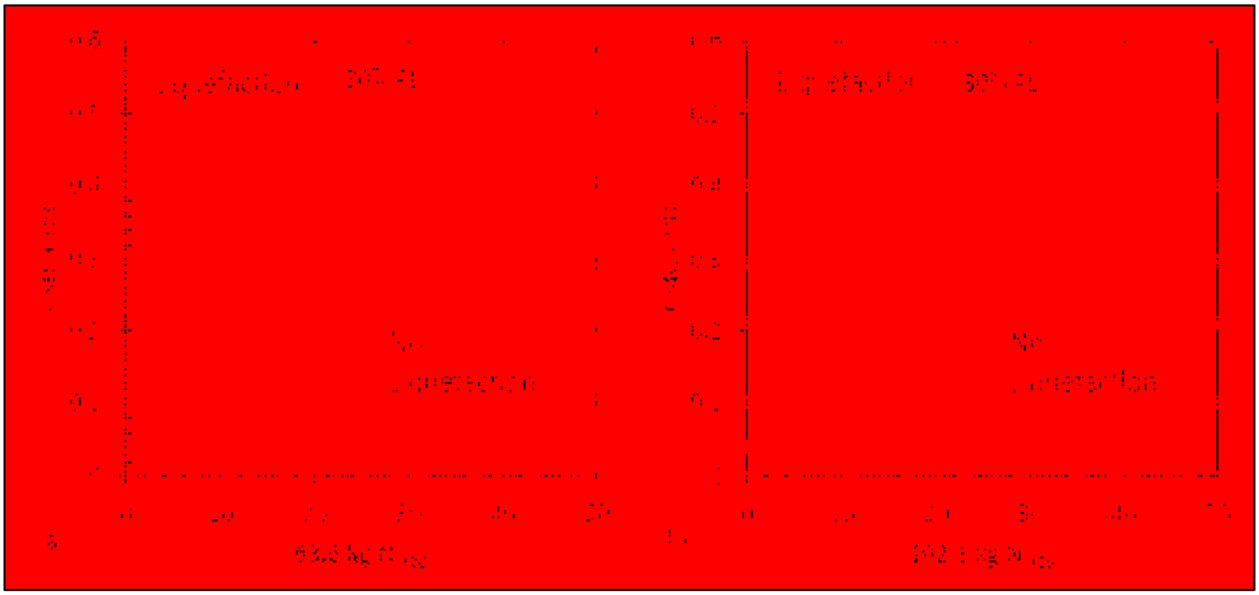

Figure 8-14. Comparison of CSR vs DPT N'$_{120}$, using a) the 63.6 kg (140 lb.) hammer, and b) the 102.1 kg (225 lb.) hammer, for Millsite Dam Hole 3-15. Solid dots are from a potentially liquefiable unit and open dots are from a non-liquefiable unit.

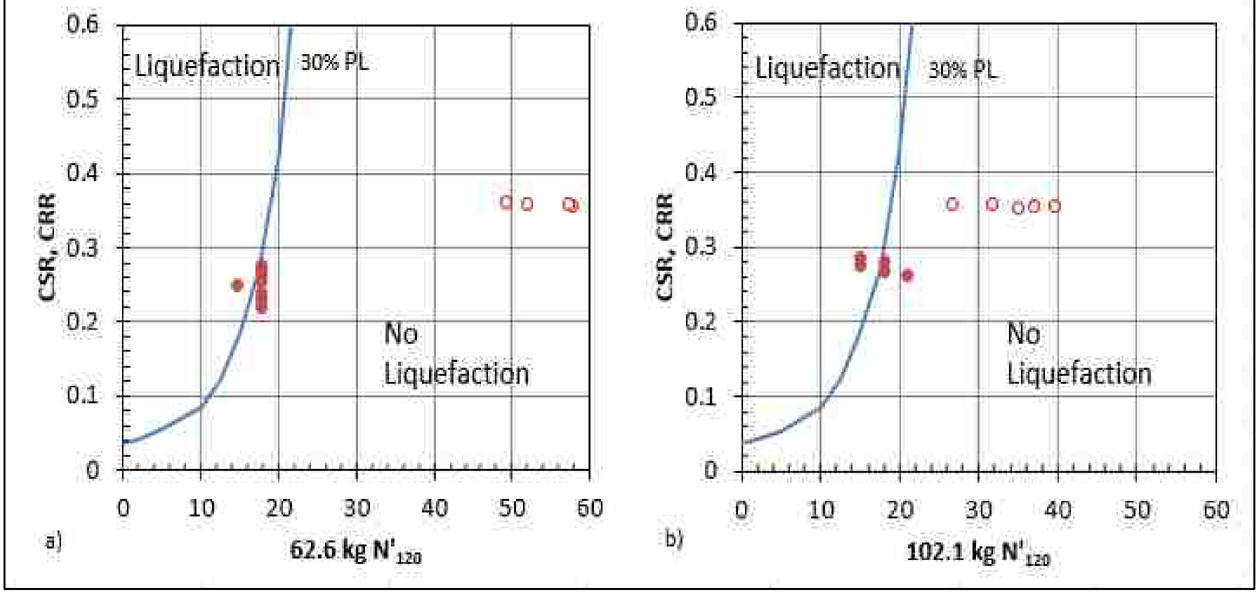

Figure 8-15. Comparison of CSR vs DPT N'$_{120}$, using a) the 63.6 kg (140 lb.) hammer, and b) the 102.1 kg (225 lb.) hammer, for Millsite Dam Hole 5-15. Solid dots are from a potentially liquefiable unit and open dots are from a non-liquefiable unit.

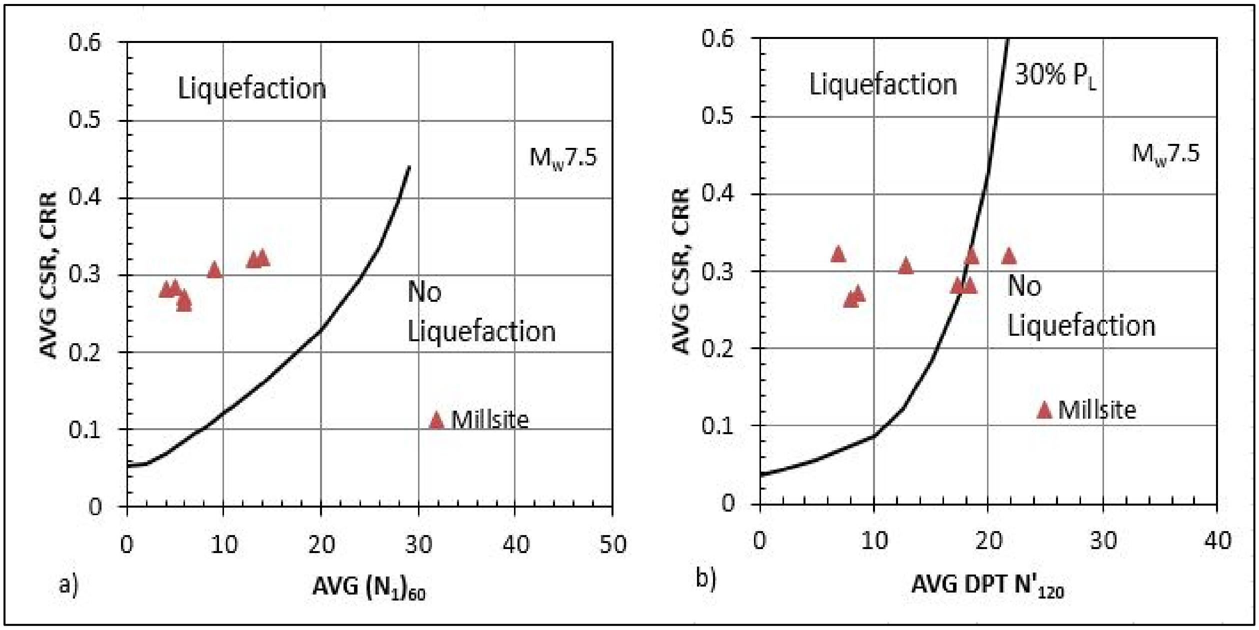

Figure 8-16. Comparison of a) CSR vs BPT-based $(N_1)_{60}$ data points for Millsite Dam in comparison with triggering curve, and b) CSR vs. DPT N'$_{120}$, data points for Millsite Dam in comparison with triggering curve for 30% probability of liquefaction (Cao et al. 2013) for M_w7.5 earthquakes.

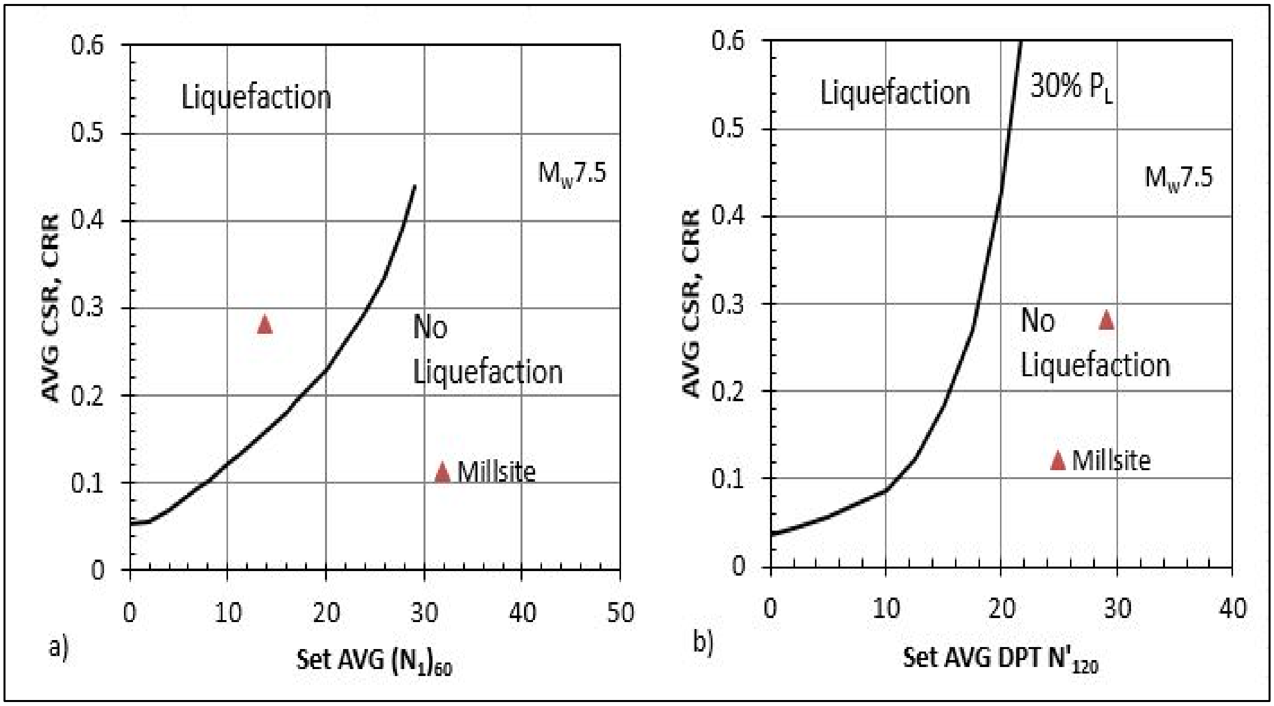

Figure 8-17. Comparison of the set average (Figure 8-16) for a) CSR vs BPT-based $(N_1)_{60}$ data points for Millsite Dam in comparison with triggering curve, and b) CSR vs. DPT N'_{120}, data points for Millsite Dam in comparison with triggering curve for 30% probability of liquefaction (Cao et al. 2013) for M_w7.5 earthquakes.

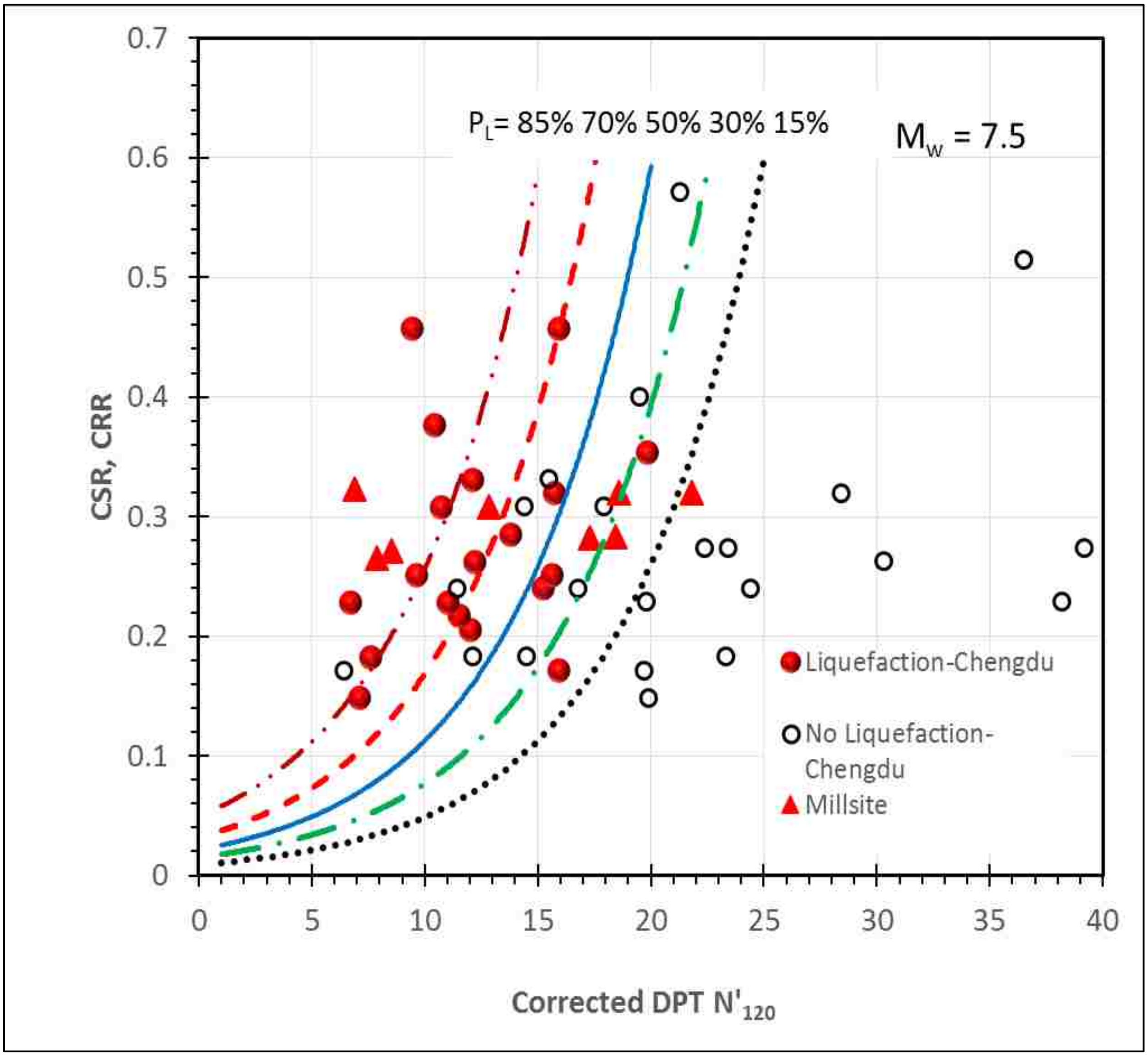

Figure 8-18. CSR vs. DPT N'120 curves for various probabilities of liquefaction in gravelly soils developed by (Cao et al. 2013*)* along with liquefaction/no liquefaction data points from Chengdu Plain. Points from Millsite Dam, Figure 8-16 b) are shown.

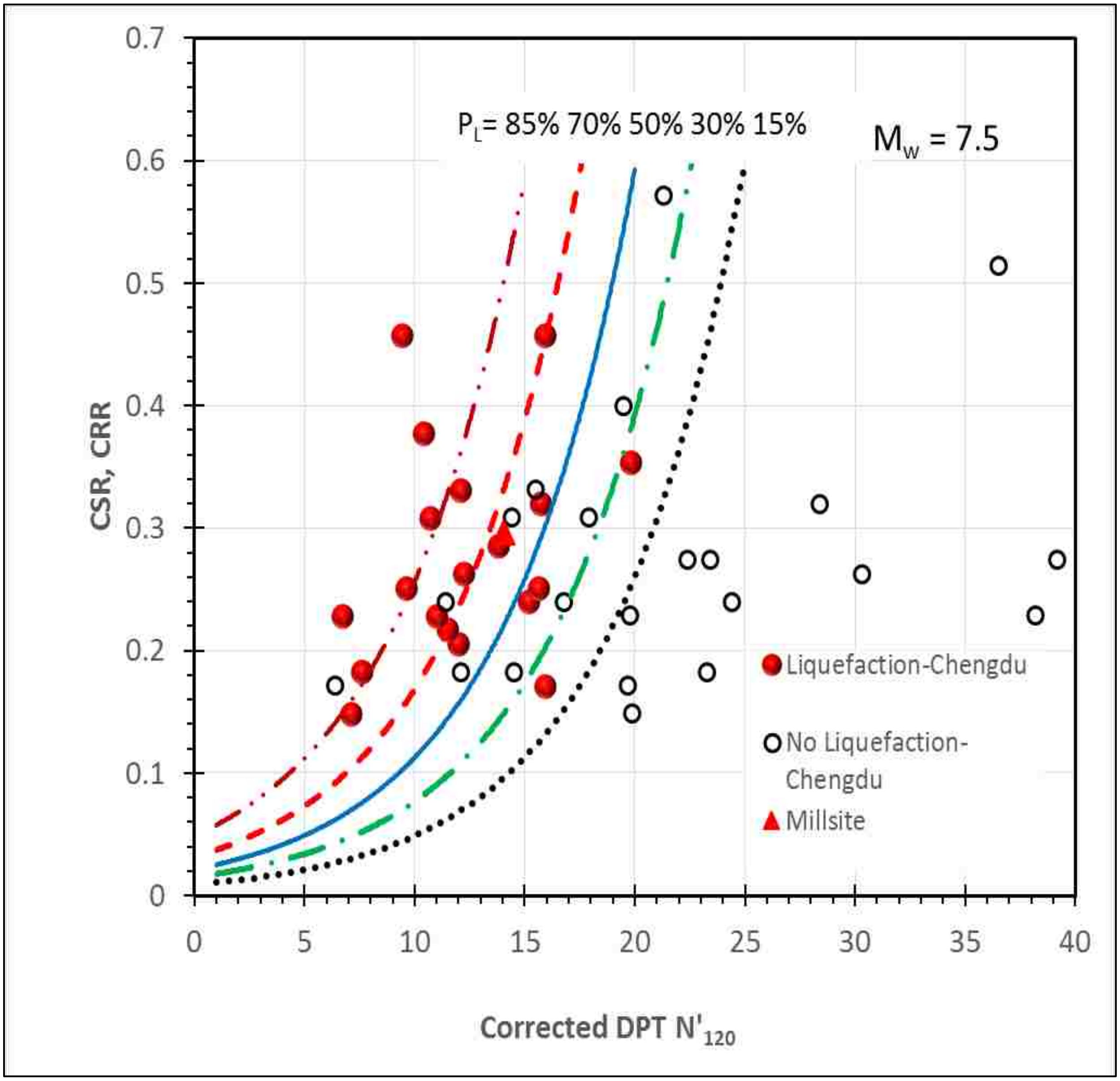

Figure 8-19. CSR vs. DPT N'120 curves for various probabilities of liquefaction in gravelly soils developed by Cao Z. et al. (2013*)* along with liquefaction/no liquefaction data points from Chengdu Plain. Set point from Millsite dam Figure 8-17 is shown.

8.7 DPT vs SPT

Similar to Chapter 7, a good indicator of the results of the study is the comparison of the DPT results with previous SPT results. Figures 8-20 through 8-23 demonstrate the correlation between the SPT N_{60} and the DPT N_{120} at Millsite Dam.

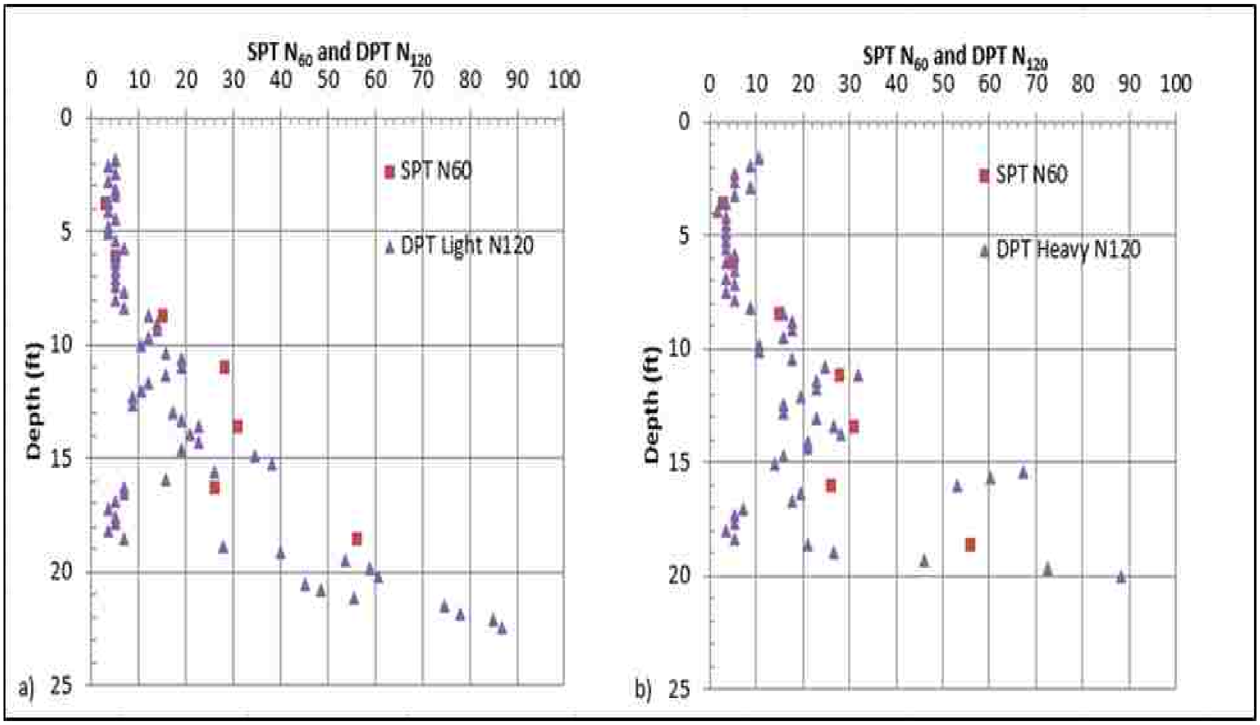

Figure 8-20. Correlation of DPT N_{120} and 2007 SPT N_{60} for Hole number DPT 1-15 given a) the light 63.6 kg (140 lb.) hammer and b) the heavy 154.4 kg (225 lb.) hammer at Millsite Dam.

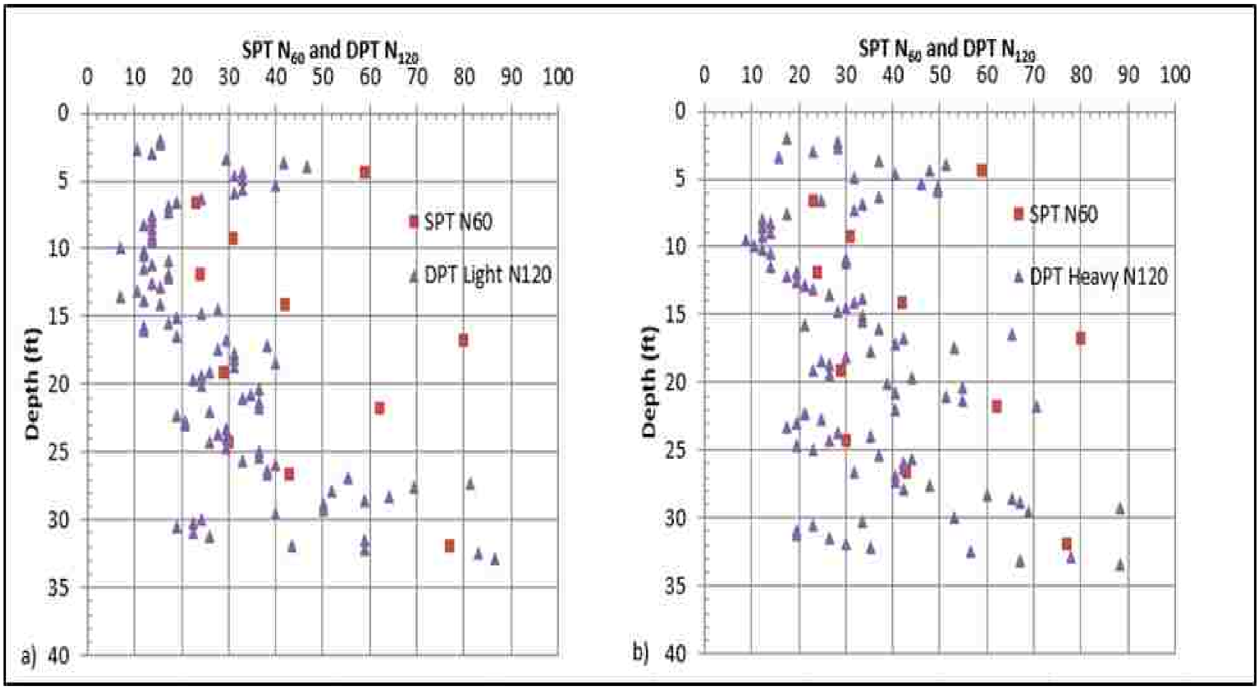

Figure 8-21. Correlation of DPT N_{120} and 2007 SPT N_{60} for Hole number DPT 2-15 given a) the light 63.6 kg (140 lb.) hammer and b) the heavy 154.4 kg (225 lb.) hammer at Millsite Dam.

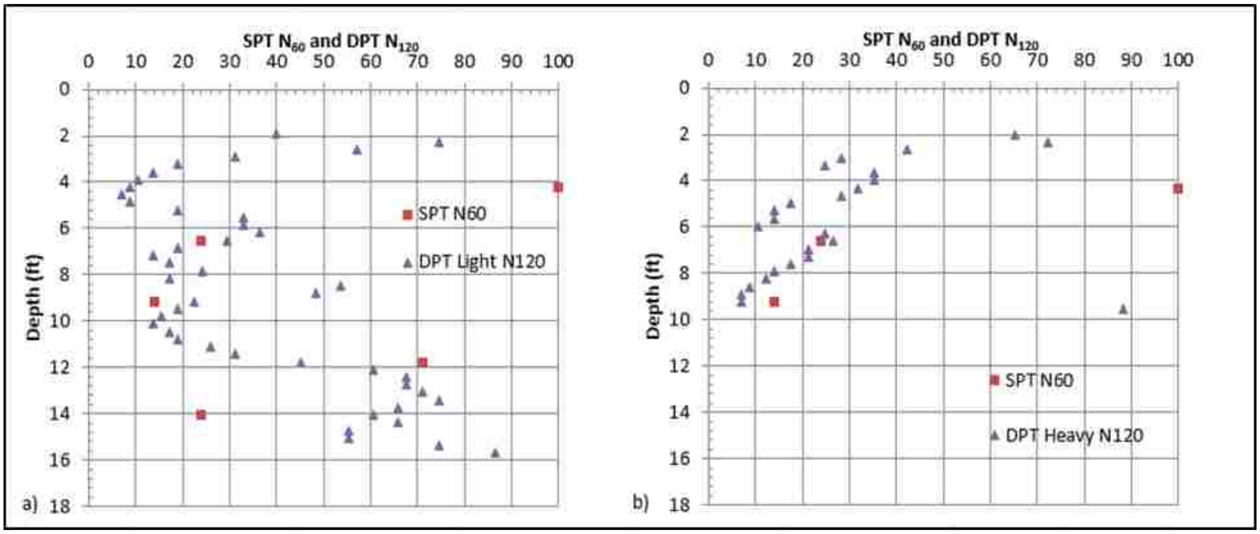

Figure 8-22. Correlation of DPT N_{120} and 2007 SPT N_{60} for Hole number DPT 3-15 given a) the light 63.6 kg (140 lb.) hammer and b) the heavy 154.4 kg

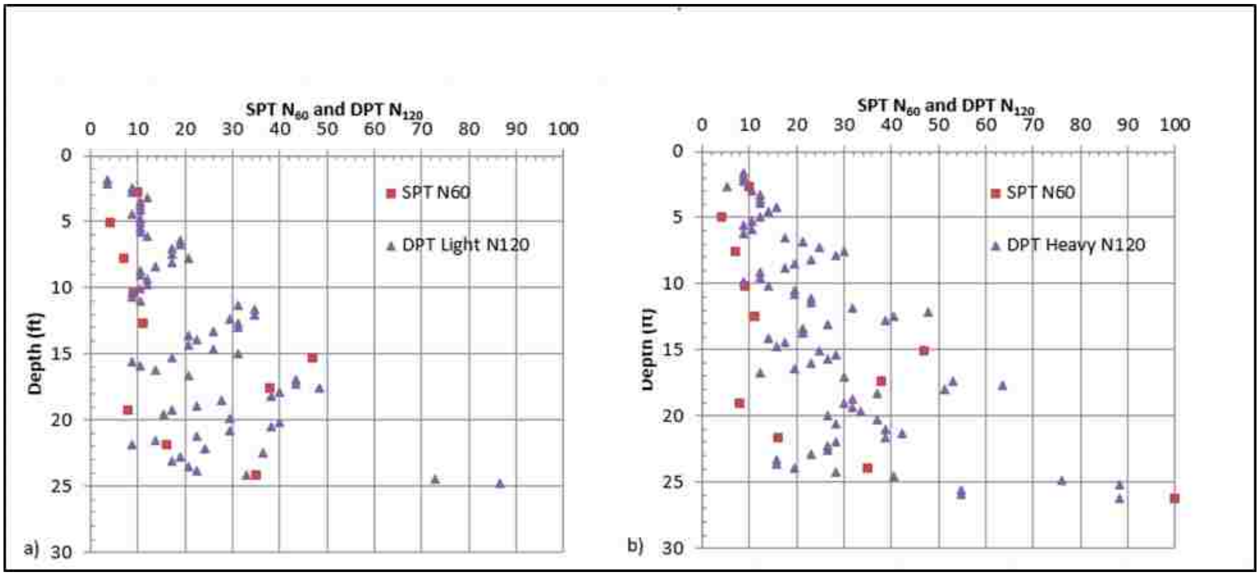

Figure 8-23. Correlation of DPT N_{120} and 2010 SPT N_{60} for Hole number DPT 5-15 given a) the light 63.6 kg (140 lb.) hammer and b) the heavy 154.4 kg (225 lb.) hammer at Millsite Dam.

The 2015 DPT vs. 2007/2010 SPT data was plotted to gain an understanding of the correlation between the DPT soundings accomplished at the site and the previous SPT soundings. As can be seen from Figure 8-24 there is only weak correlation between the two. Even though the R^2 value is 0.21, indicating a weak correlation (R^2=1.0 is a perfect fit), the value associated with x in the correlation equation is the slope of the regression line and should be close to 1.0 for good correlation. 1.17 is reasonably good.

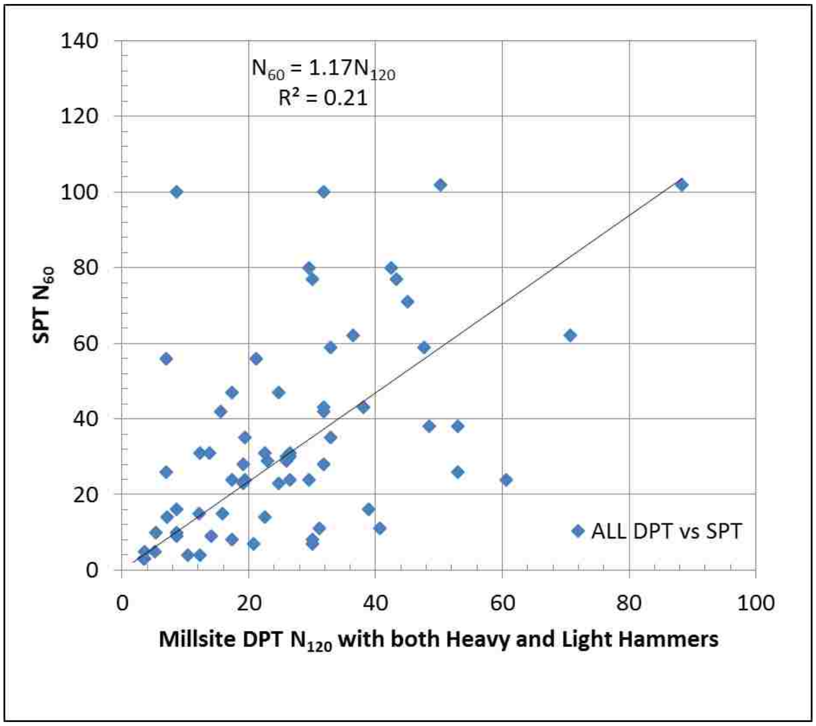

Figure 8-24. Plot comparing the 2015 DPT N120 vs. the 2007 SPT N60 for all holes at Millsite Dam using both the 63.6 kg (140 lb.) hammer, and the 102.1 kg (225 lb.) hammer.

8.8 Probability of Liquefaction vs. Depth from DPT

The probability of liquefaction P_L was calculated and plotted for all DPT holes at Millsite Dam and is shown in Figure 8-25 below. Equation 5-2 is referred to as the probability function for liquefaction.

Cao et al. (2013) validated this equation using data from the Wenchuan event where 15 of 19 sites with surface liquefaction effects (79%) plotted on or above the P_L=50% curve of Figure 2-8, and 17 of 19 (89%) liquefaction sites plot on or above the P_L=30% curve. Similarly, 23 of 28 (82%) of sites exhibiting no surface liquefaction effects plot on or below the P_L=50% curve and 26 of 28 (93%) nonliquefaction sites plot on or below the P_L=70% curve. He states that this correlation is therefore generally verifiable for gravelly soils in the Chengdu plain shaken by the 2008 Wenchuan earthquake, and that this relationship may be used for other sites underlain by gravelly soils with soil types similar to those that liquefied during the Wenchaun quake.

The probability of liquefaction, P_L, seen below, corresponds well with the calculated critical zone of liquefaction of 0.61-2.4 m (2-8 ft.) for Hole-1. For Hole-2 the calculated critical zone is 7 to 13 ft. and corresponds somewhat with Figure 8-23. Hole-3 also correlated reasonably well for the critical zone of 2.4 to 3.4 m (8 to 11 ft.). And lastly, the P_L for Hole-5 corresponded reasonably with the calculated critical zone of 0.91 to 2.1 m (3 to 7 ft.).

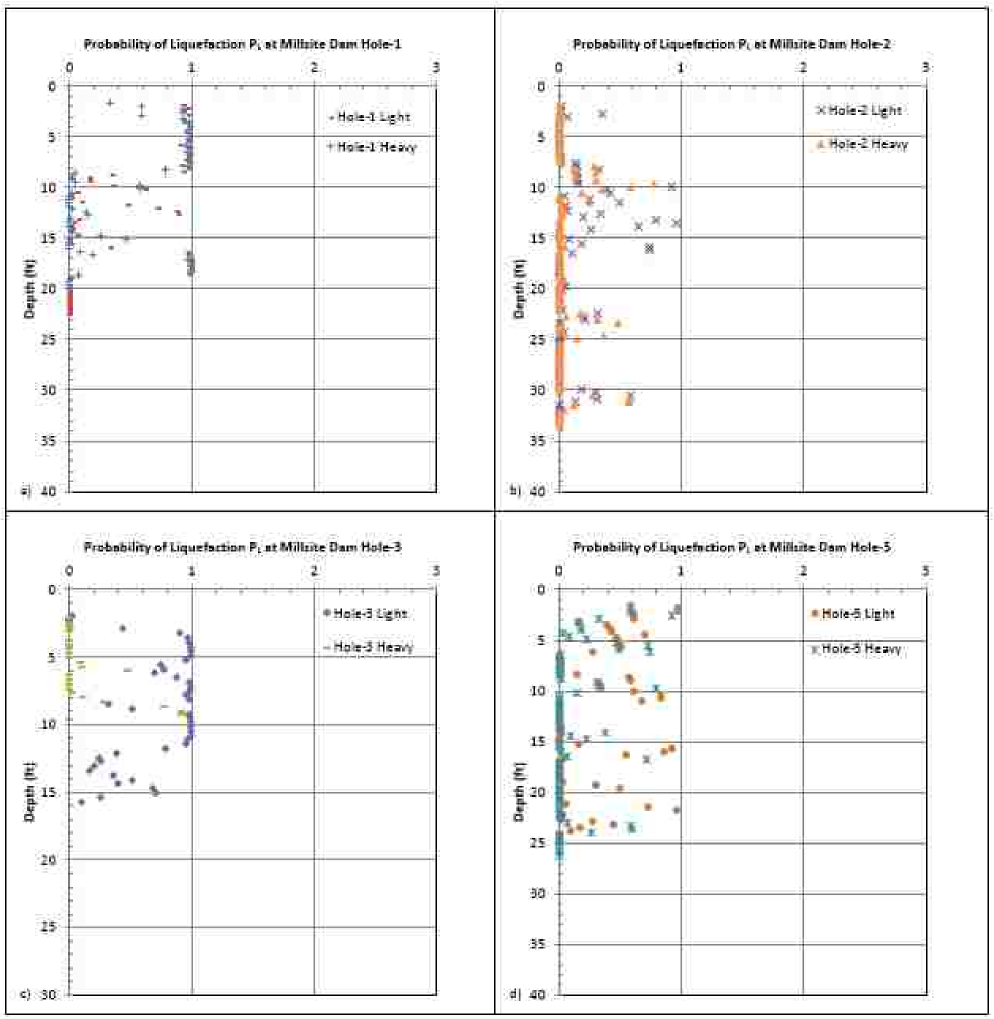

Figure 8-25. Probability of Liquefaction, P_L, for all holes at Millsite Dam, vs. Depth, from DPT. For a) Hole-1, b) Hole-2, c) Hole-3, d) Hole-5.

9 ANALYSIS OF RESULTS FROM ALL TEST SITES

9.1 Summary of CSR vs DPT N'_{120} Data for All Sites

Figure 9.1 provides a summary of the CSR vs DPT N'_{120} data pairs obtained in Idaho during this study in comparison with those obtained from China by Cao et al. (2013). CSR values have been adjusted for hammer energy and magnitude as discussed previously. One average data point is shown for each test site in Idaho. In all cases, the sites which liquefied plot above the 50% probability of liquefaction curve which is in excellent agreement with field observations where liquefaction was observed.

9.2 Determination of Improved Liquefaction Triggering Curves

Probabilistic liquefaction triggering curves had already been developed based on the Chinese data set of gravel liquefaction that occurred in Chengdu Plain in China from the 2008 M_w7.9 Wenchuan earthquake. In this chapter, those curves have been updated by adding three additional points obtained from three different sites of Idaho, viz. Pence Ranch, Larter Ranch and Whiskey Springs, where gravel liquefied during the 1983 M_w6.9 Borah Peak earthquake. Logistical regression analysis has been performed in this study to obtain the updated probabilistic liquefaction triggering curves.

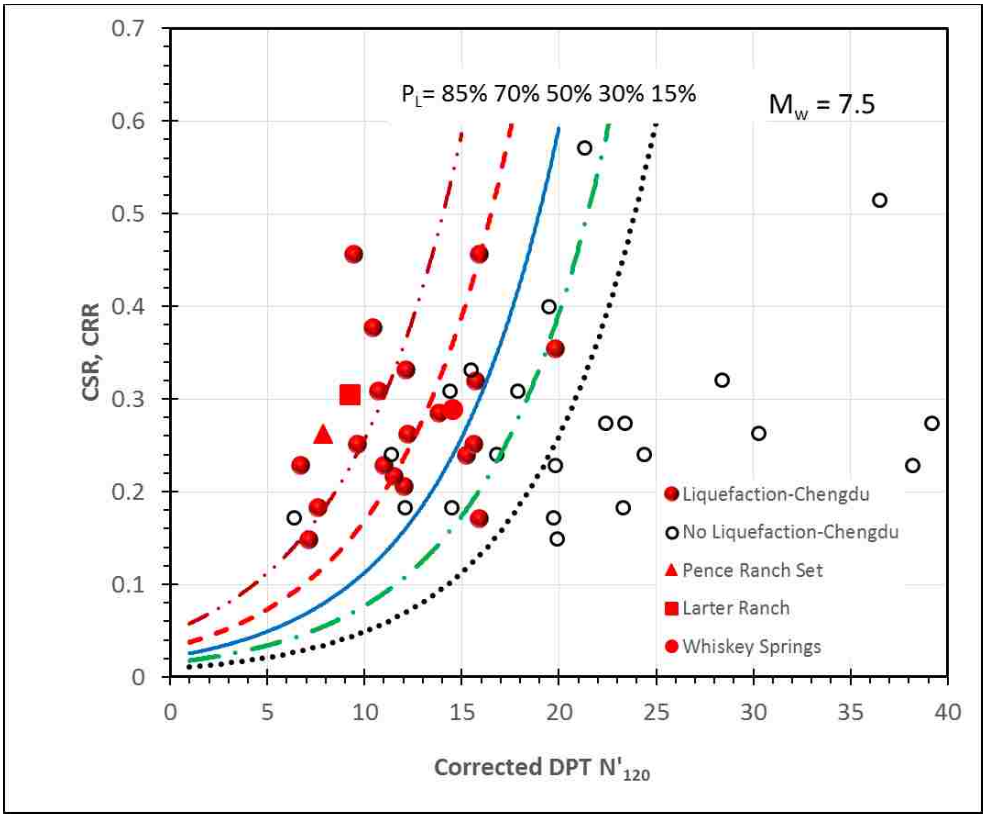

Figure 9-1. CSR vs. DPT N'_{120} curves for various probabilities of liquefaction in gravelly soils developed by Cao et al. (2013) along with liquefaction/no liquefaction data points from Chengdu plain. Points from DPT tests at Larter Ranch, Pence Ranch, and Whiskey Springs are also shown.

To accomplish the analysis, the average N_{120} and CSR pairs obtained from three individual sites were combined with the results from the Chinese data set. In all cases, the CSR values for each site were determined from the simplified procedure as defined by Youd et al. (2001). Then the equivalent $CSR_{M=7.5}$ was obtained by dividing the original CSR by the Magnitude Scaling Factor (MSF) which was obtained from the Seed and Idriss model used by Youd et al. (2001), as given in equation 2-2 and 2-4.

To perform this analysis, all the data for the three Idaho sites were averaged to get one single point for each site and added to the Chinese data set. Consequently, the variables and corresponding values for all the sites including the Chinese data are shown in the following

Table 2 below. To obtain the final regression coefficients 'JMP Pro13' software was used. In this analysis a regression equation has been obtained to predict the Probability of Liquefaction (P_L) using the variables N'_{120}, and $\ln(CSR_{M=7.5})$. The probability of liquefaction is then given by the equation

$$P_L = 1/(1 - 9.05_1 + 0.378N'_{120} - 2.42Ln(CSR)) \qquad 3\text{-}1$$

Substituting different values of $N'_{120,}$ the corresponding CSR values are computed and plotted for different probabilities of liquefaction to obtain the probabilistic liquefaction triggering curves. These updated curves are compared with the curves based on Chinese data set as shown in in Figure 9-1.

Table 2. Three Idaho Sites added to the Chinese Data Set.

Sites	N'_{120}	CSRM=7.5	M_w	MSF	$Ln(CSR_{M=7.5})$	Liquefaction
Xinshi	10.400	0.377	7.900	0.875	-0.975	Y
Pilu	9.600	0.251	7.900	0.875	-1.381	Y
Banqiao	12.100	0.331	7.900	0.875	-1.104	Y
Songbai	10.700	0.309	7.900	0.875	-1.176	Y
Guoyuan	15.900	0.171	7.900	0.875	-1.764	Y
Jingqiao	7.600	0.183	7.900	0.875	-1.699	Y
Xiangliu	19.800	0.354	7.900	0.875	-1.038	Y
Xinglong	9.400	0.457	7.900	0.875	-0.783	Y
Shihu	13.800	0.286	7.900	0.875	-1.253	Y
Oifu	12.200	0.263	7.900	0.875	-1.336	Y
Guihua	15.900	0.457	7.900	0.875	-0.783	Y
Zhenjiang	15.700	0.320	7.900	0.875	-1.140	Y
Sanyuan	15.200	0.240	7.900	0.875	-1.427	Y
Shengli	12.000	0.206	7.900	0.875	-1.581	Y
Xiaojia	7.100	0.149	7.900	0.875	-1.907	Y
Lichun	11.500	0.217	7.900	0.875	-1.527	Y
Jingxing	15.600	0.251	7.900	0.875	-1.381	Y
Quanshui	6.700	0.229	7.900	0.875	-1.476	Y
Longqiao	11.000	0.229	7.900	0.875	-1.476	Y

Table 2. (cont.) Three Idaho Sites added to the Chinese Data Set.

Wulan	12.100	0.183	7.900	0.875	-1.699	N
Chuanmu	17.900	0.309	7.900	0.875	-1.176	N
Tonglin	21.300	0.571	7.900	0.875	-0.560	N
Nangui	11.400	0.240	7.900	0.875	-1.427	N
Mianzhu	15.500	0.331	7.900	0.875	-1.104	N
Heping	23.300	0.183	7.900	0.875	-1.699	N
Quezhu	19.800	0.229	7.900	0.875	-1.476	N
Bayi	14.400	0.309	7.900	0.875	-1.176	N
Yongning	36.500	0.514	7.900	0.875	-0.665	N
Dacheng	22.400	0.274	7.900	0.875	-1.294	N
Ming'an	16.800	0.240	7.900	0.875	-1.427	N
Wufan	23.400	0.274	7.900	0.875	-1.294	N
Yangjia	19.900	0.149	7.900	0.875	-1.907	N
Linfa	19.500	0.400	7.900	0.875	-0.916	N
Business College	24.400	0.240	7.900	0.875	-1.427	N
Guangkou	30.300	0.263	7.900	0.875	-1.336	N
Jushui	61.800	0.548	7.900	0.875	-0.601	N
Pengzhou	38.200	0.229	7.900	0.875	-1.476	N
Ruikan	44.500	0.251	7.900	0.875	-1.381	N
Zipingpu	28.400	0.320	7.900	0.875	-1.140	N
Yutang	39.200	0.274	7.900	0.875	-1.294	N
Youxian	6.400	0.171	7.900	0.875	-1.764	N
Sandaovan	28.200	0.171	7.900	0.875	-1.764	N
Majiamiao	29.300	0.171	7.900	0.875	-1.764	N
Shitimiao	30.400	0.160	7.900	0.875	-1.833	N
Youngshen	19.700	0.171	7.900	0.875	-1.764	N
Jingyu	14.500	0.183	7.900	0.875	-1.699	N
Qingbaijiang Bridge	35.400	0.171	7.900	0.875	-1.764	N
Larter Ranch	9.250	0.305	6.900	1.238	-1.187	Y
Pence Ranch	7.875	0.262	6.900	1.238	-1.339	Y
Whiskey Springs	14.500	0.289	6.900	1.238	-1.242	Y

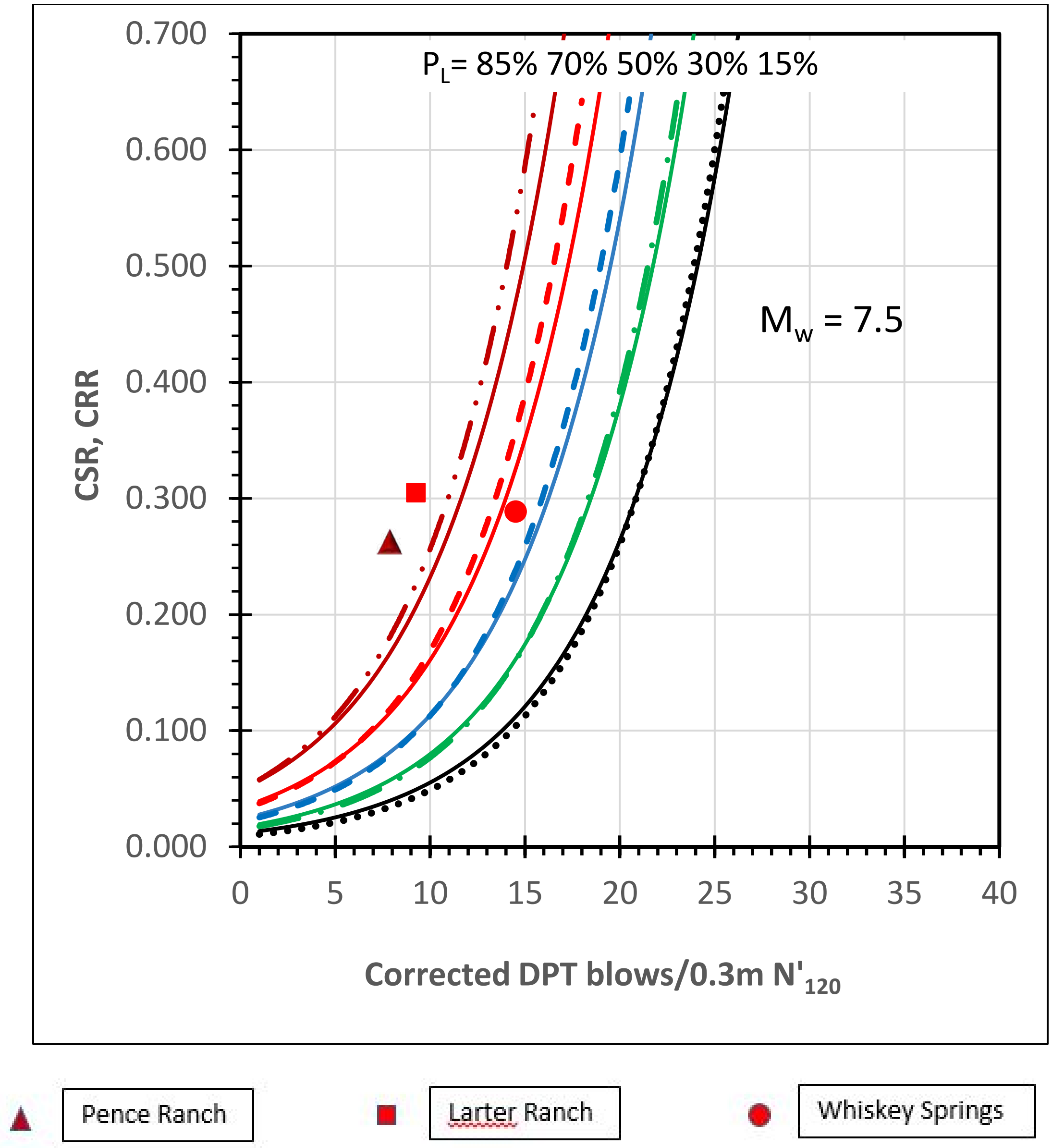

Figure 9-2. Plot showing the data set from the Idaho liquefaction sites as compared to the Chinese and the updated liquefaction triggering curves.

In Figure 9-2, the solid curves show the updated triggering curves whereas the dashed curves show the triggering curves based on Chinese data set only. The new curves are very close to what was obtained previously indicating that the data from the DPT investigations in Idaho are remarkably consistent with the observed field performance in China.

9.3 Correlation of Light and Heavy Hammers

Figure 9-3 below shows the correlation between the light, 63.6 kg (140 lb.) hammer and the heavy 154.4 kg (340 lb.) hammer for all holes at all sites in this study.

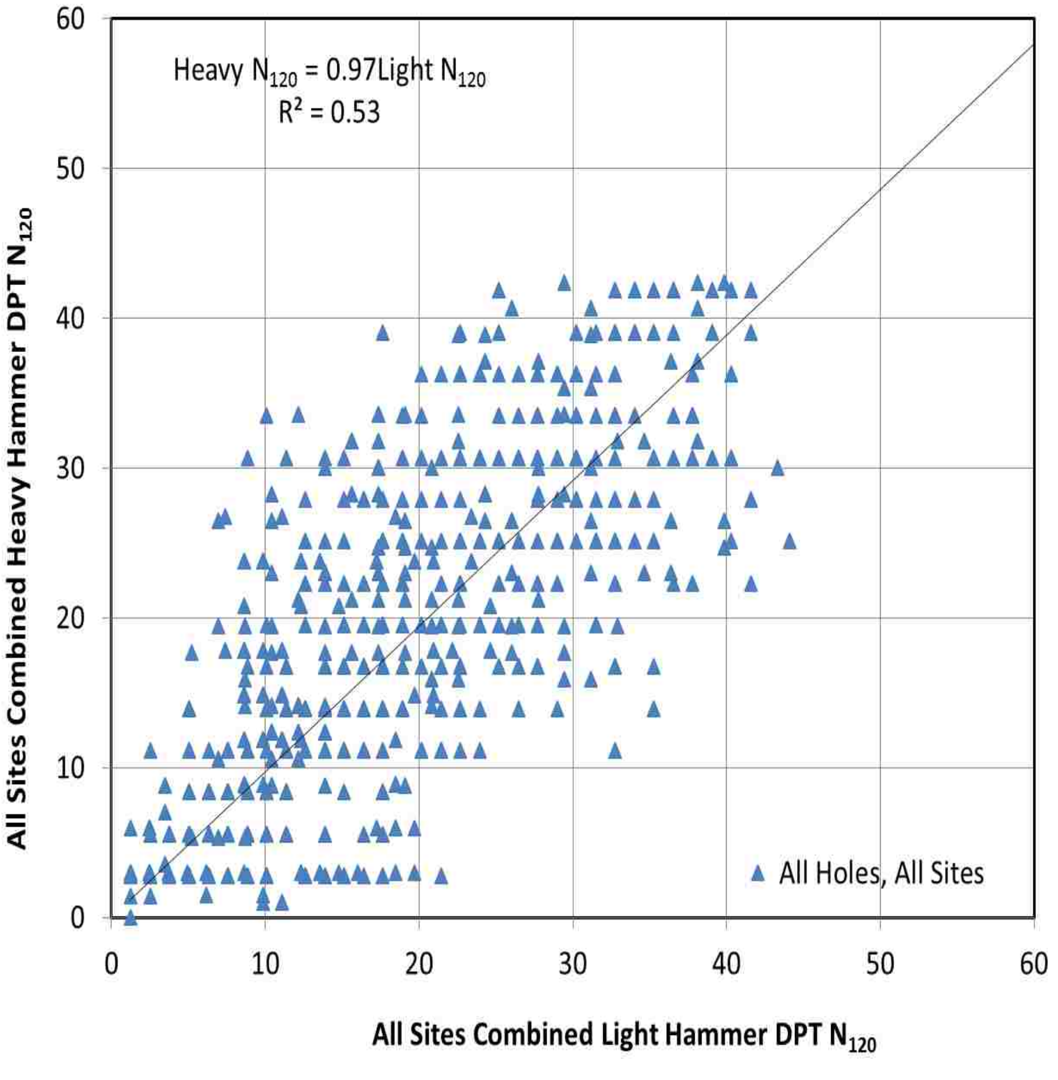

Figure 9-3. Correlation of DPT N_{120} between the light 63.6 kg (140 lb.) hammer and the heavy 154.4 kg (340 lb.) hammers for all holes at all sites.

The correlation between the light and heavy hammers is relatively good. An R^2 value of greater than 0.80 is considered a strong correlation while anything below about 0.70 is considered to be weakening. Therefore, an R^2 of 0.53 would be considered somewhat weak. The slope of the regression equation is considered good when it approaches 1.0, therefore a slope of 0.97 would indicate excellent correlation.

9.4 Overall DPT vs SPT

The summary plot shown in Figure 9-4 depicts the correlation between DPT N_{120} and the corresponding SPT N_{60} for all holes at all Idaho sites.

If the correlation is good, the scatter will be minimal around a 1:1 line. The R^2 value, or coefficient of determination, is a statistical indicator of how well the data fits a statistical model. An R^2 of 1.0 indicates that the regression line perfectly fits the data. For Pence Ranch, an R^2 of 0.73 is a fairly good indicator (0.8 is a strong correlation while 0.7 is considered weakening). The coefficient of the x value, or slope of the regression equation, is also an indicator of good correlation. The x coefficient should be close to 1.0, and for Pence Ranch, 0.9539 is a good correlation.

Figure 9-5 shows the correlation line determined by Chinese researches that best depicts the expected relationship between the DPT N_{120} and the SPT blowcount N_{60}, for a given soil. This correlation curve has also been added to Figure 10-9 for ease of comparison.

DPT data was collected for this study while the SPT data was obtained from (Andrus 1994) in the case of Pence Ranch, Whiskey Springs, and Larter Ranch, and from the Utah State Division of Water Resources for Millsite Dam.

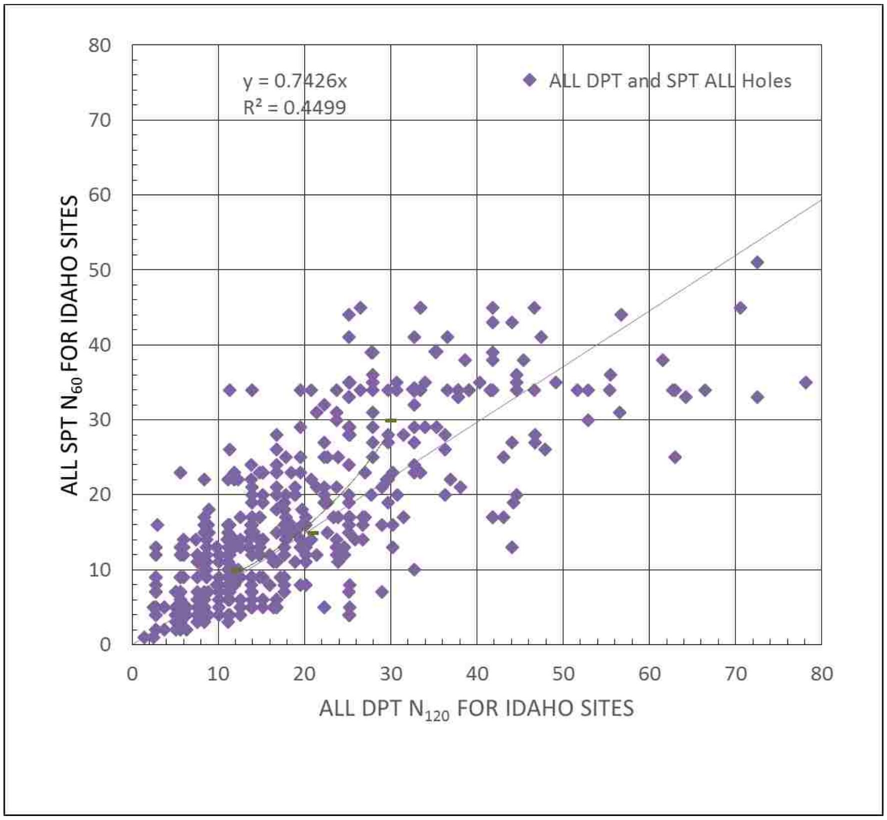

Figure 9-4. Correlation of DPT N_{120} vs SPT N_{60} for all holes at all Idaho sites using both the light, 63.6 kg (140 lb.) hammer, and the heavy, 154.4 kg (340 lb.) hammer. The Chinese line depicts the expected relationship between the N_{120} blow count and the SPT blow count N_{60}, as detailed in Figure 9-5 below.

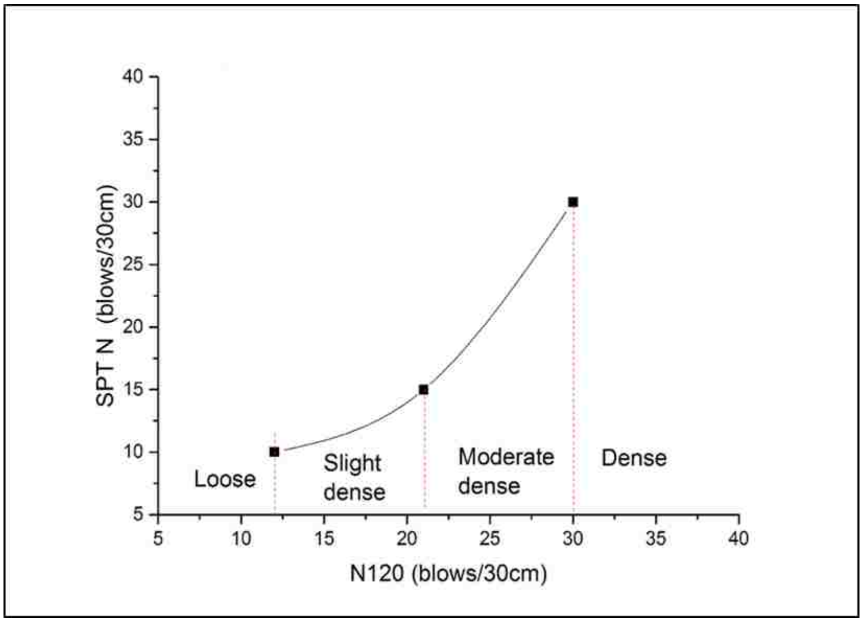

Figure 9-5. Chinese correlation line depicting the expected relationship between the N_{120} blow count and the SPT blow count N.

10 CONCLUSIONS

The Chinese dynamic cone penetration test (DPT) provides a simpler, more economical approach for evaluating liquefaction resistance than the Becker penetration test (BPT). In addition, the DPT liquefaction resistance curves for gravels are based on direct field performance while the BPT requires an intermediate correlation to obtain an equivalent sand SPT blow count. Correlations between DPT N'_{120} and the BPT $(N_1)_{60}$ were reasonable for gravels when using an automatic hammer to increase consistency and reduce data scatter. Regression analysis indicates that separate correlation curves would be required for sand and gravel. Cyclic resistance ratio curves from the DPT for the 30% probability curve are generally consistent with results from the BPT at a field test site; however, the DPT consistently identified a thin potentially liquefiable layer than was apparently not resolved by the BPT. Therefore, the DPT liquefaction resistance curves should only be used to evaluate liquefaction in gravels. Additional field testing would be very desirable in understanding the performance of the DPT versus the BPT in field tests sites.

Based on the results of the field investigations conducted for this study, the following conclusions have been developed.

1. The Chinese dynamic cone penetrometer can generally be driven through sandy gravel alluvium profiles using only the conventional SPT hammer energy despite the larger particle sizes.
2. Typical hammer energy correction factors provide a reasonable means for adjusting the blow count from the SPT hammer to give blow counts that would be obtained with the

conventional Chinese DPT hammer energy. However, use of this procedure will lead to additional uncertainty in the blow count due to depth and particle size. Ideally, the heavier hammer should be used for liquefaction evaluation whenever possible.

3. When the DPT rods are more than about 5º from vertical, the side friction can increase, reducing the energy that is actually transferred to the cone tip, and producing artificially high N'_{120} values which are unreliable. If this condition develops, the DPT cone should be withdrawn and the test repeated.
4. Liquefaction triggering correlations based on the DPT N'_{120}, correctly identified sites where liquefaction features were observed. In addition, layers which would not be expected to liquefy based on the BPT approach were also correctly predicted to not liquefy using the DPT approach.
5. Although an expanded database is clearly necessary to adequately evaluate the effectiveness of the DPT based approach, the DPT-based triggering curve assuming a 30% probability of occurrence seems to provide a reasonable boundary relative to the BPT.
6. The results of this study suggest that the DPT can provide liquefaction hazard evaluations quickly, reliably, and more economically than the BPT at depths less than about 15 m or 50 ft. and use more direct correlations with field performance.
7. Adding the CSR vs DPT N'_{120} data points from the three Idaho DPT to the Chinese Data Set list had little effect on the probabilistic triggering curves originally developed by Cao et al. (2013). This result indicates that the field performance data from Idaho is consistent with the results obtained in China.

8. Correlation equations between SPT N_{60} and DPT N_{120} have relatively low R^2 values and are not particularly reliable. These should be used with appropriate caution.

Table 3. Summary of DPT-based Liquefaction Data.

Earthquake	Site	Mag	a_{max}	Liq (yes/no)	Critical interval (ft.)	Avg Depth (ft.)	Depth to GWT (ft.)	r_d	CSR (Eq.)	% gravel	% fines	Hammer Weight (lb.)
None	**Millsite Dam**											
	DPT 1-15 Light	N/A	N/A	No	3.3-8.2	5.7	3.0	1.0	0.36	0.0	10-15	140
	DPT 1-15 Heavy	N/A	N/A	No	3.3-8.2	5.7	3.0	1.0	0.35	0.0	10-15	225
	DPT 2-15 Light	N/A	N/A	No	8.0-11.0	9.5	3.0	1.0	0.40	20.0	10.0	140
	DPT 2-15 Heavy	N/A	N/A	No	8.0-11.0	9.5	3.0	1.0	0.40	20.0	10.0	225
	DPT 3-15 Light	N/A	N/A	No	7.8-11.1	9.5	3.0	1.0	0.39	20.0	15.0	140
	DPT 3-15 Heavy	N/A	N/A	No	7.8-11.1	9.5	3.0	1.0	0.38	20.0	15.0	225
	DPT 5-15 Light	N/A	N/A	No	2.0-8.1	6.0	3.0	1.0	0.32	0.0	46.0	140
	DPT 5-15 Heavy	N/A	N/A	No	2.0-8.1	6.0	3.0	1.0	0.32	0.0	46.0	225
1983Borah Peak	**Pence Ranch**											
	BPc-A Light	7.3	.39	Yes	5.0-10.0	7.5	5.0	.98	0.30	35-65	1-9	140
	BPc-A Heavy	7.3	.39	Yes	5.0-10.0	7.5	5.0	.98	0.30	35-65	1-9	340
	BPc-B Light	7.3	.39	Yes	5.0-12.0	8.5	5.0	.98	0.31	1-71	2-5	140
	BPc-B Heavy	7.3	.39	Yes	5.0-12.0	8.5	5.0	.98	0.31	1-71	2-5	340
	BPc-C Light	7.3	.39	Yes	7.0-14.0	10.5	3.7	.98	0.35	8-50	6-9	140
	BPc-C Heavy	7.3	.39	Yes	7.0-14.0	10.5	3.7	.98	0.36	8-50	6-9	340
	BPc-3 Light	7.3	.39	Yes	5.0-12.0	8.5	4.0	.98	0.34	46-71	3-8	140
	BPc-3 Heavy	7.3	.39	Yes	5.0-12.3	8.6	4.0	.98	0.32	46-71	3-8	340
1983Borah Peak	**Whiskey Springs**											
	BC-3 Light	7.3	0.5	Yes	22.0-28.0	25.0	20.0	.90	0.32	38-58	9	140
	BC-3 Heavy	7.3	0.5	Yes	22.0-28.0	25.0	20.0	.90	0.31	38-58	9	340
	BC-4 Light	7.3	0.5	Yes	36.7-38.3	37.5	20.0	.91	0.39	56	4	140
	BC-4 Heavy	7.3	0.5	Yes	37.3-40.3	38.8	20.0	.91	0.40	56	4	340
1983Borah Peak	**Larter Ranch**											
	BPc-1 Light	7.3	0.5	Yes	20.0-22.3	21.2	19.6	.95	.32	N/A	N/A	140
	BPc-1 Heavy	7.3	0.5	Yes	20.0-22.0	21.0	19.6	.95	.32	N/A	N/A	340
	BPc-2 Light	7.3	0.5	Yes	20.0-30.0	25.0	14.6	.95	.38	42-64	6-22	140
	BPc-2 Heavy	7.3	0.5	Yes	20.0-30.0	25.0	14.6	.94	.38	42-64	6-22	340
	BPc-3 Light	7.3	0.5	Yes	19.0-29.0	24.0	14.6	.94	.38	50-64	6-10	140
	BPc-3 Heavy	7.3	0.5	Yes	19.0-29.0	24.0	14.6	.94	.38	50-64	6-10	340
	BPc-4 Light	7.3	0.5	Yes	15.0-22.0	18.5	8.3	.96	.41	33-42	13-18	140
	BPc-4 Heavy	7.3	0.5	Yes	15.0-20.0	17.5	8.3	.96	.41	33-42	13-18	340

REFERENCES

Andrus, R. D. et.al (1986). Geotechnical Evaluation of a Liquefaction Induced Lateral Spread, Thousand Springs Valley, Idaho. Proceedings of the 22nd Symposium on Engineering Geology and Soils Engineering, 383-402.

Andrus, R. D. and Youd, T.L. (1987). Subsurface Investigation of a Liquefaction-Induced Lateral Spread Thousand Springs Valley, Idaho. Brigham Young University, Civil Engineering. Provo, Utah: US Army Engineer Waterways Experiment Station.

Andrus, R.D., and Youd, T.L. (1989). Penetration Tests in Liquefiable Gravels. Proceedings of 12th ICSMFE, 1, 679-682.

Andrus, R. D. et.al. (1991). Liquefaction of Gravelly Soil at Pence Ranch during the 1983 Borah Peak, Idaho Earthquake. Soil Dynamics and Earthquake Engineering, 251-262.

Andrus, R. D. (1994). In situ characterization of gravelly soils that liquefied in the 1983 Borah Peak Earthquake. PhD Dissertation, Civil Engineering Dept. University of Texas at Austin, p. 579.

Bowler, J.M., and Polach, H.A. (1971). Radiocarbon Analyses of Soil Carbonates: An Evaluation from Paleosols in Southeastern Australia. (D. H. Yaalon, Ed.) Paleopedology-Origin, Nature, and Dating of Paleosols, 97-108.

Bull, W. B. (1972). Recognition of alluvial-fan deposits in the stratigraphic record. (J. K. Rigby, Ed.) Recognition of Ancient Sedimentary Environments, 63-83.

Callen, R.A., Wasson, R.J., and Gillespie, R. (1983). Reliability of Radiocarbon Dating of Pedogenic Carbonate in the Australian arid Zone. Sedimentary Geology, 35, 1-14.

Cao, Z., Youd, T. Yuan, X. (2011). Gravelly soils that liquefied during 2008 Wenchuan, China earthquake, Ms=8.0. *Soil Dynamics and Earthquake Engineering*, Elsevier, 1132-1143.

Cao, Z. Y. (2012). Chinese Dynamic Penetration Tests (DPT) at Liquefaction Sites Following 2008 Wenchuan Earthquake. Proceedings of 4th International Conference on Site Characterization.

Cao, Z. Youd, T., Yuan, X. (2013). Chinese Dynamic Penetration Test for Liquefaction Evaluation in Gravelly Soils. *Journal of Geotechnical and Geoenvironmental Engineering*, ASCE 139(8), 1320-1333.

Chameau, J.L., Clough, G.W., Reyna, F., and Frost, G.D. (1991). Liquefaction Response of San Francisco Bayshore Fills. Seismic Society of America, 81(5), 1998-2009.

Chinese Design Code (2001). *Design Code for building foundation of Chengdu region*. Administration of Quality and Technology supervision of Sichuan Province PRC (in Chinese), DB51/T5026-2001.

Chinese Specifications (1999). *Specification of Soil Test*. Ministry of Water Resources of the People's Republic of China, SL237-1999.

Coulter, H., and Miglaccio, R. (1966). The Alaska Earthquake, March 27, 1964: Effects on Communities, Effects of the Earthquake of March 27, 1964 at Valdez, Alaska. *U.S. Geological Survey Professional Paper,* 542-C.

Elgamal, A. W., Amer, M. (1993). Soil Liquefaction during the October 12, 1992 Egyptian Dahsur Earthquake. NCEER Bulletin, 7(4), 22-24.

Florin, V. A., Ivanov, P.L. (1961). Liquefaction of Saturated Sandy Soils. Proceeding of the 5th International Conference of Soils Mechanics and Foundation Engineering, 1, 107-111.

Funk, J. M. (1976). Climatic and Tectonic Effects on Alluvial Fan Systems, Birch Creek Velley, East-Central Idaho. Ph.D. Dissertation, University of Kansas, Dept. of Geology.

Ghafghazi, M., DeJong, J. (2014). Instrumented Becker Penetration Test for Liquefaction Assessment in Gravelly Soils. Vancouver Geotechnical Society.

Ghafghazi, M., DeJong, J.T., Sturm, A.P., Temple, C.E. (2017). Instrumented Becker PenetrationTest. II:iBPT-SPT Correlation for Characterization and Liquefaction Assessment of Gravelly Soils. *Journal of Geotechnical and Geoenvironmental Engineering,* 143(9); 04017063.

Harder, L., and Seed, H. (1986). Determination of Penetration Resistance for coarse-grained soils using the Becker Hammer drill. University of California-Berkeley: Report UCB/EERC-86/06 Earthquake Engineering Resource Center.

Harder, L. (1988). Use of Penetration Tests to Determine the Liquefaction Potential of Soils During Earthquake Shaking. PhD Dissertation, University of California, Berkeley, 456 p.

Harder, L. (1997). Application of the Becker Penetration Test for Evaluating the Liquefaction Potential of Gravelly Soils. Salt Lake City, Utah: *NCEER Workshop on Evaluation of Liquefaction Resistance.*

Holzer, T.L., Young, T.L., and Hanks, T.C. (1989). Dynamics of Liquefaction during the 1987 Superstition Hills, California, Earthquake. Science, 244(4900), 56-59.

Holzer, T. L, Clark, M.M. (1993). Sand Boils without Earthquakes. Geology, 21, 873-876.

Holzer, T., Bennett, M.J. (1994). A Paleoliquefaction Signature in Natural Sand Deposits (abs). EOS, Trans. Am. Geoph. Union, 75(44), 452.

Holzer, T., Bennett, M.J. (1995). Searching for a Paleoliquefaction Signature in Geotechnical Borings in Sands. Geological Society of America: Abstract with Programs, 26(7), A252-A253.

Ishihara, K., Shimizu, K., and Yasuda, Y. (1981). Porewater Pressure Measured in Sand Deposits during an Earthquake. Soils and Foundations, 21(4), 85-100.

Ishihara, K. (1985). Stability of Natural Deposits during Earthquakes. Proceedings of 11th Int. Conf. on Soil Mech. and Foundation Engineering, San Francisco, Calif.., Vol. 1, 321-376.

Jackson, S.M. and Boatright, J. (1985, November). The Borah Peak Earthquake of October 28, 1983-Strong Ground Motion. Earthquake Spectra, 2.

Jackson, S.M. and Boatright, J. (1987). Strong Ground Motion in the 1983 Borah Peak, Idaho, Earthquake and its Aftershocks, Bulletin of the Seismological Society of America, Vol. 77, No.3, pp.724-738.

Kanamori, Y., Kawakami, S.I., Yairi, K., and Hattori, T. (1993). Liquefaction and Flowage at Archaelogical Sites in the Inner Belt of Central Japan: Tectonic and Hazard Implications. Engineering Geology, 335, 65-80.

Keefer, D. K. (1984). Landslides Caused by Earthquakes. Geological Society of America Bulletin, 95, 406-421.

Koester, J.P., Daniel, C., and Anderson, M. (2000). In Situ Investigation of Liquefied Gravels at Seward, Alaska. Geotechnical Site Characterization, 1714, 33-48.

Kokusho, T., Tanaka, Y., Kudo, K., and Kawai, T. (1995). Liquefaction Case Study of Volcanic Gravel Layer during 1993 Hokkaido-Nansei-Oki Earthquake. Proceedings 3rd International Conference on Recent Advances in Geotechnical Earthquake Engineering and Soil Dynamics, 235-242.

Kulhawy, F., Mayne, P. (1990). Manual on Estimating Soil Properties for Foundation Design, Electric Power Research Institute, EL-6800, Project 1493-6, Palo Alto, CA.

Lin, C., et al. (2004). Impact of Chi-Chi earthquake on occurrence of landslides and debris flow. Engineering Geology, Vol. 71. P.49-61.

Liu, H. (1989). The 1976 Great Tangshan Earthquake. Siesmological Press.

Maurenbrecher, P.M., Den Outer, A., and Luger, H.J. (1995). Review of Geotechnical Investigations Resulting from the Roermond April 13, 1992 Earthquake. Proceedings 3rd International Conference on Recent advances in Geotechnical Earthquake Engineering and Soil Dynamics, 645-652.

McIntyre, D.H., and Hobbs, S.W. (1978). Geologic Map of the Challis Quadrangle, Custer County, Idaho. U.S. Geological Survey Open-File Report 78-1059.

National Research Council. (1985). Liquefaction of Soils during Earthquakes. National Academy Press, 240.

Nelson, W.B., and Ross, C.P. (1969). Geologic Map of the Mackay Quadrangle, South-Central Idaho. U.S. Geological Survey Miscellaneous Geologic Investigations Map I-580.

Nikolaou, S. (2014). GEER/EERI/ATC Earthquake Reconaissance January 26th/February 2nd 2014 Cephalonia, Greece Events. NSF/GEER/EERI/ATC.

O'Rourke, T.D., Palmer, M.C. (1994). Earthquake Performance of Gas Transmission Pipelines during the Northridge Earthquake. NCEER Bulletin, 8(2), 1-5.

Pierce, K.L., and Scott, W.E. (1982). Pleistocene Episodes of Alluvial Gravel Deposition, Southeastern Idaho. (B. a. Breckenridge, Ed.) Idaho Bureau of Mines and Geology Bulletin 26-Cenozoic Geology of Idaho, 685-702.

Pierce, K.L., Covington, H.R., Williams, P.W., and McIntyre, D.L. (1983). Geologic Map of the Cotterel Mountains in the Northern Raft River Valley, Cassia County, Idaho. U.S. Geological Survey Miscellaneous Geologic Investigations Map I-11450.

Pierce, K. L., Machette, M. N., U.S. Geological Survey, oral communication, 1986).

Rember, W. C., Bennett, E.H. (1979a). Geologic Map of the Dubois Quadrangle, Idaho. Idaho Bureau of Mines and Geology Geologic Map Series, 2 Degree Quadrangle.

Rember, W. C., Bennett, E.H. (1979b). Geologic Map of the Dubois Quadrangle, Idaho. Idaho Bureau of Mines and Geology, Geologic Map Series 2 Degree Quadrangle.

Rollins, K. et al. (2017). Liquefaction Evaluationat a Gravel Site using the Dynamic Penetration Test and the Becker Penetration Test. Earthquake Geotechnical Engineering.

Sasaki, Y., Taniguchi, E. (1982). Shaking Table Tests on Gravel Drains to Prevent Liquefaction of Sand Deposits. Soils and Foundations, 22(3), 1-14.

Sasaki, Y. T. (1992). Mechanism of Permanent Displacement of Ground caused by Seismic Liquefaction. Soils and Foundations, 32(3), 79-96.

Scott, W. E. (1982). Surficial Geologic Map of the Eastern Snake River Plane and Adjacent Areas, 111 deg to 115 deg West, Idaho and Wyoming. US Geological Survey Miscellaneous Investigation Series Map I-1372.

Seed, H.B., Idriss, I.M. (1971). Simplified Procedure for Evaluating Soil Liquefaction Potential, Journal of Geotechnical Engineering Division, ASCE, Vol. 97, No. 3, pp.458-482.

Seed, H. a. (1983). Evaluation of Liquefaction Potential using Field Performance Data. Journal of Geotechnical Engineering, 109(3), 458-482.

Seed, H., et al. (1984). The Influence of SPT Procedures in Soil Liquefaction Resistance Evaluations, Report No. UBC/EERC-84/15. Berkely, California: Earthquake Engineering Research Center, UC Berkeley.

Seed, H.B., Tokimatsu, K., Harder, L.F., and Chung, R.M. (1985). Influence of SPT Procedures in Soil Liquefaction Resistance Evaluations. Journal of Geotechnical Di., 111(12), 1425-1445.

Seed, H.B., and De Alba, P. (1986). Use of SPT and CPT Tests for Evaulating the Liquefaction Resistance of Sands. (V. Tech, Ed.) Proceedings of In-Situ 1986(6), 281-302.

Sekiguchi, K. O. (1988). Liquefaction Analyses of Layered Sand Deposits considering Overconsolidated Ratio. Proceedings of 9th World Conference on Earthquake Engineering, 3, 279-284.

Sims, J.D., and Garvin, C.D. (1995). Recurrent Liquefaction induced by the 1989 Loma Prieta Earthquake and 1990 and 1991 Aftershocks: Implication for Paleoseismicity Studies. Seismic Society of America, 85(1), 51-65.

Sirovich, L. (1996). Repetitive Liquefaction at a Gravelly Site and Liquefaction in Overconsolidated Sands. Soil and Foundations, 36(4), 23-34.

Sirovich, L. (1996a). In-situ Testing of Repeatedly Liquefied Gravels and Liquefied Overconsolidated Sands. Soils and Foundations, 36(4), 35-44.

Stamatopolous, C. S. (1995). Effect of Prestress on the Liquefaction Potential of Silty Sands. (A. a. Cakmak, Ed.) Soil Dynamics and Earthquake Engineering VII, 181-188.

Stokoe, K., Rix, G. et al (1988a). Liquefaction of Gravelly Soils during the 1983 Borah Peak, Idaho Earthquake. Proceedings of 9th World Conference on Earthquake Engineering, 3, 183-188.

Stover, C. (1985). The Borah Peak Earthquake of October 28, 1983-Isoseismal Map and Intensity Distribution. Earthquake Spectra, 2.

Sy, A. (1993). Energy Measurements and Correlations of the Standard Penetration Test (SPT) and the Becker Penetration Test (BPT). University of British Columbia, Department of Civil Engineering, Vancouver, B.C.

Sy, A. and Campanella, R.G. (1993). Dynamic Performance of the Becker Hammer Drill and Penetration Test. Canadian Geotechnical Journal, 30(4), 607-619.

Sy, A., and Campanella, R. (1994). Becker and Standard Penetration Tests (BPT-SPT) Correlations with Considerations of Casing Friction. *Canadian Geotechnical Journal*, 31(3), 343-356.

Sy, A. a. (1995). Becker and Standard Penetration Tests (BPT-SPT) Correlations.

Sy, A. (1997). Twentieth Canadian Geotechnical Colloquium: Recent developments in the Becker penetration test: 1986-1996. *Canadian Geotechnical Journal*, 23(4), 56-74.

Tanaka, Y., Kokusho, T., Yoshida, Y., and Kudo, K. (1989). Dynamic Strength Evaluation of Gravelly Soils. Proceedings of Discussion Session on Influence of Local Conditions on Seismic Response, 12th International Conference on Soil Mechanics and Foundation Engineering.

Tatsuoka, F. K. (1988). Liquefaction Strength of Sands Subjected to Sustained Pressure. Soils and Foundations, 28(1), 119-131.

Tokimatsu, K., Yoshimi, Y. (1983). Empirical Correlation of Soil Liquefaction based on SPT N-value and Fines Content. Soils and Foundations, 23(4), 56-74.

Varnes, D. J. (1978). "Slope Movement Types and Processes" Landslides-Analysis and Control. Washington D.C.: National Academy of Sciences.

Wang, W. (1984). Earthquake Damages to Earth Dams and Levees in Relation to Soil Liquefaction and Weakness in Soft Clays. *Proceedings of International Conference of Case Histories in Geotechnical Engineering.* St. Louis, Missouri, Vol.1, 511-521.

Williams, G.E., and Polach, H.A. (1969). The Evaluation of 14C Ages for Soil Carbonate from the Arid Zone. Earth and Planetary Science Letters, 7, 240-242.

Williams, G.E., and Polach, H.A (1971). Radiocarbon Dating of Arid-zone Calcareous Paleosols. Geologic Society of America Bulletin, 82, 3069-3086.

Yasuda, S. and Tohno, I., (1988). Sites of Reliquefaction caused by the 1983 Nihonkai-Chubu Earthquake. Soils and Foundations, 28(2), 61-72.

Yegian, M. G. et al. (1994). Liquefaction and Embankment Failure Case Histories, 1988 Armenian Earthquake. Journal of Geotechnical Engineering, 120(3), 581-596.

Youd, T. L. et al. (1978). Mapping Liquefaction-Induced Ground Failure Potential. Journal of the Geotechnical Engineering Division, 104(GT4), 433-466.

Youd, T. L. (1984). Recurrence of Liquefaction at the Same Site. Proceedings of 8th World Conference of Earthquake Engineering, 3, 231-238.

Youd, T. L., EERI, Harp, E.L., Keefer, D.K., Wilson, R.C. (1985). The Bora Peak, Idaho Earthquake of October 28, 1983-Liquefaction. Earthquake Spectra: The Professional Journal of the Earthquake Engineering Research Institute, 71-89.

Youd, T. L., Idriss, I.M., Andrus, R.D., Arango, I., Castro, G., Christian, J.T., Dory, R., Finn, W.D.L., Harder, L.F., Hynes, M.E., Ishihara, K., Koester, J.P., Liao, S.S.C., Marcuson, W.F., Martin, G.R., Mitchell, J.K., Moriwaki, Y., Power, M.S., Robertson, P.K., Seed, R.B., and stoke, K.H. (2001). Liquefaction Resistance of Soils; Summary Report from the 1996 NCEER and 1998 NCEER/NSF Workshops on Evaluation of Liquefaction Resistance of Soils. *Journal of Geotechnical and Geoenvironmental Engineering*, 127(10), 817-833.

Yuan, X., et al. (2009). Preliminary research on liquefaction characteristics of Wenchuan 8.0 earthquake (in Chinese). China Journal of Rock Mechanics and Engineering, 28(6), 1288-1296.